Odor representations in Drosophila receptor neurons analyzed by in vivo calcium imaging

Dissertation zur Erlangung des akademischen Grades eines Doktors der Naturwissenschaften, *Dr. rer. nat.*

vorgelegt von:

Daniel Münch

an der

Universität Konstanz

Mathematisch-Naturwissenschaftliche Sektion

Fachbereich Biologie

Tag der mündlichen Prüfung: 28. Februar 2014

1. Referent: Prof. Dr. C. Giovanni Galizia
2. Referent: Dr. Christoph J. Kleineidam
Prüfungsvorsitz: Prof. Dr. Elisa Ferrando-May

Contents

General Introduction

> *»A scent organ is designed to set the scene olfactorily,« she explained in a whisper. »It's unique to Bookholm – unique to this theatre! Together with the music, it contributes an olfactory dimension to the production. Sight, hearing, smell! Even a blind member of the audience knows what's happening onstage when the scent organ gets going. Playing the thing is an art in itself. There are seven scent organists in Bookholm, but Krakenbeyn is by far the greatest virtuoso. He designed and built that instrument himself. A grand master of nasal scene-setting! His compositions smell the best. Pay attention, the solo is beginning!«*
>
> from *The Labyrinth of Dreaming Books* by Walter Moers

Technically we are far away from having an organist playing a "scent organ" in theater, manipulating the olfactory world and drawing the audience right into the play. But everybody experienced the power of olfaction when a familiar scent suddenly brought back long forgotten memories or the stink of rotten food induced strong feelings of disgust. These examples illustrate how we are influenced by the sense of smell and how we rely on it for example in telling apart nutritious from malicious food sources. Other examples for the importance of olfaction from across the animal kingdom include the finding of mating partners and egg-laying habitats, finding friends and avoiding foes. Extracting all these relevant cues reliably from an olfactory environment that is consisting of myriads of odorous molecules, is the task of olfactory systems.

Organization of olfactory systems

While olfactory systems of different species vary largely in their complexity and evolved to serve specific ecological needs of a given species, their gross organization is remarkably conserved (Niimura and Nei, 2007; Dekker et al., 2006; Stensmyr, 2009; Hildebrand and Shepherd, 1997). Olfactory receptor neurons (ORN) are housed on the olfactory organs like the mammalian nose or the insect antenna and palps. These ORNs usually express a single type of olfactory receptor protein although there are exceptions from this rule (Malnic et al., 1999; Serizawa et al., 2003; Couto et al., 2005; Fishilevich and Vosshall,

2005). An odorant receptor is able to bind a variety of chemical compounds which subsequently leads to activation of the ORN. ORNs are surrounded by liquid, the mucus in vertebrates or the sensilla lymph in insects. Different proteins involved in olfaction are expressed in lymph and mucus. Odorant binding proteins bind and transport e.g. hydrophobic molecules to the receptors, odorant degradation enzymes decompose molecules to clean the lymph of them (Bignetti et al., 1985; Tegoni et al., 2000; Xu et al., 2005; Swarup et al., 2011; Chertemps et al., 2012)

ORNs send their axons to a first olfactory processing center in the brain, the olfactory bulb (OB) in vertebrates or the antennal lobe (AL) in insects. Axons of a given class of ORN, as defined by the receptor they express, converge onto the same spherical structure within AL and OB called a glomerulus (Feinstein and Mombaerts, 2004; Couto et al., 2005; Fishilevich and Vosshall, 2005). Glomeruli are heavily interconnected by a lateral network of different types of local interneurons (LNs). Local neurons of another type, projection neurons (PNs) in insects or mitral cells (MCs) in vertebrates, convey olfactory information from the glomeruli to higher brain areas (Hildebrand and Shepherd, 1997).

However, there also exist differences between olfactory systems. Nematodes for example express multiple receptors per ORN, comprising a completely different way of olfactory coding (Troemel et al., 1995). A specialty in insect olfactory systems is the organization of 2-4 ORNs in hairlike structures called sensilla where they are able to influence each others response (Stocker, 1994; Shanbhag et al., 1999; Su et al., 2012; Vermeulen and Rospars, 2004; Figure 0.1). Vertebrate olfactory receptors are metabotropic 7-transmembrane proteins that activate g-protein signaling cascades upon ligand binding (Buck and Axel, 1991). Insect odorant receptors of the OR family are also 7-transmembrane proteins but they possess an inverted membrane topology (Benton et al., 2006). In addition to ORs insect olfaction involves another class of ionotropic receptors (IRs). Signal transduction in insect olfaction is not as well understood as that of vertebrates. IRs seem to signal exclusively ionotropic while ORs together with an ubiquitously expressed co-receptor called ORCO seem to use ionotropic- as well as a metabotropic signaling (Larsson et al., 2004; Vosshall and Hansson, 2011; Sato et al., 2008; Smart et al., 2008; Wicher et al., 2008; Benton et al., 2009; see Silbering and Benton, 2010 for review).

Different species differ largely in the complexity of their olfactory systems. They differ with respect to the number of their ORNs or glomeruli, e.g. mouse expressing ~ 1000, humans ~ 400, bees ~ 160, ants up to 630 and fruit flies expressing only ~ 50 classes of ORNs/glomeruli (Niimura and Nei, 2007; Flanagan and Mercer, 1989; Galizia et al., 1999; Kelber et al., 2009; Laissue et al.,

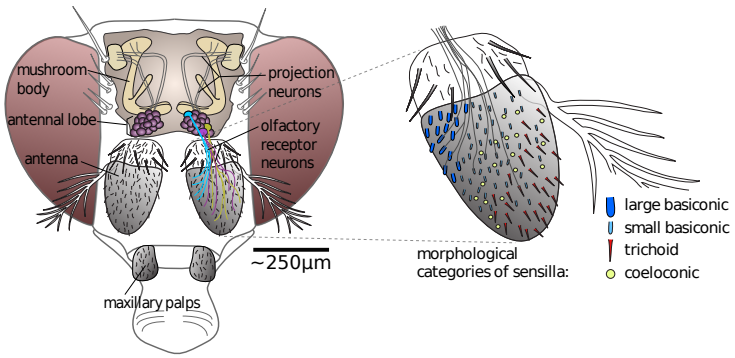

FIGURE 0.1: Schematic of the *Drosophila* olfactory system. The olfactory organs comprise the antenna and maxillary palps. ORNs are housed in different morphological categories of sensilla. ORNs of the same class converge onto a single glomerulus in the antennal lobe. Olfactory information is projected to higher brain areas like the mushroom bodies *via* projection neurons. Illustration with kind permission from Alja Lüdke.

1999; Fishilevich and Vosshall, 2005; Couto et al., 2005), and they differ with respect to the number of their central neurons, e.g. bees have around 4000 local interneurons in the antennal lobe while fruit flies have only around 100 (Witthöft, 1967; Chou et al., 2010). The comparable simple architecture of *Drosophila's* olfactory system paired with a large genetic toolbox available makes them an ideal model organism to study olfaction.

The ensemble code

The high coding capacity of olfactory systems that detect and encode thousands of odorants with a much lower number of input channels, arises from an ensemble code. A single ORN is able to respond to many odorants with different strength of activation depending on the odorants identity and concentration, its specific response profile (Araneda et al., 2000; Pelz et al., 2006). At the same time a single odorant usually elicits responses from more than one ORN. Thus, stimulation with a single odorant gives rise to a specific ensemble response consisting of all the activated and non activated ORNs of an olfactory system (Friedrich and Korsching, 1997; Malnic et al., 1999; Sachse et al., 1999; Uchida et al., 2000; Hallem and Carlson, 2006).

There is a broad range of ORN tuning widths. While generalist ORNs get activated by a large number of odorants, specifically tuned ORNs only show strong responses to a few ligands. On the extreme end lie pheromone receptors that are tuned to single or very few ligands that convey e.g. information about mating partners (Hallem and Carlson, 2006; Stensmyr et al., 2012; van der Goes van Naters and Carlson, 2007).

Response profiles get broader with increasing ligand concentration. More

ORNs get recruited as even less effective ligand–ORN pairs lead to activations and the ensemble of active cells widens (Sachse and Galizia, 2003).

Ensemble responses exist on the different levels of olfactory systems. The earliest pattern arises at the level of ORNs. In AL and OB this ensemble activation gets further shaped by lateral interactions of the different channels *via* the LN network. Presynaptic inhibitory connections on ORN terminals sharpen the pattern at an early stage, further lateral connections shape the ensemble response of PNs and MCs that is conveyed to higher brain areas (Root et al., 2008; Olsen and Wilson, 2008; Silbering et al., 2008).

Odor-response dynamics

ORN responses can be of different polarity. Depending on spontaneous firing rate or previous activation ORNs can respond to odorants with different amounts of inhibition (Duchamp-Viret et al., 1999; Boekhoff et al., 1994). Responses also differ in temporal dynamics like rise-time and response termination, some ligand–ORN combinations lead to responses that last much longer than the stimulation (Martelli et al., 2013; Montague et al., 2011; Turner et al., 2011; Spors et al., 2006). Response dynamics of long or repeated stimulations are further influenced by adaptation (Störtkuhl et al., 1999; Zufall and Leinders-Zufall, 2000).

Odor mixtures

Adding another level of complexity to odor-coding, the vast majority of natural odors appear as mixtures of varying complexity (Knudsen et al., 1993). When a mixture of two or more components hits the olfactory organ, the different ORN ensemble responses for the single ligands overlap and generate a new mixture-specific ensemble response (Johnson et al., 2010). At the same time components and responses interact at several levels, further shaping the mixture ensemble response.

On the level of the brain, many of these mixture interactions arise from a strong lateral network (Silbering and Galizia, 2007; Lei and Vickers, 2008; Olsen and Wilson, 2008; Root et al., 2008; Ignell et al., 2009). But interactions do also happen at earlier stages of olfaction where no lateral network is present. Interactions can happen chemically between odor molecules, odor components can compete for binding at the same receptor and ORNs which housed in the same sensillum can modulate each other electrically (Rospars et al., 2008; Su et al., 2012). All these different interactions make mixture responses often hard to predict from their components responses (Duchamp-Viret et al., 2003; Tabor et al., 2004; Rospars et al., 2008).

The way towards the olfactome

One approach to further decipher the olfactory code is to characterize the olfactory input channels, the ORNs, in best possible detail. The knowledge about the response profiles of all ORNs , the so called "olfactome", would reveal the complete ensemble-response patterns for individual odorants. OR response profiles are being investigated in different species (de Bruyne et al., 2001; Grosmaitre et al., 2009; Wang et al., 2010). In *Drosophila* the receptor genes are identified and facilitated by a large available genetic toolbox,their expression patterns as well as the glomeruli the ORNs project to are known (Clyne et al., 1999; Gao and Chess, 1999; Vosshall et al., 1999; Benton et al., 2009; Fishilevich and Vosshall, 2005; Couto et al., 2005). Especially the GAL4-UAS expression system makes it easy to target identified ORN classes individually and characterize their response profile (Brand and Perrimon, 1993; Dobritsa et al., 2003; Hallem et al., 2004; Pelz et al., 2006). Odorant responses are measured by different labs with a variety of methods (de Bruyne et al., 1999; Dobritsa et al., 2003; Pelz et al., 2006; Sato et al., 2008; Wicher et al., 2008). An approach to integrate this heterogeneous data into a consensus database in order to combine efforts and make a step towards a complete olfactome is presented in Chapter 1. Although in *Drosophila* lots of odor–ORN combination have been measured, there remain substantial gaps, with ORNs where no or only a few ligands have been tested and others, presumably specialized ORNs, where no good responses have been found yet.

Calcium-imaging

All physiological recordings in the work at hand were performed using calcium-imaging. Calcium-imaging makes use of recombinant reporter proteins like G-CaMP (Nakai et al., 2001; Tian et al., 2009) that change their fluorescence properties in response to concentration changes of free cytosolic calcium. Calcium concentration is highly correlated to a neuron's action potential rate and can be used as a proxy for neuronal activity (Charpak et al., 2001; Tian et al., 2009; Moreaux and Laurent, 2008). The cytosolic calcium concentration rises upon neuron activation, mainly through the influx of extracellular calcium-ions *via* voltage-gated calcium-/ or cation-channels (Charpak et al., 2001; Lucas and Shimahara, 2002; Grienberger and Konnerth, 2012; Figure 0.2). For *Drosophila* ORNs the influx of extracellular calcium *via* ligand-gated channels is discussed (Wicher et al., 2008; Sato et al., 2008). The cytosolic calcium concentration can also rise *via* influx from intracellular stores such as the endoplasmatic reticulum (Grienberger and Konnerth, 2012; Ignatious Raja,

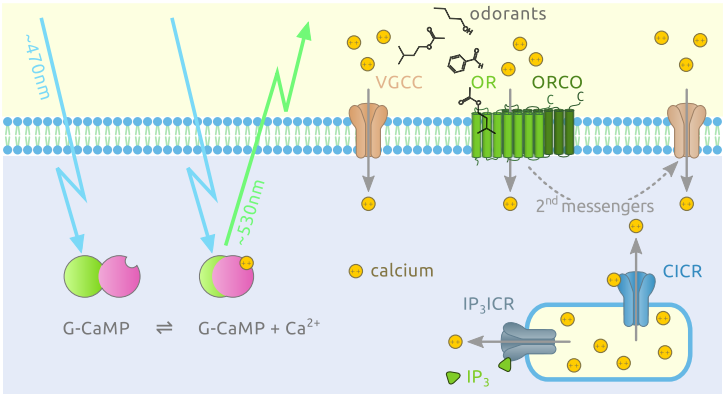

FIGURE 0.2: Schematic of G-CaMP function and Ca^{2+} sources. *VGCC* voltage gated cation channel, *OR* odorant receptor, *ORCO* canonical OR co-receptor, *CICR* Ca^{2+} induced Ca^{2+} release, *IP_3ICR* IP_3 induced Ca^{2+} release. G-CaMP consists of a calcium binding calmodulin domain and a green fluorescent protein. Upon calcium binding, the molecule changes its conformation and fluorescence properties, now emitting light at ~ 530 nm.

2013). However, in *Drosophila* ORNs the calcium release from intracellular stores seems to play only a minor role (Wicher et al., 2008; Sato et al., 2008).

Aims of this study

In this study I investigated how different aspects of odor stimuli are represented in the activity of individual ORNs and ORN ensembles of the fruit fly *Drosophila*.

In **Chapter 1** we paved the ground for the "olfactome" of *Drosophila melanogaster*, i.e. the information about all ORN response profiles. To this end we created a framework to combine the available, published data on odorant responses from *Drosophila* ORNs. The database of odorant responses (DoOR) provides information on tuning properties of individual ORNs and the resulting ensemble codes elicited by single odorants. It is highly accessed from all over the world and used as a tool by scientists of different fields (Andersson et al., 2012; Gabler et al., 2013).

In **Chapter 2** we fill gaps in the "olfactome" by characterizing the odor response profiles of eight types of ORNs. One of these ORNs was completely uncharacterized before, for others we expand the response profiles.

In **Chapter 3** we investigated the complexity of ORN response dynamics. We characterized response dynamics elicited by ~ 100 odorants in eight different ORNs. We found response dynamics to be odorant–ORN specific and to be differentially distributed across ORNs.

In **Chapter 4** we studied mixture effects in ORNs and identified a possible underlying mechanisms. We analyzed responses towards a 15 component mixture and binary sub-mixtures and found hypoadditive mixture interactions. We could determine syntopic interactions as a possible mechanism for these mixture effects.

In **Chapter 5** we screened for possible mixture effects on the *Drosophila* antenna to get an idea of how frequently these effects happen. The measurement of 100 mixture–ORN combinations revealed that strong mixture effects happen sporadically at this peripheral level of the olfactory system.

Chapter One

Integrating heterogeneous odor response data into a common response model: A DoOR to the complete olfactome.

Abstract

We have developed a new computational framework for merging odor response data sets from heterogeneous studies, creating a consensus meta-database, the database of odor responses (DoOR). As a result, we obtained a functional atlas of all available odor responses in *Drosophila melanogaster*. Both the program and the data set are freely accessible and downloadable on the Internet (`http://neuro.uni.kn/DoOR`). The procedure can be adapted to other species, thus creating a family of "olfactomes" in the near future. *Drosophila melanogaster* was chosen because of all species this one is closest to having the complete olfactome characterized, with the highest number of deorphanized receptors available. The database guarantees long-term stability (by offering time-stamped, downloadable versions), up-to-date accuracy (by including new data sets as soon as they are published), and portability (for other species). We hope that this comprehensive repository of odor response profiles will be useful to the olfactory community and to computational neuroscientists alike.

1.1 Introduction

The aim of neuroscience is to understand the brain based on empirically measured physiological data. The community, therefore, relies on access to good experimental data, and considerable effort is being made to create databases that offer large, annotated data sets from physiological experiments made across the world in many laboratories (Herz et al., 2008). However, a major difficulty lies in the comparability of data that come from different places and times. Small changes in experimental parameters can influence the outcome of a physiological experiment, and even under similar conditions, different groups might use other readout parameters for physiological activity. For

example, stimulus response intensity might be reported in spike counts, spike rates, or calcium concentration changes.

Odors consist of volatile airborne molecules that can be perceived by an organism. In the olfactory system, odors are recognized by a large family of odor receptors (ORs). In most animals, including humans, mice, and the fruit fly *Drosophila melanogaster*, each receptor cell expresses one or a few receptor proteins, which give that cell a specific odor response profile. This profile can be represented by a function: to any given chemical representing an odor stimulus we can map a response intensity. Because most chemicals will elicit responses in more than one receptor cell type, each odor elicits a combinatorial activity pattern across these channels. It is this combinatorial nature of olfaction that allows the brain to recognize and remember thousands or maybe millions of different odors with a limited number of receptor types: approximately 350 in humans (Glusman et al., 2001), 1000 in mice (Buck and Axel, 1991), and 60 in *D. melanogaster*(Vosshall et al., 1999). In order to understand how the brain perceives an odor, the ideal situation would be to know all response profiles of all receptors for a given species. Because of technical difficulties, most receptor types are still orphans, that is, their ligands are unknown. The most prominent exception to this is the fruit fly *D. melanogaster*, where many studies have measured odor response patterns in individual cells and in small groups of cells, either *in vivo* or *in vitro*. These odor response profiles in *D. melanogaster* come from different research groups, which have used different techniques (e.g., heterologous expression, Smart et al., 2008; in situ recordings in wild-type sensilla, de Bruyne et al., 1999; in situ recordings in the "empty neuron", Hallem et al., 2004; calcium imaging of cellular responses, Pelz et al., 2006). Furthermore, the set of tested odors differed across studies. As a consequence, it is difficult to compare different studies numerically. Yet, no study has covered all receptor cells so far, and given the resources needed for such an enterprise, it would appear as a waste to do so now, where many receptors have already been deorphanized in great detail.

Exploiting this wealth of data available from the fruit fly, we have therefore developed a new approach that allows us to compare and combine odor response profiles from many studies even when their physiological responses are hetero- geneous due to different techniques used and when the odors tested are only partially overlapping. As a result, we obtain consensus profiles that are based on many studies and thus are statistically more reliable than any single study. We have developed a software platform that allows to extract odor response profiles across chemicals for individual receptors or to extract the entire combinatorial response pattern elicited by a given chemical. The software is open source and can be modified by the user. Although we will

update the database on a regular basis, the database includes a feature that allows for retrieving the state of the database at any given time in the past. This is important to allow for comparative computational studies on reference data sets.

The database is suitable for further studies into the combinatorial nature of olfactory coding, into the logic of ligand receptor interaction in olfactory receptors, and for other applications. Furthermore, the software can be used to create similar databases for other species, including mice and humans, as soon as enough data will be available. Thus, it joins related efforts for databases of olfactory receptor sequences and their ligands (Crasto et al., 2002), as well as other data repositories, for example, `http://senselab.med.yale.edu/senselab/ordb` or `http://gara.bio.uci.edu/`. The database of odor responses (DoOR) package is available from `http://neuro.uni.kn/DoOR`.

1.2 Material & Methods

Nomenclature

Receptors (e.g., Or22a and Ir76b), receptor cells (e.g., ab3A and ac3B), and corresponding glomeruli (e.g., DM2 and VC3l) were labeled following the standards in *D. melanogaster* literature (see Laissue et al. 1999 for glomerulus nomenclature). ORs in *D. melanogaster* belong to three major families: ORs, gustatory receptors, and ionotropic receptors (Larsson et al., 2004; Kwon et al., 2007; Benton et al., 2009). Each odor is given by its chemical name (e.g., 2-heptanone) and the unique Chemical Abstracts Service number (`http://www.cas.org`).

Sources for published odor response profiles

Odor responses were taken from studies with at least five odors tested for a given receptor. Each study enters the database with its own name based on the author, the publication year, and a short data descriptor. For example, the data from Hallem (Hallem et al., 2004) enter the database as two data sets called Hallem.2004.EN and Hallem.2004.WT. Here, EN stands for an empty neuron recording, where receptor proteins are ectopically expressed in an empty olfactory neuron, whereas WT signifies a wild-type recording, that is, a recording from an olfactory neuron that naturally expresses its receptor protein. A list of all studies with nomenclature and details on the respective experiments is provided (Supplementary Table). As most studies reported only one odorant concentration level, no information about response properties across concentration ranges is included in the present version of the database.

Sources for unpublished odor response profiles

We recorded odor response profiles for Or13a, Or67b, and Or92a. We used OrXX:GAL4 and UAS:G-CaMP flies and recorded calcium responses using a CCD (charge-coupled device) camera and a $50\times$ air objective through the intact antenna cuticle as described in detail elsewhere (Pelz et al., 2006). Odors were diluted in mineral oil in decadic steps (10^{-2}, 10^{-3}, ...), with 1:100 (10^{-2}) as the highest concentration, to measure complete odor response curves. Five milliliters of diluted odor was kept in sealed 20 ml vials filled with nitrogen, and 2 ml headspace was used for each stimulation. Odor delivery was automated using a headspace multisampler adapted from gas chromatography (CombiPAL, CTC analytics). For each odor stimulus, a train of 80 fluorescent frames was recorded, with a sampling rate of 4 frames per second. Odor stimuli were applied as two pulses, each 1 s long, at time points 6 and 9 s in each measurement. Bleach-corrected odor responses were converted into relative fluorescence changes as $\Delta F/F$, with F being the background fluorescence before odor stimulation. For each measurement, odor response magnitude was quantified as the average calcium increase in $\Delta F/F$ during 4 s after first stimulus onset. Maximum response magnitude varies across animals, mostly due to difference in G-CaMP expression levels and cuticle pigmentation darkness. Before averaging across animals, responses were therefore normalized within each animal by setting the response to a reference stimulus to 1 and scaling all other responses accordingly. The reference odor was 3-octanol (589-98-0) for Or13a, 1-hexanol (111-27-3) for Or67b, and 2,3-butanedione (431-03-8) for Or92a.

Preprocessing of odor response profiles

We transformed all data sets where values decrease for better ligands (i.e., data reported as 50 % effective concentration (EC50) values of odor dilution) by inverting their values in the database (e.g., in Pelz.2006.AntEC50 an EC50 value of -4.13 is coded as +4.13 in the database) in order to comply with our assumption that $R_1(a) < R_1(b) \Rightarrow R_2(a) < R_2(b)$ for all odors a,b (see Results). Before fitting an odor response vector, its values were all scaled to the range $[0, 1]$ in order to avoid unequal weighting of the two vectors in the fitting procedure.

Finding the best-fitting function

Take a data set of odor response profiles covering o_A odors in r_A receptors. We write this data set as a matrix (see Supplementary Figure S7). We have several

such data sets from different studies, and each study may cover a different (but overlapping) set of odors and a different (but overlapping) set of receptors. Let there be s such studies, and let us denote them $A^1, \ldots A^s$. Thus, the response to odor i in receptor j for study k is A^k_{ij}. For better readability, where useful, we denote columns by the corresponding receptor names and omit subscripts where the entire range is intended. Thus, $A^k_{[Or22a]}$ contains the column of odor responses for receptor 22a in the kth study. We will follow the Or22a example throughout this section. The goal of the algorithm is to merge all available A^k in order to obtain a single consensus matrix $M \in \mathbb{R}^{r \times o}$, where r is the number of all receptors and o is the number of all odors. Merging is done sequentially for each receptor, and within each receptor, merging is done iteratively (Supplementary Figure S7). First, two data sets are merged and then the resulting consensus data set is merged to the next original data set. For small s (s may differ for different receptors), all possible merging sequences can be calculated. For large s, this exhaustive approach is not possible due to computing time constraints, and we follow a heuristic instead (see below).

For each merging step, we first fit five different monotonic functions to the pairs of data sets. The functions used are linear, exponential, sigmoid, asymptotic, and asymptotic with an offset (see Supplementary Figure S1 and user manual on the DoOR homepage). Fitting is done using the R routine `nls()`. This routine minimizes the square distance of the dependent variable $f(x)$ against the independent variable x. Graphically this corresponds to the vertical distances from each point onto that function. However, this is not the optimal solution because there is no "dependent" and "independent" data set. The best solution would be to minimize not the vertical distances but the perpendicular projections onto the fitted function. However, there is no efficient algorithm yet to do this calculation. Until such an algorithm will be implemented, we have taken an alternative approach: all five functions are also fitted flipping the two data sets, effectively optimizing not the vertical projections on the fit but the horizontal projections. In our algorithm, these are the "inverse" functions, so that effectively a total of 10 fitting functions were tested.

For each of these 10 fits, we calculate the average orthogonal distance (unlike the fitting of best parameters, for a set of given parameters this statistic is easily computed). We select the fitting function $f_{best}(x)$ with the smallest average orthogonal distance (mean distance [MD]). This function is only well defined within the data range of the two odor response vectors that have been fitted, and an extrapolation beyond that range would create unwarranted results. Therefore, for values outside this range, we expand the function with a linear function, $f(x) = x + intercept$, where intercept is chosen to create a

continuous function. Thus, the complete $f_{best}(x)$ consists of a linear function to the left, a fitted function in the center, and a linear function to the right.

Merging two data sets

For all odors present in both studies to be merged (or the study to be merged into the consensus set), the location of that odor on the trajectory of $f_{best}(x)$ is calculated by orthogonal projection. All odors that are present in only one of the two studies are also projected onto the function. The odor response values of the newly merged set are calculated by measuring the distances along $f_{best}(x)$. Specifically, given a data point $p_1 = (x_1, y_1)$, we compute the distance from $p_{min} = (x_{min}, y_{min})$ to p_1 as follows:

$$d(p_{min}, p_1) = \int_{x_{min}}^{x_1} \sqrt{1 + (f'_{best}(x)^2)} dx$$

This step is followed by scaling the whole range to $[0, 1]$. Now the complete data set, for this receptor, has one study less, and the procedure is iterated (Supplementary Figure S7).

Data set merging order and data set exclusion

When the number of data sets to be merged is large, not all merging orders can be tested. In this case, we first calculate merging quality (in terms of mean orthogonal distance) for all possible pairs and merge the two data sets that yield the best merging quality. This procedure is iterated until all data sets have been matched.

There are cases where no match is possible, and these data sets are excluded. First, the minimum overlap requested (in terms of common odors of both studies) is 4. Fewer overlapping odors do not give sufficient degrees of freedom to fit the monotonic functions. Second, only pairs that result in a mean orthogonal distance below 0.1415 (which corresponds to $10\,\%$ of the maximum possible distance) are merged.

Global scaling

For comparison of responses across receptors (see Figure 1.3B), we developed a global scaling introducing a weighting factor w_j for each receptor, making use of the information in studies that contain more than one receptor. Because studies that include many odors and receptors contain more across-receptor information, they are weighted more. Thus, for a study k, let $n.rec_k$ be the number of receptors covered and $n.odo_k$ the number of odors recorded. For each receptor j, in that study, we calculate R_j^k as the maximum odor response

within that receptor, and for that study, S^k is the maximum odor response across all receptors (in the units of that study, e.g., spikes per second). We then calculate:

$$w_j = \frac{\sum_{k=1}^{s} n.rec_k \frac{R_j^k}{S^k} + \sum_{k=1}^{s} n.odo_k \frac{R_j^k}{S^k}}{\sum_{k=1}^{s} n.rec_k + \sum_{k=1}^{s} n.odo_k}$$

Implementation and availability

All methods used in this work are implemented in the open source statistical environment R (R Development Core Team, 2013). Apart from the source codes, the DoOR packages for R comprise the original data sets and a precomputed model response matrix. With a few R commands, the user can add data, compute his or her own model response matrix, and reproduce the plots from this paper. R can be obtained from `www.r-project.org`. The DoOR package is available from `http://neuro.uni.kn/DoOR`. A help file with detailed instructions can also be downloaded from that site.

For users who just wish to query the database without using the R package, we provide a web interface for the latest version of the database including 2D and 3D visualizations of the response patterns at `http://neuro.uni.kn/DoOR`.

1.3 Results

Fitting two data sets onto each other

Different odor response profile data sets can have very different qualities and data ranges. For example, studies reporting spike counts may have discrete values, for example, ranging from 0 to 500 spikes/s. Data based on calcium imaging may have percentage of fluorescence change values ranging from negative values (for inhibitory responses) to positive values (e.g., –5 to +18 $\Delta F/F$). Measurements that report receptor sensitivities calculated from entire dose response curves report data as the effective odor concentration that elicit half-maximal responses (EC50), with values ranging from, say, –6.0 to –2.0 (corresponding to log-based odor dilutions). Unlike the first two cases, better ligands have a lower value when expressed as EC50. With this heterogeneity in the qualitative nature of different data types, how could we combine them? Which is the property of odor response profiles that is, in theory, consistent across all data sets? We start with the observation that all odor response profiles of a particular receptor must be based on the same monotonic relationship. Given two odors a and b, we denote their responses with method 1 as $R_1(a)$ and $R_1(b)$ and with method 2 as $R_2(a)$ and $R_2(b)$. Our postulate states that

$R_1(a) < R_1(b) \Rightarrow R_2(a) < R_2(b)$ for all a,b of a given odor response profile. Because all measurements have noise, this postulate will not be true in all real data sets, but the basic principle is that a better ligand in one data set should also be a better ligand in another data set.

We mapped data sets onto each other as pairs. In order to avoid too many free parameters, we selected five possible fitting models and their inverse (see Materials & Methods): a linear model, an exponential, a sigmoid model, and two types of asymptotic nonlinear functions, one with an offset and one without (see Supplementary Figure S1). We show the merging of two data sets for Or22a in Figure 1.1. This receptor has a broad response pattern, that is, many chemicals elicit responses (Figure 1.1A). Responses are plotted against each other for all odors that were measured in both sets (Figure 1.1B); note that values in Pelz.2006.AntEC50 range from 2 to 7 (negative logarithm of odor dilution necessary to elicit the half-maximal response), whereas responses in Hallem. 2006.EN range from 0 to 250 (these are response frequencies in spikes per second, compare with Figure 1.1D). Different dimensionalities along the axes influence the fitting procedure (e.g., deviation along the spike axis would weigh more because the value ranges are larger). Therefore, each data set was linearly scaled to a common range [0,1] before mapping (compare the axes in Figure 1.1B and C). A clear monotonic relationship (plus noise) is apparent between the two data sets.

Next, we mapped each point onto the regression function (Figure 1.1C). Because in these regressions both data sets are equal (i.e., there is no dependent variable), mapping is done by perpendicular projection, that is, we projected each data point onto the closest point on the regression function. Some odors were measured only in one of the two data sets. These odors were also projected onto the regression line. We did not extrapolate the fitting function beyond the data range covered by the two data sets. Rather, we projected values outside this range onto a unitary line (45° slope), thus leaving that range of the data set unaltered. Finally, we gave each point on the regression a value by calculating its position on the curve, scaled to the range [0,1]. The resulting odor response profile was not the average of the two data sets but a fitted consensus set (Figure 1.1D). A comparison of the consensus set with the two original sets showed a good correspondence but also showed that for some odors the information in one set differed from the information in the other set. In no case, we attempted to weigh data sets based on our judgment of their quality: the more data sets are integrated the more individual outliers should become irrelevant.

Note that scaling to the [0,1] interval might cause problems, for example, in case of a data set consisting only of weak ligands when compared with a data

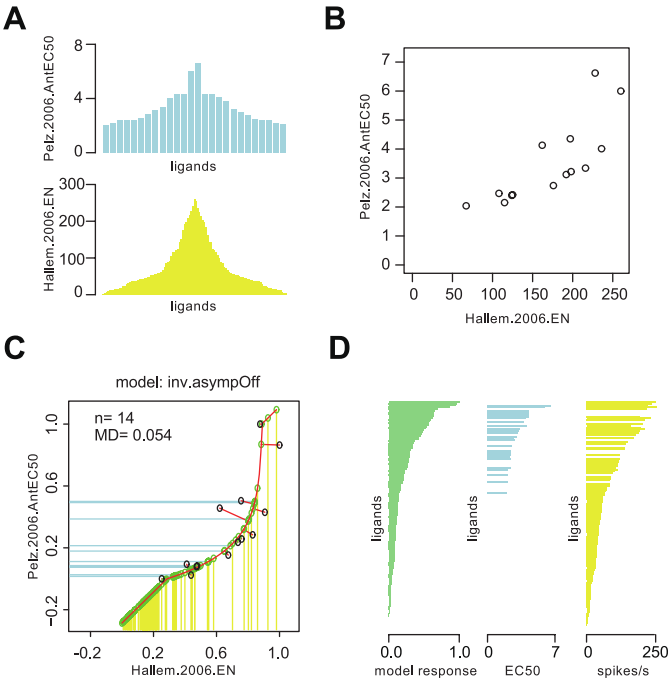

FIGURE 1.1: Merging two response data sets for one receptor. **A** Tuning breadth of odor response profiles for Or22a taken from 2 published sets: Pelz.2006.AntEC50 (Pelz et al., 2006) (top, ordinate units are percentage of calcium responses) and Hallem.2006.EN (Hallem and Carlson, 2006) (bottom, ordinate values are spikes per second). Responses are arranged with strongest odor at the center in order to show the broad odor response profile confirmed in both studies, irrespective of the recording technique. Pelz reported EC50 values based on calcium responses from dose responseprofiles. Hallem reported action potential frequencies in the empty neuron preparation. **B** Plotting odor responses to substances that were measured in both data sets against each other shows a strong correspondence. Note that the values differ: spikes range (abscissa) from approximately 0 to 250 (spontaneous rate was not subtracted) and EC50 (ordinate) ranges from 1 to 7 (negative logarithm of odor dilution). **C** Generation of a consensus data set. Vertical projections from the circles as in B to a fitted regression function yield the consensus odor response. Odors that were measured only in one study are projected from the respective axis onto the regression curve (blue lines for Pelz and yellow lines for Hallem). Consensus responses are calculated from the position along the regression curve. **D** Comparison of odor response profiles of the overlapping odor set for the model responses and the two original data sets (EC50 and spikes per second, respectively). The model responses were arranged in decreasing order, whereas the other two data sets were ordered by matching the odors to the model response plot. The model response covers the normalized range [0,1].

set with mostly strong ligands or when several receptors are compared. The first problem is addressed by not extrapolating the fitting function but using a unitary line beyond the range of each study. For the second case, we employed a global scaling to enable across-receptor comparisons (see Material & Methods and below).

Merging multiple data sets

Ideally, each receptor has been recorded in several studies giving rise to several data sets, with many overlapping odor responses. Merging data sets was done by iteration. To this end, we performed pairwise data set mapping with each of the fitting functions, and the function with the fit performance (lowest "MD") was noted. This results in a fit-quality matrix of all data sets, from which a cluster dendrogram can be derived for visualization when fit quality is interpreted as similarity (Figure 1.2A). Note that this data set is also influenced by how many odors overlap between two data sets. In the extreme case, two sets with an overlap of just two odors would have a perfect fit even though they would not share any information about the odor response profile. Therefore, to create the dendrogram, we did only use those pairs that had at least four common values.

Next, the pair with the best fit-performance was merged. In Figure 1.2A, this corresponds to joining the two data sets with the highest node. As a result, the complete data contained one set less altogether. In the next step, the created merged set was taken as reference, and its fit performance with all other data sets was measured (Figure 1.2B). The data set with the lowest MD was merged into the reference, and this procedure was iterated until either all sets were merged into the consensus set or the breakout criterion was reached (see Material & Methods). With increasing number of studies, the reference set contains an increasing number of odor responses. Figure 1.2C shows the whole procedure for Or22a, which is the receptor for which most studies were available. Because the sequence of merging studies slightly influences the outcome of the consensus data set, in cases where computationally feasible, we merged the data calculating all possible merging sequences and selected the best sequence on the basis of the mean deviation of the merged sequence to each original data set.

Validation and rescaling

As a result, we obtained a consensus odor response profile as shown for a subset of odors with Or22a in Figure 1.2D. How reliable are the individual values? We ran the merging process as many times as there were data sets,

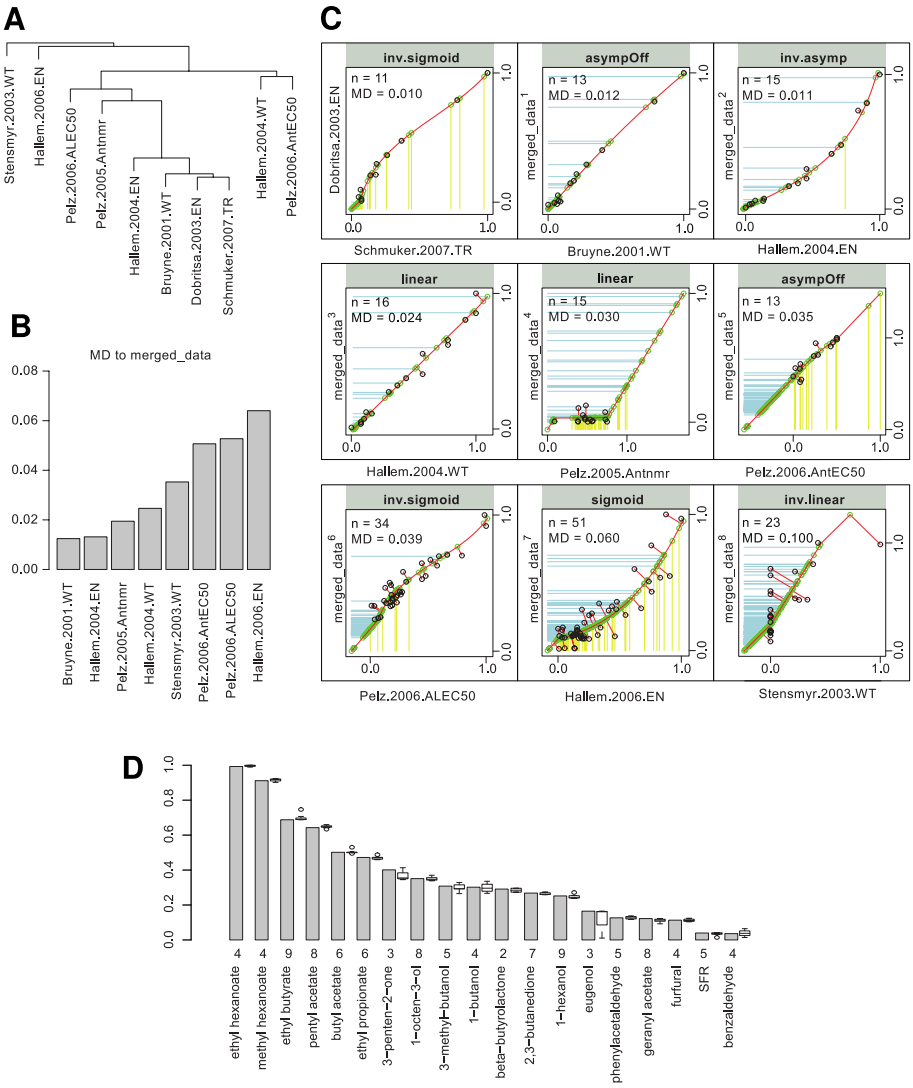

FIGURE 1.2: Mapping many response sets for one receptor. **A** Hierarchical cluster dendrogram based on best-fit values of 10 data sets from 8 studies (de Bruyne et al., 2001; Dobritsa et al., 2003; Stensmyr et al., 2003; Hallem et al., 2004; Pelz, 2005; Hallem and Carlson, 2006; Pelz et al., 2006; Schmuker et al., 2007) with odor responses for Or22a. The two sets with the best pairwise fit are Dobritsa.2003.EN and Schmuker.2007.TR. These two sets are then merged and create the first model response. **B** Best fit of the remaining 8 data sets with this modeled response (merged_data) shows that Bruyne.2001.WT is the next best match (smallest MD). This set is now merged with merged_data. This procedure is iterated for all sets that match merging criteria (see text). **C** Iterative sequence for Or22a showing how for each step a different mapping function might be best. Here, Dobritsa.2003.EN is first merged to Schmuker.2007.TR (see A) using inv.sigmoid as function, yielding $merged\_data^1$. Each of the next frame gives the fitting function used, the number of odors common to both sets (n), and indicates new odors added into $merged\_data^{i+1}$ by yellow vertical lines and odors present in $merged\_data^i$ but not in the data set by blue horizontal lines.(*Continued on next page*)

with each time one data set being dropped from the list. Therefore, for each odor, we obtained several data points, that is, as many as the number of studies that covered that odor and obtained error bars as shown in Figure 1.2D. These error bars confirmed that our approach yields reliable values.

Although remapping of odor responses to [0,1] is useful for theoretical analysis of olfactory coding, in an experimental setting, odor responses are more useful if they are given in the same unit as the experiments themselves. Therefore, the package can be used to back project the merged data set onto the experimental data sets. Most importantly, the back projected data set contained data points that were not measured in the original study but that can be directly compared with their numerical value (see Supplementary Figure S2).

SFR denotes "spontaneous firing rate", which is not an odor response but background activity in the absence of a stimulus. If upon stimulation with an odor firing rate drops below SFR this indicates an inhibitory response. Not all studies reported the SFR value, and some techniques have no access to this value. For example, calcium-imaging studies cannot measure uniform spontaneous activity (bursty spontaneous activity can be measured, Galán et al., 2006). In calcium-imaging studies, however, inhibitory responses are visible as calcium concentration decreases, as opposed to the responses to control, air or mineral oil, which generally give no responses. In our procedure, as explained so far, the merged data were scaled to the range [0,1]. SFR, air, and solvent were always treated as if they were stimuli, and thus, inhibitory responses could be recognized as values smaller than the SFR value. However, this is not always satisfactory, in particular when comparing different receptors that might have different levels for SFR. Therefore, data can be linearly rescaled to have the range SFR to maximum map into the range [0,1], and negative values as large as dictated by the linear fitting.

Comparisons across receptors

Up to this point, all procedures were applied to each receptor *per se* without any comparison to responses in other receptors. Tuning breadth displays for six different receptors are shown in Figure 1.3A: for example, Or67a had a

FIGURE 1.2: (*Continued*) **D** Responses to 19 selected odors in Or22a, as calculated from all available data sets. Ethyl hexanoate and methyl hexanoate are the best ligands in this subset. The numbers under the bars indicate how many studies contribute to the given value. For example, ethyl butyrate or 1-hexanol were covered in nine studies, whereas ethyl hexanoate or benzaldehyde were only measured in four studies. Gray bars give the consensus values. White box plots right to the gray bars give median, quartiles (where available), and outliers (oval circles) obtained by using a leave-one-out strategy.

broad response profile, whereas Or59b had a sharp response profile. Note also that for some receptors, only few odor responses were known (e.g., Or59c). For each receptor, the maximum response was set to 1 and SFR was set to 0, making negative responses immediately visible.

However, the very nature of olfactory coding is combinatorial, and for the olfactory system as a whole, no response in a single receptor neuron type contains information without a comparison to other receptors (with the possible exception of very few labeled line systems). Assume, for example, that a receptor, OrX, has so far only been measured with very weak ligands (i.e., no better ligand is as yet known). In this case, the procedure above would still give the best odor in the test set a value of 1, which when compared across receptors would be misleading. In order to compare receptors, it was therefore necessary to rescale them (see Material & Methods).

For the six receptors shown in Figure 1.3A, the rescaled results are shown in Figure 1.3B (see also Supplementary Figure S6). Note that the pattern changes somewhat for Or59a and changes dramatically for Or59c and Or65a. The most likely explanation is that for these receptors, the best ligands have not yet been found. Studies including more odors might find a better ligand, and targeted studies that exploit the combinatorial knowledge from the entire database might help. Nevertheless, it might also be that some receptors never reach the same strong responses as other receptors. In such cases, even though the individual best ligand has been found, the elicited response might still be weak as compared with maximal responses in other cells. With the globally scaled responses, it was possible to create response breadth plots for each single odor (Figure 1.3C), similar to the tuning breadth plots shown above. 2-heptanone elicited responses in many receptors, some of which were negative. Methyl salicylate in contrast showed a very sharp profile evoking strong responses only in a few receptors.

Scaling odor responses across receptors is also a prerequisite for the creation of spatial odor response maps. In the *Drosophila* olfactory system, axons of sensory cells that express a given receptor converge stereotypically onto one glomerulus of the antennal lobe (AL), and thus, an activity map across receptor cells results in an activity map across olfactory glomeruli. These maps can be recorded directly, for example, using calcium imaging (Fiala et al., 2002; Wang et al., 2003; Silbering and Galizia, 2007; Silbering et al., 2008). With the database presented here, virtual spatial activity maps in the antennal lobe can be generated; the map for 2-heptanone is shown in Figure 1.3D. On the webpage, the map for any of the odors in the database can be downloaded. The map visualizes activated glomeruli in shades of red, inhibited glomeruli in shades of blue, and indifferent glomeruli in white. Some glomeruli cor-

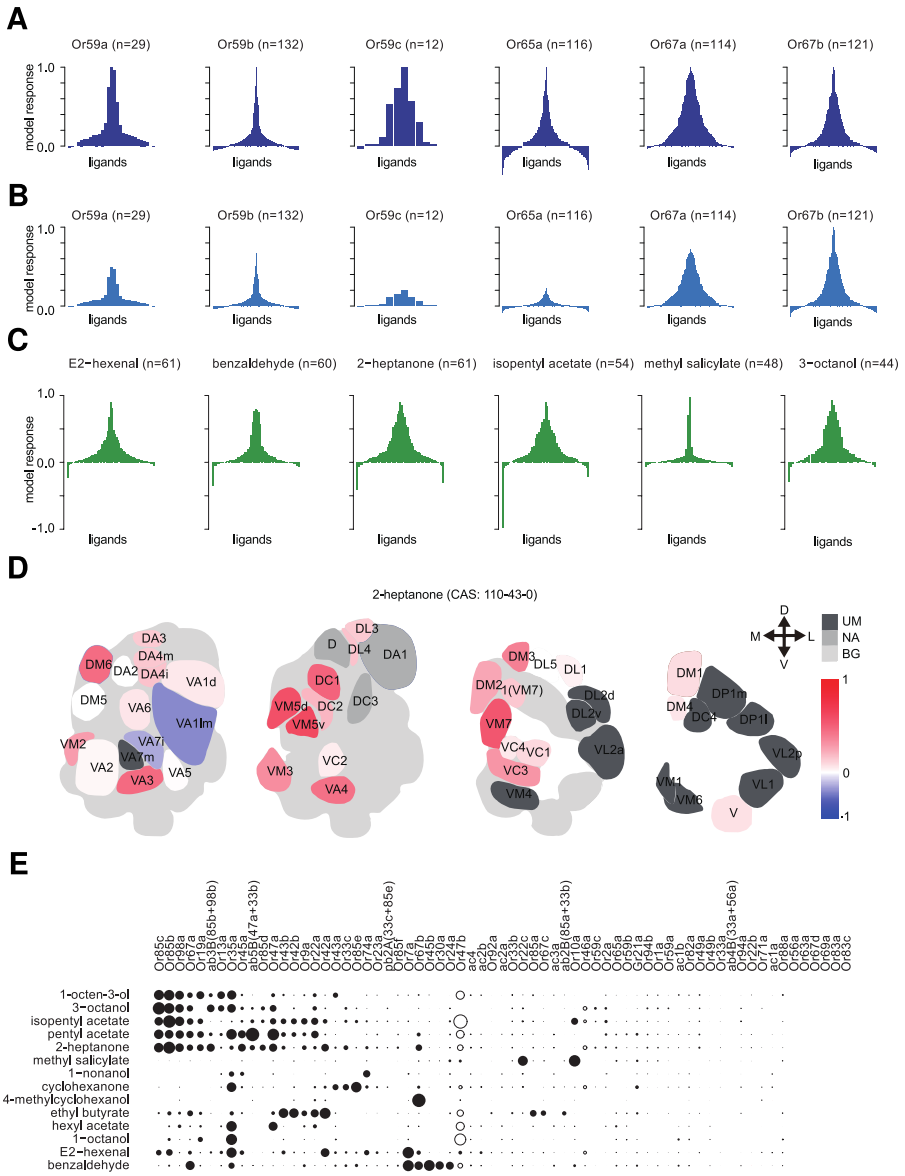

FIGURE 1.3: The complete consensus data set. **A** Tuning breadth plots (compare with Figure 1.1a) for 6 receptors based on the respective consensus data set.Note the pointed shape and negative responses in Or59b and Or65a and the broader profiles in Or67a and Or67b. Only few odor responses are available for Or59c. n Gives the number of odors but not the number of studies merged. Each receptor has been calculated separately and was therefore scaled independently of the other receptors. **B** Same as A but normalized across receptors (see text). Or59a, Or59c, and Or65a do not reach strong responses,indicating that these receptors have a different physiology or that the best ligands have not yet been identified. See Supplementary Figure S6 for additional plots. **C** Response breadth plots for 6 odors, that is, plotting responses against Or. Note that odors differ in their response breadth, for example, broad range for 2-heptanone and isopentyl acetate and narrow range to methyl salicylate. n Gives the number of receptors included. (*Continued on next page*)

respond to receptors, for which there is no response data yet, in the case of 2-heptanone, these are the glomeruli D, DA1, and DC3 (see Figure 1.3D, light gray glomeruli). Other glomeruli do not have a value because the morphological mapping of these glomeruli onto a receptor is as yet unclear (e.g., glomerulus DP1m). Thus, the graphical display of these functional antennal lobes can also be used to earmark gaps in our knowledge of the *D. melanogaster* olfactome, gaps that need to be filled by targeted measurements. Interactive 3D renderings of these AL maps are also available from the website. A ball plot of OR response profiles is shown in Figure 1.3E for a subset (see also Supplementary Figure S8). Note that many entries are still missing, that is, unknown.

Matching neurons, receptors, and glomeruli

Odor response profiles in *D. melanogaster* have been measured in several ways: sensory cells that were identified morphologically, without knowing what receptor they expressed, expression of ORs in other receptor cells or heterologously, expression of calcium sensors in the receptor cells, and measurement of odor responses either in the dendrites or in the axon terminals. This diversity is possible because of a basic mapping property in this system: one receptor, one class of receptor cells, and one glomerulus. There are some exceptions to this scheme: some cells express more than one receptor, and some of the glomerular mapping strategies are more complex. Therefore, we included these cases into the database. The simplest one is given by Or22a, which is coexpressed with Or22b: because no function for Or22b is known, only Or22a has been mapped to the neuron ab3A and the glomerulus DM2. In cases where two receptors are coexpressed and each contributes to the odor response profile, we created a separate mapping for ORs (ligand-binding properties) and for receptor cells (odor response properties). For example, Or85e and Or33c are coexpressed in the receptor neuron pb2A (Goldman et al., 2005). The database contains three entries, but only the entry for pb2A is matched with glomerulus VC1 in the visualization of the antennal lobe. In this case, the functional

FIGURE 1.3: (*Continued*) **D** Physiological antennal lobe response to the odor 2-heptanone. By mapping each receptor to the glomerulus it innervates, we generate a fictive spatial response pattern in the antennal lobe. Excitatory responses are given in red and inhibitory responses in blue in 4 consecutive slices through the antennal lobe. UM, unmapped glomeruli, where the respective receptor is not yet known; NA, non-available glomeruli, where no odor responses have been measured for the corresponding receptor; BG, background material used for the shape of glomeruli beneath the indicated plane; D, dorsal; V, ventral; M, medial; L, lateral. Antennal lobe figure modified from Vosshall and Stocker (2007). **E** Plot of normalized odor responses across all available receptors, for a set of odors, including odors often used in behavioral studies in *Drosophila melanogaster*. Negative responses are given as empty circles. The complete table is in Supplementary Figure S8.

relevance is high because the three odor response profiles differ.

Mapping unlabeled response profiles into database

In some cases, the mapping of receptor cell and receptor is not yet known. Here, the database can be used to find an appropriate match. To test this procedure, we used the database to find the receptor cell that expresses Or13a. We expressed the calcium indicator G-CaMP under the control of the Or13a promoter (Figure 1.4A and B) and recorded calcium odor responses to a total of 111 odors at a dilution of 1:100 (selected responses in Figure 1.4C, full results in Supplementary Table S3). For all odors that elicited responses, we further decreased the dilution in decadic steps until no responses were left. The best ligand was 1-octen-3-ol, and furfural elicited a calcium decrease (Nissler, 2007). At this stage, the odor response profile of Or13a was known, but the corresponding receptor cell was not. We thus used the consensus database to calculate how well the recorded response profile matched each of the known consensus response profiles. Data set ab6A had the best match (Figure 1.4D), which is a receptor neuron that had been characterized previously (de Bruyne et al., 2001) but for which the expressed receptor was not yet known. We also used a recently published data set in which odor responses in Or13a were recorded (Kreher et al., 2008) and confirmed our result (data not shown). To confirm our link of Or13a with ab6A, we mapped the area on the antenna where Or13a is expressed (Figure 1.4A) and found that area to match the published location of ab6A (de Bruyne et al., 2001). The glomerulus that is innervated by neurons expressing Or13a is DC2 (Couto et al., 2005) (Figure 1.4B). Thus, we conclude that ab6A expresses Or13a, correcting previous suggestions that Or13a might be expressed in intermediate sensilla (Couto et al., 2005). Taken together, we used a comparison between physiological recordings and the consensus database to find a match between receptor cells and receptor proteins and confirmed this by neuroanatomical analysis. A similar procedure might also be useful for interspecific studies, finding functionally homologous receptors across species.

Estimating unknown receptor responses

As shown above, even with this comprehensive meta-analysis, our current knowledge of the *D. melanogaster* olfactome is quite incomplete. Thus, the database might lead to targeted studies toward a more complete olfactome. However, in several instances, it would be useful to have an estimate for an odor response even if none has been measured yet. Could the DoOR database be used for this purpose? We used local least squares imputation (Kim et al.,

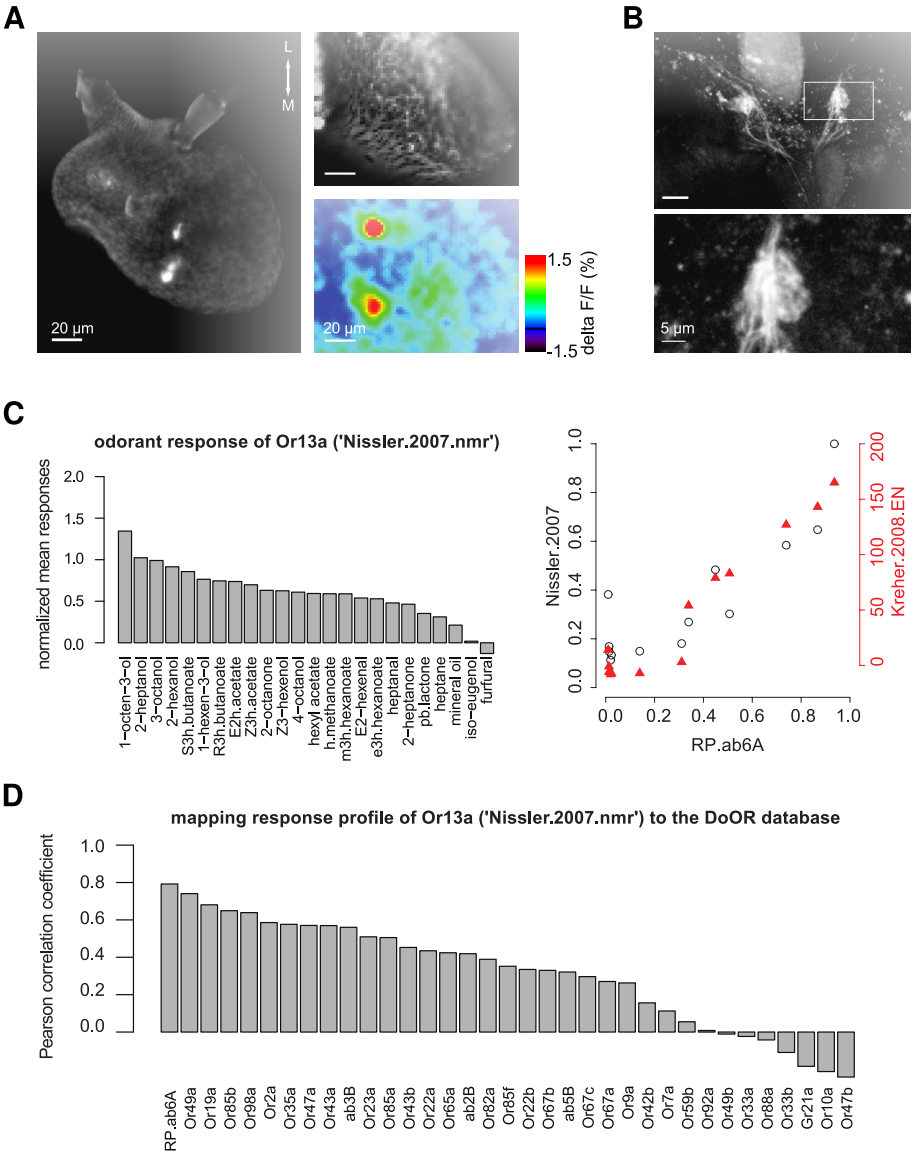

FIGURE 1.4: Mapping response profiles to ORs. **A** Left panel: Confocal picture of the antenna of Or13a:GAL4;UAS:G-CaMP shows expression in a small number of olfactory sensilla. The location corresponds to that published for ab6A sensilla. Right upper panel: Anatomical picture of the antenna as seen in wide-field microscopy for calcium imaging. Right lower panel: False color coded spatial response pattern to 3-octanol shows focalized responses. **B** Confocal picture of the antennal lobes of a Or13a:GAL4;UAS:G-CaMP fly shows fluorescence in one glomerulus for each antennal lobe (arrows), indicating that this GAL4 line targets a single receptor neuron population. The lower panel shows a magnification of the boxed area in the upper panel. ES, esophagus; D, dorsal; V, ventral. **C** Left: 24 selected odors that evoked calcium responses. S3h.butanoate, (S)-(+)-3-hydroxybutanoate; R3h.butanoate, (R)-(-)-3-hydroxybutanoate; E2h.acetate, E2-hexenyl acetate; Z3h.acetate, Z3-hexenyl acetate; h.methanoate, hexyl methanoate; m3h.hexanoate, methyl 3-hydroxyhexanoate; e3h.hexanoate, ethyl 3-hydroxyhexanoate; pb.lactone, gamma-propyl-gamma-butyrolactone; right: plotting the data measured knowing the receptor gene by calcium imaging (left ordinate) and electrophysiological recording (right ordinate) against the response data measured from ab6A (abscissa). **D** Pearson's correlation of the response profile over 111 odors measured by calcium imaging in Or13a:GAL4;UAS:G-CaMP flies to each known model response of antennal receptors. The best match was found with RP.ab6A.

2005), which is a method for estimating missing values in a matrix (Supplementary Figure S4). As an example, Supplementary Figure S5A shows estimated responses in red. However, validating this approach using the leave-one-out technique, we found that this imputation technique is only reliable for a subset of odor responses (Supplementary Figure S5B and C; Wilcoxon test, $P = 0.5616$). Future studies will need to develop more appropriate algorithms for response estimation, possibly including external information such as chemical odor similarity.

Relating olfactory space with other data

The *D. melanogaster* olfactome as it will be available with increasingly complete versions of the DoOR database can be used to answer several important questions in olfactory coding. As a teaser, we mention 4.

1. Odor response properties can be mapped onto chemical space (Schmuker and Schneider, 2007). In this approach, large data sets of chemical descriptors are used for characterizing chemicals, and multivariate statistics is used to extract those chemical descriptors that have the highest predictive values for odor responses of individual receptors or receptor families. This approach yields two very important results: first, it can be used to predict better ligands and/or unknown ligands for particular receptors (see above). Second, knowing which chemical properties best predict a receptor odor response profile can be used to understand mechanisms of ligand receptor interactions.

2. Bioinformatic analysis of OR sequences. Mathematically, we have a similar approach as before, in which two related but distinct multidimensional spaces are compared and analyzed with respect to which parameters/factors are most predictive for the interaction of the two spaces. Specifically, such a comparison might yield which sequence positions of the genes are correlated with odor response properties and which are not, thus generating hypotheses for odor-binding sites. Similar approaches have been taken for individual receptors, for example, the mouse MOR42 subfamily and could be tested experimentally (Abaffy et al., 2007).

3. Odor response properties can be mapped onto the behavioral meaning of odors: repellent or attractive odors (Semmelhack and Wang, 2009) or pheromones and non-pheromones. Using the spatial representation of odor response patterns in the antennal lobe that can be generated from the DoOR package, it is possible to answer questions as whether behaviorally relevant odor responses are clustered and/or concentrated

in particular antennal lobe areas or whether they are distributed and compare these results with experimental data.

4. The logic of spatial arrangement of odor response properties in the antennal lobe can be analyzed. Supplementary Figure S3a shows an odor response similarity matrix for all glomeruli in the antennal lobe: some glomeruli have very similar odor response profiles (shown with dark red squares) and others are anticorrelated (blue). Is there a relationship between the spatial distance of glomeruli in the antennal lobe (Laissue et al., 1999) and their physiological similarity? We found the relationship to be significant, with a tendency of similar glomeruli to be closer neighbors (Supplementary Figure S3B), except when only cases with small odor counts (6:31) are considered. However, the slope of this relationship is small, accounting for 0.28 correlation value difference across the entire antennal lobe. We conclude that functional odor response properties have only a limited influence on the spatial location of glomeruli in the *D. melanogaster* antennal lobe, a conclusion that has significant implications for models of interglomerular computations in the antennal lobe (Galizia and Menzel, 2001).

1.4 Discussion

The use of a functional atlas

Here, we create a functional atlas of odor responses for olfactory receptors, receptor cells, and olfactory glomeruli of the fruit fly *D. melanogaster*. This functional atlas represents a consensus data set combining all available data. It will serve as a reference work for olfactory physiologists, but it also represents a new approach of how to map different data sets onto each other. The only strict assumption made is that of a monotonic odor response function.

Most odors elicit a combinatorial pattern of activity across olfactory receptors, resulting in a stereotypical combinatorial pattern of activated glomeruli in the primary olfactory center (the mammalian bulb or the insect antennal lobe) (Galizia and Menzel, 2001). In such a combinatorial system, the effect of removing individual receptors is difficult to predict. For example, silencing Or22a in *D. melanogaster* did not lead to a behavioral deficit in the response to any of the better ligands of this receptor, but it did create a deficit in response to a weak ligand (Keller and Vosshall, 2007). This example shows that it is not sufficient to know the response of a single receptor class. Hence, the goal of this functional atlas is to generate the full olfactome of a species, in this case *D. melanogaster*. The data currently available do not yet include all receptors (see

Supplementary Table S1), but the framework is open to new additions and will grow as more data will be collected by different laboratories.

Based on the complete olfactome, it will be possible to understand and to model the combinatorial nature of olfactory coding. In particular, the biological "olfactory space" can be derived from the data, that is, a description of how similar and dissimilar different odors are at the level of primary receptor input. At a later stage, when a similar database will be created for other species, it will be possible to compare these olfactory spaces for different species and thus to understand for what odors individual species have evolved higher resolution either in terms of discrimination capacity or in terms of sensitivity.

The need of new mathematical tools

In principle, two approaches can be taken to create a complete functional atlas. In one approach, a mass screen using a dedicated technique would be used to create a homogeneous data set that results in a functional atlas. For example, in the visual system, the spectral response properties of photoreceptors can be mapped in great detail by electrophysiological recordings and once done the description is complete. Although attractive, this approach is not feasible in the olfactory system where the number of receptors is high in all species (*D. melanogaster* being among the most tractable) and the number of odors is infinite: every single study will always grasp but a partial view of the olfactome. Therefore, it is necessary to take the second approach, that is, to merge different data sets. Because these data sets differ in many respects, new mathematical tools are necessary. We have created a framework which allows for merging data sets of any kind as long as a single assumption is fulfilled: that the relationship be monotonic, that is, that better ligands in one study are expected to be better ligands in all studies (give or take variability).

This approach might also be useful in other studies where heterogeneous data sets need to be merged into metadatabases. Our entire package is open source. Without any change in the code, it can be adapted to the olfactory systems of other species: the only thing to do is to feed the data into a spreadsheet, create a graphical template for the antennal lobe output (if necessary), and a consensus database can be created. Thus, as soon as sufficient data will be available, the same platform will be usable to create olfactomes for other species, for example, mice or humans. With appropriate changes, the software could also be used for non-olfactory systems.

Although conceptionally and practically attractive, a database that is constantly evolving and including new data also creates problems: computational studies, for example, need to access standardized data sets because a change

in the data set creates a situation where different results cannot be attributed unambiguously to a different model any more. Therefore, we will make older versions available indefinitely: the “DoOR 1.0” or “DoOR 2.0” will represent different stages in the publicly available data, such that computational studies will be able to consistently use a single reference olfactome, allowing for creating statistical or computational benchmarks.

Limitations of the database

From a biological-physiological point of view, the data set presented here has three major drawbacks: it lacks information about 1) odor concentration, 2) complex stimuli, and 3) temporal response profiles. First, at the current stage, no information about responses to odor concentrations is included. This is a serious drawback because odor concentration is a fundamental parameter in olfaction. Some studies have measured odor responses across concentrations for all odors tested: in these cases, receptor responses can be coded as odor dilution that elicits half-maximal response strength (Pelz et al., 2006). In other studies, dose response curves were only measured for a subset of odors or not measured at all. For ligands with high affinity, this can create distortions in the database: for example, ethyl hexanoate and methyl hexanoate are currently the best-known ligands for Or22a (Pelz et al., 2006). At high concentrations, however, the responses to these substances decrease due to fast receptor adaptation. Thus, in some studies that did not include dose response curves but tested many odors at high concentrations, these odors erroneously appear to be good, but not exceptional ligands. Some receptors have complex dose response curves for particular odors, further complicating the concentration aspect. Currently, there are not enough published data sets to include odor concentration into the database, but with an increasing number of studies, this will be possible. Including odor concentration as a parameter into the database will add one difficulty: measuring absolute odor concentration of a stimulus at the receptor cell in an experimental situation is not trivial. Thus, a concentration of 1:100 in one laboratory may not correspond to a concentration of 1:100 in another laboratory. Relative concentrations are less problematic: the relationship of 1:100 to 1:1000 will be 1:10 in all laboratories. Additional mathematical tools will be necessary to allow for automatic dose response curve shifts for data from different laboratories.

Second, complex stimuli are not covered in the database. These include odor mixtures but also other properties. For example, in a dynamical situation where odors are given as turbulent plumes, responses to some odors can be quite different as compared with the response to the same odor as a single

odor pulse (Schuckel et al., 2009). A related aspect needs to be considered for negative responses: many receptors respond to some odors with an activity decrease measured as a drop in firing rate or a decrease in intracellular calcium. However, some receptors have almost no spontaneous activity but might show inhibitory responses if activated beforehand. Here, an odor response is no longer a simple stimulus response property but rather dependent on previous activation. Such complexities cannot be covered in a functional atlas that is, in essence, a lookup table of simplified odor responses. However, these complexities are certainly important for the olfactory system and need to be considered in our quest to understand olfactory coding at large by generating dedicated physiological data sets.

Third, this functional data set maps odors to single values, disregarding the fact that odor responses are temporally structured at the level of olfactory receptors already. Response onsets to an odor have different time lags in different receptors, a property that could be included into the database as more data become available. Including more temporal information (e.g., phasic, phasic–tonic, tonic, or complex response patterns) will require additional tools. Temporal properties are more dependent on recording techniques than response magnitude: calcium imaging, intracellular recordings, or sensilla recordings might all reveal different aspects of the temporal complexity in a receptor neuron. Thus, including temporal information at the current stage would reduce the available data too much to make a consensus database useful.

Taken together, we present an open access software to assemble the complete olfactome of a species – here *D. melanogaster*. We hope that this service to the community will be of use for many further studies into olfaction of this and other species, and we will update the database as new odor response profiles become available.

Acknowledgements

We thank David Samuelson for creating the 3D visualizations on the webpage and Konrad Polthier (TU Berlin) for technical support in adapting VRML import in JavaView. Thanks to Birgit Rapp and Gabriele Pszolla for physiological recordings.

Chapter Two

Response profiles for eight olfactory receptor neurons

Abstract

The olfactory system of *Drosophila melanogaster* consist of only ~ 50 types of olfactory receptor neurons. For some of these receptor neurons detailed response profiles are available, others are less well investigated or completely uncharacterized. In order to get a complete view on the olfactory code of *Drosophila* it is necessary to characterize receptor neuron profiles in great detail. Here we describe the response profiles of eight classes of receptor neurons. Using calcium imaging on the fruit fly's antenna we recorded responses elicited by a set of ~ 100 odorants of different chemical classes. For these eight receptor neurons we found different tuning-widths, ranging from broadly tuned generalists responding to many odorants to narrowly tuned receptor neurons tuned responding only to a few odorants. The response profile of the receptor Or69a was uncharacterized before, for the other receptor neurons we add responses of many new odorant–receptor combinations to the *Drosophila* olfactome.

2.1 Introduction

The world around us is an olfactory world that consists of myriads of different volatile molecules – odors. May it be danger or attraction, a foe to avoid or a possible mating partner to approach, these odors convey essential information for all animals. Olfactory systems of different complexity have evolved to reliably detect the relevant stimuli within the olfactory environment. Across species, from invertebrates to vertebrates, many of these systems share a common structural principle: Several classes of olfactory receptor neurons (ORNs) housed for example on an insects antenna or in a mammals nose, serve as differentially tuned input channels (Hildebrand and Shepherd, 1997). ORNs convey the sensory input to a first processing area of the brain, e.g. the insect antennal lobe or the olfactory bulb of vertebrates, from where it is then send to higher brain areas. The differential tuning of ORNs arises from the

expression of one or a few specific chemoreceptors, creating an ORN's individual response profile (Hallem et al., 2004). As most of these different response profiles overlap, stimulation with a ligand will elicit an odor-specific ensemble response consisting of all the activated and non-activated ORNs of the olfactory system (Friedrich and Korsching, 1997; Malnic et al., 1999; Hallem and Carlson, 2006).

With this principle of ensemble coding, even species with simple olfactory systems like *Drosophila* with its around 50 classes of ORNs are able to distinguish a manifold of odorants (Couto et al., 2005; Fishilevich and Vosshall, 2005; Hallem and Carlson, 2006; Galizia et al., 2010). The more complex olfactory systems consist of e.g. $\sim$1000 ORNs in mice, up to $\sim$600 in ants, $\sim$400 in humans or $\sim$160 ORNs in honeybees (Niimura and Nei, 2007; Kelber et al., 2009; Galizia et al., 1999).

In order to understand the complex ensemble code of olfactory systems it is desirable to know all the possible activation patterns that ligands might elicit from such a system, the so called olfactome. Because of its low number of ORNs, the olfactory system of *Drosophila melanogaster* is particularly well suited to reach near to a complete olfactome.

Another big advantage of *Drosophila* is that some information about the olfactome is already existing. Different labs all over the world are working on *Drosophila* olfaction and recorded response profiles for many ORNs with varying sets of odorants. In order to pool all available odor response data we created the DoOR database (Galizia et al., 2010; `http://neuro.uni.kn/door`; Chapter 1). DoOR integrates the heterogeneous response data that was recorded using different techniques and in different labs into one single consensus response data set, providing a view on the up-to-date known olfactome and a useful tool for olfactory research. Looking at the existing *Drosophila* olfactome reveals its gaps, with some ORNs being tested with only a few odorants, and others not being characterized at all.

Here we present data for eight ORNs, four that add up to existing profiles, one response profile for an ORN that to our knowledge had not been characterized before, and three that we published together with the DoOR database but did not present in detail.

2.2 Material & Methods

Animals

All recordings were performed on female *Drosophila melanogaster* expressing the calcium reporter G-CaMP 1.3 (Nakai et al., 2001) or G-CaMP 3 (Tian et al.,

2009) in specific sets of olfactory receptor neurons under the control of the GAL4-UAS expression system. UAS-G-CaMP 1.3 flies were provided by Jing Wang, University of California, San Diego, La Jolla, CA; UAS-GCaMP 3.0 flies were provided by Loren L. Looger, Howard Hughes Medical Institute, Janelia Farm Research Campus, Ashburn, Virginia. Stable GAL4-UAS fly lines were of the following genotypes: P[UAS:GCaMP1.3]; P[GAL4:X] (X being one of Or10a, Or13a, Or42b, Or47b, Or67b, Or69a or Or92a), and w;P[Or56a:GAL4]; P[UAS:GCaMP3]attP40. Experiments with Or56a were conducted using three different GAL4 driver-lines, all obtained from the Bloomington Stock Center (Department of Biology, Indiana University, Bloomington, USA), general recordings were performed with Bloomington stock #23896, control experiments were performed with stocks #9987 and #9988.

Flies were kept at $25\,^{\circ}$C in a 12/12 light/dark cycle. Animals were reared on standard medium (100 mL contain: 2.2 g yeast, 11.8 g of sugar beet syrup, 0.9 g of agar, 5.5 g of cornmeal, 1 g of coarse cornmeal and 0.5 mL of propionic acid).

Odorant preparation

Odorants were purchased from Sigma-Aldrich in the highest purity available. Pure substances were diluted in 5 mL mineral oil (Sigma-Aldrich, Steinheim, Germany). All odorants were applied at 10^{-2} dilution except geosmin which was applied at 10^{-4}. For dose-response curves pure odorants were diluted in mineral oil in decadic steps from 10^{-2} to 10^{-8}. Odorants were prepared in 20 mL headspace vials sealed with a Teflon septum (Axel Semrau, Germany). Information and abbreviations for all odorants used are given in Table S4.

Stimulus application

A computer-controlled autosampler (PAL, CTC Switzerland) was used for automatic odor application. A headspace of 2 mL was injected in two 1 mL portions at time points 6 s and 9 s with an injection speed of $1\,\mathrm{mL\,s^{-1}}$ into a continuous flow of purified air flowing at $60\,\mathrm{mL\,min^{-1}}$. The stimulus was directed to the antenna of the animal *via* a Teflon tube (inner diameter 2 mm, and length 39.5 cm).

Four to eight odorants were presented in a row (one block) interspaced by solvent control, room air control and an OR specific reference odorant. After each injection the autosampler syringe was flushed with purified air for 30 s. After each block of stimuli, the syringe was washed with hexane or pentane (Merck, Darmstadt, Germany), heated up to $48\,^{\circ}$C, and rinsed with continuous clean air for 6 min.

We were able to increase stimulus precision in the newer data sets (Or10a, Or47b, Or56a, Or69a) by using a different injection protocol in the Cycle Composer software controlling the PAL system. At the same time the injection protocol changed from a three step protocol (1: needle penetrates injector; 2: injection of first pulse; 3: injection of second pulse) to a two step protocol (1: needle penetrates injector and injection of the first pulse in a single step; 2: injection of the second stimulus pulse). In the three step protocol (used for Or13a, Or42b, Or67b, Or92a) the needle penetrated the injector $\sim 2\,\mathrm{s}$ before injection of the first pulse. The mere penetration of the syringe into the continues airflow was sufficient for some potent ligand–ORN combinations to produce strong responses (see phenethyl alcohol in Figure 2.7).

Calcium imaging

Calcium imaging was performed on two setups which consisted of a fluorescence microscope (BX50WI or BX51WI, Olympus, Tokyo, Japan) equipped with a $50\times$ air lens (Olympus LM Plan FI $50\times/0.5$). A CCD camera (TILL Imago, TILL Photonics, Gräfelfing, Germany or SensiCam, PCO, Kelheim, Germany) was mounted on the microscope recording with 8×8 pixel on-chip binning, which resulted in 80×60 pixel sized images. For each stimulus recordings of $20\,\mathrm{s}$ at a rate of $4\,\mathrm{Hz}$ were performed using TILLvisION (TILL Photonics, Gräfelfing, Germany). A monochromator (Polychrome II or Polychrome V, TILL Photonics, Gräfelfing, Germany) produced excitation light of $470\,\mathrm{nm}$ wavelength which was directed onto the antenna *via* a $500\,\mathrm{nm}$ low-pass filter and a $495\,\mathrm{nm}$ dichroic mirror, emission light was filtered through a $505\,\mathrm{nm}$ high-pass emission filter.

Data analysis

Data analysis was performed using custom written routines in IDL (ITT VIS, USA) and R (R Development Core Team, 2013).

As long as animals showed stable responses to the reference odor measurements were included into the analysis. Recorded movies were manually corrected for movement artifacts, and an area of interest was defined for the parts of the antenna that showed fluorescence increase upon stimulation. All calculations were done within that area.

Relative fluorescence change was calculated as $\Delta F/F = ((F_i - F_0)/F_0) \times 100$ with F_i being the fluorescence at $frame_i$ and F_0 being the mean fluorescence of the first 10 frames of a recording.

The data was manually corrected for movement and an area of interest was defined on a false color coded image of the reference odor measurement, all

calculations were done within that area. Response traces of the average pixel value within the area were exported.

To correct for the photo-bleaching of the dye, an exponential decay function of the form $A * exp^{-x/B} + C$ was fitted to the data using the `nls()` function in R. Because some odorant responses would not reach baseline within measurement time, the fit parameter B was estimated by an initial fit on the median mineral oil control response within each animal. For fitting three frames at the beginning of the time-trace and 44 frames during stimulus presentation were omitted and the pre-stimulus part of the recording was weighted 100 fold.

Response values were calculated as the mean response during 5 s after stimulus onset (corrected for setup specific stimulus onset delays) subtracted by the mean response during the first 2.5 s of a recording.

As ORN responses decrease over time a linear regression was fitted on each reference odor measurement within each individual animal. The value of this function at each corresponding timepoint was set to the value of the first reference odor presentation elicited.

We quantified the tuning widths of individual ORNs by calculating the lifetime kurtosis (LTK) as follows:

$$LTK = \left\{ \frac{1}{M} \sum_{i=1}^{M} \left[\frac{r_i - \overline{r}}{\sigma_r} \right]^4 \right\} - 3$$

with M being the number of stimuli tested, r the response elicited and $\overline{r}$ and σ_r the mean and the standard deviation of the responses (Willmore and Tolhurst, 2001; Silbering et al., 2011).

Plotting was performed using the R core functions and the `ggplot2` package (Wickham, 2009).

2.3 Results

We recorded odorant dependent calcium-changes in olfactory receptor neurons (ORN) of *Drosophila melanogaster*. Using the GAL4-UAS system we expressed the calcium sensitive dies G-CaMP 1.3 (Nakai et al., 2001) or G-CaMP 3.0 (Tian et al., 2009) in single ORN classes and were able to perform imaging directly through the cuticle of the intact antenna.

Or10a – a receptor tuned to aromatics and esters

Or10a is expressed in ab1D neurons which project to the DL1 glomerulus (Couto et al., 2005; Fishilevich and Vosshall, 2005; Table S1). These neurons also express the gustatory receptor Gr10a (Fishilevich and Vosshall, 2005). Or10a showed strong activation when stimulated with aromatics. Some acids

and esters also elicited clear responses (Figures 2.2 and 2.1). Especially the responses to some aromatics (methyl salicylate, ethyl benzoate, benzonitrile and benzyl alcohol) and one acid (butyric acid) were long lasting and did not reach baseline within recording time (right panel in Figure 2.2). From the acids, butyric acid led to the strongest activation while longer or shorter acids produced weaker activity or induced to inhibition (e.g. acetic acid, Figure 2.1). Or10a responded to aldehydes in a graded manner with the responses increasing with molecular weight.

Integration of our data expanded the the DoOR database by 55 odor responses (Figure 2.2). The best ligands of Or10a in DoOR matched the best ligands from our data set (methyl salicylate and ethyl benzoate). Propanal, acetic acid and 2,3-butanedione produced stronger inhibitions as compared to the DoOR data. Among others propanoic acid, butyric acid and benzyl alcohol produced clear activations in our data whereas only weak excitations or inhibitions were listed in DoOR.

Alcohols and esters activate Or13a

Or13a is expressed in ab6A neurons which send their axons to glomerulus DC2 (Couto et al., 2005; Fishilevich and Vosshall, 2005; Table S1). Or13a was specifically tuned to esters (e.g. ethyl (S)-(+)-3-hydroxybutanoate, Z3-hexenyl acetate, E2-hexenyl acetate) and alcohols (e.g. 2-hexanol, 1-hexen-3-ol, 3-octanol) and did show any strong responses to ligands of other chemical classes in our set (Figures 2.1 and 2.3). Or13a signals were very weak in general, reaching only around $1\,\%$ change in mean fluorescence during stimulation.

The Or13a data set was integrated into DoOR previously (see Galizia et al. (2010)). It expanded responses in DoOR from 57 to 135 and added four good ligands (Figure 2.3). While alcohols were known to be good ligands before, our set also added many esters. Responses to 1-butanol, 3-methyl-butanol and propanoic acid produced excitation of Or13a bearing neurons in our data whereas slight inhibitions were reported from DoOR.

Or42b – activated by esters and ketones.

Or42b is expressed in ab1A neurons that innervate glomerulus DM1 (Couto et al., 2005; Fishilevich and Vosshall, 2005; Table S1). Most responses we measured for Or42b were weak inhibitions. The few ligands that evoked clear excitatory responses belonged to ketones (3-hexanone and 3-penten-2-one), esters (ethyl (S)-(+)-3-hydroxybutanoate and ethyl propionate) and alcohols (2-hexanol; Figures 2.1 and 2.4). Interestingly, ethyl (R)-(-)-3-hydroxybutanoate

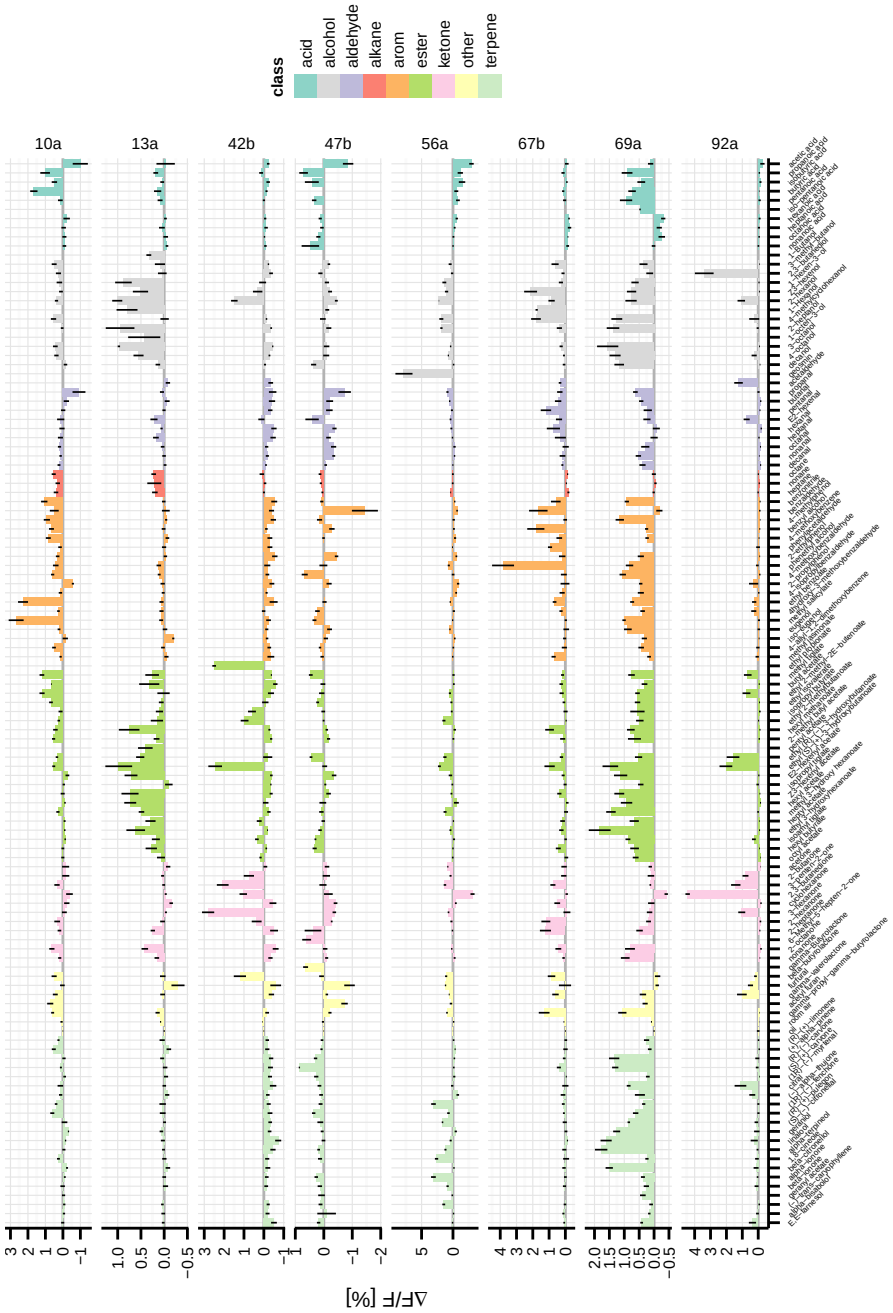

FIGURE 2.1: Response profiles of eight ORNs. Odorants were grouped by chemical class and sorted by molecular weight. Bars show mean fluorescence changes during stimulation (see Material & Methods for exact calculation), error-bars indicate SEM. Colors indicate chemical classes.

FIGURE 2.2: Response profile of Or10a. First panel: Our data set, bars show mean fluorescence changes during stimulation (see Material & Methods for exact calculation), error-bars indicate SEM (n = 4–11, higher for references). Second and third panel: Bars give response values from the DoOR database. Second panel shows data before, third panel after integrating our data into DoOR. All bars are ordered according to the updated DoOR response values. Colors of bars indicate the chemical class. Fourth panel: Mean color-coded response traces over the 20 s recordings. *Gray* lines indicate stimulus pulses. The two pulses of stimulation lasted for 1 s each. *Red* indicates fluorescence increase, *blue* fluorescence decrease respectively. Dark odorant names indicate odor–receptor pairs that were not existing in DoOR before. Solvent control (oil) was set to zero for all plots.

FIGURE 2.3: Response profile of Or13a. First panel: Our data set, bars show mean fluorescence changes during stimulation (see Material & Methods for exact calculation), error-bars indicate SEM (n = 3–10, higher for references). Second and third panel: Bars give response values from the DoOR database. Second panel shows data before, third panel after integrating our data into DoOR. All bars are ordered according to the updated DoOR response values. Colors of bars indicate the chemical class. Fourth panel: Mean color-coded response traces over the 20 s recordings. *Gray* lines indicate stimulus pulses. The two pulses of stimulation lasted for 1 s each. *Red* indicates fluorescence increase, *blue* fluorescence decrease respectively. Dark odorant names indicate odor–receptor pairs that were not existing in DoOR before. Solvent control (oil) was set to zero for all plots.

produced weak inhibitions whereas its stereo-isomer ethyl (S)-(+)-3-hydroxybutanoate was one of the best ligands.

Our data added a total of 76 new odorants to DoOR (Figure 2.4). Four odorants produced inhibitions in our data whereas excitation (E2-hexenyl acetate) or almost no response (3-octanol, cyclohexanone and 2-heptanone) was listed in DoOR.

No strong responses for Or47b

Or47b was the only receptor in our set that is expressed in ORNs housed in trichoid sensilla. at4 neurons expressing Or47b project to the VA1lm glomerulus (Couto et al., 2005; Fishilevich and Vosshall, 2005; Table S1). We found the best activation for (S)-(+)-carvone, propanoic acid and 4-methoxybenzaldehyde. The strongest inhibitions we found for benzaldehyde, acetic acid and furfural (see Figures 2.1 and 2.5). Overall there was no very strong activation of Or47b by any of the ligands in our set.

Our set expanded the Or47b profile in DoOR by 61 new odorants adding (S)-(+)-carvone and 4-methoxybenzaldehyde as new best ligands (Figure 2.5). Some odorants we recorded as being excitatory were listed as inhibitory in DoOR, especially propanoic acid elicited clear excitatory responses in our recordings.

Or56a – a response profile beyond geosmin

Or56a is expressed in ab4B neurons together with the co-expressed Or33a (Couto et al., 2005; Fishilevich and Vosshall, 2005; Table S1). ab4B neurons target glomerulus DA2 but occasionally show innervations of an additional area in the vicinity to the DL4 glomerulus (Fishilevich and Vosshall (2005)). ab4B neurons were recorded previously by de Bruyne et al. (2001) who did not find any responses to their set of odorants using single-sensillum recordings. Recently Stensmyr et al. (2012) reported ab4B to respond to geosmin solely.

We found odor induced activity in Or56a bearing neurons on the antenna of *Drosophila melanogaster*. These responses included excitation as well as inhibition, we could confirm geosmin as best ligand for Or56a (Figures 2.1 and 2.6). Geosmin elicited strong, long lasting activations while tested at 100 times lower concentrations (10^{-4} dilution) as compared to the other odorants. The best excitatory ligands for Or56a, despite geosmin, were terpenes like alpha-ionone, (1R)-(-)-fenchone, 1,8-cineole, (-)-trans-caryophyllene and (S)-(-)-citronellal as well as some alcohols like 2-hexanol, 4-methylcyclohexanol and 2-heptanol and the ester ethyl (S)-(+)-3-hydroxybutanoate. We found inhibitory responses elicited by most acids in the set (e.g. acetic acid, isobu-

FIGURE 2.4: Response profile of Or42b. First panel: Our data set, bars show mean fluorescence changes during stimulation (see Material & Methods for exact calculation), error-bars indicate SEM (n = 3–9, higher for references). Second and third panel: Bars give response values from the DoOR database. Second panel shows data before, third panel after integrating our data into DoOR. All bars are ordered according to the updated DoOR response values. Colors of bars indicate the chemical class. Fourth panel: Mean color-coded response traces over the 20 s recordings. *Gray* lines indicate stimulus pulses. The two pulses of stimulation lasted for 1 s each. *Red* indicates fluorescence increase, *blue* fluorescence decrease respectively. Dark odorant names indicate odor–receptor pairs that were not existing in DoOR before. Solvent control (oil) was set to zero for all plots.

FIGURE 2.5: Response profile of Or47b. First panel: Our data set, bars show mean fluorescence changes during stimulation (see Material & Methods for exact calculation), error-bars indicate SEM (n = 6–16, higher for references). Second and third panel: Bars give response values from the DoOR database. Second panel shows data before, third panel after integrating our data into DoOR. All bars are ordered according to the updated DoOR response values. Colors of bars indicate the chemical class. Fourth panel: Mean color-coded response traces over the 20 s recordings. *Gray* lines indicate stimulus pulses. The two pulses of stimulation lasted for 1 s each. *Red* indicates fluorescence increase, *blue* fluorescence decrease respectively. Dark odorant names indicate odor–receptor pairs that were not existing in DoOR before. Solvent control (oil) was set to zero for all plots.

tyric acid, propanoic acid, pentanoic acid and hexanoic acid). Within the acids the amount of inhibition was related to the molecular weight of the molecule, with smaller acids eliciting stronger inhibition (Figure 2.1). Inhibitions elicited by 2,3-butanedione and acetic acid were particularly strong and long lasting (Figure 2.6).

We confirmed the Or56a response profile with a subset of odorants for two other available Or56a GAL4-lines (data not shown).

Or67b – tuned to aromatics and alcohols

Or67b is expressed in ab9 neurons which send their axons to the VA3 glomerulus (Couto et al., 2005; Fishilevich and Vosshall, 2005; Table S1). The best ligands were aromatics and alcohols (phenethyl alcohol followed by Z3-hexenol, 4-methylcyclohexanol, benzyl alcohol and 1-hexanol; Figure 2.7). Alkanes and acids with six to nine carbon atoms elicited weak inhibitions. Phenethyl alcohol was a particular potent ligand for Or67b. Penetrating the stimulus air-flow with the odor syringe without injecting the odorant actively (see Material & Methods for protocol details), was sufficient to elicit a strong excitatory response.

Integration expanded the existing DoOR profile from 30 to 121 odor responses. Our set added phenethyl alcohol as new best ligand as well as a few other strong alcohols and aromatics (Z3-hexenol, 4-methylcyclohexanol, benzyl alcohol).

Esters and terpenes activate Or69a

Or69a is expressed in ab9 neurons projecting to the D glomerulus (Couto et al., 2005; Fishilevich and Vosshall, 2005; Table S1). The response spectrum we recorded exhibited a broadly tuned receptor (LTK of -0.33, see below) with some terpenes like alpha-terpineol, linalool, beta-citronellol, (R)-(-)-carvone and (S)-(+)-carvone as good ligands (Figures 2.1 and 2.8). The best ligands were ethyl 3-hydroxyhexanoate and alpha-terpineol. Acids with seven to nine carbon atoms and 2,3-butanedione produced inhibitory responses.

No data for this receptor was existing in DoOR before.

Or92a – narrowly tuned to 2,3-butanedione and 2,3-butanediol

Or92a is expressed in ab1B neurons and targets the VA2 glomerulus (Couto et al., 2005; Fishilevich and Vosshall, 2005; Table S1). Or92a bearing neurons were narrowly tuned (LTK = 19.33), showing strong responses for 2,3-butanedione, 2,3-butanediol (Figures 2.1 and 2.9).

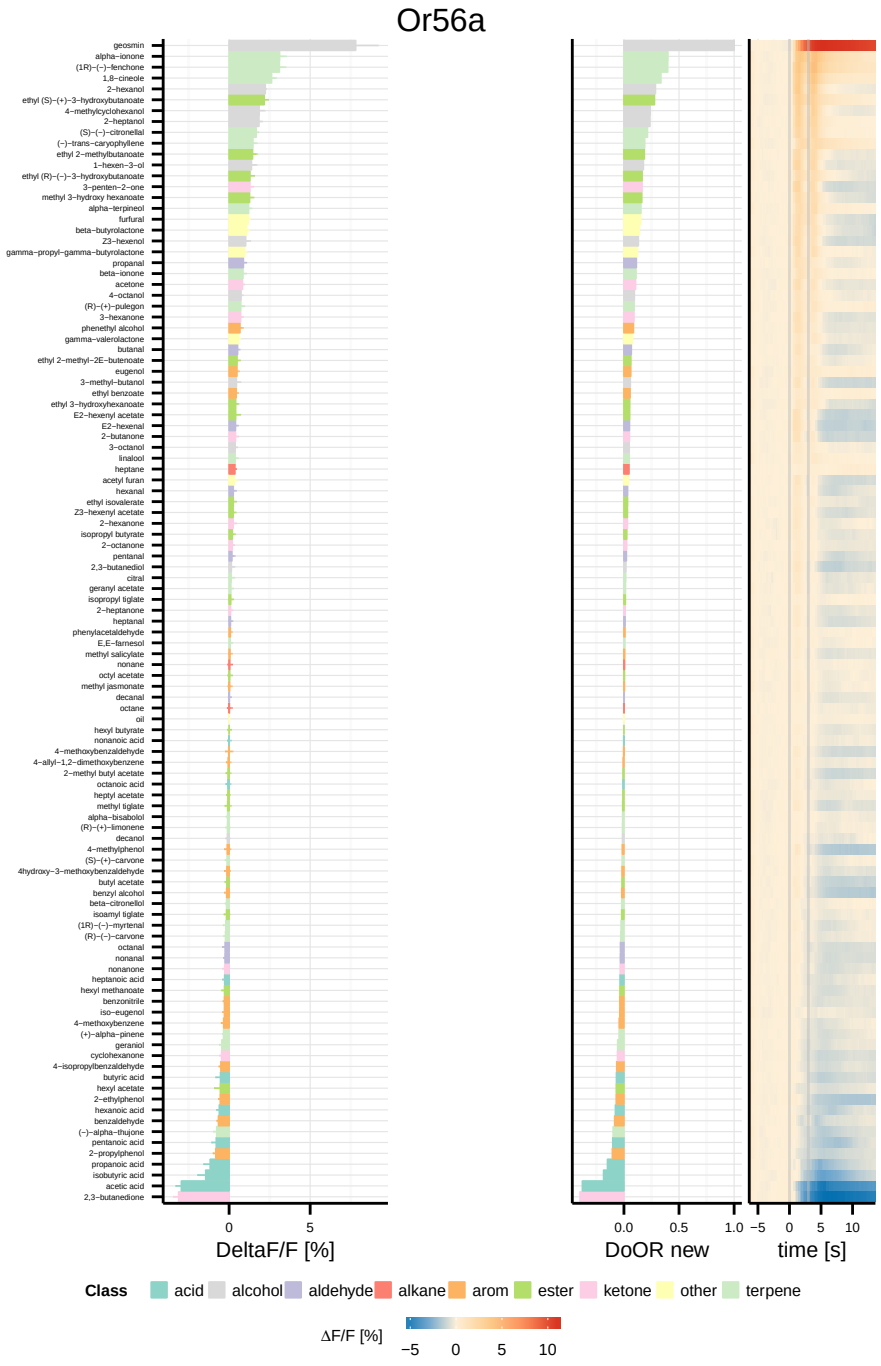

FIGURE 2.6: Response profile of Or56a. First panel: Our data set, bars show mean fluorescence changes during stimulation (see Material & Methods for exact calculation), error-bars indicate SEM (n = 7–13, higher for references). Second panel: Bars give response values after integration into the DoOR database. All bars are ordered according to the updated DoOR response values. Colors of bars indicate the chemical class. Third panel: Mean color-coded response traces over the 20 s recordings. *Gray* lines indicate stimulus pulses. The two pulses of stimulation lasted for 1 s each. *Red* indicates fluorescence increase, *blue* fluorescence decrease respectively. Dark odorant names indicate odor–receptor pairs that were not existing in DoOR before. Solvent control (oil) was set to zero for all plots.

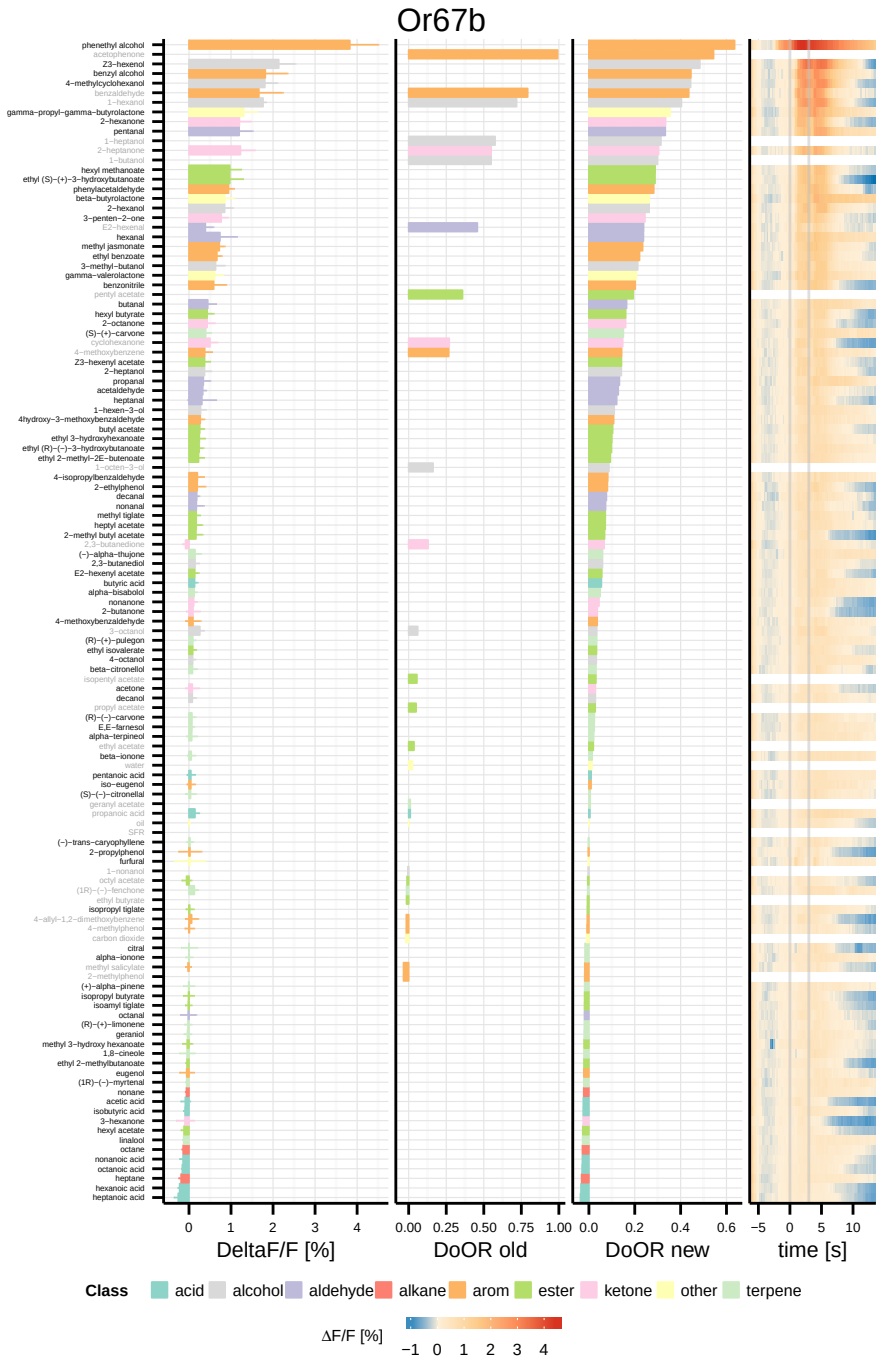

FIGURE 2.7: Response profile of Or67b. First panel: Our data set, bars show mean fluorescence changes during stimulation (see Material & Methods for exact calculation), error-bars indicate SEM (n = 4–7, higher for references). Second and third panel: Bars give response values from the DoOR database. Second panel shows data before, third panel after integrating our data into DoOR. All bars are ordered according to the updated DoOR response values. Colors of bars indicate the chemical class. Fourth panel: Mean color-coded response traces over the 20 s recordings. *Gray* lines indicate stimulus pulses. The two pulses of stimulation lasted for 1 s each. *Red* indicates fluorescence increase, *blue* fluorescence decrease respectively. Dark odorant names indicate odor–receptor pairs that were not existing in DoOR before. Solvent control (oil) was set to zero for all plots.

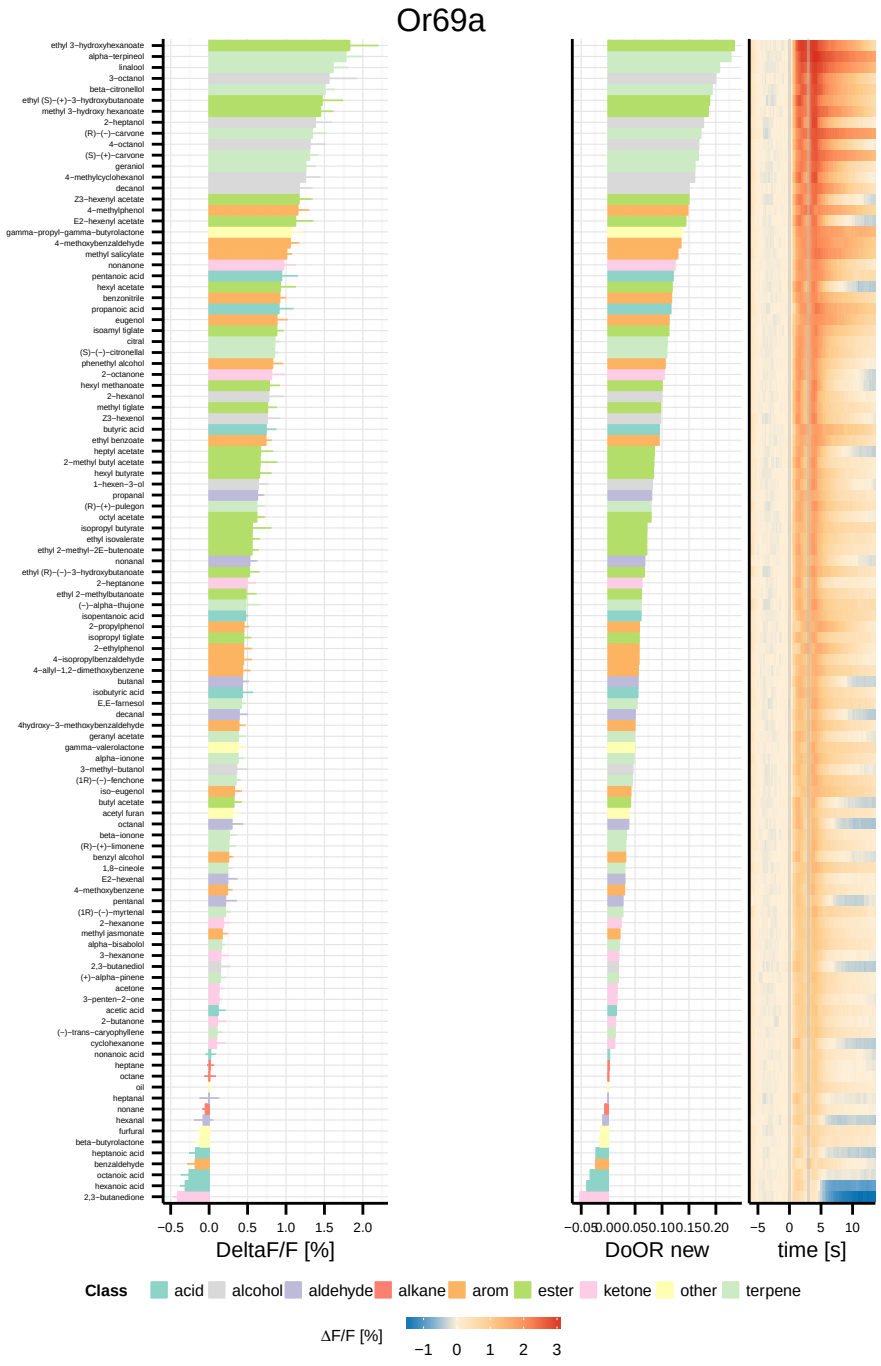

FIGURE 2.8: Response profile of Or69a. First panel: Our data set, bars show mean fluorescence changes during stimulation (see Material & Methods for exact calculation), error-bars indicate SEM (n = 5–8, higher for references). Second panel: Bars give response values after integration into the DoOR database. All bars are ordered according to the updated DoOR response values. Colors of bars indicate the chemical class. Third panel: Mean color-coded response traces over the 20 s recordings. *Gray* lines indicate stimulus pulses. The two pulses of stimulation lasted for 1 s each. *Red* indicates fluorescence increase, *blue* fluorescence decrease respectively. Dark odorant names indicate odor–receptor pairs that were not existing in DoOR before. Solvent control (oil) was set to zero for all plots.

Our data set added 81 new odor responses to DoOR. We confirmed 2,3-butanedione as best ligand and added the closely related 2,3-butanediol as strong ligand.

Receptor tuning

The set of eight ORNs already revealed a variety of tuning breadths. Or56a and Or92a were sharply tuned to only a few odorants (high LTK of 14.82 and 19.33; Willmore and Tolhurst, 2001; Silbering et al., 2011), Or69a and Or13a were the ORNs with the lowest LTK in our set (LTK of -0.33 and 1.99 respectively, Figure 2.10). The profiles of Or42b, Or47b and Or56a exhibited some clear inhibitory responses towards our set of odors with Or56a showing some particular strong inhibitory responses (Figures 2.6 and S9). The maximum response strength differed between the measured ORNs, which might have been an intrinsic property of the ORN or due to different accessibility of the neurons for calcium imaging. It might also indicate that good ligands for a particular receptor were missing in our set.

Ensemble responses

Looking at the pattern a given odorant elicited from our set of eight ORNs we saw distinct ensemble responses already with the small subset of eight ORNs analyzed here. Most odorants elicited responses across many ORNs (e.g. see 2-hexanol and 3-penten-2-one in Figures 2.11A and S10). Some odorants activated a more specific subset of ORNs. The alcohol 2,3-butanediol elicited strong responses from Or92a only while the corresponding ketone 2,3-butanedione also activated Or42b and strongly inhibited Or56a (Figure 2.11A). A differential activation of the three ORNs by 2,3-butanedione could also be observed across concentrations. The dose-response curve for 2,3-butanedione in Or42b started to rise at a 10^{-4} dilution and reached saturation with the next dilution step 10^{-3} (Figure 2.11B). Or92a started to respond at slightly lower concentrations and did not reach saturation at the highest concentration tested (10^{-2} dilution). Inhibition of Or56a towards 2,3-butanedione was only recorded from 10^{-3} dilutions on. Phenethyl alcohol strongly activated Or67b while it produced much weaker responses in Or56a and Or67b (Figure 2.11A).

Inhibitory responses

Olfactory receptor neurons can respond to odorant stimulation with excitation as well as inhibition. Although the majority of responses we recorded were of an excitatory nature, we also found some inhibitions. Many weak, but no

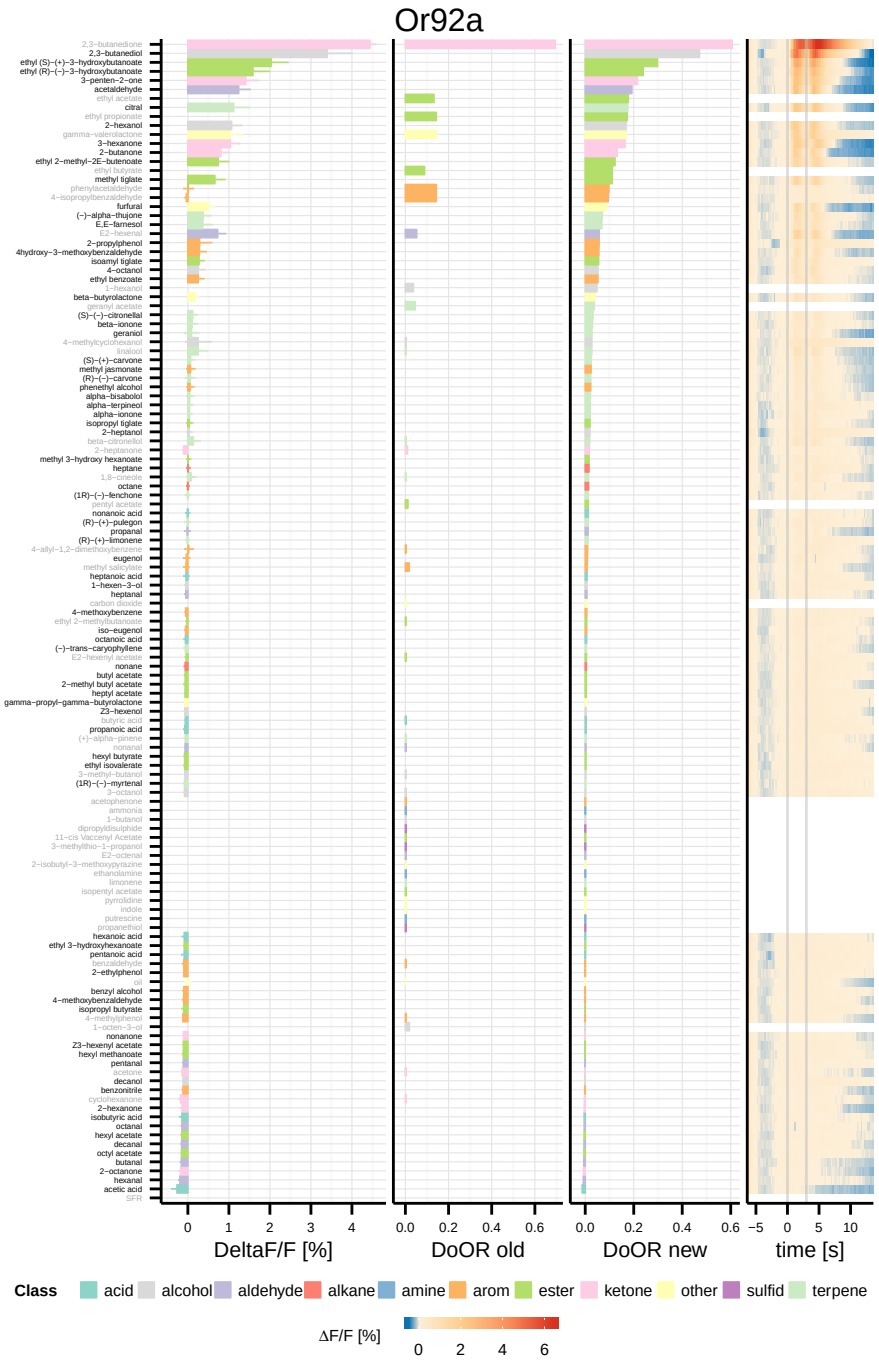

FIGURE 2.9: Response profile of Or92a. First panel: Our data set, bars show mean fluorescence changes during stimulation (see Material & Methods for exact calculation), error-bars indicate SEM (n = 4–12, higher for references). Second and third panel: Bars give response values from the DoOR database. Second panel shows data before, third panel after integrating our data into DoOR. All bars are ordered according to the updated DoOR response values. Colors of bars indicate the chemical class. Fourth panel: Mean color-coded response traces over the 20 s recordings. *Gray* lines indicate stimulus pulses. The two pulses of stimulation lasted for 1 s each. *Red* indicates fluorescence increase, *blue* fluorescence decrease respectively. Dark odorant names indicate odor–receptor pairs that were not existing in DoOR before. Solvent control (oil) was set to zero for all plots.

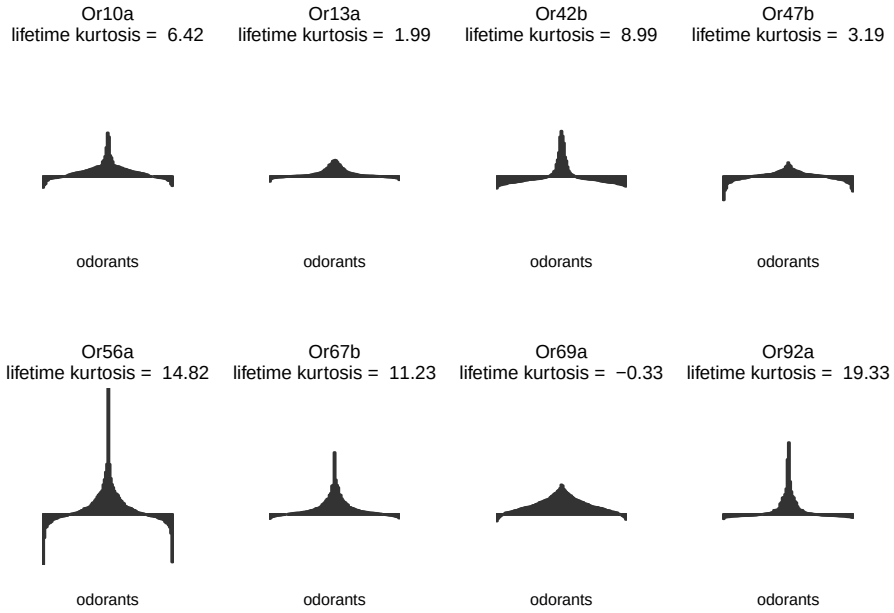

FIGURE 2.10: Tuning width plots for eight ORNs. Bars indicate mean responses towards the set of ~ 100 odorants. Lifetime kurtosis (LTK) gives a measure of tuning width, see Material & Methods for calculation. Note that geosmin in Or56a was measured at 10^{-4} dilution whereas all other odorants were used at 10^{-2}. This likely reduced the calculated LTK value.

strong inhibitions were recorded in Or42b while Or56a had only a few but very strong inhibitions (Figures 2.4 and 2.6). Acetic acid was inhibitory in most ORNs while others like 2-hexanol and 3-penten-2-one were mostly excitatory (Figure 2.11).

Inhibitions were usually found at the same recording sites as excitations. In some Or56a recordings we found two spatially separated areas. While responses in these areas could be of both polarities, fluorescence increases towards excitatory ligands were stronger in the one, fluorescence decreases upon stimulation with inhibitory ligands were stronger in the other area (Figure S9B). In no case did an odorant elicit responses of opposing polarity from both areas.

2.4 Discussion

Olfactory sensory systems consist of a set of olfactory receptor neurons that differ in their sensitivity towards volatiles defining their specific response profile. These response profiles overlap, thereby creating an ensemble-pattern of activation upon ligand stimulation. Receptor response profiles do also differ in the

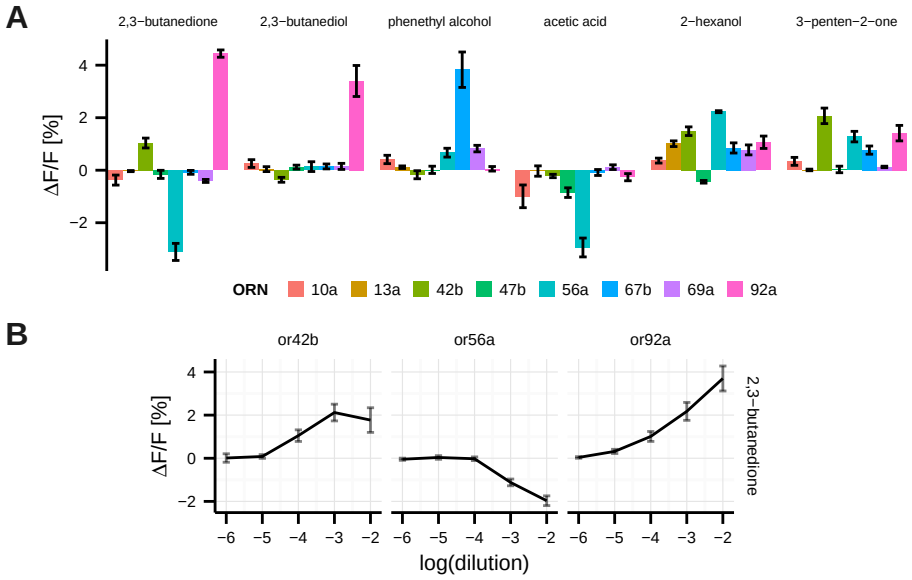

FIGURE 2.11: A Odor responses across receptors. Bars show mean fluorescence changes ($\Delta F/F$), error-bars indicate SEM, colors indicate ORN type (n = 3–289). See Figure S10 for all odorants. **B** Dose-response curve for 2,3-butanedione in three ORNs (n = 6–14).

number of ligands that they respond to, defining their tuning-width. The here presented response profiles for eight *Drosophila* ORNs already show a variety of tuning widths, with LTK values ranging from -0.33 for the very broadly tuned receptor Or69a, to 19.33 for Or92a that responds strongly to 2,3-butanedione and 2,3-butanediol only.

Or10a, Or13a, Or42b, Or67b and Or69a are rather broadly tuned, responding to many odorants in our set. Still their tuning widths vary with LTKs ranging from -0.33 to 11.23. Interestingly, except for Or69a, these receptors are to some degree tuned to given classes of chemicals, with most of their best ligands coming from two chemical classes, respectively. Or10a and Or67b are both tuned to different sets of aromatics. While Or10a is also activated by esters, Or67b also responds to alcohols. From the old DoOR data, Or13a looked like being tuned to alcohols mainly. Our data also added esters as good ligands. Responses towards the best ligands were rather low with $\sim 1\,\%$ fluorescence increase. As previous electrophysiology studies measured AP-rate changes of up to $200\,\mathrm{Hz}$ (de Bruyne et al., 2001; Kreher et al., 2008), the low fluorescence signals in our data might have originated from cells not being easily accessible visually from the top of the antenna. Or42b is mainly activated by esters and ketones. With an LTK of 8.99 its tuning-width is narrower than that of Or92a, Or13a and Or10a. A narrower tuning means a higher specialization of a receptor and this suggests its involvement in specific tasks. In line with this,

Or42b was shown to play a special role in food-odor detection. Or42b ORNs mediate food search behavior (Semmelhack and Wang, 2009) and the sensitivity of Or42b ORNs towards vinegar compounds is increased upon starvation *via* sNPF signaling (Root et al., 2011). Of the here newly described ligands for Or42b, ethyl-3-hydroxybutanoate, also known as grape-butyrate is a fermentation product produced by yeast (Kometani et al., 1993) and was reported to be present in vinegar and wine (Cha et al. 2012, racemic mixture reported). Interestingly, in our data only the S-enantiomer elicited a response from Or42b while the R-enantiomer did not (Figure 2.4).

Like Or42b, Or67b also had a rather high LTK of 11.23. There were some good ligands for the receptor in our set but phenethyl alcohol was the strongest. Or67b activation by phenethyl alcohol was so effective, that a strong and longlasting signal was induced when the odor-syringe penetrated stimulus airstream, before actually injecting the odor. Phenethyl alcohol is a fruit volatile (Stensmyr et al., 2003) which could make it a relevant odor for fruit flies *per se*. Phenethyl alcohol was shown to act antibacterial and fungostatic (Lilley and Brewer, 1953) and as such might add a positive value to a possible egglaying site. Whether phenethyl alcohol really plays a special role in *Drosophila* ecology, which the tuning of Or67b indicates, remains to be elucidated.

We presented for the first time a response profile for Or69a. It is the broadest tuned receptor in our set with the lowest LTK (-0.33). A very low LTK together with a low maximum response could also indicate that a much better ligand is yet to be found, like e.g for Or47b.

Or56a and Or92a are strongest activated by only a few ligands. Or56a ORNs are mainly tuned to geosmin (Figure 2.6; Stensmyr et al. 2012) and Or92a to 2,3-butanedione (Figure 2.9, de Bruyne et al. 2001; Dobritsa et al. 2003). Besides their best ligands, both receptors show responses to some of the other ligands, although with lower intensities. Or56a is excited by a set of terpenes and strongly and long lasting inhibited by 2,3-butanedione and acetic acid. Or92a also gets activated by the reduction product of 2,3-butanedione, 2,3-butanediol, both being fermentation products appearing in wine and vinegar (Callejón et al., 2008; Caligiani et al., 2007; Romano et al., 1998).

Or47b likely also belongs to the group of narrowly tuned ORNs. We found no strong ligand from our set of odorants which matches results from previous studies using general odors (Hallem et al., 2004; Hallem and Carlson, 2006). However, Or47b ORNs do respond to extracts of male and virgin-female *Drosophila* (van der Goes van Naters and Carlson, 2007). Or47b ORNs are suggested to be involved in pheromone detection as they are housed in trichoid sensilla, express the male specific transcription factor fru^M and target the VA1v glomerulus which is enlarged in male flies (Kondoh et al., 2003; Manoli et al.,

2005; Stockinger et al., 2005; van der Goes van Naters and Carlson, 2007). Stimulating these ORNs with the single components of fly extracts, separated by a gas-chromatograph could be a way to identify the specific Or47b ligands.

Like Or42b, Or92a is involved in the innate attractiveness of *Drosophila* towards vinegar. Or92a silencing reduces vinegar search behavior, while Or92a alone is sufficient to restore search behavior when rescued in an ORCO-mutant background (Semmelhack and Wang, 2009). As Or56a is involved in geosmin aversion (Stensmyr et al., 2012) and Or92a and Or42b are involved in innate vinegar attractiveness (Semmelhack and Wang, 2009), it is interesting to see that 2,3-butanedione activates Or42b and Or92a while it inactivates Or56a, suggesting that 2,3-butanedione is a very attractive component that might interfere with aversive olfactory channels. Like geosmin, CO_2 is also an aversive stimulus for *Drosophila*, strikingly, CO_2 sensitive ORNs get also strongly and longlasting inhibited by 2,3-butanedione (Turner and Ray, 2009).

Stensmyr et al. (2012) and de Bruyne et al. (2001) did not find Or56a responses for any odors other than geosmin. Here we present a profile that shows some clear excitations and inhibitions for other ligands, although much weaker than those for geosmin. Fluorescence changes elicited by these additional ligands were comparable to best ligands recorded in other sets. These comparably strong signals might have resulted from the much more sensitive calcium-sensor G-CaMP 3.0 that we used in Or56a ORNs, as compared to G-CaMP 1.3 in the other ORNs in this study. The very strong inhibitions we recorded for 2,3-butanedione were not visible in the single sensillum recordings of de Bruyne et al. (2001). The authors report a spontaneous firing rate for the ab4B neuron of 3 ± 1 spikes per second. Inhibitions would thus not have a prominent influence on the AP-rate of these neurons but they might play a role in mixtures or influence subsequent stimuli. We confirmed a subset of the response profile with two different Or56a-GAL4 lines.

The two areas responding with different strength to excitatory or inhibitory odorants which we found for Or56a (Figure S9) could be calcium-signals originating from two different cell compartments. It is unlikely however, that responses originated from different types of ORNs as these different areas essentially have the same odor response profiles, only with different amplitudes for inhibitory or excitatory responses respectively. As the Or56a profile was recorded using the more sensitive G-CaMP 3.0, response-strength differences between recording areas might have been observed here but not in the other lines recorded with G-CaMP 1.3.

Here we presented eight response profiles that fill gaps on the way towards the complete *Drosophila* olfactome. One ORN was uncharacterized before, for others our data extended existing profiles. However, it is important to keep on

adding ligand-receptor combinations, describing ORN-profiles in greater detail in order to expand our knowledge of the *Drosophila* olfactome. Or10a for example was initially described as a receptor activated by methyl salicylate and some structurally similar aromatics (de Bruyne et al., 2001), Or13a looked like being tuned to alcohols mainly. Further experiments revealed Or10a's responsiveness to esters and acids (Hallem et al., 2004; Hallem and Carlson, 2006; Figures 2.2 and 2.1) and our data added some esters to best known ligands of Or13a (Figure 2.3). Still many gaps remain and existing profiles will improve with every data set added.

Chapter Three

Complex dynamics of olfactory receptor neuron responses

Abstract

Olfactory receptor neuron responses vary depending on odor-stimulus identity and concentration. Not only do they vary in activation strength but also in their temporal dynamics. A receptor neuron might be activated by one odor but inhibited by the next, one odor might induce a transient response while the response to another odor might last beyond stimulus offset. Response dynamics are diverse and convey information about odor identity. We analyzed the dynamics of more than 800 responses recorded from eight classes of *Drosophila* olfactory receptor neurons. We performed calcium imaging on the antenna of fruit flies and used a double pulse stimulation protocol to access temporal response features and adaptation. We confirm that response dynamics are odor–receptor neuron specific and we show that different dynamical features are differentially distributed across receptor neuron classes. We found activity after stimulus offset with some odor–receptor neuron combinations producing particular strong and long lasting responses. Euclidean distances between odorants were elevated after stimulus offset demonstrating that odor identity information was still present after stimulation.

3.1 Introduction

Olfactory systems have evolved to deal with chemical and temporal complex stimuli. Olfactory stimuli usually consist of multiple components in different concentrations and they appear together with competing stimuli, traveling through the air in a chaotic manner (Riffell et al., 2008). In addition to the complexity of the odor stimulus, the responses of olfactory receptor neurons can be complex too: even short stimuli consisting of mono molecular odors often elicit complex responses from olfactory receptor neurons (ORNs) (Hallem et al., 2004; Turner et al., 2011; Montague et al., 2011; Martelli et al., 2013).

Depending on its identity and concentration, an odorant activates an ensemble of differentially tuned olfactory receptor neurons (ORNs) (Friedrich

and Korsching, 1997; Malnic et al., 1999; Sachse et al., 1999; Uchida et al., 2000; Hallem and Carlson, 2006; Pelz et al., 2006; Galizia et al., 2010). As individual ORN responses do not only differ in polarity and amplitude but also in their temporal dynamics (de Bruyne et al., 1999, 2001; Martelli et al., 2013; Getahun et al., 2012), elicits a specific spatio-temporal ensemble response (Lei et al., 2004). Responses towards a short stimulus can follow stimulus dynamics or can be shorter or longer and can even outlast the stimulus by several minutes (Turner et al., 2011; Montague et al., 2011). Response dynamics depend on the specific odorant–ORN combination and are thought to be mainly mediated by the type of receptor expressed in an ORN (Hallem et al., 2004; Getahun et al., 2012).

Response dynamics are also shaped by the cells activity state. A ORN might be adapted due to a previous stimulation, being less sensitive for a stimulus. In contrast to response dynamics, adaptation is thought to be not an intrinsic property of the OR (Nagel and Wilson, 2011).

Odor specific response dynamics might enable single ORNs to encode odorant quality in the absence of an ensemble response. Flies with a single functioning type of ORN are able to differentiate between odorants and response dynamics are thought to underly this type of odorant quality coding (DasGupta and Waddell, 2008). Response dynamics are to a large degree concentration invariant (Martelli et al., 2013), further underlining an involvement in odor quality coding.

Here we used calcium imaging to investigate response dynamics of eight *Drosophila* ORNs in response to 115 odorants. We used a double pulse stimulus regime in order to access adaptation. We show that response dynamics depend on the ligand–ORN combination while different dynamical features are differentially distributed across ORNs.

3.2 Material & Methods

Animals

All recordings were performed on female *Drosophila melanogaster* expressing the calcium reporter G-CaMP 1.3 (Nakai et al., 2001) or G-CaMP 3 (Tian et al., 2009) in specific sets of olfactory receptor neurons under the control of the GAL4-UAS expression system. UAS-G-CaMP 1.3 flies were provided by Jing Wang, University of California, San Diego, La Jolla, CA; UAS-GCaMP 3.0 flies were provided by Loren L. Looger, Howard Hughes Medical Institute, Janelia Farm Research Campus, Ashburn, Virginia. Stable GAL4-UAS fly lines were of the following genotypes: P[UAS:GCaMP1.3]; P[GAL4:X] (X being one of

Or10a, Or13a, Or42b, Or47b, Or67b, Or69a or Or92a), and w;P[Or56a:GAL4]; P[UAS:GCaMP3]attP40.

Flies were kept at $25\,°C$ in a 12/12 light/dark cycle. Animals were reared on standard medium ($100\,mL$ contain: $2.2\,g$ yeast, $11.8\,g$ of sugar beet syrup, $0.9\,g$ of agar, $5.5\,g$ of cornmeal, $1\,g$ of coarse cornmeal and $0.5\,mL$ of propionic acid).

Odorant preparation

Odorants were purchased from Sigma-Aldrich in the highest purity available. Pure substances were diluted in $5\,mL$ mineral oil (Sigma-Aldrich, Steinheim, Germany), dilutions ranged from 10^{-2} to 10^{-8}. Odors were prepared in $20\,mL$ headspace vials sealed with a Teflon septum (Axel Semrau, Germany). For dose-response curves pure odorants were diluted in mineral oil in decadic steps from 10^{-2} to 10^{-8}. Information and abbreviations for all odorants used are given in Table S4.

Stimulus application

A computer-controlled autosampler (PAL, CTC Switzerland) was used for automatic odor application. A headspace of $2\,mL$ was injected in two $1\,mL$ portions at time points $6\,s$ (frame 24) and $9\,s$ (frame 36) with an injection speed of $1\,mL\,s^{-1}$ into a continuous flow of purified air flowing at $60\,mL\,min^{-1}$. The stimulus was directed to the antenna of the animal *via* a Teflon tube (inner diameter $2\,mm$, and length $39.5\,cm$).

Four to eight odorants were presented in a row (one block) interspaced by solvent control, room air control and an OR specific reference odorant. After each injection the autosampler syringe was flushed with purified air for $30\,s$. After each block of stimuli, the syringe was washed with hexane or pentane (Merck, Darmstadt, Germany), heated up to $48\,°C$, and rinsed with continuous clean air for $6\,min$.

We were able to increase stimulus precision in the newer data sets (Or10a, Or47b, Or56a, Or69a) by using a different injection protocol in the Cycle Composer software controlling the PAL system. At the same time the injection protocol changed from a three step protocol (1: needle penetrates injector; 2: injection of first pulse; 3: injection of second pulse) to a two step protocol (1: needle penetrates injector and injection of the first pulse in a single step; 2: injection of the second stimulus pulse). In the three step protocol (used for Or13a, Or42b, Or67b, Or92a) the needle penetrated the injector $\sim 2\,s$ before injection of the first pulse. The mere penetration of the syringe into the

continues airflow was sufficient for some potent ligand–ORN combinations to produce strong responses (see phenethyl alcohol in Or67b).

Calcium imaging

Calcium imaging was performed on two setups which consisted of a fluorescence microscope (BX50WI or BX51WI, Olympus, Tokyo, Japan) equipped with a $50\times$ air lens (Olympus LM Plan FI $50\times/0.5$). A CCD camera (TILL Imago, TILL Photonics, Gräfelfing, Germany or SensiCam, PCO, Kelheim, Germany) was mounted on the microscope recording with 8×8 pixel on-chip binning, which resulted in 80×60 pixel sized images. For each stimulus recordings of $20\,\mathrm{s}$ at a rate of $4\,\mathrm{Hz}$ were performed using TILLvisION (TILL Photonics, Gräfelfing, Germany). A monochromator (Polychrome II or Polychrome V, TILL Photonics, Gräfelfing, Germany) produced excitation light of $470\,\mathrm{nm}$ wavelength which was directed onto the antenna *via* a $500\,\mathrm{nm}$ low-pass filter and a $495\,\mathrm{nm}$ dichroic mirror, emission light was filtered through a $505\,\mathrm{nm}$ high-pass emission filter.

Data analysis

Data analysis was performed using custom written routines in IDL (ITT VIS, USA) and R (R Development Core Team, 2013).

As long as animals showed stable responses to the reference odor measurements were included into the analysis. Recorded movies were manually corrected for movement artifacts, and an area of interest was defined for the parts of the antenna that showed fluorescence increase upon stimulation. All calculations were done within that area.

Relative fluorescence change was calculated as $\Delta F/F = ((F_i - F_0)/F_0) \times 100$ with F_i being the fluorescence at $frame_i$ and F_0 being the mean fluorescence of the first 10 frames of a recording.

The data was manually corrected for movement and an area of interest was defined on a false color coded image of the reference odor measurement, all calculations were done within that area. Response traces of the average pixel value within the area were exported.

To correct for the photo-bleaching of the dye, an exponential decay function of the form $A * exp^{-x/B} + C$ was fitted to the data using the `nls()` function in R. Because some odorant responses would not reach baseline within measurement time, the fit parameter B was estimated by an initial fit on the median mineral oil control response within each animal. For fitting three frames at the beginning of the time-trace and 44 frames during stimulus presentation were omitted and the pre-stimulus part of the recording was weighted 100 fold.

Response values were calculated as the mean response during 5 s after stimulus onset (corrected for setup specific stimulus onset delays) subtracted by the mean response during the first 2.5 s of a recording.

As ORN responses decrease over time a linear regression was fitted on each reference odor measurement within each individual animal. The value of this function at each corresponding timepoint was set to the value fo the first reference odor presentation elicited.

Headspace concentrations in ppm, were estimated using the published information about the relation of liquid- and vapor-phase concentrations of volatile compounds in mineral oil (Cometto-Muñiz et al., 2003) and interpolating based on available vapor pressure information (Pelz, 2005; Pelz et al., 2006).

Plotting was performed using the R core functions and the ggplot2 package (Wickham, 2009).

Response classification

We defined the following four time windows of a response and used the mean response during these time windows for further calculations (see Figure S11 for a graphical representation of the different time windows): *peak$_1$* – the mean response between frames 30 and 34; *between peaks* – the mean response between frames 35 and 39; *peak$_2$* – the mean response between frames 40 and 44; *post-stimulus phase* – the mean response between frames 52 and 56.

We defined the following response classes based on the time windows described above: *responders* – responses that showed fluorescence changes stronger than $0.3\,\%$ in at least one of peak$_1$, peak$_2$ or the post-stimulus phase; *excitatory* – responders with fluorescence changes $> 0\,\%$ at peak$_1$ and $> -0.3\,\%$ at the post-stimulus phase; *inhibitory* – responders with responses fluorescence changes $< 0\,\%$ at peak$_1$; *biphasic* – responders with fluorescence changes $> 0\,\%$ at peak$_1$ and $< -0.3\,\%$ at the post-stimulus phase.

3.3 Results

Responses differed in their polarities

Responses of olfactory receptor neurons (ORNs) were of different polarity. We grouped responses into three categories according to their polarity at different timepoints after stimulus onset (Figure 3.1A and C; see Material & Methods for details). Recordings with fluorescence changes between -0.3 or below 0.3 percent were defined as “non-responders”. Responses that were purely excitatory (fluorescence increase) or inhibitory (fluorescence decrease) were grouped in the correspondingly called categories. Responses that had a first excitatory

phase followed by an inhibitory post-stimulus phase (de Bruyne et al., 1999, 2001; Hallem et al., 2004; Silbering et al., 2008) were called biphasic.

Excitation was the predominant response type we found in six of eight ORNs we recorded. For Or42b we recorded mainly inhibitory responses while the majority of responses in Or56a was biphasic. We found inhibitory and biphasic responses in all ORNs but Or13a and Or92a.

Responses differed in their dynamics

In order to access temporal features of the odorant responses, we applied double pulses with $1\,$s pulse length and an inter-pulse interval of $3\,$s. We analyzed the three following dynamical features:
1) Peakiness – the ability of the response to return to baseline between pulses measured as:

$$1 - (response_{betweenpeaks}/response_{peak_1})$$

2) Relative height of peak$_2$ in comparison to peak$_1$, calculated as:

$$(response_{peak_2}/response_{peak_1}) - 1$$

3) Response duration – the time the response was as strong as $30\,\%$ of the first peak.

Response duration was differentially distributed for different response polarities. Excitatory responses covered the complete range from short to long-glasting responses (Figure 3.2A). Most excitatory responses in Or42b, Or56a and Or92a were short while short and long responses appeared in other receptors in similar proportions (Figure 3.2A). Biphasic responses were all short, distributing in two clusters around two and four seconds. Note that response duration was calculated based on the first peak, thus the inhibitory phase of biphasic responses was not included in the calculation of response duration.

Inhibitory reponses split into two clusters of long and short inhibitory responses (Figure 3.2A). Both types were present in Or42b, with short inhibition occurring more often. In Or47b we observed more long-lasting inhibitions which was also the exclusive type of inhibition found in Or56a bearing ORNs (Figure 3.2A).

Peakiness of excitatory responses in Or10a and Or47b and Or69a distributed around 0 meaning the majority of responses did not reach back to baseline between pulses (Figure 3.2B). For most of the Or67b responses peakiness was slightly below 0 indicating responses that were still rising after the first odor pulse. Excitatory responses in Or42b, Or56a and Or92a were more “peaky” distributing between 0 and 1. Responses in Or13a distributed into two clusters, one below 0 and one centered around a peakiness of 0.3. Most inhibitory

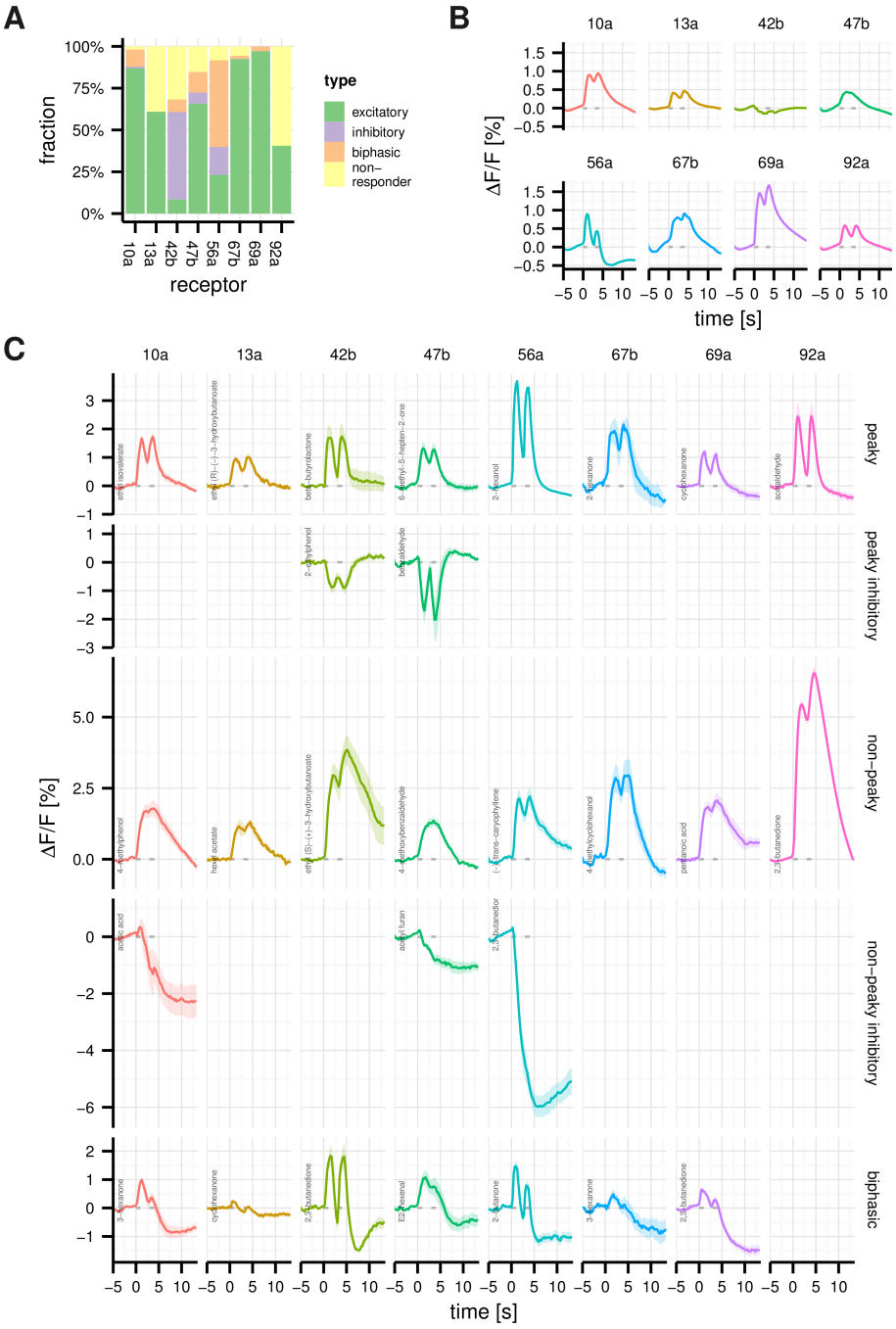

FIGURE 3.1: Response polarity and dynamics are diverse across ORNs. **A** Distribution of different response polarities across receptors (n = 105–110). For definition of classes see Material & Methods. **B** Mean traces of all odorants measured for a given receptor (n = 3 – 289)). **C** Example responses for different polarities across ORNs (mean traces, n = 5 – 10), *shaded* areas indicate SEM, *gray dashes* indicate stimulus pulses.

responses were not peaky in Or56a while responses in Or42b were of both kind. Biphasic responses were all peaky, with the highest peakiness values among all recordings (Figure 3.2B).

For most of the excitatory responses in Or10a, Or13a, Or47b, Or67b and Or69a the response to the second pulse was stronger as the response to the first pulse (Figure 3.2C). The majority of Or92a responses had a larger first peak. In Or42b and Or47b both, inhibitory responses with larger first as well as larger second peaks were found. All inhibitory responses in Or56a had larger second peaks. Biphasic responses in general had a larger first peak.

The differential distribution of dynamical features and response polarities across receptors is also reflected in the mean response curves shown for each receptor in Figure 3.1B. The Or56a mean response is clearly biphasic, Or42b is inhibitory. The other mean receptor curves are excitatory, showing different width and peakiness.

Response dynamics depend on odorant–ORN combination

As described above, a given ORN could respond with more than one polarity, having excitatory, as well as inhibitory or biphasic responses. An ORN responses could also differ in dynamical features, exhibiting different response durations, peakiness or relative peakheights towards different odorants. Thus the response dynamics did not depend on the ORN type alone. Response dynamics did also not depend on the odorant identity alone as a given odorant was able to elicit different response polarities from different receptors (Figure 3.3). Responses towards 2,3-butanediol for example were excitatory in Or92a, biphasic in Or56a and inhibitory in Or42b. Responses towards gamma-propyl-gamma-butyrolactone were long lasting and non-peaky in Or10a, Or67b and Or69a while they were short and peaky in Or56a. Taken together these results show response polarity as well as complex dynamical features depend on the specific odorant–ORN combination.

Some dynamical features were weakly correlated to concentration

We performed all measurements with pure odorants diluted 1:100 vol/vol in mineral oil. Due to different vapor pressures even when equally diluted, odorants are present in headspace at different absolute concentrations. Thus our data contained odorants at different headspace concentrations which enabled us to check whether some dynamical features were depending on ligand concentration. We estimated the ppm concentration in the headspace using the published information about the relation of liquid- and vapor-phase concentrations of volatile compounds in mineral oil (Cometto-Muñiz et al., 2003)

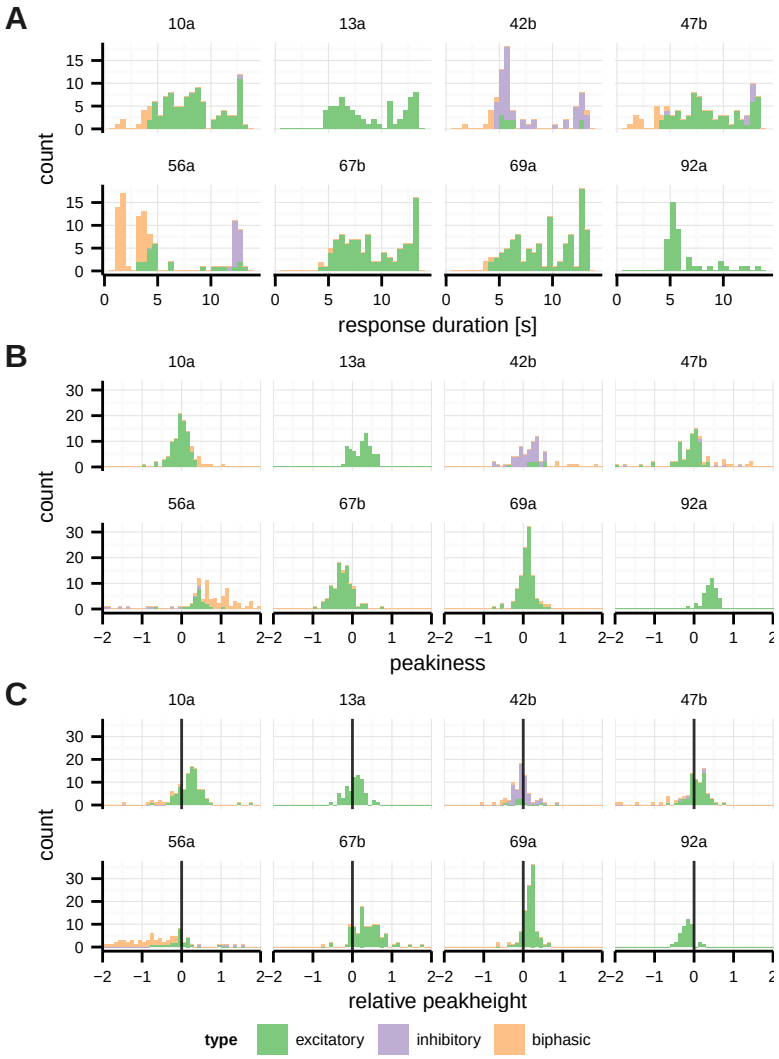

FIGURE 3.2: Distribution of dynamical features across ORNs and polarities. **A** Stacked histograms showing the distribution of the response duration (bin width = 0.5 s). **B** Stacked histograms showing the distribution of "peakiness"."Peakiness" = 0: no return to baseline; "peakiness" = 1: full return to baseline; "peakiness" > 0: response still rising (see Material & Methods for exact calculation; bin width = 0.1). **C** Stacked histograms showing the distribution of "relative peakheight". "relative peakheight" < 0: $peak_1$ > $peak_2$; "relative peakheight" > 0: $peak_2$ > $peak_1$ (see Material & Methods for exact calculation; bin width = 0.1). X-axes in **B** and **C** are trimmed, see Figure S12 for full range. *Color* indicates polarity

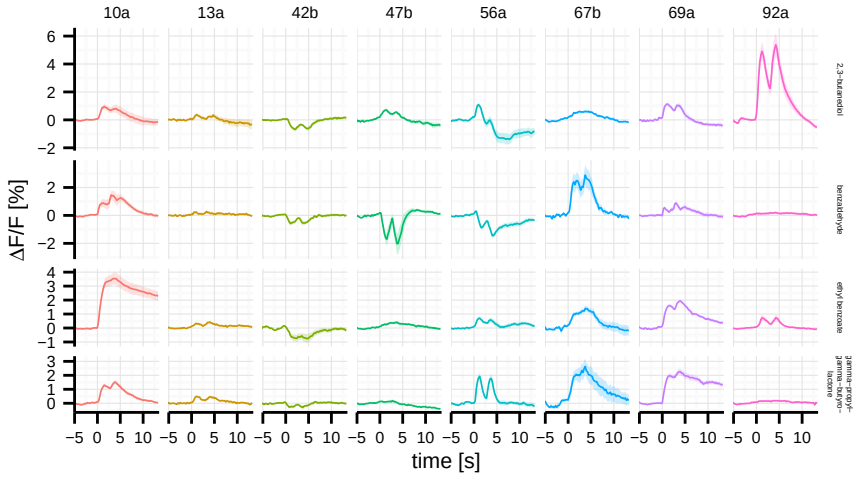

FIGURE 3.3: Response dynamics differ between odorant and ORN. Mean reponse traces (n = 4–13) for four odorants across ORNs. *Shaded* areas indicate SEM, *gray dashes* indicate stimulus pulses.

and interpolating based on available vapor pressure information (Pelz, 2005; Pelz et al., 2006). Response strength measured as the absolute amplitude of peak_1 and headspace concentration (log ppm) were weakly correlated (Pearson's product-moment correlation / t-test, $r = 0.09, P < 0.05$; Figure 3.4A). Response duration and concentration were weakly anti correlated (Pearson's product-moment correlation / t-test, $r = -0.15, P < 0.001$; Figure 3.4A). Peakiness and relative peak heights were not correlated to concentration.

None of the dynamical features we analyzed was significantly correlated to response strength.

For some odorant–ORN combinations we measured responses at different concentrations by diluting the odorants in decadic steps (Figure 3.4B). While response strength was only weakly linked to concentration across odorants and ORNs, it was affected by concentration changes for given odorant–ORN combinations. Response strength increased with increasing amount of ligand present, as commonly observed (Figure 3.4B; Malnic et al., 1999; de Bruyne et al., 1999; Sachse and Galizia, 2003). For excitatory responses, response duration increased slightly with increasing odorant concentration, while peakiness was not affected (2,3-butanediol, 2,3-butanedione an 2-hexanol in Figure 3.4B). This could be best seen when the responses were normalized to the first peak (Figure 3.4C). A similar observation was made by Martelli et al. (2013) who compared ORN responses towards single stimuli. The second peak did increase relative to the first peak with concentration for one odorant (2-hexanol - Or56a in Figure 3.4C) while it did not change for another odorant (2,3-butanedione - Or92a in Figure 3.4C) Response dynamic was less preserved across concentra-

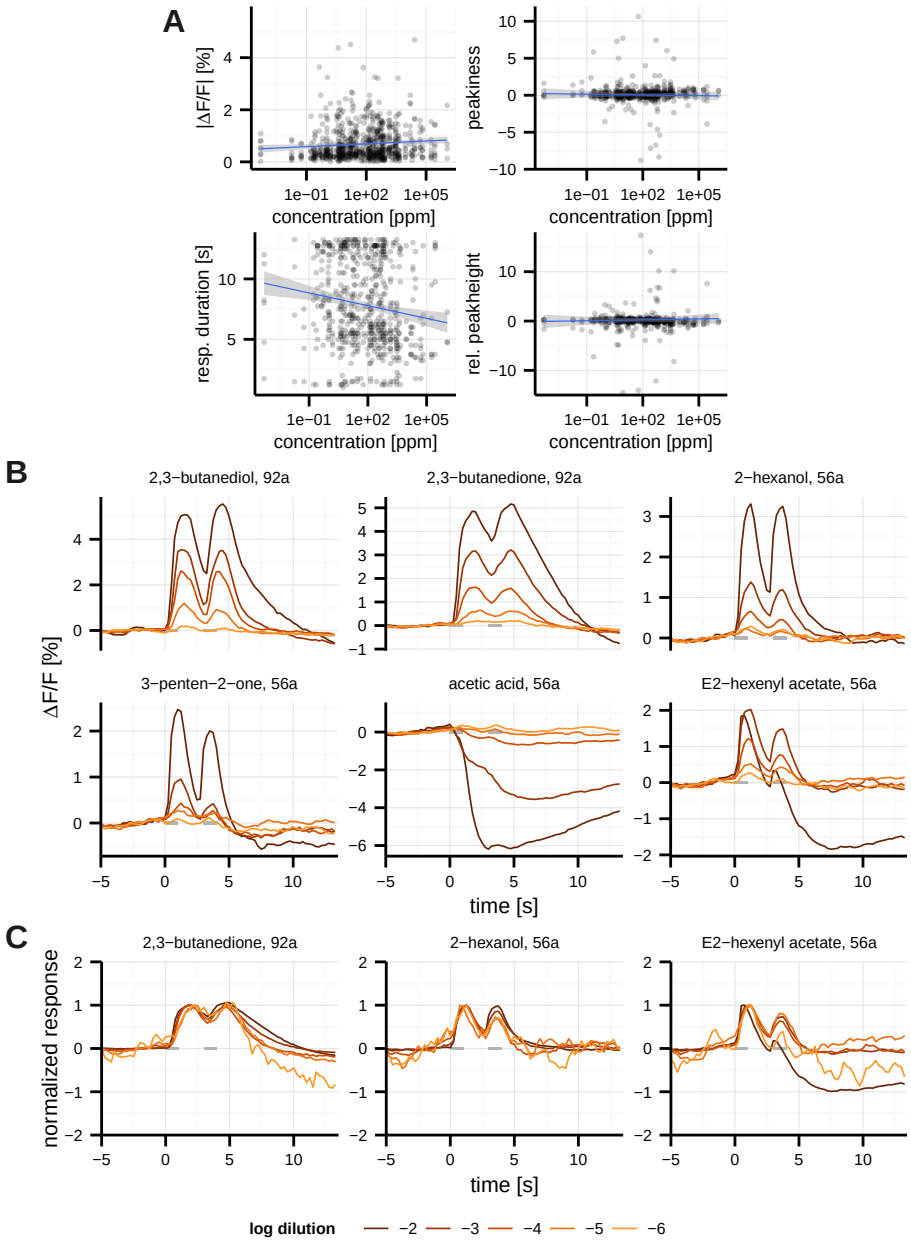

FIGURE 3.4: Concentration dependency of dynamical features. **A** Concentration in ppm estimated from available vapor pressures of odorants plotted against response strength (measured as absolute amplitude of peak$_1$, n=751), peakiness, response duration and relative peakheight (see Material & Methods for calculation of the different features). Response strength was weakly correlated to concentration (Pearson's product-moment correlation / t-test, $r = 0.09, P < 0.05$), response duration was weakly anti-correlated (Pearson's product-moment correlation / t-test, $r = -0.15, P < 0.05$). "Peakiness" and "relative peakheight" were not significantly correlated. **B** Mean response traces of six odorants measured at five different dilutions of three odorants (n = 9–17). **C** Data from **B** for three odorants, normalized to peak$_1$ (n = 9–17). *Gray dashes* indicate stimulus pulses.

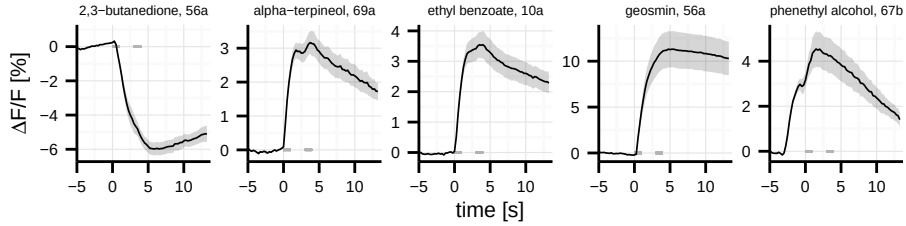

FIGURE 3.5: Strong and prolonged responses. Five mean traces of odorants (n = 6-10) that elicited particularly strong and prolonged responses from individual ORNs. *Shaded* areas indicate SEM

tions in the responses elicited by E2-hexenyl acetate in Or56a. These responses were excitatory but became biphasic at the highest concentration tested (Figure 3.4B). The normalized responses in Figure 3.4C overlap only for the lower concentrations. 3-penten-2-one on the other hand was weakly biphasic also at lower concentrations. Biphasic responses towards E2-hexenyl acetate at higher concentrations could have been linked to an additional small acetic acid peak that we observed in GC-MS measurements (data not shown). Response dynamics of acetic acid changed at high concentrations. While the second peak was stronger as compared to the first peak at a 10^{-3} dilution, both peaks were equally strong at 10^{-2} (Figure 3.4B).

Strong and prolonged responses

Some ORN–odorant combinations lead to particular strong and prolonged responses (Figure 3.5). This prolonged activation could also result from a prolonged stimulation through ligands sticking to the stimulus tube (Martelli et al., 2013). At least for some of the responses this can be excluded as the same odorants elicited faster responses in other ORNs (compare ethyl benzoate in Figure 3.3).

Strong and longlasting responses in Figure 3.5 had weak to no double peaks (low peakiness). This was not a general rule as peakiness and also response duration were not correlated to response strength.

Odor-response distance was correlated to chemical distance

We calculated Euclidean distances based on the complete response traces after stimulus onset for 98 odorants recorded in all eight receptors. A 2D visualization of odor distances in Figure 3.6A shows that especially the odors that elicited longlasting responses from some ORNs are located more distant from other odorants. Additionally we calculated odor distances for every timepoint individually. In Figure 3.6B mean distances at every timepoint are plotted

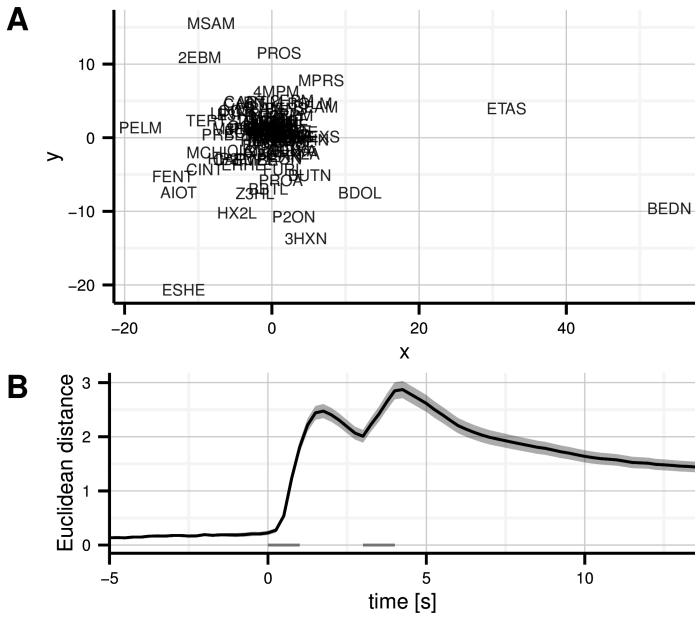

FIGURE 3.6: Euclidean distances between odor-responses. **A** 2D visualization of odor-response distances calculated using the Kruskal's non-metric multidimensional scaling. **B** Mean odor distances across recording time, *shaded* area indicates SEM, *gray dashes* indicate stimulus pulses.

over time. Mean odor-distance was elevated even after stimulus-offset, likely due to the contribution of strong longlasting responses described above (Figure 3.5)13.

When comparing odor distances calculated from our data to chemical distances calculated on an optimized set of chemical descriptors from Haddad et al. (2008) we found a weak correlation ($r = 0.22$, P < 0.001). This correlation was slightly stronger when distances were not calculated on the whole response trace but on the post-stimulus response ($r = 0.24$, P < 0.001) or the response duration alone ($r = 0.25$, P < 0.001).

3.4 Discussion

We analyzed response dynamics of eight *Drosophila* ORNs towards a set of 115 odorants. Responses differed in polarity as well as in their dynamics. In accordance with previous studies odorants elicited responses of different polarity from different ORNs and a given ORN could respond with different polarity to different odorants (de Bruyne et al., 1999; Hallem et al., 2004; Pelz et al., 2006). Similar, response dynamics depended on ligand–ORN combination, not on ligand or ORN alone.

One dynamical feature, response duration, was more or less equally dis-

tributed across excitatory responses whereas the distribution of response duration across inhibitory responses was bimodal and split into short and long lasting responses (Figure 3.2A). We found short and long responses in Or42b, the inhibitory responses in other ORNs were almost exclusively long lasting. Although response duration could be directly based on receptor–ligand binding properties such as affinity and residence time (Tummino and Copeland, 2008), the bimodal distribution of response durations in inhibitory responses could indicate the involvement of two signaling mechanisms with different dynamics. While it is clear that insect ORs are involved in ionotropic signaling (Wicher et al., 2008; Sato et al., 2008; Smart et al., 2008), a metabotropic function is discussed (Wicher et al., 2008). The involvement of signaling cascades with different temporal dynamics could explain the observation that inhibitory responses were in general slow with long lasting responses and peakiness < 0 meaning the response was still rising in between stimuli. Alternatively, the slower dynamic of inhibitory responses could indicate that the removal of intracellular calcium is slower than the influx of calcium. In crustaceans it has been demonstrated that two different signaling cascades mediate excitation and inhibition within a single ORN (Boekhoff et al., 1994).

We measured changes in calcium concentrations *via* a genetically encoded calcium indicator. Albeit the relationship between calcium concentration and action potential rates are well established in general (Charpak et al., 2001; Tian et al., 2009; Moreaux and Laurent, 2008), calcium dynamics in response to inhibitory responses were not studied in detail. Thus, experiments that combine electrophysiology and calcium imaging on ORNs would be interesting. However, slow response dynamics for inhibitory responses have also been described in electrophysiological recordings (Su et al., 2011; Getahun et al., 2012) and thus seem to comprise a general phenomenon in insect OR bearing ORNs.

We observed many biphasic responses, i.e. excitatory responses with an inhibitory post-stimulus phase. Biphasic responses are commonly observed in insect ORNs (de Bruyne et al., 1999, 2001; Hallem et al., 2004; Faucher et al., 2013; Galili et al., 2011) and ORNs which respond biphasic to a particular odor often also have a high temporal resolution for this odor (Lei and Hansson, 1999). Matching these observations, all biphasic responses we observed had short excitatory phases and a peakiness > 1 (high return to baseline rate between stimuli). The second peak of most biphasic responses was smaller than the first peak which would can be interpreted as fast adaptation happening. Hyperpolarizing phases after adapting stimulus pulses were also observed in LFP recordings of *Drosophila* ORNs (Nagel and Wilson, 2011). We observed responses with similar dynamics in another data set containing binary mixtures of excitatory and slow inhibitory components (see Chapter 5 Figure 5.3B). As

hypothesized above, if different signaling pathways would mediate excitatory and slow inhibitory responses, a biphasic response could result from both these pathways being active in parallel. For at least one odorant (E2-hexenyl acetate) that elicited a biphasic response in Or56a we found an additional peak of acetic acid in GC-MS measurements. As acetic acid elicited strong inhibitory responses in Or56a, this particular biphasic response could have been a mixture response. However such a peak could not be found for at least one other odorant. The source of the additional acetic acid remains unclear, it might be contained in the ($\geqslant 98\,\%$) pure odorant or be a product of chemical decomposition.

Within the sensillum lymph, odorant-degrading enzymes are actively degrading odorant molecules in order to clear the lymph from it (Chertemps et al., 2012). Response dynamics, especially response termination, are thought to be influenced by these processes (Syed et al., 2006). By-products of odorant-degradation could in theory again be ligands for a given OR and influence response dynamics additionally.

Dynamical features were differentially distributed across ORNs in our data. Misexpression experiments where ORs have been expressed in the wrong ORN have shown that e.g. response termination is directly mediated by the OR-protein (Hallem et al., 2004). Adaptation in contrast appears to be independent of the OR-protein (Nagel and Wilson, 2011). Also the expression of odorant binding proteins (Shanbhag et al., 2001) and odorant degradation enzymes (Syed et al., 2006) might be sensillum specific and thus might determine the temporal response properties of an ORN. Repeating our experiments with misexpressed ORs is necessary to identify the OR, cell and sensillum specific response properties.

The double pulse stimulation allowed us to access adaptation. While adaptation is most pronounced after prolonged stimuli like e.g. a constant background odor , neurons are less sensitive for a few seconds already following adapting stimuli of $500\,$ms length (de Bruyne et al., 1999). Mechanisms leading to adaptation of vertebrate ORNs are well studied (see Zufall and Leinders-Zufall (2000) for review), whereas the involved mechanisms in insect ORNs remain largely unknown. There are hints that like in vertebrates calcium plays a role in feedback signaling in adaptation (Störtkuhl et al., 1999), it is acting on the activation of transduction and the OR itself is not directly involved in the process (Nagel and Wilson, 2011). Whether a response towards the second pulse of our double pulse stimulation was adapted or not could not easily be distinguished. The response towards the first pulse did in most cases not reach back to baseline before the second pulse arrived at the antenna (“peakiness” $<$ 1). Thus the second peak was riding on top of the first response. While a lower

second peak clearly indicates an adapted response, the amount of contribution of the initial response to the second peak (peakiness and relative height of the second peak were strongly anti-correlated; Pearson's product-moment correlation / t-test, $r = 0.97, P < 0.001$) could still include adaptation but a stronger ligand concentration in the lymph (e.g. due to slow degradation processes) could have compensated for that.

In contrast to biphasic responses, most excitatory and inhibitory responses had stronger second peaks. The amount of adaptation happening seemed to depend on the ORN class to some degree as excitatory responses in Or92a and Or56a had smaller second peaks. In line with adaptation leading to a shift of the dose-response curve to higher concentrations, a smaller second peak could be overcome by increasing the ligand concentration while for a response with equal strong 1st and 2nd peak, the ratio did not change (Figure 3.4). As adaptation in *Drosophila* ORNs can be blocked by mutating the trp-Ca^{2+} channel (Störtkuhl et al., 1999), repeating some of our experiments under this condition could give more insight in involvement of adaptation on the second peak.

Martelli et al. (2013) described *Drosophila* ORN responses dynamics to be concentration invariant over a wide range of concentrations. Our data confirms this finding regarding peakiness (i.e. return to baseline between pulses) but adds that subsequent responses can vary with concentration when adaptation is happening. Thus odor dynamics can carry information on odor quality as behavioral data indicated before (DasGupta and Waddell, 2008). On the same time it might contribute to concentration invariant coding of odor quality.

Concentration invariant odor-coding is an important task to be solved by an olfactory system. When for example an animal approaches an odor source, the odor concentration increases. The odor-quality however should stay the same. Different mechanism like sequential ORN recruitment, syntopic interactions and network effects in the brain are thought to contribute to this concentration invariant odor-coding (Sachse and Galizia, 2003; Uchida and Mainen, 2007; Root et al., 2008; Asahina et al., 2009; Cleland et al., 2012; Münch et al., 2013). Odor dynamics are an additional mechanism to preserve odor quality across concentrations.

Some ligand–ORN combinations in our data produced responses that were strong (high efficacy) and long-lasting (high affinity, but see Tummino and Copeland, 2008; Figure 3.5). One of these responses was elicited by geosmin in Or56a bearing ORNs. Geosmin was shown to activate Or56a ORNs selectively and to convey an ecologically relevant aversive signal for *Drosophila* (Stensmyr et al., 2012). In order to reliably detect low doses of relevant odorants, like e.g. low volatile pheromone compounds like cis-vaccenyl acetate (Brieger and But-

terworth, 1970; Kurtovic et al., 2007), it is beneficial for an olfactory system to have ORNs that are efficiently activated and very affine to this odorant. A high affinity would ensure that the ligand is able to bind even at low concentrations or in a mixture when competing with other ligands for binding. A high efficacy would guarantee that already low dosages lead to sufficient ORN activation.

A prolonged activation of an ORN could be especially important for flying insects that rapidly pass filaments of odors. Some odor cues become more meaningful when they appear together, like for example host plant volatiles and sex pheromones that in some moth species (Ochieng et al., 2002; Yang et al., 2004). Prolonged activation of an ORN could facilitate such detection of coincidental stimuli, even if they are traveling in different odor-filaments and thus hit the antenna with a delay. The mean Euclidean distance between odorants stayed elevated even after stimulus offset. This shows that odorant information is indeed present even when the stimulus is not present anymore. Taken together it might be interesting to specifically look for a ecological relevance in highly efficient and affine ligand–ORN combinations that elicit strong and long lasting responses.

Chapter Four

Weaker ligands can dominate an odor blend due to syntopic interactions

Abstract

Most odors in natural environments are mixtures of several compounds. Perceptually, these can blend into a new "perfume," or some components may dominate as elements of the mixture. In order to understand such mixture interactions, it is necessary to study the events at the olfactory periphery, down to the level of single-odorant receptor cells. Does a strong ligand present at a low concentration outweigh the effect of weak ligands present at high concentrations? We used the fruit fly receptor Or22a and a banana-like odor mixture as a model system. We show that an intermediate ligand at an intermediate concentration alone elicits the neuron's blend response, despite the presence of both weaker ligands at higher concentration, and of better ligands at lower concentration in the mixture. Because all of these components, when given alone, elicited significant responses, this reveals specific mixture processing already at the periphery. By measuring complete dose-response curves we show that these mixture effects can be fully explained by a model of syntopic interaction at a single-receptor binding site. Our data have important implications for how odor mixtures are processed in general, and what preprocessing occurs before the information reaches the brain.

4.1 Introduction

Naturally occurring odors usually consist of tens or even hundreds of different components at varying concentrations (Knudsen et al., 1993). Depending on the olfactory receptor (OR) it expresses, an olfactory receptor neuron (ORN) is able to respond to a large set of odorants (Hallem et al., 2004). Odor response profiles overlap, thereby leading to an ensemble of activated ORNs upon odorant presentation (de Bruyne et al., 2001; Hallem and Carlson, 2006; Galizia et al., 2010). Because even a single ligand is able to elicit an ensemble response across ORNs, in a mixture, the ensemble responses of the different components overlap and generate a novel mixture activation pattern (Johnson

et al., 2010). On a perceptional level, humans have difficulties to recognize individual components with increasing mixture complexity and instead perceive the stimulus as a new odor quality (Jinks and Laing, 2001). In other cases, honeybees have been shown to learn odor mixtures *via* selection of only a few key components (Reinhard et al., 2010). These, and similar, mixture effects are thought to derive from mixture interactions in odor coding. In the brain network, the overlapping input channels influence each other laterally *via* neural circuits, resulting in mixture interactions (Silbering and Galizia, 2007; Lei and Vickers, 2008; Olsen and Wilson, 2008; Root et al., 2008; Ignell et al., 2009). The presence of one component might for example suppress the response to the other (suppression or hypoadditivity) or enhance it (synergism; Duchamp-Viret et al., 2003; Silbering and Galizia, 2007; Kuebler et al., 2011).

However, mixture interactions can also be found prior to any brain network at a single ORN level in the olfactory periphery (Cromarty and Derby, 1998; Duchamp-Viret et al., 2003; Rospars et al., 2008; Hillier and Vickers, 2011). Thus, these effects directly shape the sensory input the brain receives. Studying the mechanisms underlying mixture interactions in the periphery is therefore important to understand how natural odors are perceived.

Here, we measured odor-evoked calcium responses in the dendrites and somata of Drosophila ORNs. We used the well-characterized receptor dOR22a (Pelz et al., 2006; Galizia et al., 2010), which responds strongly to banana extract (Hallem and Carlson, 2006), and an artificial banana-like odor blend (Jordán et al., 2001), which allowed us to dissect the contribution to the odor response of different components. As not only the quality of components but also their relative concentration is an important feature of a mixture, we used different concentrations and recorded full dose-response curves. We found that mixture responses are hypoadditive in dOR22a. Responses to odor-concentration series demonstrate that the observed hypoadditivity is likely due to syntopic interactions at a single-odorant receptor-binding site (Rospars et al., 2008). Thus, a relatively simple peripheral mechanism already explains a large part of mixture interactions that render odor mixtures unique and identifiable “perfume”.

4.2 Material & Methods

We recorded odor-evoked responses in Or22a ORNs using calcium imaging. In each animal, up to 31 stimulus responses were recorded aiming at 1) screening for responses toward 15 selected banana-scent components, 2) measuring mixture interactions, or 3) characterizing full dose-response curves. All measurements were performed at the same experimental setup using the same

strain of flies. A total of 40 animals were used for this study.

Animals

Flies were kept at $25\,^{\circ}$C in a 12/12 light/dark cycle. Animals were reared on standard medium (100 mL contain: 2.2 g yeast, 11.8 g of sugar beet syrup, 0.9 g of agar, 5.5 g of cornmeal, 1 g of coarse cornmeal and 0.5 mL of propionic acid). Female *Drosophila melanogaster* were used for experiments 1-3 weeks after eclosion. Flies were of genotype P[UAS:GCaMP];P[GAL4:Or22a]/CyO, expressing the calcium reporter G-CaMP 1.3 in Or22a-bearing cells (crossed from wP[UAS:G-CaMP];CyO/Sp;+ flies provided by Jing Wang, University of California, San Diego, La Jolla,CA; Nakai et al., 2001; Wang et al., 2003.

Flies were mounted in custom made holders, placed with their neck into a slit, the head was fixed to the holder with a drop of dental glue (Tetric EvoFlow, Ivoclar Vivadent, Ellwangen, Germany). A half electron microscopy grid was placed on top of the head, stabilizing the antenna by touching the second, but not the third antennal segment.

Odorant preparation

Odorants were purchased from Sigma-Aldrich in the highest purity available (Table 4.1). Pure substances were diluted in 5 mL mineral oil (Sigma-Aldrich, Steinheim, Germany), dilutions ranged from 10^{-2} to 10^{-8}. Odors were prepared in 20 mL headspace vials sealed with a Teflon septum (Axel Semrau, Germany).

Information and abbreviations for all odorants used are given in Table 4.1, the tested mixtures were MIX15 (all 15 components: 1-butanol [BO], 1-hexanol [HO], 2-pentanol [PO], 2-pentanone [PN], 3-hydroxy-2-butanon [BN], 3-methyl-1-butanol [MO], butyl acetate [BA], butyl butyrate [BB], E-2-hexenal [HE], ethyl butyrate [EB], hexanal [HL], hexyl acetate [HA], isoamyl butyrate [IAB], isobutyl acetate [IBA], and isopentyl acetate [IA]); MIX4 (IA, BA, EB, and PO); MIX3 (BA, EB, and PO); IA.BA (IA and BA); IA.EB (IA and EB); and IA.PO (IA and PO).

Odorant dilutions for the artificial banana blend and its components were prepared in order to match the concentrations appearing in natural banana fruit reported by Jordán et al. (2001). For producing the desired headspace concentrations in ppm, the corresponding vol/vol dilutions in mineral oil were estimated using the published information about the relation of liquid- and vapor-phase concentrations of volatile compounds in mineral oil (Cometto-Muñiz et al., 2003) and interpolating based on available vaporpressure information (Pelz, 2005; Pelz et al., 2006).

For dose-response curves pure odorants were diluted in mineral oil in decadic steps from 10^{-2} to 10^{-8}, headspace concentrations in ppm were calculated as explained above. The ratios of the single components within the binary mixtures were 1:1 (vol/vol), which corresponds to the following ppm ratios in the headspace: $ratio_{PO/IA}$ = 0.78 and $ratio_{EB/IA}$ = 3.34.

Compound concentrations in all mixtures are the same as in single odors, for example, mixture AB contains A + B and not 0.5 A + 0.5 B.

TABLE 4.1: Table of odorants and concentrations used in the experiments together with their Chemical Abstracts Service (CAS) number and the abbreviated code used in the text

CODE	Name	CAS	ppm	Dilution	Class
HE	E-2-hexenal	6728-26-3	32.2	$10^{-3.9}$	Aldehyde
HL	hexanal	66-25-1	21.47	10^{-4}	Aldehyde
BN	3-hydroxy-2-butanon	513-86-0	20.33	$10^{-3.5}$	Ketone
PO	2-pentanol	6032-29-7	14.26	$10^{-3.8}$	Alcohol
MO	3-methyl-1-butanol	123-51-3	7.9	$10^{-3.6}$	Alcohol
IAB	isoamyl butyrate	106-27-4	7.13	$10^{-3.1}$	Ester
IA	isopentyl acetate	123-92-2	4.85	$10^{-4.3}$	Ester
PN	2-pentanone	107-87-9	2.71	$10^{-5.6}$	Ketone
IBA	isobutyl-acetate	110-19-0	2.45	$10^{-5.2}$	Ester
BA	butyl acetate	123-86-4	1.32	$10^{-5.3}$	Ester
HO	hexanol	111-27-3	1.17	$10^{-3.8}$	Alcohol
BO	butanol	71-36-3	1.06	10^{-5}	Alcohol
BB	butyl butyrate	109-21-7	0.83	$10^{-4.8}$	Ester
HA	hexyl acetate	142-92-7	0.57	$10^{-4.9}$	Ester
EB	ethyl butyrate	105-54-4	0.15	$10^{-6.4}$	Ester

Stimulus application

A computer-controlled autosampler (PAL, CTC Switzerland) was used for automatic odor application. A headspace of 2 mL was injected in two 1 mL portions at time points 6 s and 9 s with an injection speed of $1\,\text{mL}\,\text{s}^{-1}$ into a continuous flow of purified air flowing at $60\,\text{mL}\,\text{min}^{-1}$. The stimulus was directed to the antenna of the animal *via* a Teflon tube (inner diameter 2 mm, and length 39.5 cm).

The interstimulus interval was approximately 2 min. Solvent control, room air control, and reference odorant were measured after every 7 or 8 stimuli (1 block). The autosampler syringe was flushed with purified air for 30 s after each injection. After each block of stimuli, the syringe was washed with hexane (Merck, Darmstadt, Germany), heated up to $48\,^{\circ}$C, and rinsed with continuous clean air for 6 min.

Gas chromatography

A gas chromatography-mass spectrometry system (GC-MS, Trace GC Ultra & DSQ II, Thermo Fisher Scientific, equipped with a $60\,\mathrm{m} \times 0.25\,\mathrm{mm}$ forte bpx5 nonpolar capillary column, SGE International, Australia) was used to measure headspace concentrations of compounds in mixtures and single compounds. Headspace of $1\,\mathrm{mL}$ was injected with an autosampler (PAL, CTC, Switzerland), the GC run started at $40\,°\mathrm{C}$ and increased $10\,°\mathrm{C\,min^{-1}}$ up to $250\,°\mathrm{C}$. MS profile identification and GC peak measurement was performed in Xcalibur (Thermo Fisher Scientific).

Calcium imaging

Calcium imaging was performed with a fluorescence microscope (BX51WI, Olympus, Tokyo, Japan) equipped with a $50\times$ air lens (Olympus LM Plan FI 50×/0.5). A CCD camera (TILL Imago, TILL Photonics, Gräfelfing, Germany) was mounted on the microscope recording with 8×8 pixel on-chip binning resulting in 80×60 pixel sized images. For each stimulus recordings of $20\,\mathrm{s}$ at a rate of $4\,\mathrm{Hz}$ were performed using TILLvisION (TILL Photonics, Gräfelfing, Germany).

A monochromator (Polychrome II, TILL Photonics, Gräfelfing, Germany) produced excitation light of $470\,\mathrm{nm}$ wavelength that was directed onto the antenna *via* a $500\,\mathrm{nm}$ low-pass filter and a $495\,\mathrm{nm}$ dichroic mirror, emission light was filtered through a $505\,\mathrm{nm}$ high-pass emission filter.

Data analysis

Data were analyzed in custom written routines using IDL (ITT VIS), R (`http://www.r-project.org`), and LibreOffice (`http://www.libreoffice.org`). Statistics were done in SigmaStat (Systad Software).

Animals that showed stable responses to the reference odor (ethyl propionate) throughout the experiment were included into the analysis. Recorded movies were manually corrected for movement artifacts, and an area of interest was defined for the parts of the antenna that showed fluorescence increase upon stimulation. All calculations were done within that area.

Relative fluorescence change was calculated as $\Delta F/F = ((F_i - F_0)/F_0) \times 100$ with F_i being the fluorescence at $frame_i$ and F_0 being the mean fluorescence of 19 frames before stimulus onset.

We corrected for bleaching artifacts by fitting a logarithmic function for frames 4–22 and 70–80 to the ΔF trace leaving out $12\,\mathrm{s}$ after stimulus on-

set and weighting frames 4–22, 3-fold compared with after response end (see Silbering and Galizia, 2007 for details).

The response amplitude was calculated as the average of three frames around the response maximum within 2 s after stimulus onset.

To compare across animals, responses were normalized as follows: within each animal response to solvent control was set to 0 and response to reference odor ethyl propionate was set to 1. Because responses decrease over time, all other responses were calculated by linear interpolation.

A Hill function as shown in Formula 4.1 was fitted to the concentration series of odors using the `CURVEFIT` function in IDL (Sachse and Galizia, 2003; Pelz et al., 2006). The obtained parameters of the single odor-concentration series (hill [slope], Rmax [maximum response], and EC50 [concentration eliciting the half maximal response]) were used to predict the mixture parameters according to Rospars et al. (2008). The Hill parameter (slope) was estimated from the best two fits within an animal.

$$R(x) = \frac{x^{hill}}{x^{hill} + EC50^{hill}} \times Rmax \tag{4.1}$$

Response estimation

Two models for binary mixture response prediction were compared with our data. Tabor et al. (2004) used the measured responses to the single and double concentration of the individual compounds to gather local information on their dose-response curves. The logic is that if a stimulus A elicits a response, adding molecules of B to it that are also excitatory should increase the response, if we assume that no interaction happens between the odorants. Mathematically, a mixture response can be estimated using a "linear interpolation" of this local dose-response data.

$$R_{pred} = max_{1x}(R_A, R_B) + \sqrt{\Delta_{2x-1x}R_A \times \Delta_{2x-1x}R_B} \tag{4.2}$$

With R_{pred}, R_A, and R_B being the predicted response and the responses toward odorant A and B, respectively. For the purpose of this study, we define a measured response that differs from this prediction as a mixture interaction.

Rospars et al. (2008) argue that if the two substances A and B interact with the same binding pocket of interaction site, then the presence of molecules B in addition to A will interfere with the response. In order to predict this syntopic interaction mathematically, it is necessary to know the complete dose-response curve for both mixture components. The model then predicts the parameters $EC50$ and $Rmax$ of the dose-response curves for the mixtures as:

$$EC50_{pred} = (1+r)EC50_A EC50_B \sqrt[n]{\frac{1}{r^n EC50_B^n + EC50_A^n}} \tag{4.3}$$

$$Rmax_{pred} = \frac{Rmax_A r^n EC50_B^n + Rmax_B EC50_A^n}{EC50_A^n + r^n EC50_B^n} \tag{4.4}$$

With r being the ratio of the two components, n being the Hill value, $EC50$ the dose that elicits the half maximal response, and $Rmax$ the maximum response a ligand elicits. It is important to note that this model only works with concentrations measured as molecular concentrations in ppm and not for dilution units.

4.3 Results

Which odor component does Or22a respond to when a banana-like mixture is presented?

The *D. melanogaster* olfactory receptor Or22a is an especially well-described receptor that is tuned to fruity odors and strongly activated by banana (de Bruyne et al., 2001; Dobritsa et al., 2003; Stensmyr et al., 2003; Hallem and Carlson, 2006; Pelz et al., 2006). Interestingly, when comparing the Or22a response profile to the aromatic profile of banana fruit (Jordán et al., 2001), we recognized that the most abundant banana component HE is only a weak ligand, whereas the low concentrated EB strongly activates Or22a (Figure 4.1A).

In order to analyze the role of single components in the banana blend response, we created an artificial banana mixture containing 15 prominent components from banana scent (MIX15). We used published data about the relationship between liquid- and vapor-phase concentrations (Cometto-Muñiz et al., 2003) to prepare the single banana components and their mixture by diluting odorants in mineral oil in a way that vapor-phase concentrations matched those of the aromatic banana profile reported by Jordán et al. (2001)(Table 4.1).

We performed GC-MS analyses of MIX15 and the single components alone to exclude possible interactions at a chemical level that could prevent compounds from evaporation. For those peaks that were detectable, we could show that the GC-MS peak areas were the same whether diluted individually or in the mixture. Figure 4.1C shows the GC-MS measurement for the mixture overlaid with those of IA and PO alone (see Figure S13 for comparison of all detected peaks).

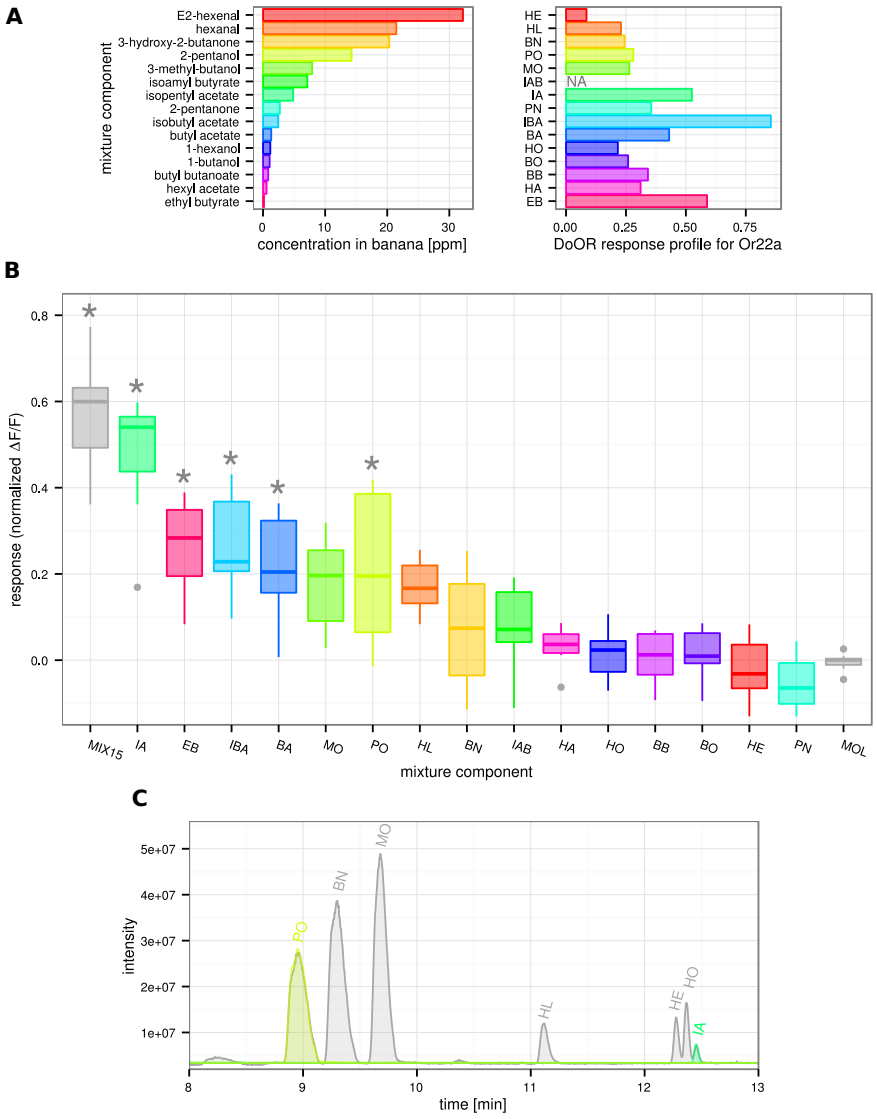

FIGURE 4.1: Selected banana compounds tested on Or22a. **A** Barplot on the left is showing the concentration in ppm of 15 compounds as they appear in the aromatic profile of banana fruit (Jordán et al., 2001), barplot on the right is giving the corresponding response profile of Or22a as in the DoOR database (Galizia et al., 2010). **B** Boxplot showing calcium imaging data recorded on the antenna of *Drosophila melanogaster*, responses are normalized to ethyl propionate and shifted by mineral oil solvent (MOL) within each animal. Asterisks indicate significant responses compared with solvent MOL (Kruskal–Wallis/Dunn's multiple comparisons vs. solvent group, $p < 0.05$, $n = 8–9$). Five of the components elicited a significant response when given alone. **C** Sample GC traces for MIX15 (gray), PO and IA. Traces of mixture and single component overlap their respective peaks. For abbreviations and odor concentrations/dilutions see Table 4.1. Boxplot shows median, lower, and upper quartile, whiskers extend to lowest and highest value that lies within 1.5 times the interquartile range from the box.

Or22a responds to many components in the mixture

We performed calcium imaging of sensory neuron dendrites using the calcium indicator G-CaMP (Nakai et al., 2001) in Or22a neurons. The mixture MIX15 and five of the 15 components elicited responses that were significantly different from the solvent control (mineral oil (MOL); Figure 4.1B). The artificial banana blend lead to the strongest activation followed by IA, EB, IBA, BA, and PO (Kruskal-Wallis, $P < 0.001$; multiple comparisons vs. control group, Dunn's method, $p < 0.05$).

Mixture responses are hypoadditive

We compared the responses elicited by the five active components from above to those elicited by the complete 15-component mixture. The response of Or22a toward IA alone was not different from the response elicited by the complete mixture that was very surprising as there were at least four other active compounds in the mixture (Kruskal-Wallis, $p < 0.001$; multiple comparisons vs. control group, Dunn's method, $P < 0.05$). We therefore asked whether IA somehow suppresses the activity of the other mixture components.

Out of the effective banana components, we selected the two at lowest concentration (EB and BA) and the most abundant (PO) for the creation of binary mixtures with IA. We also composed one mixture containing all three components (MIX3) and one mixture containing the three components and IA (MIX4). Again we performed calcium imaging of Or22a ORNs on the antenna of *D. melanogaster* with the odors at their natural banana blend concentration (Figure 4.2A). IA and MIX15 gave the same responses, and all the other responses of mixtures containing IA as a component did not differ from IA alone. Interestingly the response elicited by MIX3 was almost as high as the response of the IA containing mixtures, producing a higher Or22a response than its components alone.

Responses to binary mixtures A.B can be grouped in three types: suppressive, when the mixture response is lower than the response toward the stronger component A; hypoadditive, when the mixture response is equal to the stronger component A; synergistic, when the mixture response is higher than the response to substance A at the mixture concentration [A+B] (Duchamp-Viret et al., 2003; Silbering and Galizia, 2007; Figure 4.3).

Assuming no interaction, responses to binary mixtures can be interpolated along the dose-response curves of the single components, sometimes misleadingly referred to as "linear summation". This has been elaborated by Tabor et al. (2004) who derived Formula 4.2 for an expected mixture response (see Materials and Methods).

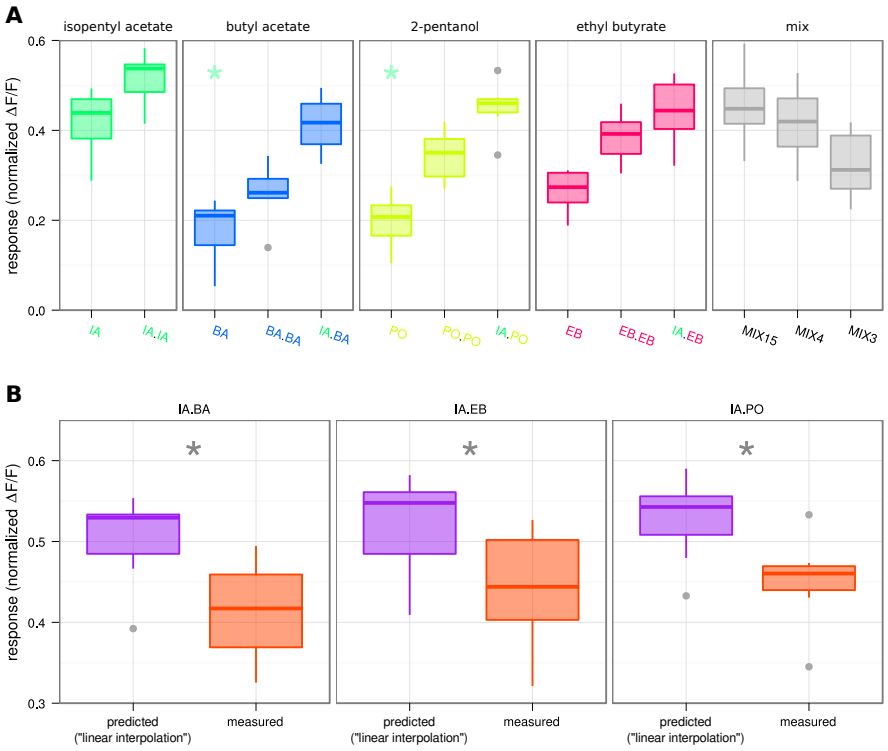

FIGURE 4.2: Binary mixtures with IA. **A** Boxplot comparing mixture components in single concentration (concentration as from banana profile, left in each panel), double concentration (second plot in each panel), the binary mixtures with IA(third plot in panels 2–4), and responses to different submixtures containing 15, 4, or 3 components (panel 5). No difference could be found between IA and the IA containing binary mixtures or between IA and the different multi component mixtures (MIX15: all 15 tested compounds; MIX4: IA, BA, EB and PO; MIX3: MIX4 without IA) (Kruskal–Wallis/Dunn's multiple comparisons vs. control group, $P < 0.001$, $n = 7$). **B** Boxplot of responses to binary mixtures as predicted assuming no interactions ("linear interpolation", *purple*) and as measured (*orange*). Prediction and measurement was significantly different in all cases (Wilcoxon Signed Rank Test, $p < 0.05$, $n = 7$). Boxplots show median, lower and upper quartile, whiskers extend to lowest and highest values that lie within 1.5 times the interquartile range from the box.

We predicted mixture responses for the three binary mixtures from measurements of the single and double concentrations of their components using Formula 4.2. We found the measured responses to be significantly lower than the predictions in all cases (Figure 4.2B; Wilcoxon signed rank test, $p < 0.05$). Thus, all responses to mixtures were hypoadditive. Specifically, adding a component to IA as stimulus – even if a good ligand – did not contribute to the response.

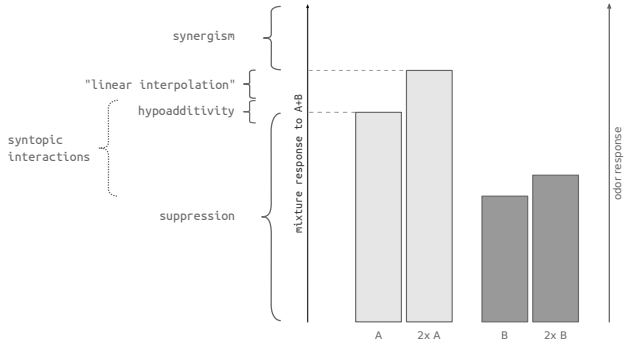

FIGURE 4.3: Scheme of mixture interaction types. Note that different authors use different wording and ranges according to different interaction mechanisms. A mixture response is termed suppressive when it is lower than the response towards the stronger component (A); hypoadditive, when the mixture response is equal to the stronger component (A); synergistic, when the mixture response is higher than the response to the stronger component A at the mixture concentration [A+B] "2× " in the figure because in this figure we consider the case of [A] = [B] for simplicity). "Linear interpolation" refers to the case where no interactions happen and the response can be calculated according to Formula 4.2. Syntopic interaction at the receptor level generally results in responses within the upper suppression range, but cannot be calculated precisely without the full dose-resonse curves (Formulas 4.3 and 4.4).

Mixture components compete at receptor level

Given that the observed mixture interactions already occurred at receptor cell level, we further tested for syntopic interaction at the receptor-binding site. Syntopic interaction describes the competition of two ligands for binding to the same or at two overlapping binding sites on the same receptor (Neubig et al., 2003). The model from Rospars et al. (2008) assumes a two-step mechanism of ligand binding and receptor activation and predicts a mixture dose-response curve from the dose-response curves of its components (Formulas 4.3 and 4.4).

We measured dose-response curves for PO and EB (the highest and the lowest concentrated component of our artificial banana blend), for IA and for their binary mixtures IA.PO and IA.EB. Pure odorants were diluted in mineral oil in decadic steps from 10^{-2} to 10^{-8}, and a Hill function was fitted to the data.

PO was a weaker ligand for Or22a than IA, showing a lower efficiency (eliciting a lower maximum response, $Rmax$, 0.67 compared with 0.94) and a lower affinity (a higher $EC50$ value, 32.73 ppm compared with 7.26 ppm; Figure 4.4A). The mixture of both in the ppm ratio measured here ($ratio_{PO/IA}$ = 0.78) followed the stronger component IA. EB on the other hand was a much stronger ligand for Or22a than IA, showing a higher affinity ($EC50$ of 36.47 ppmcompared with 67.92 ppm) and higher efficiency ($Rmax$ of 1.63 compared with 0.95; Figure 4.4B). Their mixture IA.EB also followed the stronger ligand, EB in this case ($ratio_{EB/IA}$ = 3.34). Note that IA $EC50$ and $Rmax$

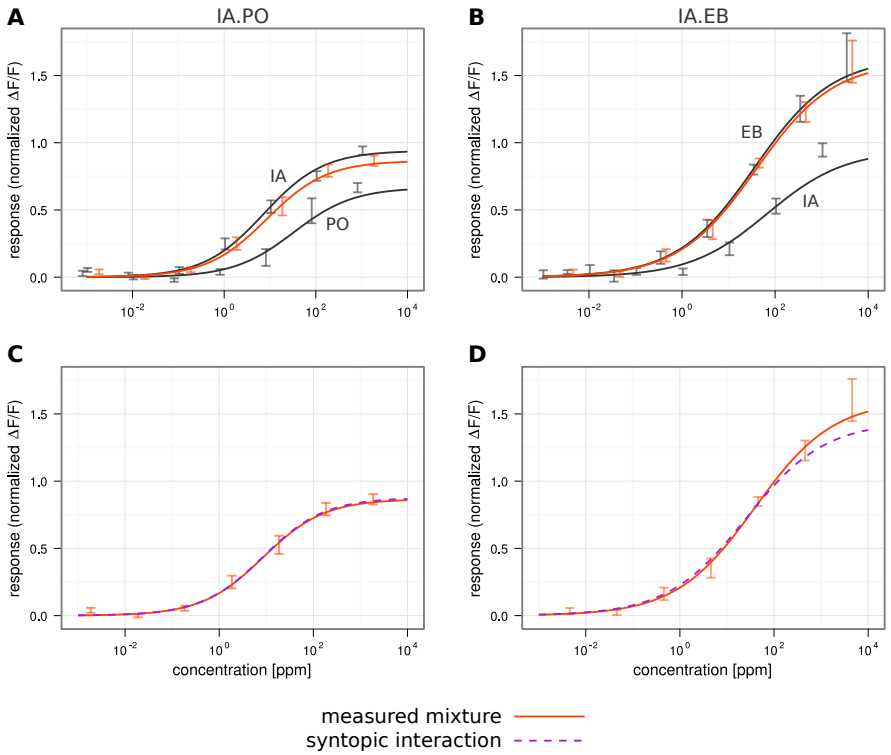

FIGURE 4.4: Dose-response curves for the single odorants IA,PO, EB and the binary mixtures IA.PO and IA.EB. **A** and **B** All dose-response curves can be fitted by the Hill equation. **C** and **D** Overlay of the measured mixture responses and the modeled mixture following syntopic interaction (Rospars et al., 2008). The model is a good estimate of the data. *light grey* IA; *dark grey* PO or EB respectively; *orange* measured mixture; *dashed purple* predicted mixture; error bars indicate SEM; n = 7.

values differed slightly as the data were obtained in two different data sets in different seasons. We could not investigate this seasonal effect in this study.

The mixture dose-response curves in Figure 4.4A and B are located between their component curves, indicating the presence of syntopic interaction. Using the model of syntopic interaction to derive a mixture dose-response curve from the component curves leads to a very accurate prediction of the actually measured mixture dose-response curves (IA.PO: predicted $EC50$: 8.59 ppm, measured $EC50$: 8.55 ppm, predicted $Rmax$: 0.88, measured $Rmax$: 0.87; IA.EB: predicted $EC50$: 25.28 ppm, measured $EC50$: 38.9 ppm, predicted $Rmax$: 1.44, measured $Rmax$: 1.6; Figure 4.4C and D). Thus mixture interactions in IA.PO and IA.EB are fully accounted for by the ligands competing for the same Or22a receptor-binding site.

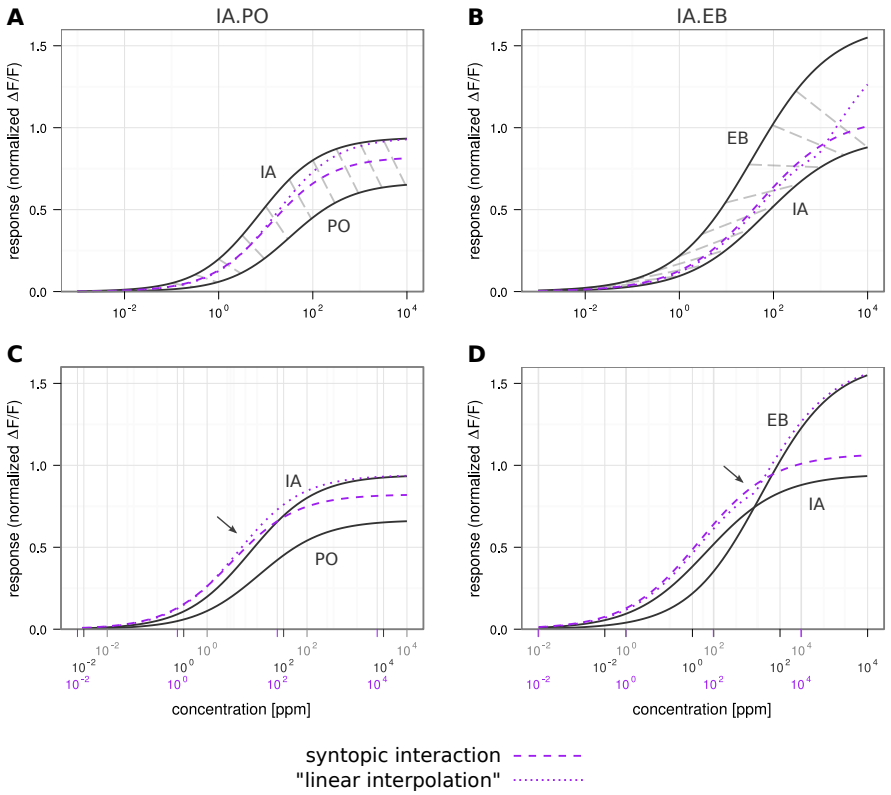

FIGURE 4.5: Mixture dose-response curves estimated for banana ratios. **A** and **B** Grey curves are the individual components IA and PO or EB, mixture curves in *purple* show predictions for syntopic interaction (*dashed*, Rospars et al. (2008)) and for linear interpolation (*dotted*, Tabor et al. (2004)). *Grey dashed* lines in A and B connect corresponding points on the single compound curves according to their ratio in banana scent. **C** and **D** Data as in A and B but shifted so that corresponding single concentrations in the "banana ratio" and resulting mixture concentration are aligned vertically. Note that "linear interpolation" leads to a "kink" in the predicted dose-response curve in **D**. Arrows indicate where syntopic interaction and linear interpolation start to diverge with increasing concentration.

Syntopic interaction applies for natural concentration ratios

The prediction of the mixture dose-response curves in Figure 4.4 is based on diluting the pure odorants in decadic steps and mixing them 1:1 (vol/vol), which translates to ratios of ($ratio_{PO/IA} = 0.78$ and $ratio_{EB/IA} = 3.34$, respectively, when transformed to ppm in headspace after Cometto-Muñiz et al. (2003). As we could show that our data can be described by the model of syntopic interaction, we calculated the mixture dose-response curves for the ratios in which the components occur in banana fruit ($ratio_{PO/IA} = 2.94$; $ratio_{EB/IA} = 0.031$; Figure 4.5). With the component dose-response curves we were also able to calculate a dose-response curve according to the "linear interpolation" model (Figure 4.5).

When calculating the syntopic interaction model using the natural banana fruit ratio of IA and PO, the mixture dose-response curve moved toward PO (its concentration in the mixture was much higher); however, it still remained closer to IA (dashed purple line in Figure 4.5A). The "linear interpolation" model (dotted purple line in Figure 4.5A) and the syntopic interaction model gave the same curves at lower concentrations; for higher concentrations, the "linear interpolation" model started deviating till it reached the same $Rmax$ level as the stronger component, whereas syntopic interaction followed the measured curve.

Using EB at the low concentration present in banana, the mixture curve for the syntopic model followed the IA curve closely. Like the models for IA.PO, the two models for IA.EB looked the same at the lower concentrations, but in the higher concentrations, the "linear interpolation" model deviated toward the stronger component, leading to a kink in the IA.EB curve (Figure 4.5B), whereas syntopic interaction created a smooth sigmoidal curve.

IA is the dominant banana-odor component for 22a

For IA and PO at the banana ratio, IA presented alone elicited the stronger responses from Or22a across the whole concentration range (dashed gray lines in Figure 4.5A and B). For a better visualization we shifted the x-axis in Figure 4.5C and D in a way that corresponding component and mixture concentrations are aligned horizontally. When comparing IA with EB, IA would elicit the stronger responses only at lower concentrations but EB would overtake at some point, leading to a kink in the "linear interpolation" model (Figures 4.5B and D).

However, in the syntopic interaction model the mixture follows IA closely, preserving a stable dose-response curve across concentrations and accounting for IA as the dominant mixture component for both binary mixtures.

4.4 Discussion

Mixture interactions at the periphery of olfactory systems have been shown for many species. Suppressive effects (including hypoadditivity, see Figure 4.3) are observed more often than synergistic interactions (Cromarty and Derby, 1998; Ochieng et al., 2002; Duchamp-Viret et al., 2003; Rospars et al., 2008; Hillier and Vickers, 2011; Su et al., 2012). Suppressive mixture effects are also observed perceptually, and some of these could be linked to ORN physiology (Bell et al., 1987; Brodin et al., 2009; Chaput et al., 2012). Some of these suppressive mixture effects may arise from agonists and antagonists competing for

a common receptor-binding site (Araneda et al., 2000; Oka et al., 2004). Our data also show an example of likely agonist competition, resulting in suppressive effects for all three binary mixtures tested. These effects were fully explained by a model of syntopic interaction. Syntopic interaction describes the competition of two agonistic ligands for binding at a common or two overlapping receptor-binding sites (Neubig et al., 2003). Syntopic interaction leads to hypoadditivity or stronger suppressive effects at high concentration, whereas those competitive effects are absent at low concentrations with sufficient free binding sites where mixture responses match "linear interpolations" of their component responses (modeled responses in Figure 4.5).

The model for syntopic interaction is sufficient to explain the data that we measured. Nevertheless, this does not exclude that under other conditions, either for different odors or other receptor cells, additional mechanisms of mixture interactions may occur. Such mechanisms could include multiple binding sites on one receptor, multiple second-messenger cascades, multiple receptors on one cell (e.g., the receptor cell studied here also expresses receptor Or22b in addition to Or22a although no active role for Or22b has been shown yet), or interactions between neurons within one sensillum (e.g., ephaptic effects; Boekhoff et al., 1994; Cromarty and Derby, 1997; Dobritsa et al., 2003; Vermeulen and Rospars, 2004; French et al., 2011; Su et al., 2012). Some receptor cells show inhibitory responses to some odorants (reverse agonists), in which cases mixture interactions need to be analyzed and modeled differently (Boekhoff et al., 1994; Kang and Caprio, 1997; de Bruyne et al., 1999, 2001; Duchamp-Viret et al., 2003; Schuckel et al., 2009; Turner and Ray, 2009).

Or22a has a broad response profile with strong responses to many fruity odors, increasing the likelihood that mixture interactions occur in a natural environment. In more selective receptors, for example, Or92a with 2,3-butanedione as dominant ligand (Galizia et al., 2010), syntopic interactions may not be relevant under natural conditions. However, even Or92a has several weak ligands, so that this scenario needs to be tested specifically.

Syntopic interactions may also help the brain to create odor-concentration invariance. For example, a fruit fly that smells a banana should be able to identify this banana also when the scent gets stronger as it approaches the source. Odor-concentration invariance has been shown in behavior and physiology for different species and sequential ORN recruitment, and network effects in the brain are thought to underlie this capacity (Sachse and Galizia, 2003; Uchida and Mainen, 2007; Root et al., 2008; Asahina et al., 2009; Cleland et al., 2012). Generally, the dose-response curve to an odor follows a sigmoidal shape. However, in the absence of interactions, "linear interpolation" predicts that dose-response curves become less predictable because of

the occurrence of "kinks" as in the calculated IA.EB mixture response curve (Figure 4.5). With syntopic interaction, however, responses to mixtures follow sigmoidal dose-response curves just as single compounds, so that the brain can use the same algorithms for concentration invariance for all odors, be they pure substances or mixtures.

Furthermore syntopic interaction helps to set the working range of receptors. The single receptor measured in this study is only a small part of the whole ensemble that consists of all the activated and non activated ORNs in response to an odor. In olfactory brain areas like the antennal lobe and the olfactory bulb, this ensemble response is shaped by a lateral network generating further mixture interactions (Giraudet et al., 2002; Sachse and Galizia, 2002; Tabor et al., 2004; Silbering and Galizia, 2007; Olsen and Wilson, 2008; Root et al., 2008; Kuebler et al., 2011). If responses to mixture components would add up linearly ("linear interpolation"), many naturally occurring odors with tens or hundreds of components might quickly lead to saturated receptor cell output, thus reducing the coding capacity of the system. Our data strengthen the view that when studying mixture processing in brain networks, syntopic interaction at the periphery needs to be taken into account, even in the absence of chemical or physiological interactions.

The majority of odors consist of many chemical substances that occur together. The scent of banana, for example, was reported to contain 152 components, and Jordán et al. (2001) identified 26 substances in the headspace of fresh fruit. Is any of these the "main component" of banana, or is banana only created by the characteristic mixture? To humans, the most concentrated component in banana (HE) smells like green apple. Following the components in order of concentration, we have to reach IA (rank 7, Figure 4.1) to find a substance that by itself reminds us of banana, even though we are by no means anosmic to the higher ranked components (Jordán et al., 2001). Honeybees have been shown to learn mixtures *via* the selection of a few key components rather than learning the full bouquet (Reinhard et al., 2010). Thus, at least in some cases, certain mixture components are more salient than others, which raises the question about the responsible mechanisms. Here we show a case study where an effect similar to key component selection happens at receptor neuron level, by syntopic interaction. In this example, the Drosophila receptor Or22a "perceives" the banana-like mixture and its intermediate component IA as being equal even though there are both better and more concentrated ligands in the mixture.

4.5 Acknowledgments

We thank Sheree Pfeiffer for help with the measurements.

Chapter Five

Mixture effects on the antenna of Drosophila melanogaster

Abstract

Olfactory sensory systems usually have to deal with complex mixtures rather than with monomolecular odorants. Each component of a mixture might elicit a response pattern of differentially activated olfactory sensory neurons when presented alone, in mixtures these response patterns can overlap and interact, resulting in mixture interactions. Here we screened for mixture interactions in the periphery of the *Drosophila melanogaster* olfactory system. We measured responses of 100 mixture–olfactory receptor neuron combinations *via* calcium imaging on the antenna of fruit flies. We quantified mixture interactions and analyzed individual mixture-response traces as well as principle component trajectories of ensemble responses. We found that strong mixture interactions, namely synergism and suppression were rare and most mixtures produced weak (hypoadditivity) or no interactions. We found two cases of synergisms, both in a specialist receptor neuron with a narrow response profile. On a population level many mixtures were dominated by one component while others covered distinct areas of the receptor space.

5.1 Introduction

Almost all natural odors appear as mixtures of variable complexity. In many cases, the neuronal response to odor mixtures can not be predicted from the responses to the single components, instead complex interactions can happen such that the presence of one component suppresses or enhances the response to another component (Duchamp-Viret et al., 2003; Tabor et al., 2004; Rospars et al., 2008). Many of these mixture interactions are generated within brain networks like the insect antennal lobe (AL) (Silbering and Galizia, 2007; Kuebler et al., 2011). However, mixture interactions also appear in the olfactory periphery like the insect antenna (Hillier and Vickers, 2011; Münch et al., 2013; Chapter 4).

The majority of interactions found in the olfactory periphery are of a suppressive nature, i.e. the response towards the mixture is equally strong or weaker than the response elicited by the stronger component alone (Derby et al., 1991). Many of these suppressive interactions can be explained by syntopic interactions, i.e. the ligands competing for a single receptor binding site (Münch et al., 2013; Rospars et al., 2008; Neubig et al., 2003). Mixture responses that are much stronger than expected from the single components responses are called "synergistic". In the periphery these responses are almost exclusively found in pheromone sensitive neurons (Ochieng et al., 2002; Hillier and Vickers, 2011).

Most olfactory systems from invertebrates to vertebrate share some common features about the way they are coding odorants. A given odor molecule will almost always be a ligand for more than one olfactory receptor neuron (ORN) and thus elicit a combinatorial activation over the whole ensemble of ORNs. Typically the activation patterns for different ligands overlap (Friedrich and Korsching, 1997; Malnic et al., 1999), and mixing different ligands together will elicit peripheral mixture interactions which will additionally shape the ensemble response and thereby directly modify the input the brain receives (Cromarty and Derby, 1998; Duchamp-Viret et al., 2003; Rospars et al., 2008; Hillier and Vickers, 2011; Münch et al., 2013). Thus understanding peripheral mixture interactions is an important first step to understand odor coding in the brain.

In order to identify and classify peripheral mixture interactions we performed a screening with binary mixtures for single ORN classes on the antenna of *Drosophila melanogaster*. Using two modified, synchronized headspace autosamplers for stimulations, we were able to create binary mixtures from single components "on the fly". In addition to mixtures we also measured responses to their individual components in single and double concentrations to define expected mixture responses and identify possible mixture interactions. We performed in *vivo calcium* imaging of identified ORN types and analyzed response values as well as response dynamics at the level of individual ORNs and at the level of ORN ensemble responses.

5.2 Material & Methods

Animals

All recordings were performed on female *Drosophila melanogaster* expressing the calcium reporter G-CaMP 1.3 (Nakai et al., 2001) or G-CaMP 3 (Tian et al., 2009) in specific sets of olfactory receptor neurons under the control of the

GAL4-UAS expression system. UAS-GCaMP 1.3 flies were provided by Jing Wang, University of California, San Diego, La Jolla, CA; UAS-GCaMP 3.0 flies were provided by Loren L. Looger, Howard Hughes Medical Institute, Janelia Farm Research Campus, Ashburn, Virginia. Stable GAL4-UAS fly lines were of the following genotypes: P[UAS:GCaMP1.3]; P[GAL4:X] (X being one of Or10a, Or13a, Or22a, Or47a), and w;P[Or56a:GAL4]; P[UAS:GCaMP3]attP40.

Flies were kept at $25\,°C$ in a 12/12 light/dark cycle. Animals were reared on standard medium ($100\,mL$ contain: $2.2\,g$ yeast, $11.8\,g$ of sugar beet syrup, $0.9\,g$ of agar, $5.5\,g$ of cornmeal, $1\,g$ of coarse cornmeal and $0.5\,mL$ of propionic acid).

Calcium imaging

Calcium imaging was performed with a fluorescence microscope (BX51WI, Olympus, Tokyo, Japan) equipped with a $50\times$ air lens (Olympus LM Plan FI 50×/0.5). A CCD camera (TILL Imago, TILL Photonics, Gräfelfing, Germany) was mounted on the microscope recording with 8×8 pixel on-chip binning resulting in 80×60 pixel sized images. For each stimulus recordings of $20\,s$ at a rate of $4\,Hz$ were performed using TILLvisION (TILL Photonics, Gräfelfing, Germany). A monochromator (Polychrome II, TILL Photonics, Gräfelfing, Germany) produced excitation light of $470\,nm$ wavelength which was directed onto the antenna *via* a $500\,nm$ low-pass filter and a $495\,nm$ dichroic mirror, emission light was filtered through a $505\,nm$ high-pass emission filter. Calcium imaging of the ALs was performed on the same setup using a 40× water immersion lens (Carl Zeiss W Plan-APOCHROMAT 40×/1.0 DIC).

Odorant preparation

Odorants were purchased from Sigma-Aldrich in the highest purity available. Pure substances were diluted in $5\,mL$ mineral oil (Sigma-Aldrich, Steinheim, Germany). Odorants were applied at 10^{-3} dilutions, reference odorants at 10^{-2}. Odors were prepared in $20\,mL$ headspace vials sealed with a Teflon septum (Axel Semrau, Germany). A set of five diagnostic odorants from Silbering et al. (2008) was applied when recording set II to improve glomerulus identification. See Table 5.2 for information on all used odorants and the abbreviations used in the text.

Stimulus application

Stimuli were applied using two computer controlled autosamplers (Twin-PAL, CTC Swizerland). Each autosampler injected $2\,mL$ of headspace in two $1\,mL$

TABLE 5.1: Table of odorants and concentrations used in the experiments together with their Chemical Abstracts Service (CAS) number and the abbreviated code used in the text

Set	Name	Code	CAS	Dilution
SetI	2-pentanol	PO	6032-29-7	10^{-3}
	isopentyl acetate	IA	123-92-2	10^{-3}
	ethyl butyrate	EB	105-54-4	10^{-3}
	furfural	FF	98-01-1	10^{-3}
	phenethyl alcohol	PA	60-12-8	10^{-3}
SetII	geranyl acetate	GA	105-87-3	10^{-3}
	propanal	PL	123-38-6	10^{-3}
	Z3-hexenol	ZL	928-96-1	10^{-3}
	ethyl (S)-(+)-3-hydroxybutanoate	EH	56816-01-4	10^{-3}
	acetic acid	AA	64-19-7	10^{-3}
reference odorants	butanol		71-36-3	10^{-2}
	hexanol		626-93-7	10^{-2}
	hexyl acetate		142-92-7	10^{-2}
	ethyl propionate		105-37-3	10^{-2}
	3-octanol		589-98-0	10^{-2}
	butyl acetate		123-86-4	10^{-2}
diagnostic odorants	pentyl acetate		628-63-7	10^{-6}
	1-octen-3-ol		3391-86-4	10^{-5}
	E2-hexenal		6728-26-3	10^{-4}
	ethyl hexanotae		123-66-0	10^{-6}
	ethyl 3-hydroxybutanoate		5405-41-4	10^{-6}

portions at timepoints $6\,\mathrm{s}$ and $9\,\mathrm{s}$. Injections were performed simultaneously with an injection speed of $1\,\mathrm{mL\,s^{-1}}$ into two separate arms of a y-shaped Teflon tube (inner diameter $2\,\mathrm{mm}$, length $47.5\,\mathrm{mm}$) containing a continuous stream of purified air. The combined air-stream (resulting in an air speed of $120\,\mathrm{mL\,min^{-1}}$) was directed onto the antenna of the fly *via* the outlet of the y-tube.

Using two modified autosamplers it was possible to perform mixture experiments without pre-mixed chemicals, excluding molecular interactions of ligands in solution and possible influence on individual headspace concentrations. Both components were injected at the same time, creating an "on the fly" mixture withing the stimulus tube. The accuracy of the mixture stimulus was tested with a photoionization detector (PID; Model 200a, Aurora Scientific, Rathmines, Ireland; see Figure 5.1).

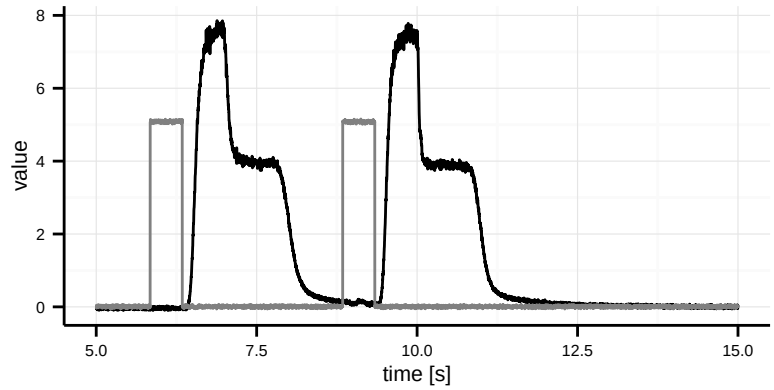

FIGURE 5.1: PID control measurement of stimulus dynamic during simultaneous injection with the Twin PAL system. The measurement was performed with 2-heptanone. *gray line* indicates the injection signal, the *black line* indicates the PID measurement. Note that the injection-signal pulse lasted only for 500 ms but the syringe injection as controlled by the PAL system lasted for 1000 ms. It took ~ 600 ms from the injection signal till the odorant reached the PID.

Five odorants were presented in a row interspaced by solvent control, room air control and an OR specific reference odorant. After each injection the autosampler syringe was flushed with purified air for at least 30 s. The syringes were washed with pentane (Merck, Darmstadt, Germany), heated up and flushed with purified air after each block of odorants automatically.

Odor vials were labeled with bar-codes containing odor and concentration information. Bar-codes were scanned and recorded by the autosampler system upon each stimulation automatically.

A setup specific delay for the odorant to reach the antenna after executing the injection protocol was calculated to be ~ 600 ms long from the data shown in Figure 5.1. Based on this, Stimulus begin was shifted three frames for all analyses.

Data analysis

Data analysis was performed using custom written routines in IDL (ITT VIS, USA) and R (R Development Core Team, 2013).

As long as animals showed stable responses to the reference odor measurements were included into the analysis. Recorded movies were manually corrected for movement artifacts, and an area of interest was defined for the parts of the antenna that showed fluorescence increase upon stimulation. For AL recordings the centers of visually identified glomeruli were marked and an area with a radius of four pixels around that spot was defined as area of interest. All calculations were done within these areas.

Relative fluorescence change was calculated as $\Delta F/F = ((F_i - F_0)/F_0) \times$

100 with F_i being the fluorescence at $frame_i$ and F_0 being the mean fluorescence of the first 10 frames of a recording.

The data was manually corrected for movement and an area of interest was defined on a false color coded image of the reference odor measurement, all calculations were done within that area. Response traces of the average pixel value within the area were exported.

To correct for the photo-bleaching of the dye, an exponential decay function of the form $A * exp^{-x/B} + C$ was fitted to the data using the `nls()` function in R. Because some odorant responses would not reach baseline within measurement time, the fit parameter B was estimated by an initial fit on the median mineral oil control response within each animal. For fitting three frames at the beginning of the time-trace and 44 frames during stimulus presentation were omitted and the pre-stimulus part of the recording was weighted 100 fold.

Response values were calculated as the mean response during 5 s after stimulus onset (corrected for setup specific stimulus onset delays) subtracted by the mean response during the first 2.5 s of a recording.

As ORN responses decrease over time a linear regression was fitted on each reference odor measurement within each individual animal. The value of this function at each corresponding timepoint was set to the value of the first reference odor presentation elicited.

In order to identify mixture interactions, i.e. responses that were unexpectedly weak or strong as compared to component responses, we defined an upper- and a lower-bound. As lower-bound we defined the response elicited by the stronger component at single concentration, the upper-bound as the strongest response elicited by any of the two components at single or double concentration. A mixture response was considered suppressive when it was significantly lower than the lower-bound and synergistic when it exceeded the upper-bound. As we were especially interested in strong mixture interactions (suppression and synergism; Figure 4.3) we performed one-sided tests against the respective bounds, not further discriminating between weak suppressive effects that lead to hypoadditivity (response equally strong as lower-bound) and additivity (no interaction; response between lower and upper-bound; Figure 4.3).

Plotting was performed using the R core functions and the ggplot2 package (Wickham, 2009).

5.3 Results

We performed calcium imaging experiments with two sets of odorants. Each set consisted of five odorants, and in a given set all possible binary combina-

tions of odorants were presented as mixtures. Responses elicited by the 20 resulting binary mixtures and their single components were measured for five ORN classes on the antenna and in the ALs of *Drosophila melanogaster*.

Excitatory mixture responses followed the stronger component

We measured 20 different binary mixtures on five different ORNs, resulting in a total of 100 mixture–ORN combinations measured. For 65 of these we tested whether their mean response during stimulation (see Methods) exceeded the respective upper-bound or was lower than the lower-bound. The remaining 35 mixture–ORN combinations contained at least one inhibitory response. Measurements with inhibitory components were excluded from this analysis as inhibitory responses do not allow to define a clear non-interaction hypothesis. Of the 65 mixture responses tested five exceeded their respective bounds (one-sided, paired Wilcoxon signed rank test, $P < 0.05$, $n = 5\text{-}17$). Figure 5.2 shows relative deviations of mixture responses from respective lower (A) or upper-bounds (B). Mixtures scatter closely around the lower-bound, meaning they were similar strong to the response elicited by the stronger mixture component (hypoadditivity) or slightly stronger (additivity). Only three mixture responses were significantly weaker than their respective lower-bounds, indicating suppression. Note that for two of the found suppressions (EH.AA and PL.AA in Or10a), although the response of all components during stimulation was excitatory, inhibitory post-stimulus responses could be observed for AA (Figure 5.2).

Two out of the 65 mixture responses were significantly stronger than their corresponding upper-bound and thus showed synergism (see Figure 5.2B; one-sided, paired Wilcoxon signed rank test, $P < 0.05$, $n = 5\text{-}17$). While the above described cases of hypoadditivity or suppression could be explained by competition of molecules for a single receptor binding site (Münch et al., 2013; Rospars et al., 2008), synergism cannot. Interestingly all three cases of synergism were measured in Or56a ORNs.

Looking at complete response traces, the vast majority of mixture responses followed the respective stronger component (Figure S16). For all mixtures where both components elicited a response when presented alone this meant: although active ligands were added, the ORN responses did not increase. Responses were certainly not saturated as the response of the stronger ligands increased with increasing concentration (Figure S16).

In summary, hypoadditivity or additivity were seen in the majority of mixtures with excitatory ligands, suppression and synergism were rare.

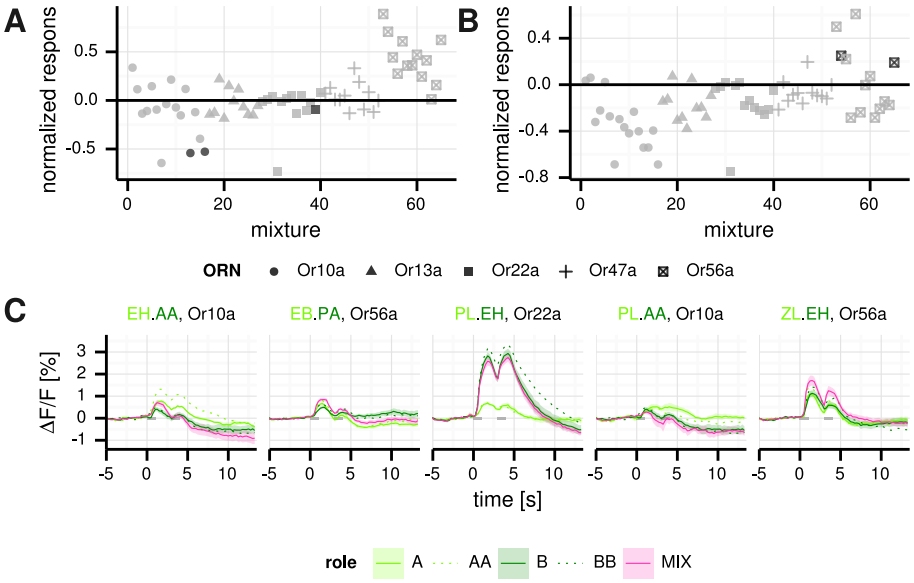

FIGURE 5.2: Scatterplot showing mean mixture-responses in relation to lower- (**A**) and upper-bound (**B**). Mixtures containing inhibitory components ($n = 35$) were excluded from this analysis. Lower and upper-bounds were set to zero for individual mixtures, mixture responses were rescaled accordingly. Bounds are indicated by horizontal lines. *Black* symbols indicate significant difference from respective bound (paired, one-sided Wilcoxon Signed Rank Test, $P < 0.05$, n = 5-17). **C** Mean response-traces of significant responses from A and B. *Shaded* areas indicate SEM, *solid lines* indicate component responses at single concentration (10^{-3} dilution), *dotted lines* indicate component responses at double concentration, *gray* dashes indicate stimulus pulses.

Inhibitory components dominate mixtures

Three of the used components elicited inhibitory responses from at least one ORN class measured (Figure 5.3). Inhibitory responses to AA were slow and long lasting, meaning they did not follow the double pulse and did neither return to baseline between the two stimulus pulses nor within the 20 s recording time. While AA responses were clearly inhibitory in Or13a, Or47a and Or56a, they had an initial excitatory component in Or22a and were biphasic in Or10a. Biphasic responses (excitatory responses with an inhibitory post-stimulus response) were observed for other odorant–ORN combinations (de Bruyne et al., 1999, 2001; Hallem et al., 2004; Galili et al., 2011; Chapter 3).

PL elicited inhibitory responses only in Or56a ORNs. Unlike AA, PL responses clearly resembled the stimulus dynamics, showing clear double peaks and returning to baseline direct after stimulation.

Responses towards FF were variable for all ORNs recorded. Responses recorded from Or22a and Or56a were excitatory in some, inhibitory in other animals. The mean responses recorded for FF at double concentration (2×10^{-3} dilution) were inhibitory for all ORNs (see dotted lines in Figures 5.3B and

S16). Strangely, FF inhibition could also be observed in unstained areas of the antenna. To check whether FF really evoked fluorescence decreases in unstained tissue, we stimulated antennae of Canton-S wildtype flies that did not express any calcium-reporter protein and observed weak "inhibition" (Figure S14). Thus fluorescence changes recorded for FF likely were a mixed signal originating from two independent sources: a calcium depending source and some other calcium-concentration unspecific source. Accordingly effects observed in FF containing mixtures have to be handled with care.

FF had an suppressive effect in Or10a and Or47a mixture responses, even when it did not elicit clear inhibition when given alone (Figure 5.3B). Inhibitory responses elicited by FF were more pronounced at an increased concentration (dotted violet lines in Figure Figure 5.3B). Thus at 10^{-3} dilution FF might already have bound but not inhibited these receptors, interfering with other molecules while not activating/inactivating the receptor on its own. In other cases the FF mixtures completely resembled the FF component trace (PA.FF in Or13a, Figure 5.3B), or the the mixture response looked like a pure subtraction of the component traces (PO.FF in Or22a, see Figure 5.3B).

PL was a fast inhibitory component for Or56a. Whether mixture traces with PL were inhibitory or excitatory seemed to depend on the strength of the excitatory component it was mixed with, with mixture responses becoming more excitatory with stronger excitatory components (Figure 5.3B). Mixing the "fast" inhibitory ligand PL (clear double peaks) with the "slow" inhibitory ligand for Or56a, AA (no double peaks, longlasting), led to a pure summation of both signals (Figures 5.3B and S15). The mixture trace showed long inhibition like measured for AA as well as clear double peaks as measured for PL alone.

AA elicited inhibition or inhibitory post-stimulus responses from all five tested ORNs (Figures 5.3A). The strongest inhibition was found for Or13a, Or22a and Or56a. In all three cases the response did not follow the double-pulse stimulus but showed an fluorescence decrease that continued beyond stimulation. AA dominated most of the mixture response traces (Figure 5.3B). This changed for Or13a and Or22a when AA was mixed with ZL or EH, where we recorded excitation during stimulation. However, the post-stimulus phase was still dominated by the inhibitory response of AA (Figures 5.3B).

ORN ensemble responses to mixtures follow the stronger component

For each mixture and its components we performed a principal component analysis (PCA). PCs were calculated in the five OR dimensions for each individual mixture together with its components. PC trajectories were plotted for

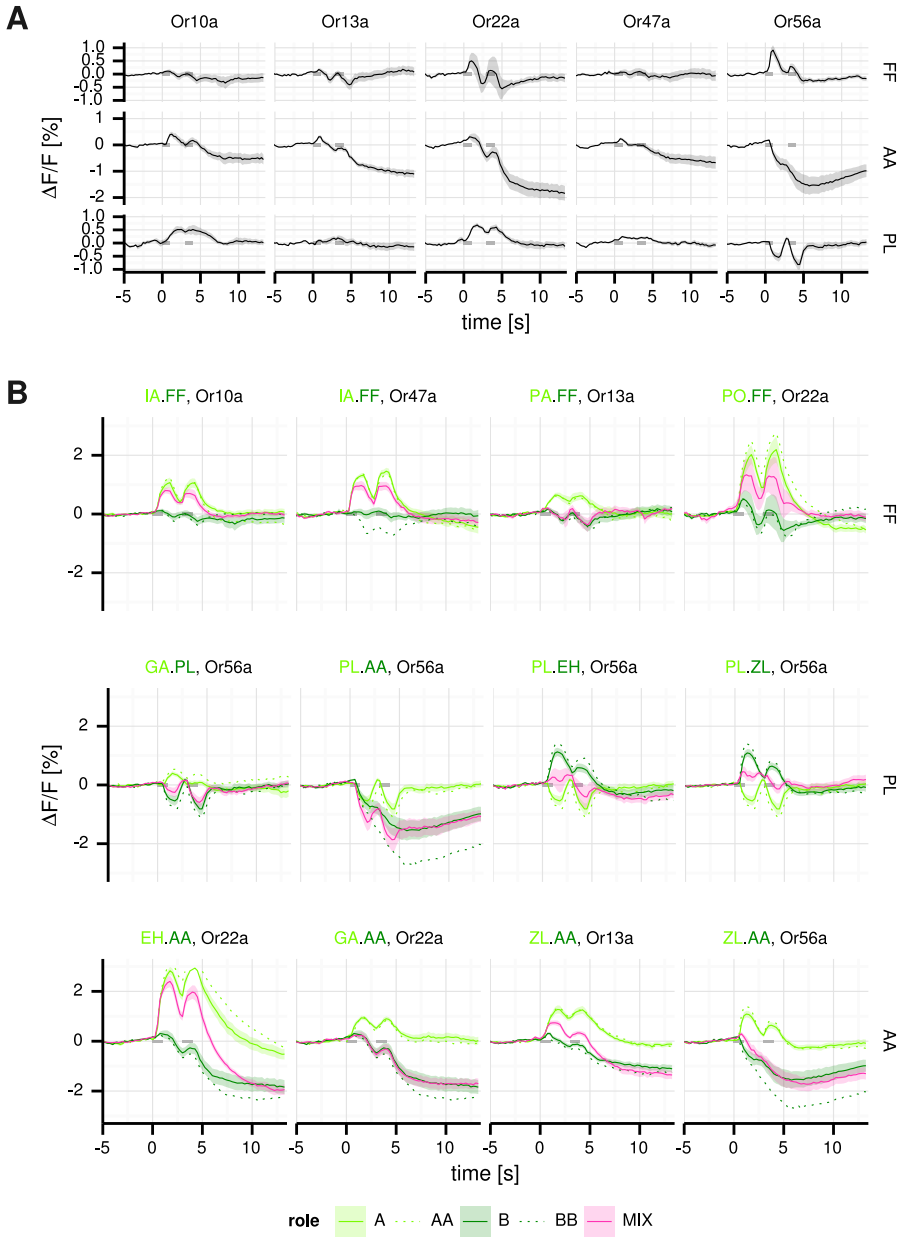

FIGURE 5.3: Components that elicited inhibitory responses. **A** Mean response traces of inhibitory components across receptors ± SEM (*gray* shaded areas; n = 6–17). **B** Mean response traces of mixtures containing inhibitory components (n = 6–17). *Shaded* areas indicate SEM, *solid lines* indicate component responses at single concentration (10^{-3} dilution), *dotted lines* indicate component responses at double concentration, *gray* dashes indicate stimulus pulses.

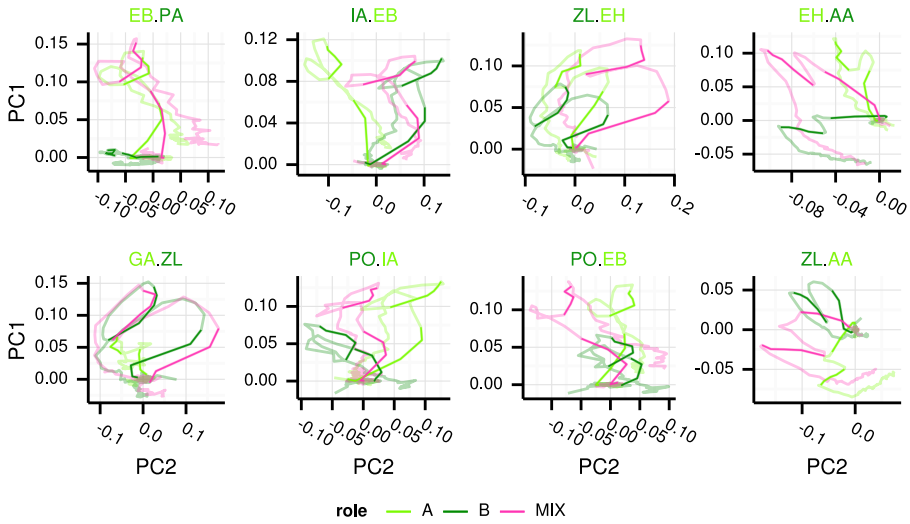

FIGURE 5.4: Selected PCA trajectories. Rotations were calculated in the five OR dimensions for each individual mixture together with its components. Darker parts of the trajectories indicate stimulus-pulses. For all PCA trajectories see Figure S17.

PC 1 & 2. Approximately half of the mixture PCA-trajectories followed the trajectory of one component (EB.PA and GA.ZL in Figure 5.4; see also Figure S17). This resembled the observation from the individual traces and was likely due to many "stronger" components consistently being the "stronger" component across receptors (Figure S16). In other cases the mixture trajectories were located between the component trajectories intermediate to the components (IA.EB and PO.IA in Figure 5.4), or covered areas of the receptorspace distinct from their component traces (ZL.EH and PO.EB in Figure 5.4). As expected from the consistently observed late inhibitions for AA, some mixture trajectories followed one component initially and then deviated towards AA (EH.AA and ZL.AA in Figure 5.4). These two mixtures elicited biphasic responses in individual ORN response traces (Figure 5.3B).

No indication for across ORN interactions within individual sensilla

Su et al. (2012) showed that ORNs sharing the same sensillum do influence each other *via* ephaptic effects, as was discussed theoretically before (Vermeulen and Rospars, 2004). We asked whether the amount of suppression we recorded for binary mixtures was correlated to the sum of activations of neighboring neurons. We correlated the relative suppression we found for each binary mixture in each ORN to the sum of the responses any of the two com-

ponents would elicit in any neighboring neuron. Data about the neighboring neuron activation was taken from the DoOR-database (Galizia et al., 2010), the relative suppression was calculated as:

$$suppresion_{rel} = \frac{lowerbound - mixtureresponse}{lowerbound}$$

We found that relative suppression and activation of neighboring neurons was weakly anti-correlated (Pearson's correlation coefficient = -0.37, $p = 1.5 \times 10^{-4}$). This suggests that suppressive mixture interactions did reflect ephaptic interactions between different ORNs of the same sensillum, but rather reflected syntopic or other interactions between different ligands at the same ORN (Münch et al., 2013; Rospars et al., 2008). Note however that in the DoOR-database the response data for neighboring neurons is not complete and taking the sum of activations is only a weak estimation of neighboring neurons activation that ignores possible mixture effects.

Comparison with ORN responses in the AL

We also measured responses to the mixtures in ORNs inside the ALs. We were able to identify five glomeruli, four of which we measured the corresponding ORN on the antenna.

ORN responses from AL and antenna were correlated, but they were not identical (Pearson's product-moment correlation / t-test, $r = 0.72, P < 0.05$), Figure 5.5A). The biggest difference between antennal and AL responses was that we did not record any inhibitions in the AL. Components that elicited fluorescence concentration decreases in ORNs on the antenna evoked fluorescence increases in the same ORNs in the AL (Figure 5.5C).

On the other hand, long lasting activations of ORNs by some odors was conserved in the AL (PO.EB in Or22a, Figure 5.5 D). For some ORN–odorant combinations ORN activation time was increased in the AL (GA.EH in Or13a, Figure 5.5 D), for others long lasting activation was only measured in the AL (ZL.EH in Or47a, Figure 5.5 D).

We computed odor distance matrices on the mean of the response during stimulation. Euclidean distances were computed for the AL and the antenna data using the four ORNs that could be mapped to their corresponding glomeruli as dimensions. Odor distances between antenna and AL were only weakly correlated, further demonstrating the differences between antennal and AL ORN responses (Pearson's product-moment correlation / t-test, $r = 0.46, P < 0.05$, Figure 5.5B).

We recorded odor responses for 20 binary mixtures and their components in five different ORN classes on the *Drosophila* antenna. We found the majority

of mixtures to evoke responses that were located within the expected bounds. In 100 ORN–mixture combinations we found three cases of mixture suppression and two cases of mixture synergism. The majority of mixtures evoked responses that followed the stronger component. Measurements of the same classes of neurons in another neuropile, the AL, was correlated but did not show any inhibitory responses.

5.4 Discussion

When olfactory neurons are stimulated with a mixture of different ligands the resulting activation is not always possible to predict from the components responses (Rospars et al., 2008; Silbering and Galizia, 2007; Duchamp-Viret et al., 2003; Tabor et al., 2004; Hillier and Vickers, 2011). The expected response elicited by two excitatory ligands in the absence of all possible interactions would be a "linear interpolation" of the components responses along their dose-response curves (Tabor et al., 2004), leading to additivity. However, ligands can interact at different levels and as soon multiple ligands are presented in a mixture they are likely to interact *via* competitive or non-competitive mechanisms, leading to different types of mixture effects. Here we defined lower- and an upper-bounds for an expected mixture response. We termed the mixture responses that were weaker than the lower-bound "suppression" and those that were stronger than the upper-bound "synergism". When excitatory and inhibitory components are mixed, bounds are not easily defined as the mixture response might gather completely new response dynamics, with excitatory responses being sharpened or completely suppressed (Su et al., 2011; Schuckel et al., 2009).

Mixture interactions occurred in five out of 65 mixtures. Three of them were suppressive, i.e. the mixture responses were significantly weaker than the lower-bound, and two were synergistic, i.e. they were stronger than the upper-bound. The remaining mixture responses were located between lower and upper-bound showing additivity or hypoadditivity. Individual mixture traces tended to follow the traces of their stronger components closely, indicating hypoadditive mixture responses.

Suppression and hypoadditivity are both suppressive effects, with either the weaker component suppressing the stronger, or vice versa. Suppressive effects are the most commonly found mixture-effects in peripheral olfactory systems of various species (Hillier and Vickers, 2011; Derby et al., 1991; Silbering and Galizia, 2007; Kang and Caprio, 1997). Several mechanisms are sufficient to explain suppressive mixture effects. We recently described cases of hypoadditivity in a complex mixture that could be fully explained by syntopic inter-

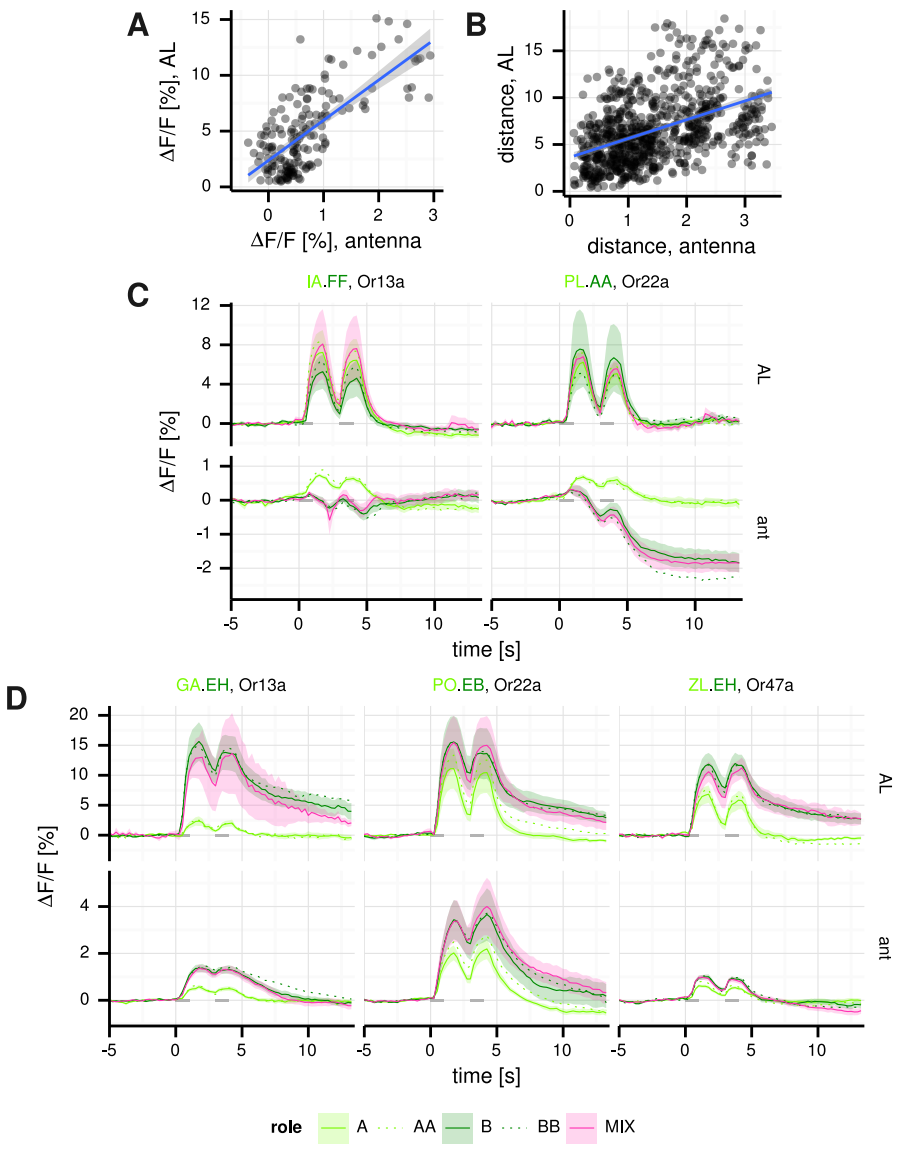

FIGURE 5.5: Antenna/AL comparison. **A** mean responses of antenna and AL recordings plotted against each other. *Blue* line indicates a linear model fitted on the data. Responses were correlated (Pearson's product-moment correlation / t-test, $r = 0.72, P < 0.001$). **B** Euclidean distances between odorants in antenna and AL recordings plotted against each other. Distances were weakly correlated (Pearson's product-moment correlation / t-test, $r = 0.46, P < 0.001$). **C** and **D** Comparison of response traces of antenna and AL recordings (n = 4–7 for AL and n = 6–13 for antenna traces). *Shaded* areas indicate SEM, *solid lines* indicate component responses at single concentration (10^{-3} dilution), *dotted lines* indicate component responses at double concentration, *gray* dashes indicate stimulus pulses.

actions (Münch et al., 2013). Syntopic interaction describes the competition of multiple agonists for binding a common or two overlapping receptor binding sites (Rospars et al., 2008; Neubig et al., 2003). Competition for receptor binding sites increases with increasing amount of molecules, and often there is no effect at lower concentrations, while hypoadditivity occurs predominantly at medium concentrations and suppression at high mixture concentrations. In the present study we used a medium dilution of 10^{-3} for all components which could explain the low number of suppressions found. Ephaptic modulation is another mechanism that could explain suppressive effects. Ephaptic modulation in insect olfaction means the electrical coupling of two neurons *via* the sensillum lymph (Vermeulen and Rospars, 2004; Su et al., 2012). However, we found no evidence for ephaptic modulation in our data. Also we did not record the full dose response curves necessary to test for syntopic interactions. Thus the exact mechanism for the suppressive effects we found remains elusive.

For two mixtures of excitatory components we found synergistic effects with the mixture responses being stronger than the respective upper-bound. Mixture synergism is an effect that is rarely found in the olfactory periphery. Most cases come from the specialized moth pheromone system and are described between sex-pheromone components ad host plant odors (Ochieng et al., 2002; Hillier and Vickers, 2011). Note that some studies use the terms synergism and additivity (Duchamp-Viret et al., 2003) interchangeably. In order to explain synergistic effects non-competitive mechanisms are needed in addition to the ones discussed above. A ligand binding to one receptor binding site could facilitate the binding of another ligand to a second binding site at the same receptor, a mechanism known as positive cooperativity. Both ligands could also activate two different receptors at the same cell or activate different intracellular second messenger cascades. An ionotropic as well as a metabotropic function of insect olfactory receptors is discussed, which could in theory both be stimulated differentially by different ligands (Wicher et al., 2008; Sato et al., 2008; Schuckel et al., 2009).

Both cases of synergism we found were recorded in Or56a expressing ab4B neurons. These neurons express at least two other ORs, the ubiquitously expressed co-receptor ORCO and Or33a (Fishilevich and Vosshall, 2005). ORN activation by ORCO agonists was recently described (Jones et al., 2011). ORCO activation in our case is not likely as ORCO should have also been activated by the same mixtures in other ORNs, leading to additional synergisms. Responses of Or33a were analyzed by Kreher et al. (2008) in the empty neuron system (Dobritsa et al., 2003), none of the odorants they tested elicited strong responses. However, the odorants that lead to synergism here have no overlap with the odorants tested by Kreher et al. (2008).

Three odorants in our set elicited inhibitory responses from at least one ORN. Inhibitions elicited by FF were to some degree ORN unspecific as weak inhibitory responses could be recorded in unstained wildtype CantonS flies as well. The origin of these signal could not be determined, but for example imaging of cell intrinsic signals is well established for measuring olfactory bulb activity (Rubin and Katz, 1999; Spors and Grinvald, 2002). However, even if the signal was cell activity specific, the type of cell that was recorded can not be distinguished.

AA and PL elicited inhibitory responses with different dynamics. While PL elicited fast inhibition from Or56a ORNs only, AA elicited different amounts of inhibition from all ORNs. In contrast to PL, responses of AA were slow and longlasting. The difference in dynamics could arise from different binding and activation properties of the ligands or different odorants might reach the antenna with different delays due to physical interactions with the stimulus tube. Differences in stimulus dynamics and their effect on response dynamics was elaborated by Martelli et al. (2013). Stimulus dynamics for individual odors were not analyzed here, the fact that AA response dynamics were longlasting and slowly decaying in all receptors tested is indicative for a "slow" stimulus dynamic. Mixtures of excitatory components with "slow" inhibitory components were also analyzed by Su et al. (2012). They described excitatory mixture responses that were sharpened by the addition of an inhbitory component. Our data confirms this observation for cases where the mixture responses were still excitatory. Moreover our double stimulus regime shows that due to the slowly increasing inhibitory response, the influence of the inhibitory component on the mixture response continuously rises, affecting the second peak stronger than the first one. The rising influence of AA on mixture responses is also visible in PCA trajectories across ORNs, where the mixture trajectory follows the excitatory component initially and then deviate towards AA. Longlasting inhibitions might also have substantial influence on subsequent stimuli and were shown to influence innate behaviors in fruit flies and mosquitoes Turner and Ray (2009).

Several models by which a given ORN can respond with excitation or inhibition depending on the ligand are discussed. These models include competitive ones with a single receptor binding site involved (Hallem et al., 2004) as well as non-competitive ones with several receptors or multiple receptor binding sites participating (Schuckel et al., 2009). For crustaceans it was shown that two different second messenger pathways are involved in excitation and inhibition (Boekhoff et al., 1994). In our data of mixed polarity mixtures we can not distinguish between competitive or non-competitive effects. However, two inhibitory ligands with different dynamics (AA, slow and PL, fast) did not seem

to influence each other in the mixture at Or56a ORNs. This could indicate non-competitive binding of both ligands. For non-competitive activation of Or56a neurons argues again the co-expression of Or33a. An activation of ORCO by AA could also be possible as we recorded similar longlasting inhibitions for all ORNs measured. Testing Or33a and ORCO specifically with these odorants would be interesting.

Inhibitory responses from *Drosophila* ORNs were described in multiple studies using different measurement techniques (de Bruyne et al., 1999; Pelz et al., 2006; Turner and Ray, 2009). Due to the usually low rates of spontaneous firing of *Drosophila* ORNs, inhibition is less obvious from AP rates as measured by single-sensillum recordings (Su et al., 2011; Hallem et al., 2004). Thus for olfactory coding inhibitory components may play a stronger role when present in mixtures as when appearing as mono molecular odorants.

Responses recorded from ORNs at two levels of the olfactory system, the antenna and the antennal lobe, were correlated but not identical. This is not surprising as ORNs get presynaptic modulatory input at the level of the ALs (Olsen and Wilson, 2008; Root et al., 2008). What was surprising was that we did not record any inhibitory responses from ORNs in the AL. Inhibitory ORN responses in the AL of *Drosophila* were successfully recorded by calcium imaging before (Pelz et al., 2006). Presynaptic modulation of ORN axon terminals is mediated by GABAergic presynaptic inhibition (Olsen and Wilson, 2008; Root et al., 2008), thus it cannot explain the mismatch between AL and antenna in our recordings as an excitatory mechanism would be necessary. A possible explanation for the missing inhibitions could be scattered light from neighboring glomeruli. We used a ORCO-GAL4 to drive the expression of G-CaMP in most of the glomeruli (Larsson et al., 2004). Scattered light was problematic for the detection of mixture suppressions in ORCO stained ALs in a previous study (Silbering and Galizia, 2007). Further recordings with a subset or a single glomerulus stained or using confocal microscopy in order to exclude the influence of scattered light from neighboring glomeruli could give more insight.

Some of the inhibitions we recorded for AA did not match data from Hallem and Carlson (2006) who recorded weak excitations for AA in Or10a, Or22a and Or47a *via* single sensillum recordings. These weak excitations could however reflect the initial excitatory component we observed in AA recordings.

In olfactory systems odor identity is encoded spatially in the ensemble of activated neurons (Friedrich and Korsching, 1997; Malnic et al., 1999; Sachse et al., 1999; Uchida et al., 2000; Hallem and Carlson, 2006; Galizia et al., 2010) as well as temporally in the specific response dynamics an odorant elicits in a receptor neuron (DasGupta and Waddell, 2008; Martelli et al., 2013; Nagel and Wilson, 2011). The same is true for odor mixtures which often elicit

ensemble responses and response dynamics that are distinct from their component responses (Joerges et al., 1997; Johnson et al., 2010; Su et al., 2011).

On a perceptional level, when two odorants are presented as a mixture, the mixture percept may be dominated by one component (Reinhard et al., 2010) or it might blend into a new perfume (Jinks and Laing, 2001). Effects in mixture perception have been linked to ORN responses before (Bell et al., 1987; Brodin et al., 2009; Chaput et al., 2012). There is a good correlation between the perceived similarity between odors and the physiological similarity measured as across ORN responses (Guerrieri et al., 2005). We assessed the physiological similarity between mixtures and components by performing a principal component analysis leading to trajectories of ORN ensemble responses to mixtures and their components in a five-dimensional receptor space. Half of the mixture trajectories were dominated by one component which suggests a mixture percept that is dominated by one component. The other half of our data occupied distinct areas of the receptor space, either lying in between component traces or exceeding them. These distinct mixture trajectories could be the basis of perceptional odor qualities that are distinct from those of their components. These observations are visible in a receptor space that covers only five out of around 50 ORNs (Couto et al., 2005; Fishilevich and Vosshall, 2005), all the more a multi dimensional analysis of mixture response dynamics across the full receptor space of *Drosophila* would be very desirable. In order to test the functional relevance of mixture interactions and whether the physiological mixture–component similarities indeed match the perceived similarities it would be interesting to perform behavioral experiments.

General Discussion & Outlook

In this doctoral thesis I gathered new insights into different aspects that odor coding in the periphery of an olfactory system.

In Chapters 1 and 2 we assessed the ensemble code of the olfactory system of *Drosophila melanogaster*. We present the DoOR database, a tool that combines all published odor-response data and creates a representation of the up to date known *Drosophila* olfactome. DoOR provides a complete as possible view on response profiles of individual ORNs as well as on ensemble responses elicited by individual odorants. Even with all available data combined, there remain substantial gaps in the known *Drosophila* olfactome. In Chapter 2 we specifically fill some of these gaps by characterizing eight ORN classes.

The ORNs analyzed in Chapter 2 featured different tuning widths (Figure 2.10). Sharply tuned ORNs are often interpreted as being part of labeled line systems, not taking part in combinatorial coding but reliably signaling the presence of a specific odorant by their activation, and directly influencing specific behaviors. Or56a bearing ORNs are thought to be such a labeled line responding to geosmin exclusively (Stensmyr et al., 2012). Our method of calcium-imaging on the antenna of *Drosophila* revealed a distinguished response profile besides the way stronger geosmin responses. Thus although extremely sensitive to geosmin, Or56a could participate in combinatorial coding when geosmin is not present. Or56a response dynamics for single odorants and binary mixtures measured in Chapters 3 and 5 were odorant/mixture specific like for the other ORNs in this study, hence Or56a bearing neurons probably are part of ensemble codes for odor-identities other than geosmin.

The responses for different odorants in Chapters 1 and 2 were quantified as single response values per ORN. However, such a representation of spatial activation patterns is only a snapshot of a complex spatio-temporal ensemble response. In Chapter 3 we therefore characterized the temporal features of ORN responses. Prolonged activations and inhibitory post-stimulus responses create a post-stimulus ensemble response that is different from the response during stimulation but still odor-specific (Galili et al., 2011). This is represented in the elevated mean Euclidean distance after stimulus offset in Figure 3.6. Response dynamics might convey odor quality information in the absence of an complete

ORN ensemble as flies with a single type of ORN are still able to differentiate between odorants (DasGupta and Waddell, 2008). Bees on the other hand are able to distinguish odorants that appear with only a few milliseconds delay (Szyszka et al., 2012). Thus, there might be cases when the odor-quality information is decoded from the response-dynamics. Discrimination experiments with odorants that elicit similar stimulus-responses but different post-stimulus responses could shed some light on the importance of response dynamics for odor discrimination.

Single response values for ligand–ORN combinations can be achieved in different ways and often vary from study to study. Researchers compress the time-traces which they measure to single values by quantifying the response amplitude or the mean response during stimulation. The raw data however contains the complete time information, and the DoOR framework could be extended to hold complete time-traces. This would not only enable us to compare temporal dynamics between different recording techniques but it could also be used to create snapshot ensemble responses by extracting response values (e.g. response amplitude or mean response during or after stimulation) from the raw data with a consistent method. A difficulty of this approach lies in the different stimulation protocols used in different studies.

In real life, odor-coding only rarely involves mono-molecular odorants but complex mixtures of different chemical substances. Coding mixtures adds more complexity as responses of single mixture components overlap and interfere, creating so-called mixture interactions (Duchamp-Viret et al., 2003; Silbering and Galizia, 2007; Kuebler et al., 2011). The mixtures analyzed in Chapters 4 and 5 evoked predominantly mixture responses of additive or hypoadditive nature. Strong effects like mixture suppressions or mixture synergisms were only observed in few cases. What does this mean for odor coding on the antenna?

As discussed in Chapter 4, suppressive effects (including hypoadditivity) might set the working range of an ORN, preventing oversaturation when natural mixtures with tens or hundreds of possible ligands reach an ORN. The cases of hypoadditive mixture effects in Chapter 4 could all be explained by syntopic interaction at a single receptor-binding site. We demonstrated that syntopic interaction allows additivity of mixture responses at lower concentrations with enough free binding sites at the ORN available, and it explains hypoadditivity at medium- and suppression at high ligand concentrations. Thus this simple mechanism could account for a common gain-control mechanism in the olfactory periphery that gets stronger with increasing ligand concentration. Assuming that the majority of components in Chapter 5 interacted syntopically, the low number of strong suppressions found could be based on the medium ligand concentrations we used in this data set.

Mixture synergisms were also rare in Chapter 5. Synergistic effects can not be explained by syntopic interactions but require non-competitive mechanisms that specifically enhance each other. Synergistic effects are in general found less often than suppressive effects in the periphery of olfactory systems (Hillier and Vickers, 2011; Derby et al., 1991; Silbering and Galizia, 2007; Kang and Caprio, 1997). Implementing such non-competitive mechanisms makes sense when for example the coincident occurrence of two ligands is ecologically relevant. Synergisms are described for specialized moth ORNs, happening between moth pheromones and host-plant volatiles (Ochieng et al., 2002; Yang et al., 2004). Having the host-plant volatiles enhancing the pheromone response on single ORN level would increase the saliency of the pheromone and might enhance behavioral output (Ochieng et al., 2002). We found mixture synergism for two mixtures in Or56a bearing neurons. Finding synergisms only in these neurons is interesting, as similar to pheromone sensitive ORNs, Or56a ORNs are narrowly tuned to a single compound. Given that Or56a neurons express an additional OR, simultaneous activation of both ORs could be a non-competitive basis for synergistic effects. However, we did not test binary mixtures with the best Or56a ligand geosmin but found the synergisms between weaker ligands. Recording binary mixtures with geosmin might yield interesting data.

When odors increase in concentration, the elicited ensemble response pattern changes as additional ORNs are recruited (Sachse and Galizia, 2003; Strauch and Galizia, 2012). Still olfactory systems have to be able to identify an odorant across concentrations. Odor concentration might for example increase when approaching an odor source while odor quality should stay the same. Different gain-control mechanisms mediating concentration-invariant coding have been described (Sachse and Galizia, 2003; Uchida and Mainen, 2007; Root et al., 2008; Asahina et al., 2009; Cleland et al., 2012). In Chapters 3 and 4 we found two additional mechanisms. In Chapter 4 we found syntopic interactions to possibly add to concentration-invariant coding as they created mixture dose-response curves of a sigmoidal shape just like general odor dose-response functions. The “linear interpolation” model on the other hand predicts that dose-response curves become less predictable because of the occurrence of “kinks” (Figure 4.5). In Chapter 3 we show that the “peakiness” of odor responses was stable across a range of concentrations. Taken together gain-control seems to happen at different levels of the olfactory system and different mechanisms seem to underly concentration-invariant coding.

The DoOR database is not finished but is an ongoing project where we aim on continuously expanding both the data and the framework by adding tools and functions. Concentration information is not yet covered by DoOR. Many

studies include measurements at different ligand concentrations or even full dose-response curves but aligning them between studies is difficult. Stimuli are applied in different ways, such that air-speed and volume differ between studies and make it hard to define the absolute concentrations reaching the antenna. One approach to include concentration information in DoOR could be to use the ensemble responses for relative alignment between studies. For example, a given odorant at 10^{-2} dilution elicits responses in ORN A and B in study I but only in ORN A in study II. Although both studies used the same odorant dilution, the concentration reaching the antenna might have been higher in study I.

Including mixtures in DoOR would be more straight forward technically but lacks sufficient data. Including algorithms to predict mixture responses from component responses, using different models could be a way to include mixture information into DoOR.

Recently several studies used optimized sets of chemical descriptors to predict new ligands for ORs (Schmuker et al., 2007; Haddad et al., 2008; Boyle et al., 2013; Gabler et al., 2013). Implementing such algorithms into DoOR to fill the gaps in the olfactome computationally would be a valuable extension and could cut short the way towards the complete olfactome.

In the work at hand we demonstrated that odor coding by a spatial activation pattern is a simplification as activation patterns vary over time, and are influenced by concentration and mixture effects. The DoOR database provides a first glance at the "spatial" *Drosophila* olfactome and it is open for expansion by other dimensions of odor-coding.

Bibliography

Abaffy, T., Malhotra, A., and Luetje, C. W. (2007). The molecular basis for ligand specificity in a mouse olfactory receptor a network of functionally important residues. *Journal of Biological Chemistry*, 282(2):1216–1224.

Andersson, M. N., Schlyter, F., Hill, S. R., and Dekker, T. (2012). What reaches the antenna? how to calibrate odor flux and Ligand-Receptor affinities. *Chemical Senses*, pages 403–420.

Araneda, R. C., Kini, a. D., and Firestein, S. (2000). The molecular receptive range of an odorant receptor. *Nature Neuroscience*, 3(12):1248–55.

Asahina, K., Louis, M., Piccinotti, S., and Vosshall, L. B. (2009). A circuit supporting concentration-invariant odor perception in drosophila. *Journal of Biology*, 8(1):9–9.

Bell, G. a., Laing, D. G., and Panhuber, H. (1987). Odour mixture suppression: evidence for a peripheral mechanism in human and rat. *Brain Research*, 426(1):8–18.

Benton, R., Sachse, S., Michnick, S. W., and Vosshall, L. B. (2006). Atypical membrane topology and heteromeric function of drosophila odorant receptors in vivo. *PLoS Biology*, 4(2):e20–e20.

Benton, R., Vannice, K. S., Gomez-Diaz, C., and Vosshall, L. B. (2009). Variant ionotropic glutamate receptors as chemosensory receptors in drosophila. *Cell*, 136(1):149–62.

Bignetti, E., Cavaggioni, A., Pelosi, P., Persaud, K. C., Sorbi, R. T., and Tirindelli, R. (1985). Purification and characterisation of an odorant-binding protein from cow nasal tissue. *European Journal of Biochemistry*, 149(2):227–231.

Boekhoff, I., Michel, W. C., Breer, H., and Ache, B. W. (1994). Single odors differentially stimulate dual second messenger pathways in lobster olfactory receptor cells. *The Journal of Neuroscience*.

Boyle, S. M., McInally, S., and Ray, A. (2013). Expanding the olfactory code by in silico decoding of odor-receptor chemical space. *eLife*, 2.

Brand, a. H. and Perrimon, N. (1993). Targeted gene expression as a means of altering cell fates and generating dominant phenotypes. *Development (Cambridge, England)*, 118(2):401–15.

Brieger, G. and Butterworth, F. M. (1970). Drosophila melanogaster: identity of male lipid in reproductive system. *Science (New York, N.Y.)*, 167(3922):1262.

Brodin, M., Laska, M., and Olsson, M. J. (2009). Odor interaction between bourgeonal and its antagonist undecanal. *Chemical Senses*, 34(7):625–30.

Buck, L. and Axel, R. (1991). A novel multigene family may encode odorant receptors: a molecular basis for odor recognition. *Cell*, 65(1):175–87.

Caligiani, A., Silva, G., and Palla, G. (2007). Determination of 2,3-Butanediol and 2-Hydroxybutanone stereoisomers in batteries of traditional balsamic vinegar. *Journal of Agricultural and Food Chemistry*, 55(19):7810–7815.

Callejón, R. M., Morales, M. L., Troncoso, A. M., and Silva Ferreira, A. C. (2008). Targeting key aromatic substances on the typical aroma of sherry vinegar. *Journal of Agricultural and Food Chemistry*, 56(15):6631–6639.

Cha, D. H., Adams, T., Rogg, H., and Landolt, P. J. (2012). Identification and field evaluation of fermentation volatiles from wine and vinegar that mediate attraction of spotted wing drosophila, drosophila suzukii. *Journal of Chemical Ecology*, 38(11):1419–1431.

Chaput, M. A., El Mountassir, F., Atanasova, B., Thomas-Danguin, T., Le Bon, a. M., Perrut, A., Ferry, B., and Duchamp-Viret, P. (2012). Interactions of odorants with olfactory receptors and receptor neurons match the perceptual dynamics observed for woody and fruity odorant mixtures. *The European Journal of Neuroscience*, 35(4):584–97.

Charpak, S., Mertz, J., Beaurepaire, E., Moreaux, L., and Delaney, K. (2001). Odor-evoked calcium signals in dendrites of rat mitral cells. *Proceedings of the National Academy of Sciences*, 98(3):1230–1234.

Chertemps, T., François, A., Durand, N., Rosell, G., Dekker, T., Lucas, P., and Maïbèche-Coisne, M. (2012). A carboxylesterase, esterase-6, modulates sensory physiological and behavioral response dynamics to pheromone in drosophila. *BMC Biology*, 10(1):56.

Chou, Y., Zheng, X., Beachy, P. a., and Luo, L. (2010). Patterning axon targeting of olfactory receptor neurons by coupled hedgehog signaling at two distinct steps. *Cell*, 142(6):954–966.

Cleland, T. a., Chen, S. T., Hozer, K. W., Ukatu, H. N., Wong, K. J., and Zheng, F. (2012). Sequential mechanisms underlying concentration invariance in biological olfaction. *Frontiers in Neuroengineering*, 4(January):1–12.

Clyne, P. J., Warr, C. G., Freeman, M. R., Lessing, D., Kim, J., and Carlson, J. R. (1999). A novel family of divergent seven-transmembrane proteins: candidate odorant receptors in drosophila. *Neuron*, 22(2):327–38.

Cometto-Muñiz, J. E., Cain, W. S., and Abraham, M. H. (2003). Quantification of chemical vapors in chemosensory research. *Chemical Senses*, 28(6):467–77.

Couto, A., Alenius, M., and Dickson, B. J. (2005). Molecular, anatomical, and functional organization of the drosophila olfactory system. *Current Biology*, 15(17):1535–1547.

Crasto, C., Marenco, L., Miller, P., and Shepherd, G. (2002). Olfactory receptor database: a metadata-driven automated population from sources of gene and protein sequences. *Nucleic Acids Research*, 30(1):354–360.

Cromarty, S. I. and Derby, C. D. (1997). Multiple excitatory receptor types on individual olfactory neurons: implications for coding of mixtures in the spiny lobster. *Journal of Comparative Physiology A*, 180(5):481–91.

Cromarty, S. I. and Derby, C. D. (1998). Inhibitory receptor binding events among the components of complex mixtures contribute to mixture suppression in responses of olfactory receptor neurons of spiny lobsters. *Journal of Comparative Physiology A*, 183(6):699–707.

DasGupta, S. and Waddell, S. (2008). Learned odor discrimination in drosophila without combinatorial odor maps in the antennal lobe. *Current biology : CB*, 18(21):1668–74.

de Bruyne, M., Clyne, P. J., and Carlson, J. R. (1999). Odor coding in a model olfactory organ: the drosophila maxillary palp. *The Journal of Neuroscience*, 19(11):4520–32.

de Bruyne, M., Foster, K., and Carlson, J. R. (2001). Odor coding in the drosophila antenna. *Neuron*, 30(2):537–552.

Dekker, T., Ibba, I., Siju, K., Stensmyr, M. C., and Hansson, B. S. (2006). Olfactory shifts parallel superspecialism for toxic fruit in drosophila melanogaster sibling, d. sechellia. *Current Biology*, 16(1):101–109.

Derby, C. D., Girardot, M. N., and Daniel, P. C. (1991). Responses of olfactory receptor cells of spiny lobsters to binary mixtures. i. intensity mixture interactions. *Journal of Neurophysiology*, 66(1):112–130.

Dobritsa, A. A., van der Goes van Naters, W., Warr, C. G., Steinbrecht, R. A., and Carlson, J. R. (2003). Integrating the molecular and cellular basis of odor coding in the drosophila antenna. *Neuron*, 37(5):827–41.

Duchamp-Viret, P., Chaput, M. A., and Duchamp, A. (1999). Odor response properties of rat olfactory receptor neurons. *Science*, 284(5423):2171–2174.

Duchamp-Viret, P., Duchamp, A., and Chaput, M. A. (2003). Single olfactory sensory neurons simultaneously integrate the components of an odour mixture. *The European Journal of Neuroscience*, 18(10):2690–6.

Faucher, C. P., Hilker, M., and de Bruyne, M. (2013). Interactions of carbon dioxide and food odours in drosophila: olfactory hedonics and sensory neuron properties. *PloS one*, 8(2):e56361–e56361.

Feinstein, P. and Mombaerts, P. (2004). A contextual model for axonal sorting into glomeruli in the mouse olfactory system. *Cell*, 117(6):817–831.

Fiala, A., Spall, T., Diegelmann, S., Eisermann, B., Sachse, S., Devaud, J., Buchner, E., and Galizia, C. (2002). Genetically expressed cameleon in drosophila melanogaster is used to visualize olfactory information in projection neurons. *Current Biology*, 12(21):1877–1884.

Fishilevich, E. and Vosshall, L. B. (2005). Genetic and functional subdivision of the drosophila antennal lobe. *Current Biology*, 15(17):1548–1553.

Flanagan, D. and Mercer, A. R. (1989). An atlas and 3-D reconstruction of the antennal lobes in the worker honey bee, apis mellifera l. (Hymenoptera : Apidae). *International Journal of Insect Morphology and Embryology*, 18(2–3):145–159.

French, A. S., Torkkeli, P. H., and Schuckel, J. (2011). Dynamic characterization of drosophila antennal olfactory neurons indicates multiple opponent signaling pathways in odor discrimination. *The Journal of Neuroscience*, 31(3):861–9.

Friedrich, R. W. and Korsching, S. I. (1997). Combinatorial and chemotopic odorant coding in the zebrafish olfactory bulb visualized by optical imaging. *Neuron*, 18(5):737–752.

Gabler, S., Soelter, J., Hussain, T., Sachse, S., and Schmuker, M. (2013). Physicochemical vs. vibrational descriptors for prediction of odor receptor responses. *Molecular Informatics*, page n/a–n/a.

Galán, R. F., Weidert, M., Menzel, R., Herz, A. V. M., and Galizia, C. G. (2006). Sensory memory for odors is encoded in spontaneous correlated activity between olfactory glomeruli. *Neural Computation*, 18(1):10–25.

Galili, D. S., Lüdke, A., Galizia, C. G., Szyszka, P., and Tanimoto, H. (2011). Olfactory trace conditioning in drosophila. *The Journal of Neuroscience*, 31(20):7240–7248.

Galizia, C. and Menzel, R. (2001). The role of glomeruli in the neural representation of odours: results from optical recording studies. *Journal of Insect Physiology*, 47(2):115–130.

Galizia, C. G., McIlwrath, S. L., and Menzel, R. (1999). A digital three-dimensional atlas of the honeybee antennal lobe based on optical sections acquired by confocal microscopy. *Cell and Tissue Research*, 295(3):383–94.

Galizia, C. G., Münch, D., Strauch, M., Nissler, A., and Ma, S. (2010). Integrating heterogeneous odor response data into a common response model: A DoOR to the complete olfactome. *Chemical Senses*, 35(7):551–63.

Gao, Q. and Chess, A. (1999). Identification of candidate drosophila olfactory receptors from genomic DNA sequence. *Genomics*, 60(1):31–9.

Getahun, M. N., Wicher, D., Hansson, B. S., and Olsson, S. B. (2012). Temporal response dynamics of drosophila olfactory sensory neurons depends on receptor type and response polarity. *Frontiers in Cellular Neuroscience*, 6(November):54–54.

Giraudet, P., Berthommier, F., and Chaput, M. (2002). Mitral cell temporal response patterns evoked by odor mixtures in the rat olfactory bulb. *Journal of Neurophysiology*, 88(2):829–38.

Glusman, G., Yanai, I., Rubin, I., and Lancet, D. (2001). The complete human olfactory subgenome. *Genome Research*, 11(5):685–702.

Goldman, A. L., Van der Goes van Naters, W., Lessing, D., Warr, C. G., and Carlson, J. R. (2005). Coexpression of two functional odor receptors in one neuron. *Neuron*, 45(5):661–6.

Grienberger, C. and Konnerth, A. (2012). Imaging calcium in neurons. *Neuron*, 73(5):862–885.

Grosmaitre, X., Fuss, S. H., Lee, A. C., Adipietro, K. A., Matsunami, H., Mombaerts, P., and Ma, M. (2009). SR1, a mouse odorant receptor with an unusually broad response profile. *The Journal of Neuroscience*, 29(46):14545–14552.

Guerrieri, F., Schubert, M., Sandoz, J., and Giurfa, M. (2005). Perceptual and neural olfactory similarity in honeybees. *PLoS Biol*, 3(4):e60.

Haddad, R., Khan, R., Takahashi, Y. K., Mori, K., Harel, D., and Sobel, N. (2008). A metric for odorant comparison. *Nature Methods*, 5(5):425–429.

Hallem, E. A. and Carlson, J. R. (2006). Coding of odors by a receptor repertoire. *Cell*, 125(1):143–60.

Hallem, E. A., Ho, M. G., and Carlson, J. R. (2004). The molecular basis of odor coding in the drosophila antenna. *Cell*, 117(7):965–79.

Herz, A. V., Meier, R., Nawrot, M. P., Schiegel, W., and Zito, T. (2008). G-Node: an integrated tool-sharing platform to support cellular and systems neurophysiology in the age of global neuroinformatics. *Neural Networks*, 21(8):1070–1075.

Hildebrand, J. G. and Shepherd, G. M. (1997). MECHANISMS OF OLFACTORY DISCRIMINATION:Converging evidence for common principles across phyla. *Annual Review of Neuroscience*, 20(1):595–631.

Hillier, N. K. and Vickers, N. J. (2011). Mixture interactions in moth olfactory physiology: examining the effects of odorant mixture, concentration, distal stimulation, and antennal nerve transection on sensillar responses. *Chemical Senses*, 36(1):93–108.

Ignatious Raja, J. S. (2013). *Role of G proteins in olfactory signaling of Drosophila*. Doctoral thesis, Universität Konstanz, Konstanz.

Ignell, R., Root, C. M., Birse, R. T., Wang, J. W., Nässel, D. R., and Winther, A. M. E. (2009). Presynaptic peptidergic modulation of olfactory receptor neurons in drosophila. *Proceedings of the National Academy of Sciences of the United States of America*, 106(31):13070–5.

Jinks, a. and Laing, D. G. (2001). The analysis of odor mixtures by humans: evidence for a configurational process. *Physiology & Behavior*, 72(1-2):51–63.

Joerges, J., Küttner, A., Galizia, C. G., and Menzel, R. (1997). Representations of odours and odour mixtures visualized in the honeybee brain. *Nature*, 387(6630):285–288.

Johnson, B. A., Ong, J., and Leon, M. (2010). Glomerular activity patterns evoked by natural odor objects in the rat olfactory bulb are related to patterns evoked by major odorant components. *The Journal of Comparative Neurology*, 518(9):1542–55.

Jones, P. L., Pask, G. M., Rinker, D. C., and Zwiebel, L. J. (2011). Functional agonism of insect odorant receptor ion channels. *Proceedings of the National Academy of Sciences*, 108(21):8821–8825.

Jordán, M. J., Shaw, P. E., and Goodner, K. L. (2001). Volatile components in aqueous essence and fresh fruit of cucumis melo cv. athena (Muskmelon) by GC-MS and GC-O. *Journal of Agricultural and Food Chemistry*, 49(12):5929–5933.

Kang, J. and Caprio, J. (1997). In vivo responses of single olfactory receptor neurons of channel catfish to binary mixtures of amino acids. *Journal of Neurophysiology*, 77(1):1–8.

Kelber, C., Rössler, W., Roces, F., and Kleineidam, C. J. (2009). The antennal lobes of Fungus-Growing ants (Attini): neuroanatomical traits and evolutionary trends. *Brain, Behavior and Evolution*, 73(4):273–284.

Keller, A. and Vosshall, L. B. (2007). Influence of odorant receptor repertoire on odor perception in humans and fruit flies. *Proceedings of the National Academy of Sciences*, 104(13):5614–5614.

Kim, H., Golub, G. H., and Park, H. (2005). Missing value estimation for DNA microarray gene expression data: local least squares imputation. *Bioinformatics*, 21(2):187–198.

Knudsen, J. T., Tollsten, L., and Bergström, L. (1993). Floral scents—a checklist of volatile compounds isolated by head-space techniques. *Phytochemistry*, 33(2):253–280.

Kometani, T., Yoshii, H., Kitatsuji, E., Nishimura, H., and Matsuno, R. (1993). Large-scale preparation of (S)-ethyl 3-hydroxybutanoate with a high enantiomeric excess through baker's yeast-mediated bioreduction. *Journal of Fermentation and Bioengineering*, 76(1):33–37.

Kondoh, Y., Kaneshiro, K. Y., Kimura, K., and Yamamoto, D. (2003). Evolution of sexual dimorphism in the olfactory brain of hawaiian drosophila. *Proceedings of the Royal Society of London. Series B: Biological Sciences*, 270(1519):1005–1013.

Kreher, S. A., Mathew, D., Kim, J., and Carlson, J. R. (2008). Translation of sensory input into behavioral output via an olfactory system. *Neuron*, 59(1):110–24.

Kuebler, L. S., Olsson, S. B., Weniger, R., and Hansson, B. S. (2011). Neuronal processing of complex mixtures establishes a unique odor representation in the moth antennal lobe. *Frontiers in Neural Circuits*, 5(May):7–7.

Kurtovic, A., Widmer, A., and Dickson, B. J. (2007). A single class of olfactory neurons mediates behavioural responses to a drosophila sex pheromone. *Nature*, 446(7135):542–546.

Kwon, J. Y., Dahanukar, A., Weiss, L. a., and Carlson, J. R. (2007). The molecular basis of CO2 reception in drosophila. *Proceedings of the National Academy of Sciences of the United States of America*, 104(9):3574–8.

Laissue, P., Reiter, C., Hiesinger, P., Halter, S., Fischbach, K., and Stocker, R. (1999). Three-dimensional reconstruction of the antennal lobe in drosophila melanogaster. *The Journal of Comparative Neurology*, 405(4):543–552.

Larsson, M. C., Domingos, A. I., Jones, W. D., Chiappe, M., Amrein, H., and Vosshall, L. B. (2004). Or83b encodes a broadly expressed odorant receptor essential for drosophila olfaction. *Neuron*, 43(5):703–714.

Lei, H., Christensen, T. A., and Hildebrand, J. G. (2004). Spatial and temporal organization of ensemble representations for different odor classes in the moth antennal lobe. *The Journal of Neuroscience*, 24(49):11108–11119.

Lei, H. and Hansson, B. S. (1999). Central processing of pulsed pheromone signals by antennal lobe neurons in the male moth agrotis segetum. *Journal of Neurophysiology*, 81(3):1113–1122.

Lei, H. and Vickers, N. (2008). Central processing of natural odor mixtures in insects. *Journal of Chemical Ecology*, 34(7):915–27.

Lilley, B. D. and Brewer, J. H. (1953). The selective antibacterial action of phenylethyl alcohol. *Journal of the American Pharmaceutical Association*, 42(1):6–8.

Lucas, P. and Shimahara, T. (2002). Voltage- and calcium-activated currents in cultured olfactory receptor neurons of male mamestra brassicae (Lepidoptera). *Chemical Senses*, 27(7):599–610.

Malnic, B., Hirono, J., Sato, T., and Buck, L. B. (1999). Combinatorial receptor codes for odors. *Cell*, 96(5):713–23.

Manoli, D. S., Foss, M., Villella, A., Taylor, B. J., Hall, J. C., and Baker, B. S. (2005). Male-specific fruitless specifies the neural substrates of drosophila courtship behaviour. *Nature*, 436(7049):395–400.

Martelli, C., Carlson, J. R., and Emonet, T. (2013). Intensity invariant dynamics and Odor-Specific latencies in olfactory receptor neuron response. *The Journal of Neuroscience*, 33(15):6285–6297.

Moers, W. (2012). *The labyrinth of dreaming books: a novel from Zamonia*. Overlook Press, New York.

Montague, S. a., Mathew, D., and Carlson, J. R. (2011). Similar odorants elicit different behavioral and physiological responses, some supersustained. *The Journal of Neuroscience*, 31(21):7891–7899.

Moreaux, L. and Laurent, G. (2008). A simple method to reconstruct firing rates from dendritic calcium signals. *Frontiers in Neuroscience*, 2(2):176–185.

Münch, D., Schmeichel, B., Silbering, A. F., and Galizia, C. G. (2013). Weaker ligands can dominate an odor blend due to syntopic interactions. *Chemical Senses*.

Nagel, K. I. and Wilson, R. I. (2011). Biophysical mechanisms underlying olfactory receptor neuron dynamics. *Nature Neuroscience*, 14(January):208–16.

Nakai, J., Ohkura, M., and Imoto, K. (2001). A high signal-to-noise ca(2+) probe composed of a single green fluorescent protein. *Nature Biotechnology*, 19(2):137–41.

Neubig, R. R., Spedding, M., Kenakin, T., and Christopoulos, A. (2003). International union of pharmacology committee on receptor nomenclature and drug classification. XXXVIII. update on terms and symbols in quantitative pharmacology. *Pharmacological reviews*, 55(4):597–606.

Niimura, Y. and Nei, M. (2007). Extensive gains and losses of olfactory receptor genes in mammalian evolution. *PloS one*, 2(8):e708–e708.

Nissler, A. (2007). *Ligand search for genetically identified Drosophila Olfactory Receptors using Calcium-Imaging*. Bachelor's thesis, Universität Konstanz, Konstanz.

Ochieng, S. A., Park, K. C., and Baker, T. C. (2002). Host plant volatiles synergize responses of sex pheromone-specific olfactory receptor neurons in male helicoverpa zea. *Journal of Comparative Physiology A*, 188(4):325–33.

Oka, Y., Omura, M., Kataoka, H., and Touhara, K. (2004). Olfactory receptor antagonism between odorants. *The EMBO Journal*, 23(1):120–6.

Olsen, S. R. and Wilson, R. I. (2008). Cracking neural circuits in a tiny brain: new approaches for understanding the neural circuitry of drosophila. *Trends in Neurosciences*, 31(10):512–520.

Pelz, D. (2005). *Functional Characterization of Drosophila melanogaster Olfactory Receptor Neurons*. Doctoral thesis, Freie Universität Berlin, Berlin.

Pelz, D., Roeske, T., Syed, Z., de Bruyne, M., and Galizia, C. G. (2006). The molecular receptive range of an olfactory receptor in vivo (Drosophila melanogaster or22a). *Journal of neurobiology*, 66(14):1544–63.

R Development Core Team (2013). R: A language and environment for statistical computing.

Reinhard, J., Sinclair, M., Srinivasan, M. V., and Claudianos, C. (2010). Honeybees learn odour mixtures via a selection of key odorants. *PloS one*, 5(2):e9110–e9110.

Riffell, J. A., Abrell, L., and Hildebrand, J. G. (2008). Physical processes and Real-Time chemical measurement of the insect olfactory environment. *Journal of Chemical Ecology*, 34(7):837–853.

Romano, P., Brandolini, V., Ansaloni, C., and Menziani, E. (1998). The production of 2,3-butanediol as a differentiating character in wine yeasts. *World Journal of Microbiology and Biotechnology*, 14(5):649–653.

Root, C. M., Ko, K. I., Jafari, A., and Wang, J. W. (2011). Presynaptic facilitation by neuropeptide signaling mediates Odor-Driven food search. *Cell*, 145(1):133–144.

Root, C. M., Masuyama, K., Green, D. S., Enell, L. E., Nässel, D. R., Lee, C., and Wang, J. W. (2008). A presynaptic gain control mechanism fine-tunes olfactory behavior. *Neuron*, 59(2):311–21.

Rospars, J., Lansky, P., Chaput, M., and Duchamp-Viret, P. (2008). Competitive and noncompetitive odorant interactions in the early neural coding of odorant mixtures. *The Journal of Neuroscience*, 28(10):2659–66.

Rubin, B. D. and Katz, L. C. (1999). Optical imaging of odorant representations in the mammalian olfactory bulb. *Neuron*, 23(3):499–511.

Sachse, S. and Galizia, C. G. (2002). Role of inhibition for temporal and spatial odor representation in olfactory output neurons: a calcium imaging study. *Journal of Neurophysiology*, 87(2):1106–17.

Sachse, S. and Galizia, C. G. (2003). The coding of odour-intensity in the honeybee antennal lobe: local computation optimizes odour representation. *The European Journal of Neuroscience*, 18(8):2119–32.

Sachse, S., Rappert, A., and Galizia, C. G. (1999). The spatial representation of chemical structures in the antennal lobe of honeybees: steps towards the olfactory code. *European Journal of Neuroscience*, 11(11):3970–3982.

Sato, K., Pellegrino, M., Nakagawa, T. T., Vosshall, L. B., and Touhara, K. (2008). Insect olfactory receptors are heteromeric ligand-gated ion channels. *Nature*, 452(7190):1002–6.

Schmuker, M., Bruyne, M. d., Hähnel, M., and Schneider, G. (2007). Predicting olfactory receptor neuron responses from odorant structure. *Chemistry Central Journal*, 1(1):11.

Schmuker, M. and Schneider, G. (2007). Processing and classification of chemical data inspired by insect olfaction. *Proceedings of the National Academy of Sciences of the United States of America*, 104(51):20285–9.

Schuckel, J., Torkkeli, P. H., and French, A. S. (2009). Two interacting olfactory transduction mechanisms have linked polarities and dynamics in drosophila melanogaster antennal basiconic sensilla neurons. *Journal of Neurophysiology*, 102(1):214–23.

Semmelhack, J. L. and Wang, J. W. (2009). Select drosophila glomeruli mediate innate olfactory attraction and aversion. *Nature*, 459(7244):218–223.

Serizawa, S., Miyamichi, K., Nakatani, H., Suzuki, M., Saito, M., Yoshihara, Y., and Sakano, H. (2003). Negative feedback regulation ensures the one Receptor-One olfactory neuron rule in mouse. *Science*, 302(5653):2088–2094.

Shanbhag, S., Hekmat-Scafe, D., Kim, M., Park, S., Carlson, J., Pikielny, C., Smith, D., and Steinbrecht, R. (2001). Expression mosaic of odorant-binding proteins in drosophila olfactory organs. *Microscopy Research and Technique*, 55(5):297–306.

Shanbhag, S., Müller, B., and Steinbrecht, R. A. (1999). Atlas of olfactory organs of drosophila melanogaster. *International Journal of Insect Morphology and Embryology*, 28(4):377–397.

Silbering, A. F. and Benton, R. (2010). Ionotropic and metabotropic mechanisms in chemoreception: 'chance or design'? *EMBO reports*, 11(3):173–9.

Silbering, A. F. and Galizia, C. G. (2007). Processing of odor mixtures in the drosophila antennal lobe reveals both global inhibition and glomerulus-specific interactions. *The Journal of Neuroscience*, 27(44):11966–77.

Silbering, A. F., Okada, R., Ito, K., and Galizia, C. G. (2008). Olfactory information processing in the drosophila antennal lobe: anything goes? *The Journal of Neuroscience*, 28(49):13075–87.

Silbering, A. F., Rytz, R., Grosjean, Y., Abuin, L., Ramdya, P., Jefferis, G. S. X. E., and Benton, R. (2011). Complementary function and integrated wiring of the evolutionarily distinct drosophila olfactory subsystems. *The Journal of Neuroscience*, 31(38):13357–75.

Smart, R., Kiely, A., Beale, M., Vargas, E., Carraher, C., Kralicek, A. V., Christie, D. L., Chen, C., Newcomb, R. D., and Warr, C. G. (2008). Drosophila odorant receptors are novel seven transmembrane domain proteins that can signal independently of heterotrimeric g proteins. *Insect Biochemistry and Molecular Biology*, 38(8):770–780.

Spors, H. and Grinvald, A. (2002). Spatio-Temporal dynamics of odor representations in the mammalian olfactory bulb. *Neuron*, 34(2):301–315.

Spors, H., Wachowiak, M., Cohen, L. B., and Friedrich, R. W. (2006). Temporal dynamics and latency patterns of receptor neuron input to the olfactory bulb. *The Journal of Neuroscience*, 26(4):1247–1259.

Stensmyr, M. C. (2009). Drosophila sechellia as a model in chemosensory neuroecology. *Annals of the New York Academy of Sciences*, 1170:468–75.

Stensmyr, M. C., Dweck, H. K. K. M., Farhan, A., Ibba, I., Strutz, A., Mukunda, L., Linz, J., Grabe, V., Steck, K., Lavista-Llanos, S., Wicher, D., Sachse, S., Knaden, M., Becher, P. G. G., Seki, Y., and Hansson, B. S. S. (2012). A conserved dedicated olfactory circuit for detecting harmful microbes in drosophila. *Cell*, 151(6):1345–57.

Stensmyr, M. C., Giordano, E., Balloi, A., Angioy, A., and Hansson, B. S. (2003). Novel natural ligands for drosophila olfactory receptor neurones. *The Journal of experimental biology*, 206(Pt 4):715–24.

Stocker, R. (1994). The organization of the chemosensory system in drosophila melanogaster: a review. *Cell and Tissue Research*, 275(1):3–3.

Stockinger, P., Kvitsiani, D., Rotkopf, S., Tirián, L., and Dickson, B. J. (2005). Neural circuitry that governs drosophila male courtship behavior. *Cell*, 121(5):795–807.

Störtkuhl, K. F., Hovemann, B. T., and Carlson, J. R. (1999). Olfactory adaptation depends on the trp Ca2+Channel in drosophila. *The Journal of Neuroscience*, 19(12):4839–4846.

Strauch, M. and Galizia, C. G. (2012). Keeping their distance? odor response patterns along the concentration range. *Frontiers in Systems Neuroscience*, 6:71.

Su, C., Martelli, C., Emonet, T., and Carlson, J. R. (2011). Temporal coding of odor mixtures in an olfactory receptor neuron. *Proceedings of the National Academy of Sciences of the United States of America*, 108(12):5075–80.

Su, C., Menuz, K., Reisert, J., and Carlson, J. R. (2012). Non-synaptic inhibition between grouped neurons in an olfactory circuit. *Nature*, 492(7427):66–71.

Swarup, S., Williams, T. I., and Anholt, R. R. H. (2011). Functional dissection of odorant binding protein genes in drosophila melanogaster. *Genes, brain, and behavior*, pages 1–10.

Syed, Z., Ishida, Y., Taylor, K., Kimbrell, D. A., and Leal, W. S. (2006). Pheromone reception in fruit flies expressing a moth's odorant receptor. *Proceedings of the National Academy of Sciences*, 103(44):16538–16543.

Szyszka, P., Stierle, J. S., Biergans, S., and Galizia, C. G. (2012). The speed of smell: Odor-Object segregation within milliseconds. *PLoS ONE*, 7(4):e36096.

Tabor, R., Yaksi, E., Weislogel, J., and Friedrich, R. W. (2004). Processing of odor mixtures in the zebrafish olfactory bulb. *The Journal of Neuroscience*, 24(29):6611–20.

Tegoni, M., Pelosi, P., Vincent, F., Spinelli, S., Campanacci, V., Grolli, S., Ramoni, R., and Cambillau, C. (2000). Mammalian odorant binding proteins. *Biochimica et Biophysica Acta (BBA) - Protein Structure and Molecular Enzymology*, 1482(1–2):229–240.

Tian, L., Hires, S. A., Mao, T., Huber, D., Chiappe, M. E., Chalasani, S. H., Petreanu, L., Akerboom, J., McKinney, S. a., Schreiter, E. R., Bargmann, C. I., Jayaraman, V., Svoboda, K., and Looger, L. L. (2009). Imaging neural activity in worms, flies and mice with improved GCaMP calcium indicators. *Nature methods*, 6(12):875–81.

Troemel, E. R., Chou, J. H., Dwyer, N. D., Colbert, H. A., and Bargmann, C. I. (1995). Divergent seven transmembrane receptors are candidate chemosensory receptors in c. elegans. *Cell*, 83(2):207–218.

Tummino, P. J. and Copeland, R. A. (2008). Residence time of Receptor-Ligand complexes and its effect on biological function. *Biochemistry*, 47(20):5481–5492.

Turner, S. L., Li, N., Guda, T., Githure, J., Cardé, R. T., and Ray, A. (2011). Ultra-prolonged activation of CO2-sensing neurons disorients mosquitoes. *Nature*, 474(7349):87–91.

Turner, S. L. and Ray, A. (2009). Modification of CO2 avoidance behaviour in drosophila by inhibitory odorants. *Nature*, 461(7261):277–81.

Uchida, N. and Mainen, Z. F. (2007). Odor concentration invariance by chemical ratio coding. *Frontiers in systems neuroscience*, 1(April):3–3.

Uchida, N., Takahashi, Y. K., Tanifuji, M., and Mori, K. (2000). Odor maps in the mammalian olfactory bulb: domain organization and odorant structural features. *Nature Neuroscience*, 3(10):1035–1043.

van der Goes van Naters, W. and Carlson, J. R. (2007). Receptors and neurons for fly odors in drosophila. *Current biology : CB*, 17(7):606–12.

Vermeulen, A. and Rospars, J. (2004). Why are insect olfactory receptor neurons grouped into sensilla? the teachings of a model investigating the effects of the electrical interaction between neurons on the transepithelial potential and the neuronal transmembrane potential. *European biophysics journal : EBJ*, 33(7):633–43.

Vosshall, L. B., Amrein, H., Morozov, P. S., Rzhetsky, A., Axel, R., Biophysics, M., and Dulac, C. (1999). A spatial map of olfactory receptor expression in the drosophila antenna. *Cell*, 96(5):725–36.

Vosshall, L. B. and Hansson, B. S. (2011). A unified nomenclature system for the insect olfactory coreceptor. *Chemical Senses*, 36(6):497–498.

Vosshall, L. B. and Stocker, R. F. (2007). Molecular architecture of smell and taste in drosophila. *Annual Review of Neuroscience*, 30:505–33.

Wang, G., Carey, A. F., Carlson, J. R., and Zwiebel, L. J. (2010). Molecular basis of odor coding in the malaria vector mosquito anopheles gambiae. *Proceedings of the National Academy of Sciences of the United States of America*, 107(9):1–6.

Wang, J. W., Wong, A. M., Flores, J., Vosshall, L. B., and Axel, R. (2003). Two-Photon calcium imaging reveals an Odor-Evoked map of activity in the fly brain. *Cell*, 112(2):271–282.

Wicher, D., Schäfer, R., Bauernfeind, R., Stensmyr, M. C., Heller, R., Heinemann, S. H., and Hansson, B. S. (2008). Drosophila odorant receptors are both ligand-gated and cyclic-nucleotide-activated cation channels. *Nature*, 452(7190):1007–11.

Wickham, H. (2009). *ggplot2: elegant graphics for data analysis*. Springer New York.

Willmore, B. and Tolhurst, D. J. (2001). Characterizing the sparseness of neural codes. *Network (Bristol, England)*, 12(3):255–70.

Witthöft, D. W. (1967). Absolute anzahl und verteilung der zellen im him der honigbiene. *Zeitschrift für Morphologie der Tiere*, 61(1):160–184.

Xu, P., Atkinson, R., Jones, D. N., and Smith, D. P. (2005). Drosophila OBP LUSH is required for activity of Pheromone-Sensitive neurons. *Neuron*, 45(2):193–200.

Yang, Z., Bengtsson, M., and Witzgall, P. (2004). Host plant volatiles synergize response to sex pheromone in codling moth, cydia pomonella. *Journal of Chemical Ecology*, 30(3):619–629.

Zufall, F. and Leinders-Zufall, T. (2000). The cellular and molecular basis of odor adaptation. *Chemical Senses*, 25(4):473–481.

Summary

Animals use olfactory receptor neurons (ORNs) to detect odors and to get a representation of the olfactory environment around them. Many of these odors convey important information for an animals daily life and thus it is essential to reliably detect them. The olfactory environment consists of myriads of different chemicals that appear in different compositions and concentrations, yet olfactory systems of varying complexity are able extract the relevant information from it. How olfactory systems are able to encode a vast number of odors with a much smaller number of ORN types is one big question in olfactory research. A given ORN is usually activated not only by one, but by many odors. The response profile of an ORN is defined by one or a few odorant receptors (OR) it expresses. The response profiles of ORNs overlap. Thus, when stimulated with an odor usually a set of ORNs gets activated creating an odor specific ensemble response.

One way to better understand how this ensemble coding works is to characterize the response profiles of individual ORNs in great detail. The ideal case would be to know the complete response profiles of all ORNs of an olfactory system and by this have access to the complete ensemble responses any odor would elicit. This knowledge about the responses produced by all possible odor–ORN combinations is the so called "complete olfactome" of a species. Of all species used in olfactory research, the best known olfactome is that of *Drosophila melanogaster*. In order to combine the information on the *Drosophila* olfactome that is scattered across different publications and not easily comparable as different studies use different recording approaches, we created the DoOR database described in Chapter 1. With DoOR it is possible to integrate all the heterogeneous response data available into one consensus model response that can then be used for further analysis or visualized in various ways. The DoOR web interface provides an easy access to the *Drosophila* olfactome e.g. as tool for designing physiological or behavioral experiments. In addition, the complete database including the model response as well as the raw data and all the functions is freely available and may be a useful source for computational approaches investigating olfactory coding.

The *Drosophila* olfactome is the completest existing olfactome but it still has

many gaps. In Chapter 2 we characterized the response profiles of eight ORNs. One of the ORNs investigated in this Chapter was completely uncharacterized before, here we describe a response profile consisting of 106 odor responses. Another one was published as being responsive to a single odorant alone, we found that many other odorants also elicit distinguished odor responses from these neurons. For six other ORNs we extended previously existing response profiles.

The ensemble activation is only one dimension of the olfactory code. Information about odor identity are also encoded in the temporal dynamics of ORNs responses. In Chapter 3 we therefore investigated the response dynamics elicited by the > 800 odorant–ORN combinations from Chapter 2 in detail. We found that response dynamics were odorant–ORN combination specific and varied largely between odorant–ORN pairs. We analyzed several features of the response dynamics and found them to be differential distributed across ORNs. We found one feature of response dynamics to be stable across concentrations, thus it could contribute to concentration invariant odor coding. We show that odor information is still present in the ORN ensemble response after stimulus offset, mainly due to some odorant–ORN combinations that lead to especially strong and long lasting responses.

While Chapters 1–3 deal with ORN responses towards monomolecular odorants, we investigated responses towards mixtures in Chapters 4 and 5. Almost all natural odors occur as mixtures. Each component of a mixture usually elicits a response pattern across ORNs and when appearing together these responses might overlap and lead to mixture interactions. In Chapter 4 we created a complex mixture of 15 components in different concentrations related to banana scent. In this mixture we found one substance, isopentyl acetate, to dominate the mixture responses elicited in Or22a ORNs. Isopentyl acetate suppressed the responses of stronger, less concentrated and weaker, higher concentrated ligands in the mixture, leading to hypoadditive mixture interactions. Further analysis revealed that the mechanism of syntopic interaction (i.e. the competition of ligands for a common receptor binding site) fully accounted for the effects we found. We discuss that syntopic interaction could account for a majority of suppressive mixture interactions found in the periphery of olfactory systems and that it might play a role in gain control and concentration invariant coding.

In Chaper 5 we expanded the mixture experiments to more mixture and ORNs. We found that strong mixture interactions, like suppression and synergism were rare, most of the 20 mixtures elicited additive or hypoadditive reponses from the five ORNs tested. With a principal component analysis we calculated trajectories of ORN ensemble responses to mixtures and their com-

ponents in a five-dimensional receptor space. We found that many mixture trajectories were dominated by one component, others covered distinct areas of receptor space. We discuss that these differences in physiological odor similarities might be a neural correlate of differences in perceived odor similarities.

Zusammenfassung

Tiere nutzen olfaktorische Rezeptorneurone um Düfte zu detektieren und um eine Repräsentation ihrer olfaktorischen Umgebung zu bekommen. Viele dieser Duftsignale beinhalte wichtige Informationen für das tägliche Leben eines Tieres und daher ist es essentiell sie zuverlässig zu erfassen. Die Duftwelt besteht aus unzähligen Chemikalien, die in unterschiedlicher Zusammensetzung und Konzentration auftreten. Dennoch schaffen es olfaktorische Systeme von unterschiedlicher Komplexität die relevanten Informationen zu extrahieren. Wie es olfaktorische Systeme schaffen eine riesige Anzahl von Düften mit einer weitaus geringeren Anzahl von unterschiedlichen Rezeptorneuronen zu kodieren ist eine der großen Fragen der Riechforschung. Ein Rezeptorneuron kann üblicherweise nicht nur von einem einzigen Duft, sondern von vielen verschiedenen aktiviert werden. Das Antwortspektrum eines Rezeptorneurons wird durch einen oder wenige Duftrezeptoren festgelegt, die es exprimiert. Die Antwortspektren verschiedener Rezeptorneurone überlappen, so dass bei der Stimulation mit einem Duft üblicherweise ein Satz an Rezeptorneuronen aktiviert wird, wodurch eine duftspezifische Ensemble-Aktivität entsteht.

Ein Weg zum besseren Verständnis der Duftkodierung durch Ensemble-Aktivität besteht darin, die spezifischen Antwortspektren sehr detailliert zu charakterisieren. Im Idealfall sind die Antwortspektren aller Rezeptorneurone eines olfaktorischen Systems bekannt und man hat somit Zugang zu den Ensemble-Aktivitäten die jeder Duft auslöst. Diese Gesamtheit aller Duft–Rezeptorneuron Kombinationen nennt man auch das komplette “Olfaktom” einer Spezies. Von allen Spezies die in der Riechforschung untersucht werden, ist das Olfaktom der Fruchtfliege *Drosophila melanogaster* bisher am besten bekannt.

Das bestehende Wissen über das Olfaktom von *Drosophila* ist über viele Publikationen verteilt und die Daten der verschiedenen Studien sind aufgrund unterschiedlicher Messmethoden nicht einfach zu vergleichen. Um dieses Problem zu lösen, haben wir die DoOR Datenbank erstellt die in Kapitel 1 beschrieben ist. Mit Hilfe von DoOR ist es möglich all die verfügbaren, heterogenen Rezeptorneuron Daten in einem Konsensmodell zu vereinen welches für weitere Analysen genutzt und auf verschiedene Arten visualisiert werden kann.

Das DoOR Webinterface ermöglicht einen einfachen Zugang zum *Drosophi-*

la Olfaktom und kann beispielsweise für die Planung von physiologischen- oder Verhaltensexperimenten genutzt werden. Zusätzlich ist die komplette Datenbank, inklusive des Konsensmodells, aller Rohdaten, sowie aller Funktionen, frei verfügbar und kann somit eine hilfreiche Quelle für neuro-informatische Untersuchungen des olfaktorischen Codes sein.

Das *Drosophila* Olfaktom ist das am besten untersuchte Olfaktom, dennoch ist es noch nicht vollständig bekannt. In Kapitel 2 haben wir daher die Antwortspektren von acht Rezeptorneuron-Typen charakterisiert. Eines dieser Rezeptoneurone war zuvor komplett uncharakterisiert, wir beschreiben hier ein Antwortspektrum bestehend aus 106 Düften. Von einem weiteren Typ von Rezeptorneuron war bisher bekannt, dass es nur auf einen einzigen Duft reagiert, wir haben herausgefunden, dass auch viele andere Düfte differenzierte Aktivitäten auslösen können. Für sechs weiter Typen von Rezeptorneuronen haben wir die bekannten Antwortspektren um eine Vielzahl an Düften erweitert.

Die Ensemble-Aktivität ist nur eine Dimension des olfaktorischen Codes. Information über Duftidentität ist auch in den zeitlichen Dynamiken der Duftantworten enthalten. In Kapitel 3 haben wir daher die Antwort-Dynamiken der > 800 Duft–Rezeptorneuron Kombinationen aus Kapitel 2 im Detail untersucht. Wir haben herausgefunden, dass die Antwort-Dynamiken Duft–Rezeptorneuron spezifisch waren und sich zwischen Duft–Rezeptorneuron Kombinationen stark unterschieden. Wir haben mehrere Merkmale der Antwort-Dynamiken untersucht und festgestellt, dass diese differenziell über die Rezeptorneurone verteilt waren. Ein Merkmal war zudem über einen Bereich von Duftkonzentrationen hinweg stabil und könnte somit an der konzentrationsunabhängigen Kodierung beteiligt sein. Wir konnten zeigen, das Duftinformation im Rezeptorneuron Ensemble auch nach Beendigung der Stimulation noch vorhanden ist. Dies beruhte unter anderem auf Duft–Rezeptorneuron Kombinationen die zu besonders starken und langanhaltenden Duftantworten führten.

Während Kapitel 1–3 von Duftanworten auf monomolekulare Düfte handeln haben wir in den Kapiteln 4 und 5 Duftmischungen untersucht. Fast alle natürlich vorkommenden Düfte bestehen aus Mischungen mehrerer Moleküle. Da jede Komponente einer solchen Mischung eine Ensemble-Aktivität verschiedener Rezeptorneurone auslösen kann, können diese Ensembles in Mischungen überlappen und zu Mischungsinteraktionen führen.

In Kapitel 4 haben wir eine komplexe Mischung aus 15 Komponenten erstellt, die sich in Konzentration und Zusammensetzung an Bananenduft orientierte. In dieser Mischung fanden wir einen Duft, Isopentyl Acetat, der die Mischungsantwort von Or22a Rezeptorneuronen dominierte. Isopentyl Acetat unterdrückte dabei sowohl stärkere, niedriger konzentrierte, als auch schwächere, höher konzentrierte Komponenten, was zu hypoadditiven Mischungs-

interaktionen führte. Weitere Analysen zeigten, dass sich die Effekte, die wir gefunden haben, durch syntopische Interaktion (Kompetition von Liganden um eine Rezeptorbindestelle) erklären ließen. Wir diskutieren, dass syntopische Interaktion für die Mehrheit an suppressiven Interaktionen in der Peripherie von olfaktorischen Systemen verantwortlich sein könnte. Außerdem könnten syntopische Interaktionen eine Rolle bei konzentrationsunabhängiger Kodierung sowie bei *gain control* spielen.

In Kapitel 5 haben wir die Mischungsexperimente erweitert und mehr Mischungen und Rezeptorneurone untersucht. Starke Mischungsinteraktionen wie Suppression oder Synergismus waren selten, die Mehrzahl von 20 Mischungen führte zu additiven oder hypoadditiven Mischungsantworten in fünf getesteten Rezeptorneuron Typen. Mittels Hauptkomponentenanalyse haben wir Zeit-Trajektorien von Mischungsantworten in einem fünfdimensionalen Rezeptorraum berechnet. Die Hälfte der Mischungs-Trajektorien wurde von jeweils einer Komponente dominiert, während die andere Hälfte der Trajektorien unterschiedliche Bereiche des Rezeptorraumes erfassten. Wir diskutieren, dass diese Unterschiede in physiologischer Duftähnlichkeit ein neuronales Korrelat von Unterschieden in wahrgenommener Duftähnlichkeit sein könnten.

List of publications and declaration of self-contribution

Chapter 1 – published as:

Integrating heterogeneous odor response data into a common response model: A DoOR to the complete olfactome.
C.G. Galizia, D. Münch, M. Strauch, A. Nissler, S. Ma
2010, *Chemical Senses*, 35(7):551-63. doi: 10.1093/chemse/bjq042

Self-contribution: designed the software together with CGG, MS and SM, created the web interface, analyzed the data for ORs 13a, 67b and 92a, wrote the paper together with CGG, MS, and SM.

Chapter 2 – in preparation:

Response profiles for eight olfactory receptor neurons
D. Münch, J.S. Ignatious Raja, A. Nissler, C.G. Galizia

Self-contribution: designed the research together with CGG, JSIR and AN, performed the research together with JSIR and AN, analyzed the data, wrote the manuscript.

Chapter 3 – in preparation:

Complex dynamics of olfactory receptor neuron responses
D. Münch and C.G. Galizia

Self-contribution: designed the research together with CGG, performed the research, analyzed the data, wrote the manuscript.

Chapter 4 – published as:

Weaker ligands can dominate an odor blend due to syntopic interactions
D. Münch, B. Schmeichel, A.F. Silbering, C.G. Galizia
2013, *Chemical Senses*, 38(4):293-304. doi: 10.1093/chemse/bjs138

Self contribution: designed the research together with BS, AFS and CGG, performed the research together with BS and AFS, analyzed the data, wrote the paper together with CGG.

Chapter 5 – in preparation:

Mixture effects on the antenna of *Drosophila melanogaster*
D. Münch and C.G. Galizia

Self contribution: designed the research together with CGG, performed the research, analyzed the data, wrote the manuscript.

Danksagung

Es gibt einige Menschen, die mich auf dem Weg zu dieser Doktorarbeit unterstützt haben und denen ich hiermit danken möchte. Zuerst möchte ich natürlich GIOVANNI danken. Nicht nur dafür, dass Du diese Arbeit betreut hast, sondern auch dafür, dass Du bei Problemen jedweder Art immer ein offenes Ohr hattest und man sich immer auf Dein Verständnis und Deine Unterstützung verlassen konnte. Ich habe in den letzten Jahren mit ihren Höhen und Tiefen wirklich enorm viel gelernt. Bei PAUL, ALJA, ANNEKE, JACOB und INA möchte ich mich für die vielen hilfreichen Kommentare und Diskussionen zu dieser Arbeit bedanken. Danke ANA für den guten Start im Projekt, auch wenn Du leider viel zu früh wieder weg warst. SABINE, danke für die Hilfe am Konfokalen und das "Enthirnen" der Fliegen. SARAH und MANUEL, danke für Eure R Probleme, die mich auch immer selbst wieder ein Stück weitergebracht haben. MARTIN, danke für die Geduld die Du aufgebracht hast um mir multidimensionale Datenauswertung irgendwie in meiner maximal dreidimensionalen Welt zu veranschaulichen. Danke DAVID, dass Du immer weißt wo alles steht. Danke BIRGIT, TINE und DIETRICH, für unzählige Kreuzungen, auf den letzten Drücker bestellte Düfte und Hilfe bei allen Setup-Basteleien. Und NICHOLAS, danke für die Hilfe bei der Verteidigung der Uni gegen die *Resistance*. Danken möchte ich auch meinen Vertiefungskursstudenten, SHEREE, BEN und ANNE, sowie GABI, SHOUWEN, MICHA, TOM und all den vielen Hiwis, ohne die diese Arbeit um einige Messungen Ärmer wäre. TOM, Dir nochmal extra danke als *Lord of the Flies*, Du hast ein paar viele Bier gut bei mir. PAUL, danke für das *Kopf-Frei-Joggen*, auch wenn ich mich so oft drücke. ALJA, danke für Tee, Äpfel, Stifte, Ladegeräte ..., demnächst räume ich mal meinen Tisch auf, versprochen. Ich möchte mich bei den kompletten AGs GALIZIA und KLEINEIDAM für die gute Stimmung im Labor, auf Konferenzen und in Damüls bedanken, ich hatte die letzten Jahre wirklich viel Spaß mit Euch!

Bei FREUNDEN und der FAMILIE möchte ich mich ganz besonders bedanken. Danke, dass Ihr immer da seid wenn es brennt, und sonst auch. Danke INA, dass ich Dich habe und Du mich unterstützt wo es nur geht. Und danke LENE, dass Du mich auch nach einem miesen Tag im Nullkommanix wieder zum Lachen bringst.

DANKE!

Supplemental Figures & Tables

Supplemental Material for Chapter 1

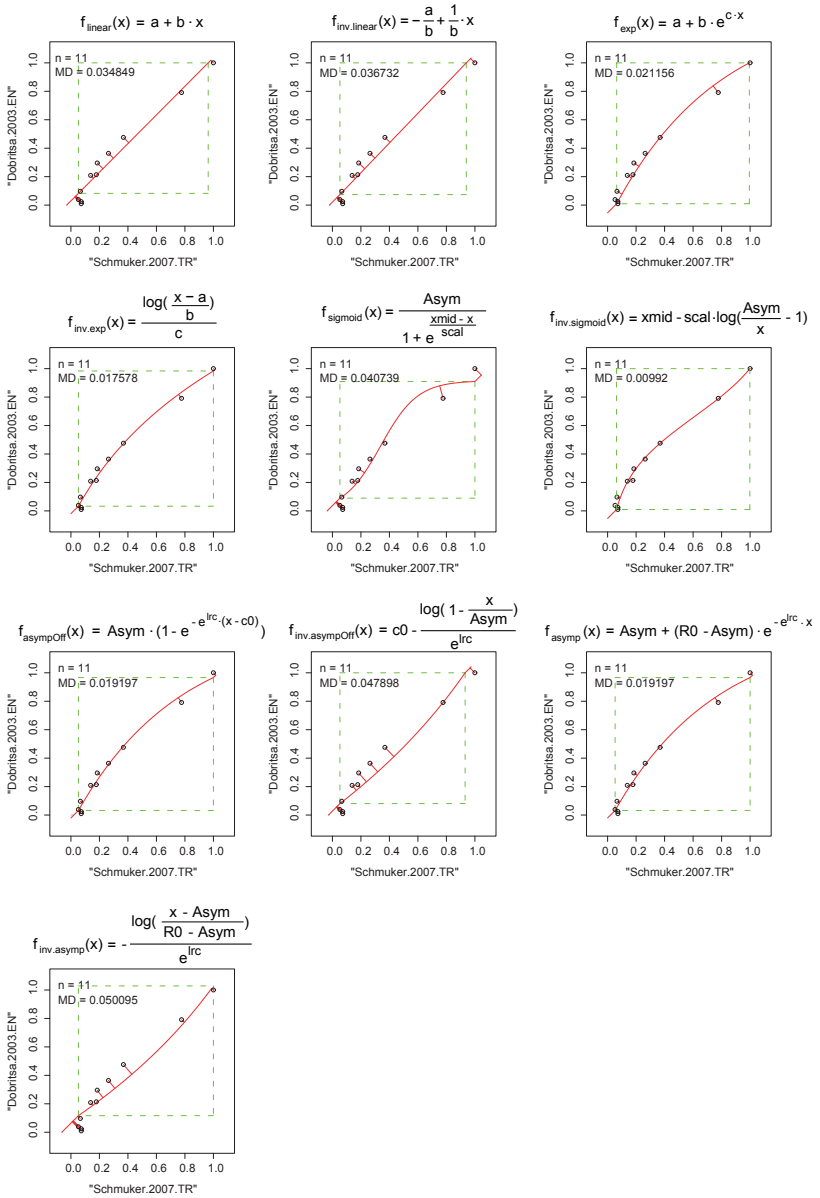

FIGURE S1: *Model functions* Performance of different model functions for *dOr22a* when plotting Dobritsa.2003.EN (Dobritsa *et al.* 2003) against Schmuker.2007.TR (Schmuker *et al.* 2007). Each fit is calculated optimizing least squares of error in y, but evaluated by calculating the mean orthogonal distance onto the best fit, given in each plot as MD. The best fit in this set is achieved with the inverted sigmoid function (MD=0.01, i.e. one hundredth of the response range [0,1]). The function is given as a mathematical formula above each inset.

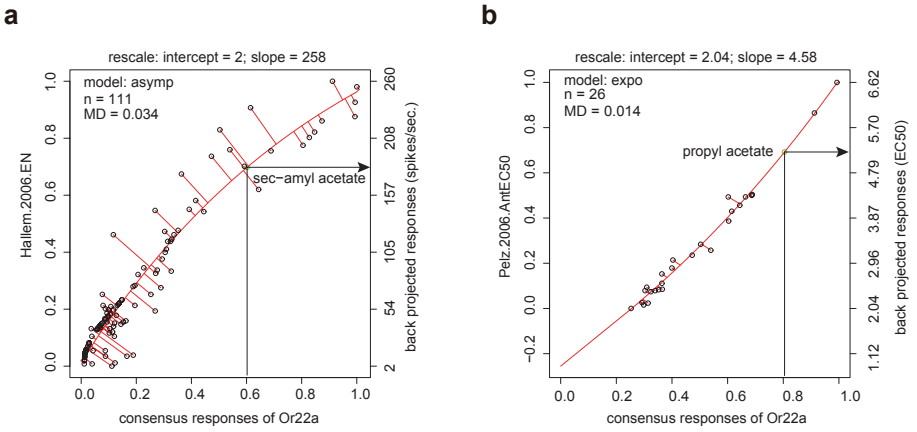

FIGURE S2: *Back projection* A consensus data set can be backprojected to the experimental data sets, allowing for the estimation of physiological responses to odors that were not tested in a particular study. In essence, the scaled axis (range [0,1], left ordinate) can be replaced by the original axis (right ordinate), and all odor response positions along the fitted curve are projected onto this axis (see example arrow). Examples for *dOr22a*. **a** example for electrophysiological data (Hallem.2006.EN, unit spikes/s) **b** example for dose-response curves (Pelz.2006.EC50, unit log-dilutions).

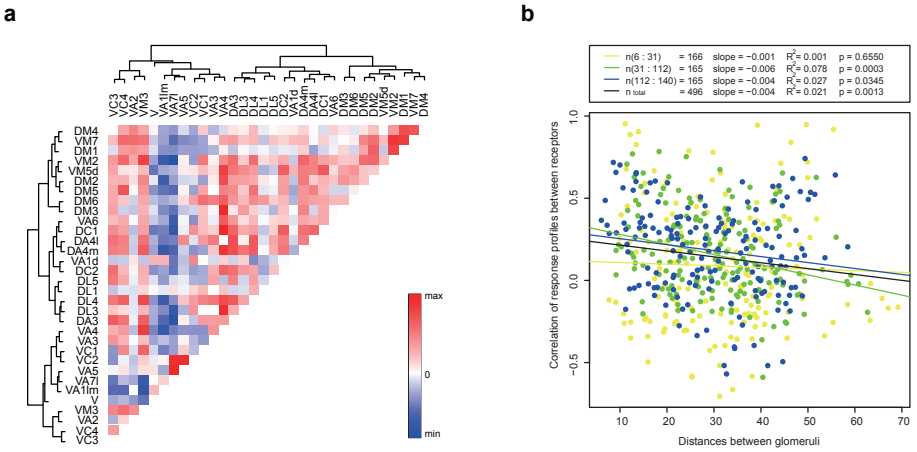

FIGURE S3: *Spatial organization of the D. melanogaster antennal lobe* **a** Pearson's correlations of odor response profiles for all glomerular pairs. Values are shown in color shades (see scale bar). The dendrograms visualize glomerular similarity. **b** Plot of odor response similarity (Pearson's correlation) between two glomeruli (ordinate) against physical distance of these glomeruli (abscissa). The observations were divided into 3 equally sized groups based on number of common odors (n, i.e. quality of the response similarity prediction). See text for details. (*Continued on next page*)

	VC3	VC4	VA2	VM3	V	VA1lm	VA7l	VA5	VC2	VC1	VA3	VA4	DA3	DL3	DL4	DL1	DL5	DC2	VA1d	DA4m	DA4l	DC1	VA6	DM3	DM6	DM5	DM2	VM5d	VM2	DM1	VM7	DM4
DM4	0.05	0.32	0.47	0.33	0.06	-0.19	-0.23	-0.04	-0.18	0.19	-0.13	-0.04	0.12	0.08	0.25	0.00	0.06	0.08	0.09	0.17	0.05	-0.03	0.18	0.11	-0.01	0.11	0.22	0.04	0.38	0.71	0.68	
VM7	0.24	0.59	0.57	0.53	-0.09	-0.21	-0.40	-0.28	-0.24	-0.19	0.07	0.32	0.36	0.22	0.25	-0.10	0.22	0.17	0.24	0.26	0.03	0.18	0.00	0.06	0.09	0.47	0.56	0.23	0.83	0.78		
DM1	-0.02	0.37	0.40	0.35	-0.02	-0.26	-0.27	-0.21	-0.21	-0.20	-0.13	0.09	-0.10	0.07	-0.02	0.02	-0.03	0.00	-0.01	0.18	-0.19	-0.05	0.01	0.16	-0.05	0.34	0.63	-0.08	0.75			
VM2	0.38	0.59	0.32	0.77	-0.20	-0.52	-0.71	0.08	-0.22	0.51	0.08	0.43	0.58	0.19	0.57	0.14	0.19	0.29	-0.08	0.60	0.48	0.33	0.29	0.19	0.22	0.57	0.59	0.24				
VM5d	0.32	0.12	0.11	0.24	-0.35	-0.17	-0.14	0.10	0.11	0.24	0.14	0.78	0.52	0.44	0.37	-0.14	-0.08	0.63	0.28	0.50	0.48	0.67	0.14	0.34	0.40	0.20	0.18					
DM2	0.27	0.28	0.13	0.45	-0.01	-0.49	-0.21	-0.04	-0.04	-0.21	0.10	0.71	0.36	0.35	0.30	0.10	0.06	0.35	-0.10	0.51	0.19	0.27	0.22	0.39	0.32	0.22						
DM5	0.30	0.67	0.06	0.39	-0.26	-0.36	-0.40	0.07	-0.20	0.32	0.04	0.47	0.44	0.20	0.55	-0.01	0.02	0.36	-0.18	0.39	0.49	0.25	-0.05	-0.05	0.09							
DM6	0.30	0.20	-0.06	0.31	-0.11	-0.18	-0.12	0.14	0.34	0.56	0.48	0.62	0.39	0.26	0.44	0.38	0.18	0.25	-0.14	0.40	0.35	0.32	0.26	0.26								
DM3	0.34	-0.06	-0.09	0.27	-0.02	-0.28	-0.36	-0.09	-0.05	0.22	0.07	0.95	0.10	0.36	0.18	-0.02	-0.13	0.22	0.05	0.47	-0.05	0.31	0.06									
VA6	0.24	0.30	0.03	0.32	-0.08	-0.17	-0.50	0.02	-0.26	0.23	0.01	0.65	0.38	0.13	0.25	0.04	0.15	0.18	-0.02	0.33	0.26	0.31										
DC1	0.43	0.34	-0.11	0.35	-0.34	-0.30	-0.59	0.00	0.41	0.23	0.17	0.94	0.60	0.31	0.35	-0.09	0.17	0.65	0.02	0.55	0.60											
DA4l	0.54	0.49	-0.07	0.54	-0.15	-0.34	-0.30	0.43	-0.02	0.38	0.51	0.05	0.70	0.08	0.66	-0.02	0.32	0.49	-0.05	0.49												
DA4m	0.49	0.45	-0.08	0.65	-0.19	-0.57	-0.43	-0.06	-0.25	-0.20	0.21	0.84	0.72	0.54	0.65	0.03	0.29	0.52	-0.15													
VA1d	-0.09	-0.07	0.11	-0.09	0.26	0.27	-0.34	-0.10	0.45	0.05	-0.04	0.17	-0.06	0.17	-0.28	-0.15	-0.05	0.03														
DC2	0.57	0.25	0.07	0.28	-0.25	-0.20	-0.35	-0.09	-0.22	-0.17	0.28	0.61	0.55	0.37	0.33	-0.18	0.23															
DL5	0.51	0.32	0.01	0.27	-0.02	-0.22	-0.03	0.00	-0.15	-0.17	0.32	-0.11	0.48	-0.04	0.35	-0.05																
DL1	-0.09	-0.01	-0.03	0.15	0.03	0.00	0.13	0.01	0.16	0.25	0.05	0.22	-0.04	-0.03	0.29																	
DL4	0.52	0.62	-0.01	0.74	-0.24	-0.52	-0.26	0.21	0.36	0.47	0.53	0.72	0.66	0.34																		
DL3	0.20	0.14	0.00	0.26	-0.16	-0.27	-0.58	-0.14	0.39	0.03	0.04	0.92	0.29																			
DA3	0.64	0.54	0.01	0.63	-0.17	-0.41	-0.66	0.08	-0.09	0.37	0.36	0.37																				
VA4	0.29	0.37	-0.12	0.79	-0.29	-0.58	-0.31	-0.25	-0.26	-0.25	0.40																					
VA3	0.41	0.27	0.05	0.23	-0.19	-0.11	-0.20	0.07	-0.13	-0.23																						
VC1	-0.24	0.45	-0.03	0.60	-0.05	-0.30	-0.21	0.18	-0.12																							
VC2	-0.25	0.01	-0.10	0.18	0.00	0.07	0.89	0.91																								
VA5	0.02	0.12	-0.06	0.13	0.13	-0.18	0.95																									
VA7l	-0.35	-0.13	-0.18	-0.52	0.04	0.17																										
VA1lm	-0.40	-0.40	0.04	-0.59	0.25																											
V	-0.18	-0.13	-0.23	-0.36																												
VM3	0.46	0.56	0.43																													
VA2	-0.15	0.16																														
VC4	0.37																															
VC3																																

FIGURE S3: (*Continued*) Data for a

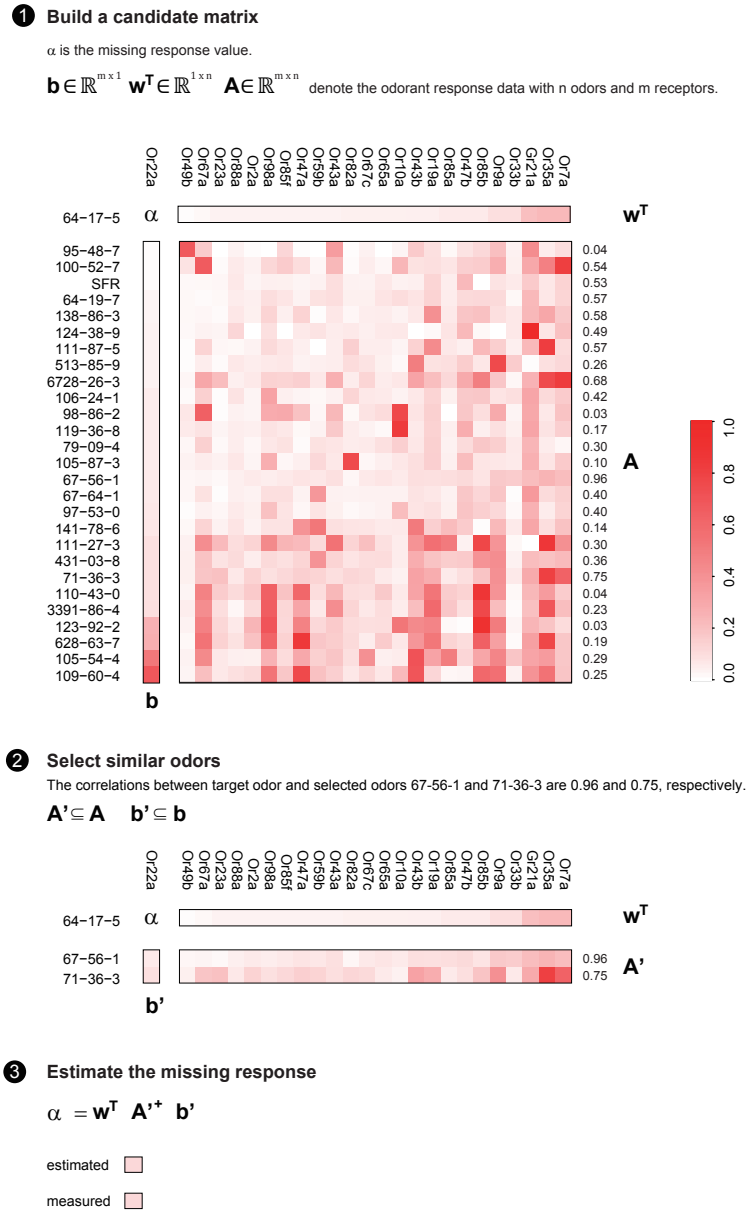

FIGURE S4: *Algorithm for missing data imputation* The missing response of *Or22a* to odor 64-17-5 (ethanol) is denoted by α. A is the NA-free submatrix of the complete odor response matrix (step 1). **w** and **b** are vectors representing the response values of odor 64-17-5 and receptor *Or22a*, respectively. The two most similar odors are selected (Pearson's correlation coefficient), and form the submatrix **A'** and the subvector **b'** (step 2). The missing response α is estimated by least squares imputation (Kim et al., 2005) (see step 3 for the formula). (*Continued on next page*)

	Or22a	Or49b	Or67a	Or23a	Or88a	Or2a	Or98a	Or85f	Or47a	Or59b	Or43a	Or82a	Or67c	Or65a	Or10a	Or43b	Or19a	Or85a	Or47b	Or85b	Or9a	Or33b	Gr21a	Or35a	Or7a
64-17-5	NA	0.01	0.03	0.03	0.03	0.04	0.04	0.04	0.05	0.05	0.06	0.06	0.06	0.06	0.07	0.08	0.09	0.10	0.10	0.11	0.15	0.15	0.21	0.22	0.23
95-48-7	0.01	0.66	0.15	0.00	0.03	0.00	0.00	0.12	0.01	0.00	0.34	0.01	0.03	0.00	0.02	0.16	0.08	0.02	0.07	0.11	0.20	0.03	0.41	0.05	0.09
100-52-7	0.03	0.07	0.65	0.01	0.05	0.03	0.11	0.16	0.09	0.02	0.22	0.01	0.04	0.02	0.23	0.08	0.09	0.07	0.14	0.15	0.26	0.04	0.29	0.47	0.79
SFR	0.03	0.01	0.02	0.02	0.06	0.03	0.04	0.04	0.03	0.03	0.09	0.03	0.03	0.06	0.03	0.04	0.12	0.04	0.22	0.00	0.08	0.05	0.16	0.06	0.13
64-19-7	0.05	0.02	0.01	0.02	0.05	0.04	0.09	0.07	0.03	0.08	0.09	0.04	0.04	0.07	0.09	0.07	0.13	0.05	0.10	0.11	0.11	0.02	0.22	0.06	0.12
138-86-3	0.06	0.02	0.02	0.01	0.06	0.03	0.12	0.04	0.13	0.01	0.06	0.02	0.04	0.05	0.03	0.06	0.40	0.05	0.17	0.19	0.09	0.06	0.22	0.29	0.16
124-38-9	0.06	0.01	0.03	0.02	0.12	0.00	0.08	0.00	0.06	0.08	0.05	0.06	0.04	0.06	0.06	0.00	0.01	0.07	0.22	0.02	0.00	0.06	0.97	0.07	0.19
111-87-5	0.07	0.01	0.12	0.02	0.02	0.03	0.10	0.07	0.04	0.00	0.05	0.14	0.04	0.04	0.02	0.13	0.42	0.06	0.04	0.22	0.14	0.04	0.22	0.79	0.10
513-85-9	0.08	0.01	0.04	0.01	0.06	0.04	0.05	0.06	0.03	0.04	0.04	0.10	0.08	0.04	0.01	0.48	0.08	0.09	0.15	0.06	0.74	0.15	0.01	0.08	0.11
6728-26-3	0.09	0.02	0.29	0.20	0.04	0.05	0.13	0.12	0.14	0.06	0.25	0.05	0.12	0.05	0.06	0.31	0.20	0.11	0.28	0.47	0.17	0.02	0.24	0.74	0.81
106-24-1	0.09	0.01	0.13	0.01	0.07	0.03	0.31	0.04	0.02	0.02	0.03	0.12	0.06	0.05	0.03	0.06	0.13	0.03	0.16	0.17	0.07	0.09	0.30	0.11	0.15
98-86-2	0.09	0.06	0.62	0.01	0.03	0.02	0.27	0.28	0.18	0.02	0.22	0.02	0.07	0.10	0.74	0.07	0.13	0.00	0.17	0.09	0.28	0.02	0.29	0.06	0.18
119-36-8	0.10	0.05	0.07	0.03	0.04	0.04	0.07	0.06	0.02	0.03	0.16	0.05	0.03	0.01	0.82	0.05	0.13	0.04	0.26	0.04	0.08	0.04	0.30	0.08	0.14
79-09-4	0.10	0.02	0.13	0.01	0.04	0.02	0.06	0.08	0.01	0.08	0.07	0.05	0.05	0.08	0.14	0.06	0.13	0.03	0.10	0.17	0.14	0.05	0.23	0.05	0.02
105-87-3	0.10	0.03	0.05	0.03	0.06	0.02	0.26	0.02	0.04	0.11	0.06	0.74	0.02	0.04	0.06	0.08	0.14	0.04	0.20	0.07	0.06	0.05	0.25	0.07	0.16
67-56-1	0.12	0.02	0.02	0.01	0.04	0.05	0.04	0.05	0.07	0.06	0.08	0.02	0.05	0.07	0.05	0.09	0.08	0.09	0.10	0.07	0.16	0.15	0.21	0.24	0.20
67-64-1	0.13	0.02	0.08	0.00	0.04	0.03	0.09	0.09	0.03	0.36	0.03	0.03	0.03	0.03	0.03	0.08	0.06	0.03	0.17	0.11	0.17	0.01	0.35	0.10	0.13
97-53-0	0.14	0.01	0.03	0.02	0.05	0.04	0.19	0.07	0.02	0.07	0.04	0.01	0.02	0.03	0.21	0.07	0.08	0.03	0.18	0.14	0.11	0.01	0.25	0.05	0.12
141-78-6	0.17	0.02	0.12	0.03	0.07	0.03	0.08	0.07	0.38	0.51	0.08	0.07	0.07	0.05	0.05	0.50	0.14	0.21	0.15	0.00	0.22	0.05	0.30	0.09	0.19
111-27-3	0.22	0.03	0.40	0.21	0.09	0.12	0.43	0.23	0.21	0.10	0.53	0.12	0.20	0.08	0.05	0.38	0.55	0.50	0.03	0.76	0.37	0.02	0.00	0.84	0.40
431-03-8	0.23	0.03	0.18	0.07	0.10	0.04	0.11	0.08	0.12	0.37	0.12	0.07	0.09	0.10	0.05	0.27	0.18	0.15	0.16	0.38	0.40	0.03	0.21	0.19	0.21
71-36-3	0.26	0.04	0.17	0.19	0.06	0.13	0.08	0.11	0.14	0.13	0.09	0.12	0.10	0.05	0.03	0.32	0.26	0.05	0.09	0.18	0.40	0.06	0.28	0.78	0.61
110-43-0	0.27	0.02	0.46	0.15	0.10	0.16	0.62	0.18	0.59	0.09	0.22	0.10	0.08	0.16	0.06	0.31	0.52	0.15	0.13	0.85	0.38	0.02	0.22	0.35	0.15
3391-86-4	0.30	0.04	0.41	0.09	0.02	0.10	0.64	0.11	0.30	0.05	0.40	0.12	0.06	0.09	0.05	0.20	0.58	0.17	0.09	0.75	0.20	0.01	0.19	0.67	0.20
123-92-2	0.53	0.03	0.47	0.11	0.06	0.23	0.68	0.11	0.46	0.11	0.16	0.10	0.08	0.09	0.51	0.42	0.45	0.01	0.00	0.89	0.49	0.02	0.23	0.18	0.10
628-63-7	0.55	0.02	0.53	0.13	0.08	0.19	0.61	0.13	0.83	0.17	0.15	0.10	0.05	0.15	0.06	0.37	0.51	0.12	0.09	0.62	0.33	0.01	0.33	0.76	0.17
105-54-4	0.59	0.03	0.42	0.06	0.04	0.04	0.24	0.10	0.28	0.14	0.18	0.09	0.40	0.04	0.05	0.69	0.31	0.49	0.12	0.30	0.44	0.17	0.30	0.34	0.17
109-60-4	0.69	0.02	0.20	0.06	0.08	0.11	0.52	0.16	0.74	0.19	0.14	0.06	0.12	0.06	0.21	0.68	0.12	0.02	0.02	0.59	0.54	0.03	0.38	0.53	0.18

Figure S4: (*Continued*) Data for Figure

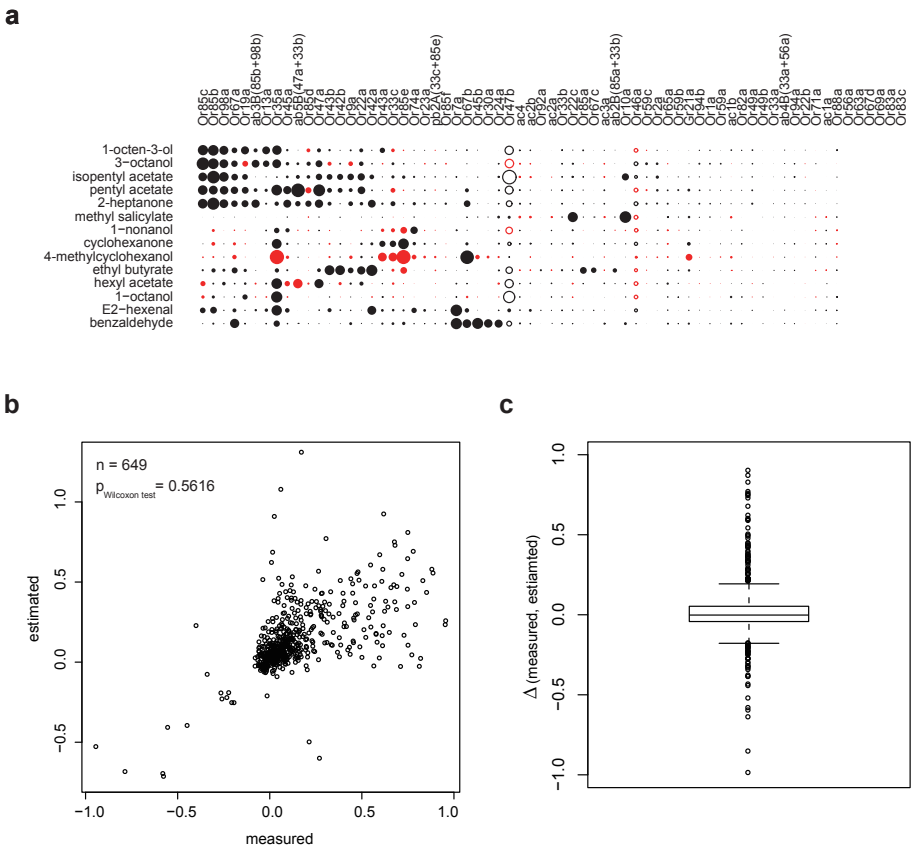

FIGURE S5: *Missing odor response estimation* **a** Plot of selected odors across all available receptors. Negative responses are given as empty circles. Black entries are measured values, red entries are those estimated. **b** Analysis of the measured values using Leave-one-out method and plotting the estimated against measured values. n indicates the number of black entries in a. A paired Wilcoxon test shows no significant relationship between the two, indicating that many estimated values are not reliable. **c** Box plot of the difference between measured and estimated values from b, again showing many unreliable estimates.

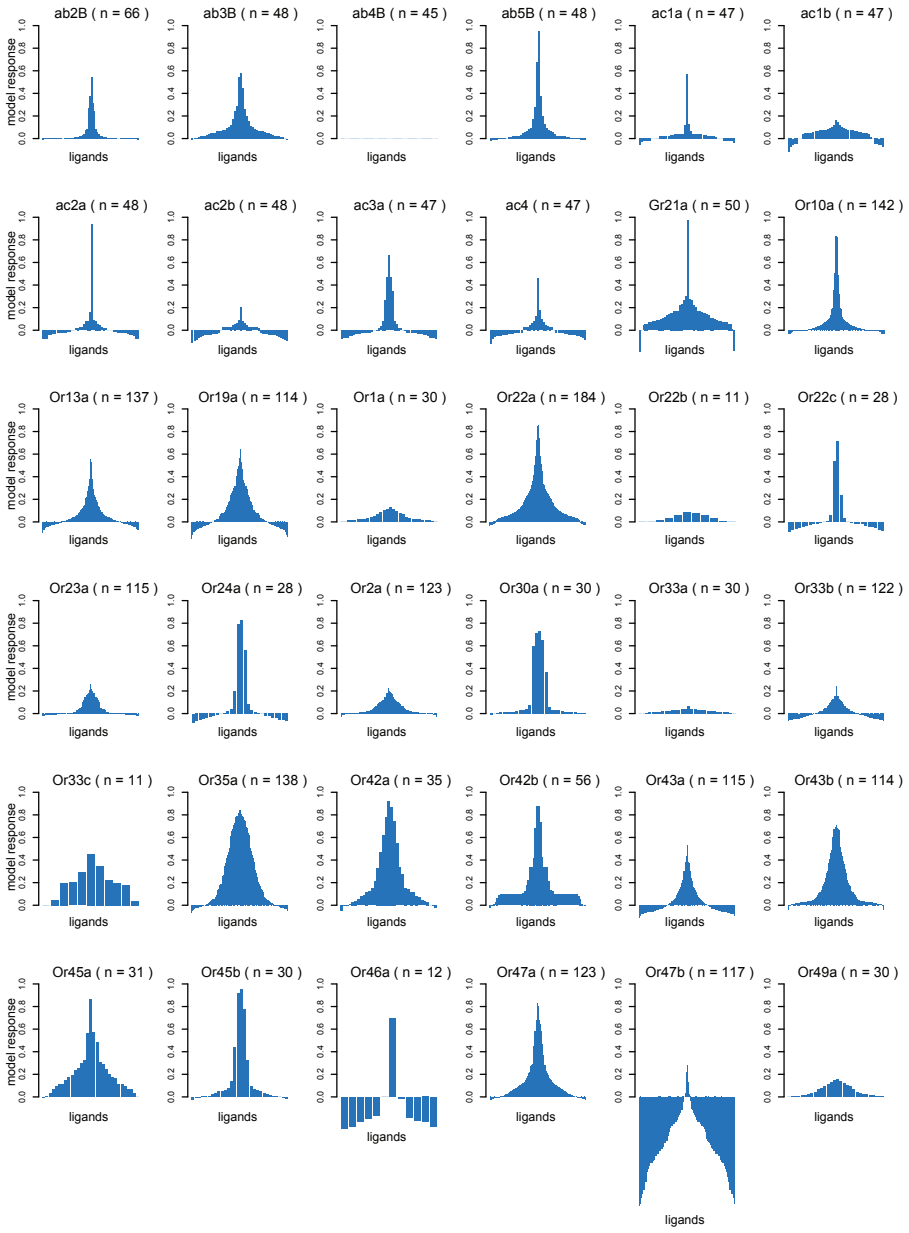

FIGURE S6: *Tuning breadth of receptor response profiles* Plot of tuning breadth for all receptors, as shown in Figure 1.4B. (*Continued on next page*)

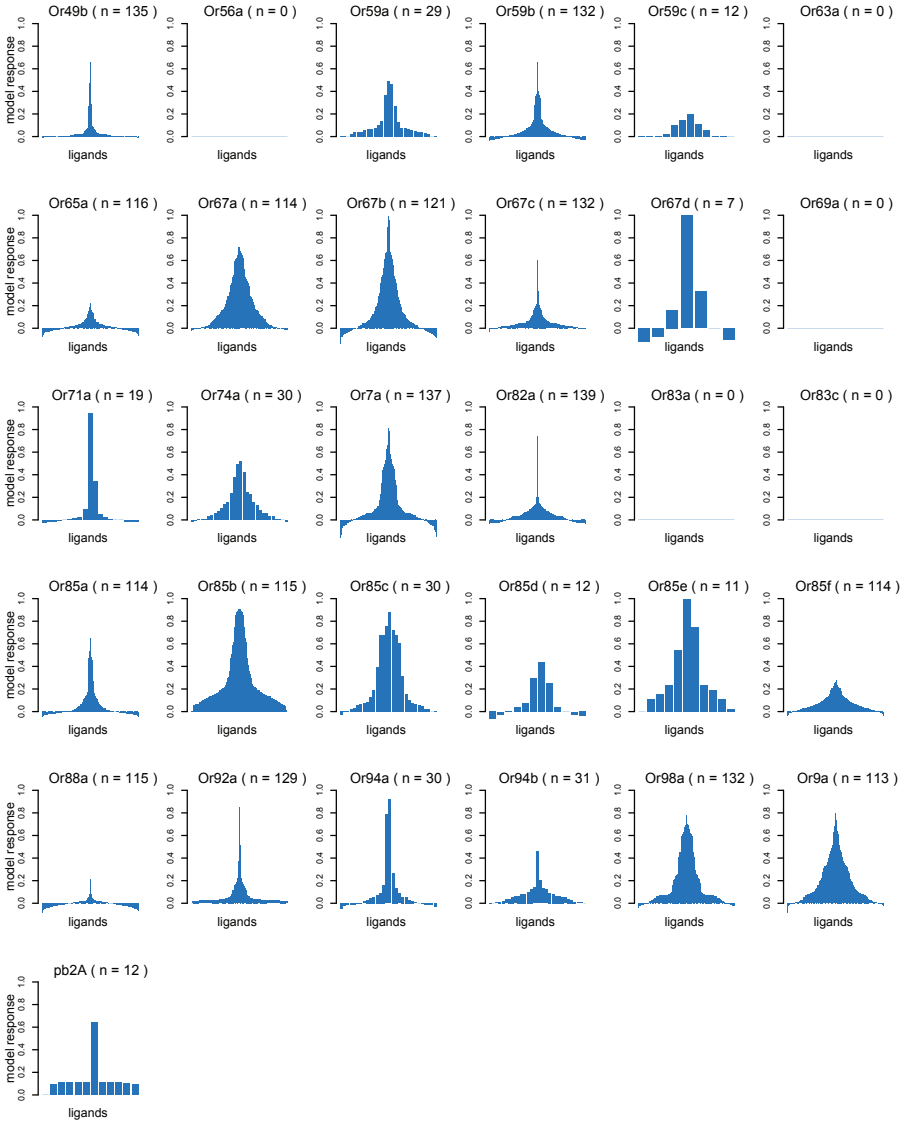

FIGURE S6: *Continued*

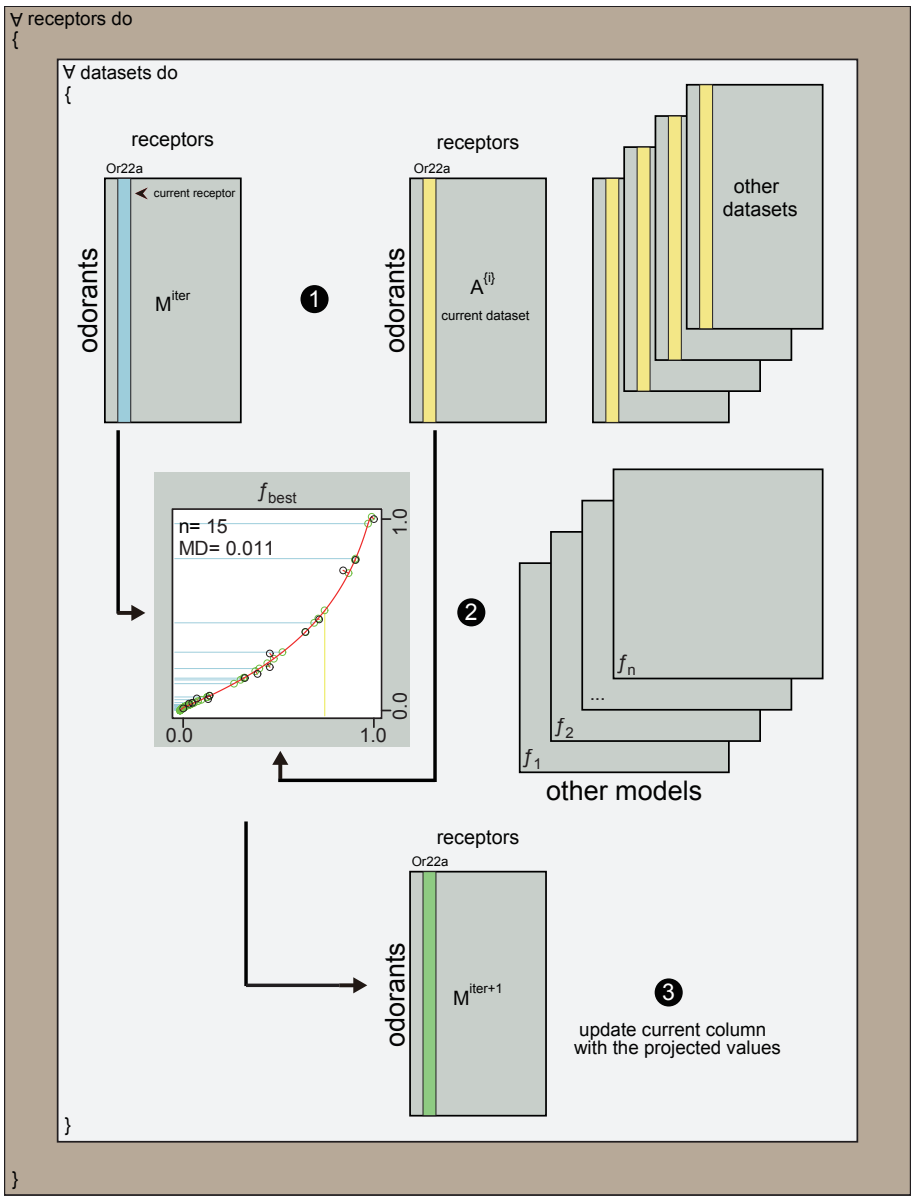

FIGURE S7: *Flow chart of the pipeline used* The Figure exemplifies the procedure taken: go through all receptors, and for each receptor (shown as a column) merge all data sets sequentially (shown as matrices, with the receptor being treated as yellow column). Each merging step selects the best from a set of available functions, and creates a consensus response (green column in the bottom matrix). This response is fed into the next iteration for this receptor.

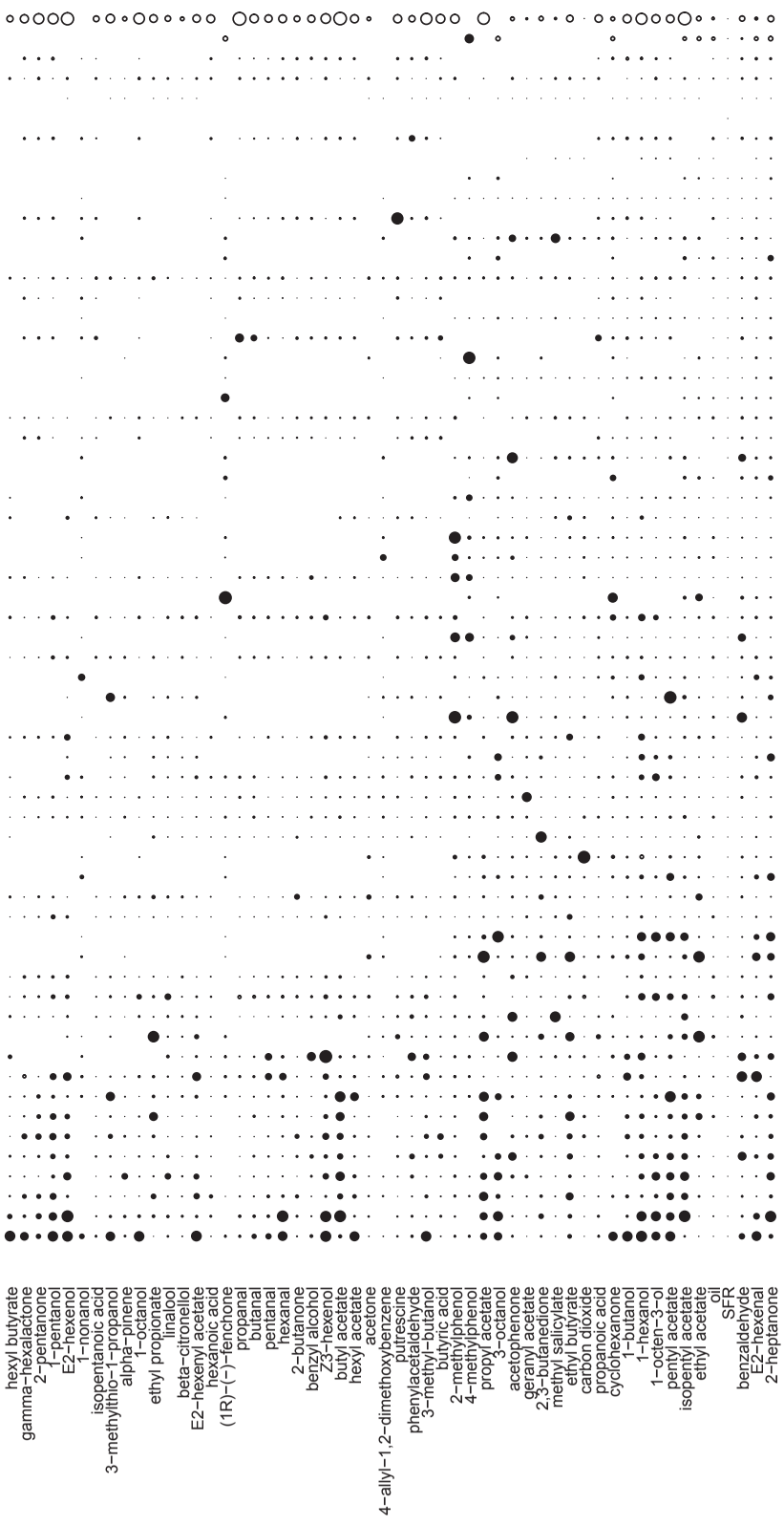

FIGURE S8: *Ball plot of response matrix* The positive responses are given as filled black circles and the negative responses are given as empty circles. Odors were sorted by descending total response across receptors. (*Continued on next page*)

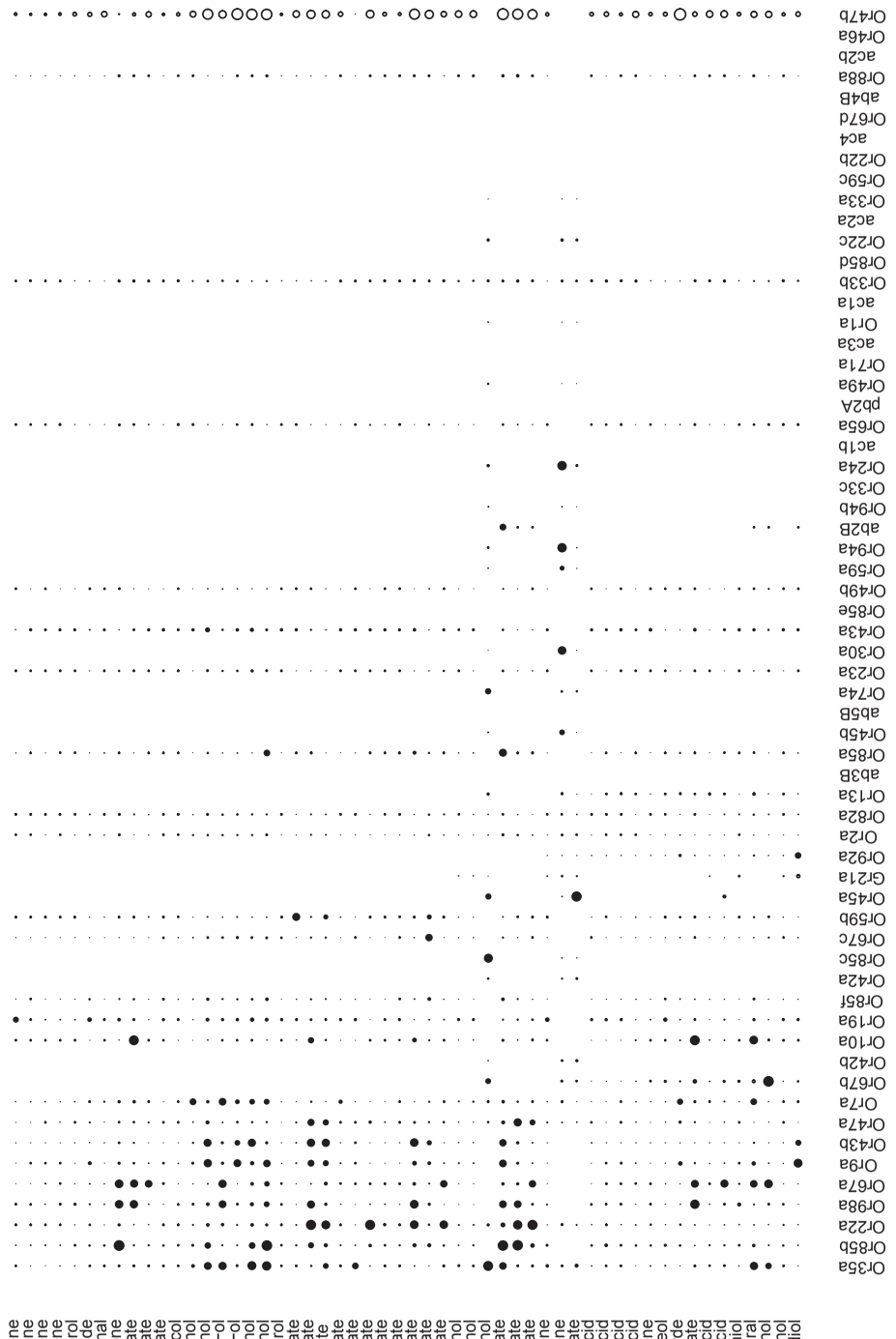

FIGURE S8: *Continued*

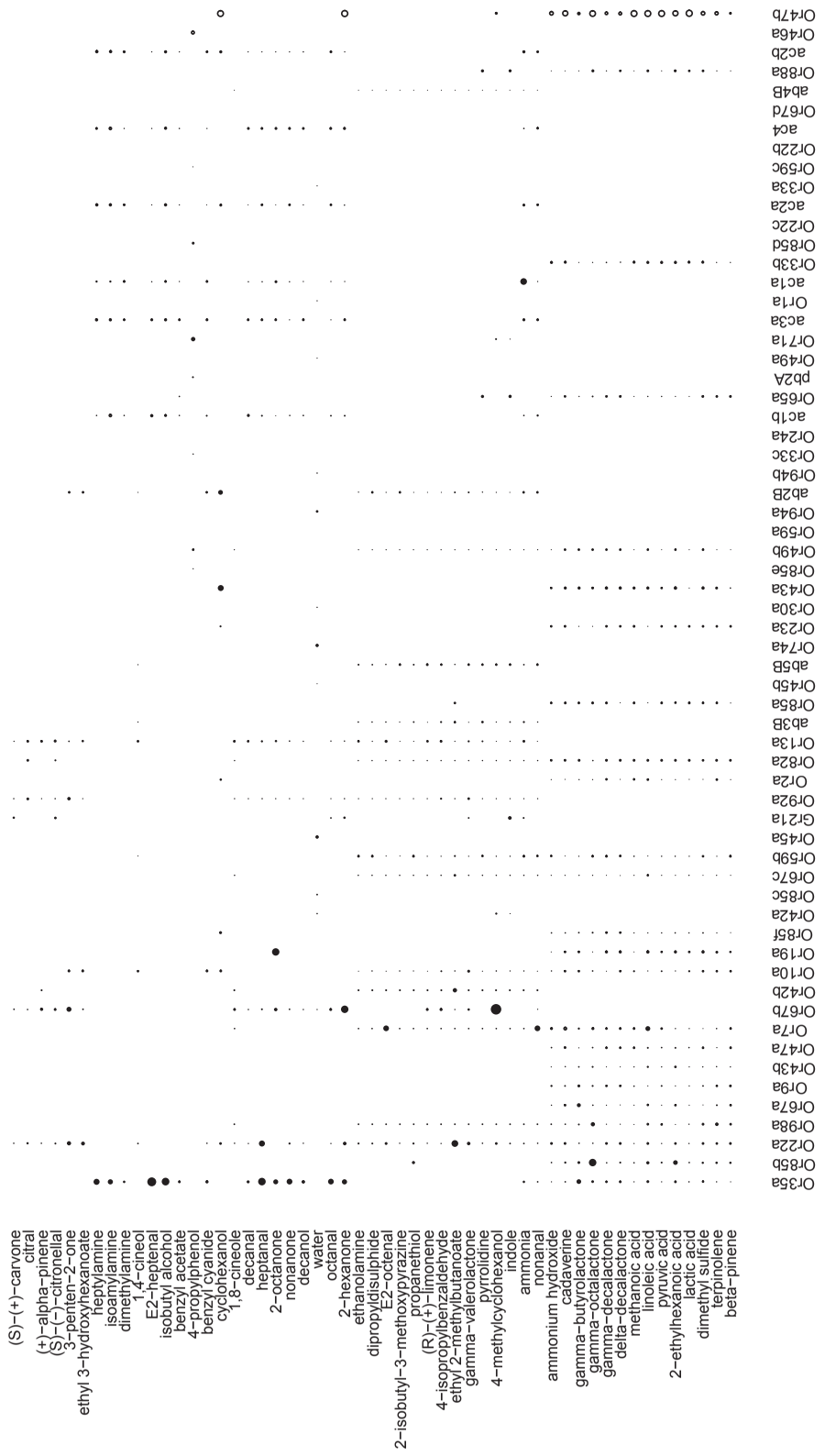

FIGURE S8: *Continued*

TABLE S1: List of receptors with their respective olfactory neuron (ORN, nomenclature based on the innervated sensillum) and glomerulus, including the best ligand, its CAS number, and the consensus response. In cases of weak maximum response the best ligand is placed in parentheses. Response breadth across the number of tested odors is given as the rank of the odor with half maximal response, scaled to [0,1]. For example, a breadth of 0.3 means that 30 % of the tested odors had responses above the half of this receptor's maximal response.

Sensillum		ORN	Receptor(s)	Glomerulus	Best Ligand	CAS	Response	Breadth	# Odors
TRICHODEA	(ANTENNA)	at1	*Or67d*	DA1	cis-vaccenyl acetate	6186-98-7	1.00	0.12	7
		at2	*Or23a*	DA3	(1-pentanol)	71-41-0	0.26	0.15	115
		at2	*Or83c*	DC3					
		at3	*Or2a*	DA4m	(isopentyl acetate)	123-92-2	0.23	0.18	123
		at3	*Or19a, Or19b*	DC1	2-octanone	111-13-7	0.64	0.17	114
		at3	*Or43a*	DA4l	1-hexanol	111-27-3	0.53	0.10	115
		at4	*Or47b*	VA1lm	(gamma-butyrolactone)	96-48-0	0.28	0.39	117
		at4	*Or65a, b, c*	DL3	(pyrrolidine)	123-75-1	0.22	0.11	116
		at4	*Or88a*	VA1d	(pyrrolidine)	123-75-1	0.22	0.02	115
BASICONICA	(ANTENNA)	ab1A	*Or42b*	DM1	ethyl acetate	141-78-6	0.88	0.07	56
		ab1B	*Or92a*	VA2	2,3-butanedione	431-03-8	0.85	0.01	129
		ab1C	*Gr21a, Gr63a*	V	carbon dioxide	124-38-9	0.97	0.06	50
		ab1D	*Or10a, Gr10a*	DL1	ethyl benzoate	93-89-0	0.83	0.05	142
		ab2A	*Or59b*	DM4	methyl acetate	79-20-9	0.66	0.05	132
		ab2B	*Or33b, Or85a*	DM5	ethyl 3-hydroxybutyrate	5405-41-4	0.54	0.05	66
		ab2B	*Or33b*	DM5	(ethyl propionate)	105-37-3	0.24	0.15	122
		ab2B	*Or85a*	DM5	3-hydroxybutyrate	5405-41-4	0.65	0.04	114
		ab3A	*Or22a, Or22b*	DM2	isobutyl acetate	110-19-0	0.85	0.09	184
		ab3B	*Or85b*	VM5d	6-methyl-5-hepten-2-one	110-93-0	0.91	0.18	115
		ab4A	*Or7a*	DL5	E2-hexenal	6728-26-3	0.81	0.15	137
		ab4B	*Or33a, Or56a*	DA2			0.00		45
		ab4B	*Or33a*	DA2	(2-heptanone)	110-43-0	0.06	0.28	30
		ab4B	*Or56a*	DA2					
		ab5A	*Or82a*	VA6	geranyl acetate	105-87-3	0.74	0.01	139
		ab5B	*Or33b, Or47a*	DM3	pentyl acetate	628-63-7	0.96	0.04	48
		ab5B	*Or33b*	DM3	(ethyl propionate)	105-37-3	0.24	0.15	122
		ab5B	*Or47a*	DM3	pentyl acetate	628-63-7	0.83	0.10	123
		ab6A	*Or13a*	DC2	1-octen-3-ol	3391-86-4	0.82	0.07	133
		ab6B	*Or49b*	VA5	2-methylphenol	95-48-7	0.66	0.02	135
		ab7A	*Or98a*	VM5v	ethyl benzoate	93-89-0	0.78	0.16	132
		ab7B	*Or67c*	VC4 (VC3m)	ethyl lactate	97-64-3	0.60	0.02	132
		ab8A	*Or43b*	VM2	ethyl trans-2-butenoate	623-70-1	0.71	0.17	114
		ab8B	*Or9a*	VM3	3-hydroxy-2-butanone	513-86-0	0.80	0.16	113
		ab9	*Or67b*	VA3	Z3-hexenol	928-96-1	0.99	0.15	121
		ab9	*Or69aA, Or69aB*	D					
		ab10	*Or49a, Or85f*	DL4					
		ab10	*Or49a*	DL4	(2-heptanone)	110-43-0	0.15	0.30	30
		ab10	*Or85f*	DL4	(acetophenone)	98-86-2	0.28	0.21	114
		ab10	*Or67a*	DM6	phenylethyl alcohol	60-12-8	0.72	0.20	114
COELOCONICA	(ANTENNA)	ac1	*Ir31a*		ammonia	7664-41-7			
		ac1	*Ir75d*		ammonia	7664-41-7			
		ac1	*Ir92a, Ir76b*		ammonia	7664-41-7			
		ac2	*Ir75a*		1,4-diaminobutane	110-60-1			
		ac2	*Ir75d*		1,4-diaminobutane	110-60-1			
		ac2	*Ir76b*		1,4-diaminobutane	110-60-1			
		ac3 (ac3a)	*Ir75a, Ir75d*		propanal	123-38-6	0.66	0.08	47
		ac3 (ac3b)	*Or35a, Ir76b*	VC3l	1-hexanol	111-27-3	0.84	0.29	138
		ac4	*Ir84a*		phenylacetaldehyde	122-78-1			
		ac4	*Ir75d*		phenylacetaldehyde	122-78-1			
		ac4	*Ir76a, Ir76b*		phenylacetaldehyde	122-78-1			
BASICONICA	(PALP)	pb1A	*Or42a*	VM7	propyl acetate	109-60-4	0.92	0.18	35
		pb1B	*Or71a*	VC2	4-methylphenol	106-44-5	0.95	0.04	19
		pb2A	*Or33c, Or85e*	VC1	(1R)-(-)-fenchone	7787-20-4	0.64	0.05	12
		pb2A	*Or33c*	VC1	(cyclohexanone)	108-94-1	0.45	0.27	12
		pb2A	*Or85e*	VC1	(1R)-(-)-fenchone	7787-20-4	1.00	0.20	11
		pb2B	*Or46a*	VA7l	4-methylphenol	106-44-5	0.70	0.06	12
		pb3A	*Or59c*	1	(3-octanol)	589-98-0	0.20	0.27	12
		pb3B	*Or85d*	VA4	(2-heptanone)	110-43-0	0.44	0.20	12

The breadth was computed as width with response of this receptor to half maximum.

Odors: number of odors that has been tested for this receptor.

(): response of this odor does not reach 0.50.

TABLE S2: A list of all studies that contributed to DoOR in the current version along with details on the respective experiments and nomenclature.

dataset	study	SFR reported	SFR substracted	technique	data type	solvents
Bruyne.1999.WT	de Bruyne et.al.,1999	yes	yes	electrophysiology	spikes	oil
Bruyne.2001.RR	de Bruyne et.al.,2001	no	no	electrophysiology	spikes	oil
Bruyne.2001.WT	de Bruyne et.al.,2001	yes	yes	electrophysiology	spikes	oil
Dobritsa.2003.EN	Dobritsa et.al.,2003	no	no	electrophysiology	spikes	oil
Goldman.2005.EN	Goldman et.al.,2005	no	yes	electrophysiology	spikes	oil
Goldman.2005.WT	Goldman et.al.,2005	no	yes	electrophysiology	spikes	oil
Hallem.2004.EN	Hallem et.al.,2004	yes	only in datasets with inhibition	electrophysiology	spikes	oil and water
Hallem.2004.WT	Hallem et.al.,2004	yes	only in datasets with inhibition	electrophysiology	spikes	oil and water
Hallem.2006.EN	Hallem et.al.,2006	yes	yes	electrophysiology	spikes	oil and water
Kreher.2005.EN	Kreher et.al.,2005	yes	no	electrophysiology	spikes	oil and water
Kreher.2008.EN	Kreher et.al.,2008	yes	yes	electrophysiology	spikes	oil and water
Kwon.2007.EN	Kwon et.al.,2007	yes	yes	electrophysiology	spikes	CO_2 was diluted in N_2
Kwon.2007.WT	Kwon et.al.,2007	no	yes	electrophysiology	spikes	CO_2 was diluted in N_2
Galizia.2009.nmr	Galizia et. al.,2009	no SFR	no SFR	calcium imaging	normalized mean responses	oil
Nissler.2007.EC50	Nissler et.al.,2007	no SFR	no SFR	calcium imaging	normalized mean responses	oil
Nissler.2007.nmr	Nissler et.al.,2007	no SFR	no SFR	calcium imaging	EC50	oil
Pelz.2005.ALnmr	Pelz et.al.,2005	no SFR	no SFR	calcium imaging	normalized mean responses	oil
Pelz.2005.Antnmr	Pelz et.al.,2005	no SFR	no SFR	calcium imaging	normalized mean responses	oil
Pelz.2005.Or47bnmr	Pelz et.al.,2005	no SFR	no SFR	calcium imaging	normalized mean responses	oil
Pelz.2006.ALEC50	Pelz et.al.,2006	no SFR	no SFR	calcium imaging	EC50	oil
Pelz.2006.AntEC50	Pelz et.al.,2006	no SFR	no SFR	calcium imaging	EC50	oil
Schmuker.2007.TR	Schmuker et.al.,2007	yes	yes	electrophysiology	spikes	oil
Stensmyr.2003.WT	Stensmyr et.al.,2003	no	no	electrophysiology	spikes	oil and water
van.der.Goes.van.Naters.2007.EN	Van der Goes van Naters et.al.,2007	yes	no	electrophysiology	spikes	oil
Yao.2005.WT	Yao et.al.,2005	yes	yes	electrophysiology	spikes	oil
Turner.2009.SC	Turner et. Al., 2009	no	yes	electrophysiology	spikes	oil

TABLE S3: Response values as measured for *dOr13a* (data set Nissler.2007.nmr and Nissler.2007.EC50) (Nissler, 2007) and *dOr67b* and *dOr92a* (data set Galizia.2009.nmr), as specifically measured for this study. Nmr values are $\Delta F/F$, EC50 values are effective odor dilutions (see Methods).

Name	CAS	Or13a	Or67b	Or92a
acetic acid	64-19-7	0.01	0.26	0.02
propanoic acid	79-09-4	0.19	0.25	0.02
butyric acid	107-92-6	0.27	0.27	0.04
pentanoic acid	109-52-4	0.17	0.17	0.03
hexanoic acid	142-62-1	0.21	0.25	0.04
heptanoic acid	111-14-8	0.22	0.22	0.05
octanoic acid	124-07-2	0.18	0.24	0.05
nonanoic acid	112-05-0	0.11	0.22	0.05
isobutyric acid	79-31-2	0.19	0.25	0.02
(-)-trans-caryophyllene	87-44-5	0.27	0.21	0.04
alpha-terpineol	10482-56-1	0.18	0.15	0.03
geraniol	106-24-1	0.24	0.16	0.05
linalool	78-70-6	0.26	0.10	0.07
beta-citronellol	106-22-9	0.14	0.24	0.07
(R)-(-)-carvone	6485-40-1	0.22	0.22	0.05
(S)-(+)-carvone	2244-16-8	0.28	0.27	0.05
1,8-cineole	470-82-6	0.18	0.19	0.05
citral	5392-40-5	0.18	0.26	0.25
(S)-(-)-citronellal	5949-05-3	0.13	0.19	0.06
(1R)-(-)-fenchone	7787-20-4	0.20	0.15	0.03
(R)-(+)-limonene	5989-27-5	0.27	0.18	0.03
(1R)-(-)-myrtenal	564-94-3	0.15	0.11	0.02
(+)-alpha-pinene	7785-70-8	0.17	0.13	0.03
(R)-(+)-pulegon	89-82-7	0.23	0.17	0.03
(-)-alpha-thujone	546-80-5	0.11	0.12	0.07
alpha-bisabolol	23089-26-1	0.22	0.22	0.05
E,E-farnesol	106-28-5	0.24	0.17	0.08
alpha-ionone	127-41-3	0.22	0.16	0.04
beta-ionone	79-77-6	0.20	0.15	0.04
acetaldehyde	75-07-0	0.12	0.30	0.31
propanal	123-38-6	0.14	0.26	0.07
butanal	123-72-8	0.18	0.29	0.02
pentanal	110-62-3	0.25	0.57	0.02
hexanal	66-25-1	0.39	0.36	0.01
E2-hexenal	6728-26-3	0.54	0.27	0.20
furfural	98-01-1	-0.13	0.01	0.16
octanal	124-13-0	0.30	0.17	0.02
decanal	112-31-2	0.21	0.25	0.03
heptanal	111-71-7	0.48	0.28	0.05
nonanal	124-19-6	0.32	0.23	0.04
acetone	67-64-1	0.16	0.22	0.03
2-butanone	78-93-3	0.32	0.24	0.21
2-heptanone	110-43-0	0.46	0.68	0.03
2,3-butanedione	431-03-8	0.27	0.30	1.24
3-penten-2-one	625-33-2	0.36	0.49	0.34
2-hexanone	591-78-6	0.31	0.68	0.05
3-hexanone	589-38-8	0.25	0.17	0.30
cyclohexanone	108-94-1	0.24	0.42	0.02
2-octanone	111-13-7	0.63	0.39	0.03
nonanone	821-55-6	0.34	0.27	0.03
phenethyl alcohol	60-12-8	0.30	1.08	0.05
benzyl alcohol	100-51-6	0.32	0.71	0.02
methyl salicylate	119-36-8	0.20	0.20	0.03
ethyl benzoate	93-89-0	0.20	0.45	0.08
benzaldehyde	100-52-7	0.12	0.61	0.02
phenylacetaldehyde	122-78-1	0.19	0.63	0.05

Name	CAS	Or13a	Or67b	Or92a
eugenol	97-53-0	0.18	0.25	0.06
4-propenyl anisole	104-46-1	0.00	NA	NA
4-methoxybenzaldehyde	123-11-5	0.25	0.20	0.03
4-isopropylbenzaldehyde	122-03-2	0.16	0.15	0.04
4-methoxybenzene	100-66-3	0.12	0.30	0.04
4-allyl-1,2-dimethoxybenzene	93-15-2	0.20	0.27	0.05
iso-eugenol	97-54-1	0.02	0.13	0.03
4-methylphenol	106-44-5	0.16	0.14	0.04
2-propylphenol	644-35-9	0.10	0.22	0.06
benzonitrile	100-47-0	0.14	0.53	0.03
methyl jasmonate	39924-52-2	0.18	0.49	0.06
2-ethylphenol	90-00-6	0.05	0.35	0.02
4hydroxy-3-methoxybenzaldehyde	121-33-5	0.22	0.24	0.10
1-butanol	71-36-3	0.61	NA	NA
1-hexanol	111-27-3	0.74	NA	NA
3-methyl-butanol	123-51-3	0.30	0.51	0.04
1-octen-3-ol	3391-86-4	1.34	NA	NA
Z3-hexenol	928-96-1	0.63	1.24	0.04
2,3-butanediol	513-85-9	0.32	0.32	0.72
decanol	112-30-1	0.29	0.25	0.02
4-methylcyclohexanol	589-91-3	0.42	1.17	0.03
3-octanol	589-98-0	0.99	0.37	0.02
4-octanol	589-62-8	0.61	0.19	0.08
2-heptanol	543-49-7	1.02	0.40	0.04
2-hexanol	626-93-7	0.91	0.72	0.24
1-hexen-3-ol	4798-44-1	0.76	0.32	0.03
butyl acetate	123-86-4	0.53	0.35	0.04
pentyl acetate	628-63-7	0.80	NA	NA
hexyl acetate	142-92-7	0.59	0.20	0.03
E2-hexenyl acetate	2497-18-9	0.74	0.33	0.03
hexyl butyrate	2639-63-6	0.34	0.42	0.03
octyl acetate	112-14-1	0.22	0.20	0.02
2-methyl butyl acetate	624-41-9	0.31	0.31	0.05
sec-amyl acetate	626-38-0	0.00	NA	NA
ethyl (R)-(-)-3-hydroxybutanoate	24915-95-5	0.75	0.26	0.23
ethyl (S)-(+)-3-hydroxybutanoate	56816-01-4	0.86	0.72	0.51
ethyl 2-methylbutanoate	7452-79-1	0.27	0.24	0.05
methyl 3-hydroxy hexanoate	21188-58-9	0.59	0.17	0.03
ethyl 3-hydroxyhexanoate	2305-25-1	0.53	0.27	0.02
isoamyl tiglate	41519-18-0	0.32	0.25	0.09
isopropyl butyrate	638-11-9	0.20	0.25	0.02
methyl tiglate	6622-76-0	0.32	0.31	0.18
ethyl 2-methyl-2E-butenoate	5837-78-5	0.17	0.28	0.18
isopropyl tiglate	1733-25-1	0.06	0.22	0.07
ethyl isovalerate	108-64-5	0.19	0.26	0.03
heptyl acetate	112-06-1	0.34	0.27	0.03
Z3-hexenyl acetate	3681-71-8	0.70	0.41	0.04
hexyl methanoate	629-33-4	0.59	0.64	0.03
beta-butyrolactone	3068-88-0	0.00	0.31	0.10
gamma-valerolactone	108-29-2	0.31	0.32	0.20
gamma-propyl-gamma-butyrolactone	105-21-5	0.35	0.57	0.03
oil	solvent	0.21	0.22	0.04
heptane	142-82-5	0.31	0.18	0.06
octane	111-65-9	0.29	0.21	0.03
nonane	111-84-2	0.25	0.21	0.04

Supplemental Material for Chapter 2

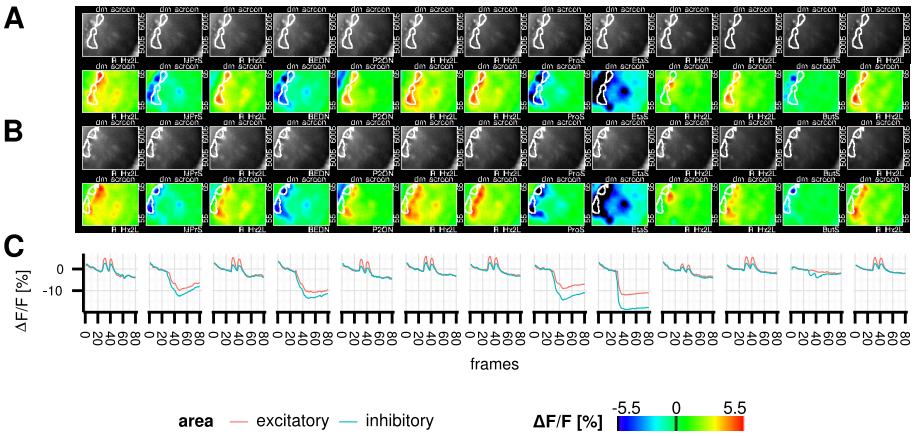

FIGURE S9: Areas of inhibition and excitation in Or56a. **A** Raw and false-color coded images of antennal calcium-imaging on GAL4-Or56a fruit fly antenna. *White* area indicates "inhibitory area" (see Text). **B** Like A, *white* area indicates "excitatory area" (see Text). **C** Response traces extracted from the corresponding "excitatory" and "inhibitory" area in A and B. Data was not corrected for bleaching

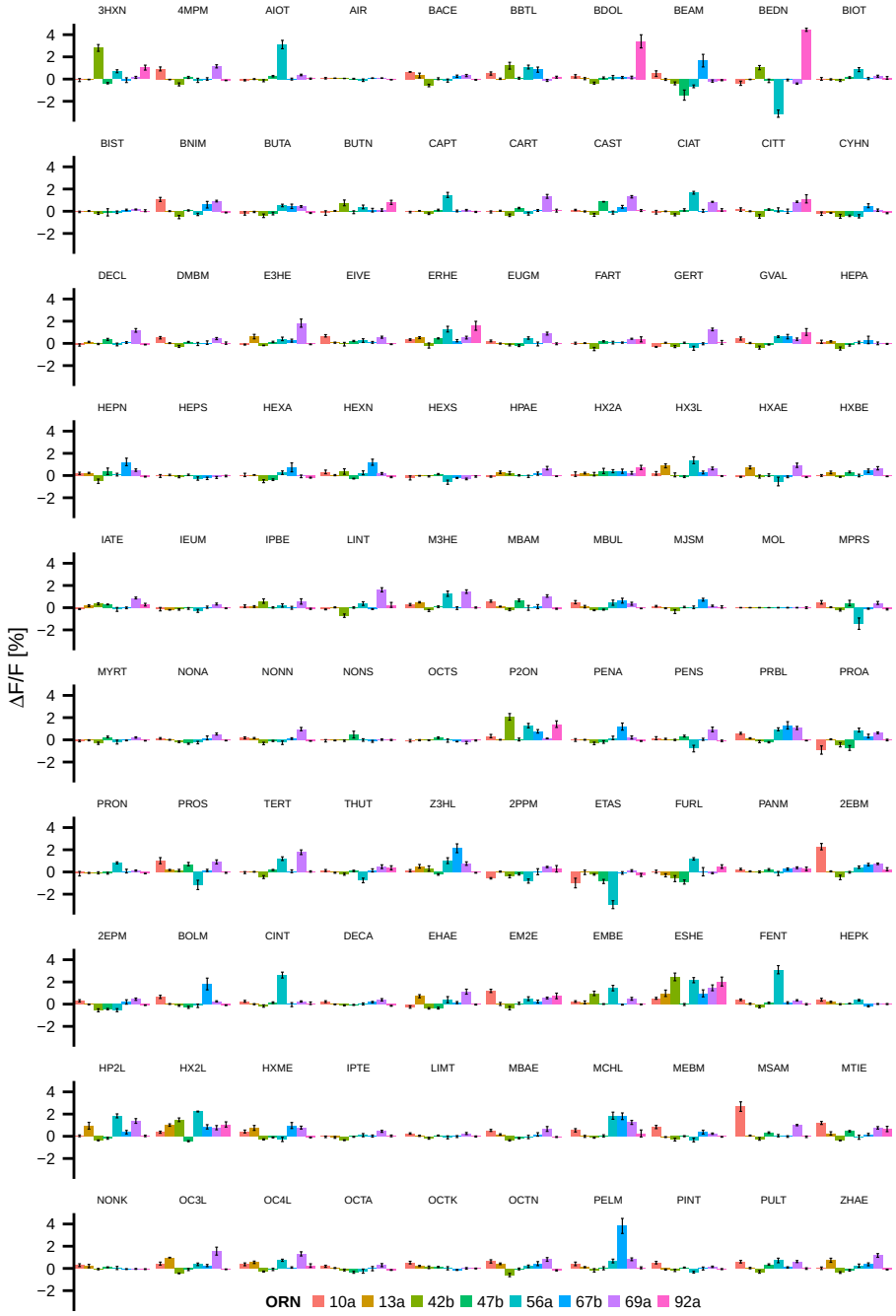

FIGURE S10: Odorant responses across receptors for 100 odorants that were tested in all eight ORNs. Bars give mean fluorescence changes ($\Delta F/F$ [%]), error-bars indicate SEM, colors indicate ORN class. See Table S4 for odorant abbreviations.

TABLE S4: Table of odorants and concentrations used in the experiments together with their Chemical Abstracts Service (CAS) number and the abbreviated code used in the text

Name	CAS	Class	Code	4-Code
(-)-alpha-thujone	546-80-5	terpene		THUT
(-)-trans-caryophyllene	87-44-5	Terpene		CAPT
(+)-alpha-pinene	7785-70-8	Terpene		PINT
(1R)-(-)-fenchone	7787-20-4	Terpene		FENT
(1R)-(-)-myrtenal	564-94-3	Terpene		MYRT
(R)-(-)-carvone	6485-40-1	Terpene		CART
(R)-(+)-limonene	5989-27-5	Terpene		LIMT
(R)-(+)-pulegon	89-82-7	Terpene		PULT
(S)-(-)-citronellal	5949-05-3	Terpene		CIAT
(S)-(+)-carvone	2244-16-8	Terpene		CAST
1-hexen-3-ol	4798-44-1	Alcohol		HX3L
1-octen-3-ol	3391-86-4	Alcohol		O13L
1,8-cineole	470-82-6	Terpene		CINT
2-butanone	78-93-3	Ketone		BUTN
2-ethylphenol	90-00-6	Aromatic		2EPM
2-heptanol	543-49-7	Alcohol		HP2L
2-heptanone	110-43-0	Ketone		HEPN
2-hexanol	626-93-7	Alcohol		HX2L
2-hexanone	591-78-6	Ketone		HEXN
2-methyl butyl acetate	624-41-9	Ester		MBAE
2-octanone	111-13-7	Ketone		OCTN
2-pentanol	6032-29-7	Alcohol	PO	PE2L
2-pentanone	107-87-9	Ketone	PN	PENN
2-propylphenol	644-35-9	Aromatic		2PPM
2,3-butanediol	513-85-9	Alcohol		BDOL
2,3-butanedione	431-03-8	Ketone		BEDN
3-hexanone	589-38-8	Ketone		3HXN
3-hydroxy-2-butanon	513-86-0	Ketone	BN	HBUN
3-methyl-butanol	123-51-3	Alcohol	MO	MBUL
3-octanol	589-98-0	Alcohol		OC3L
3-penten-2-one	625-33-2	Ketone		P2ON
4-allyl-1,2-dimethoxybenzene	93-15-2	Aromatic		DMBM
4-isopropylbenzaldehyde	122-03-2	Aromatic		IPBM
4-methoxybenzaldehyde	123-11-5	Aromatic		MBAM
4-methoxybenzene	100-66-3	Aromatic		MEBM
4-methylcyclohexanol	589-91-3	Alcohol		MCHL
4-methylphenol	106-44-5	Aromatic		4MPM
4-octanol	589-62-8	Alcohol		OC4L
4-hydroxy-3-methoxybenzaldehyde	121-33-5	Aromatic		PANM
6-methyl-5-hepten-2-one	110-93-0	Ketone		MH2N
acetaldehyde	75-07-0	Aldehyde		ACEA
acetic Acid	64-19-7	Acid	AA	ETAS
acetone	67-64-1	Ketone		PRON
acetyl furan	1192-62-7	Other		ACFL
alpha-bisabolol	23089-26-1	Terpene		BIST
alpha-ionone	127-41-3	Terpene		AIOT
alpha-terpineol	10482-56-1	Terpene		TERT

Continued on next page

Table S4 – continued from previous page

Name	CAS	Class	2-Code	4-Code
benzaldehyde	100-52-7	Aromatic		BEAM
benzonitrile	100-47-0	Aromatic		BNIM
benzyl alcohol	100-51-6	Aromatic		BOLM
beta-butyrolactone	3068-88-0	Other		BBTL
beta-citronellol	106-22-9	Terpene		CILT
beta-ionone	79-77-6	Terpene		BIOT
butanal	123-72-8	Aldehyde		BUTA
butanol	71-36-3	Alcohol	BO	BUTL
butyl acetate	123-86-4	Ester	BA	BACE
butyl butyrate	109-21-7	Ester	BB	BUBE
butyric Acid	107-92-6	Acid		BUTS
citral	5392-40-5	Terpene		CITT
cyclohexanone	108-94-1	Ketone		CYHN
decanal	112-31-2	Aldehyde		DECA
decanol	112-30-1	Alcohol		DECL
E,E-farnesol	106-28-5	Terpene		FART
E2-hexenal	6728-26-3	Aldehyde	HE	HX2A
E2-hexenyl acetate	2497-18-9	Ester		EHAE
ethyl (R)-(-)-3-hydroxybutanoate	24915-95-5	Ester		ERHE
ethyl (S)-(+)-3-hydroxybutanoate	56816-01-4	Ester	EH	ESHE
ethyl 2-methyl-2E-butenoate	5837-78-5	Ester		EM2E
ethyl 2-methylbutanoate	7452-79-1	Ester		EMBE
ethyl 3-hydroxyhexanoate	2305-25-1	Ester		E3HE
ethyl benzoate	93-89-0	Aromatic		2EBM
ethyl butyrate	105-54-4	Ester	EB	ETBE
ethyl isovalerate	108-64-5	Ester		EIVE
ethyl propionate	105-37-3	Ester		ETPE
ethyl propionate	105-37-3	Ester		ET3E
eugenol	97-53-0	Aromatic		EUGM
furfural	98-01-1	Other	FF	FURL
gamma-butyrolactone	96-48-0	Other		GBAL
gamma-propyl-gamma-butyrolactone	105-21-5	Other		PRBL
gamma-valerolactone	108-29-2	Other		GVAL
geosmin	16423-19-1	Alcohol		2MNL
geraniol	106-24-1	Terpene		GERT
geranyl acetate	105-87-3	Terpene	GA	GEST
heptanal	111-71-7	Aldehyde		HEPA
heptane	142-82-5	Alkane		HEPK
heptanoic Acid	111-14-8	Acid		HEPS
heptyl acetate	112-06-1	Ester		HPAE
hexanal	66-25-1	Aldehyde	HL	HEXA
hexanoic Acid	142-62-1	Acid		HEXS
hexanol	111-27-3	Alcohol	HO	HEXL
hexyl acetate	142-92-7	Ester	HA	HXAE
hexyl butyrate	2639-63-6	Ester		HXBE
hexyl methanoate	629-33-4	Ester		HXME
iso-eugenol	97-54-1	Aromatic		IEUM

Continued on next page

Table S4 – continued from previous page

Name	CAS	Class	2-Code	4-Code
iso-pentanoic Acid	503-74-2	Acid		IPES
isoamyl butyrate	106-27-4	Ketone	IAB	IABE
isoamyl tiglate	41519-18-0	Ester		IATE
Isobutyl-acetate	110-19-0	Ester	IBA	IBAE
isobutyric Acid	79-31-2	Acid		MPRS
isopentyl acetate	123-92-2	Ester	IA	ISOE
isopropyl butyrate	638-11-9	Ester		IPBE
isopropyl tiglate	1733-25-1	Ester		IPTE
linalool	78-70-6	Terpene		LINT
methyl 3-hydroxy hexanoate	21188-58-9	Ester		M3HE
methyl jasmonate	39924-52-2	Aromatic		MJSM
methyl salicylate	119-36-8	Aromatic		MSAM
methyl tiglate	6622-76-0	Ester		MTIE
nonanal	124-19-6	Aldehyde		NONA
nonane	111-84-2	Alkane		NONK
nonanoic Acid	112-05-0	Acid		NONS
nonanone	821-55-6	Ketone		NONN
octanal	124-13-0	Aldehyde		OCTA
octane	111-65-9	Alkane		OCTK
octanoic Acid	124-07-2	Acid		OCTS
octyl acetate	112-14-1	Ester		OCAE
pentanal	110-62-3	Aldehyde		PENA
pentanoic Acid	109-52-4	Acid		PENS
pentyl acetate	628-63-7	Ester		PACE
phenethyl Alcohol	60-12-8	Aromatic	PA	PELM
phenylacetaldehyde	122-78-1	Aromatic		PAAM
propanal	123-38-6	Aldehyde	PL	PROA
propanoic Acid	79-09-4	Acid		PROS
Z3-hexenol	928-96-1	Alcohol	ZL	Z3HL
Z3-hexenyl acetate	3681-71-8	Ester		ZHAE

Supplemental Material for Chapter 3

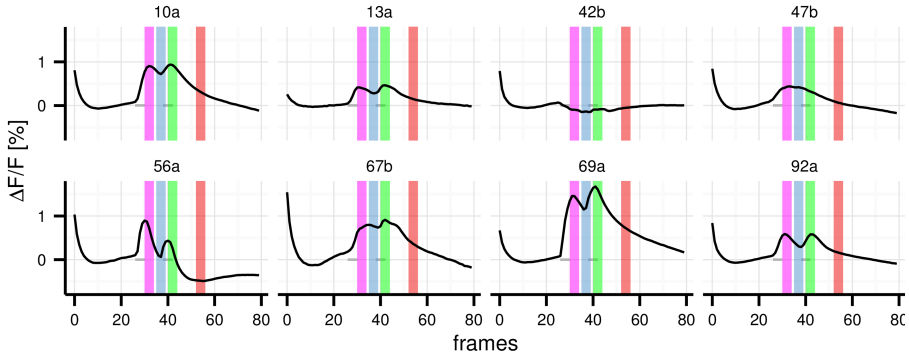

FIGURE S11: Time windows used for calculation of dynamical features. Figure shows mean response traces per ORN. Colored bars indicate $1.25\,s$ time windows (5 frames) that were used for the calculation of different dynamical features (see Material & Methods for details on calculations). Mean values during time windows were used to extract features. *violet:* peak_1, *blue:* return to baseline between peaks, *green:* peak_2, *red:* post stimulus window, *gray* dashes indicate stimulus pulses. Note that bleach correction was performed leaving out the initial three frames of a recording, pre-stimulus parts of response traces might include bleach-correction artifacts.

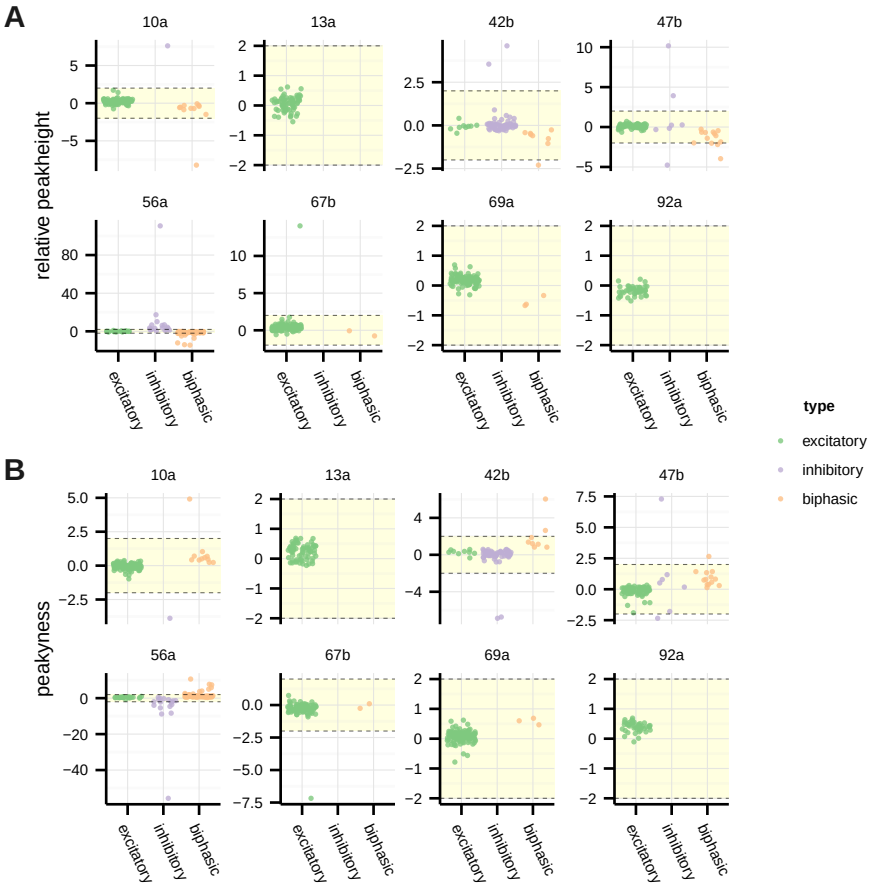

FIGURE S12: Jitterplot showing distribution across the full range of "peakiness" and "relative peakkheight" across receptors. Dashed lines indicate range shown in Figure 3.2.

Supplemental Material for Chapter 4

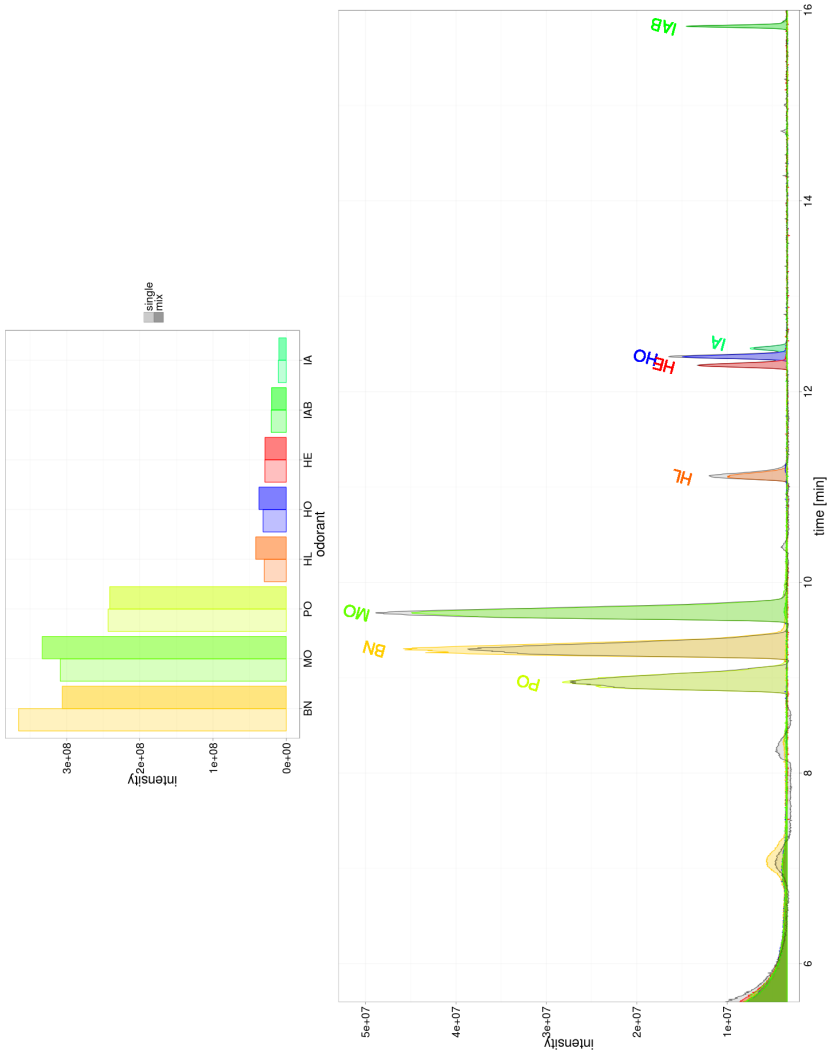

FIGURE S13: Comparison of GC-MS measurement of MIX15 vs single odorant solutions. Top, barplot comparing the GC peakareas of the detected substances diluted alone or as a mixture of all 15 components. Bottom, overlay of the GC traces of the 15 component mixture, *gray*, and the components diluted alone. Note that some odorants appear in concentrations that were below GC detection threshold.

Supplemental Material for Chapter 5

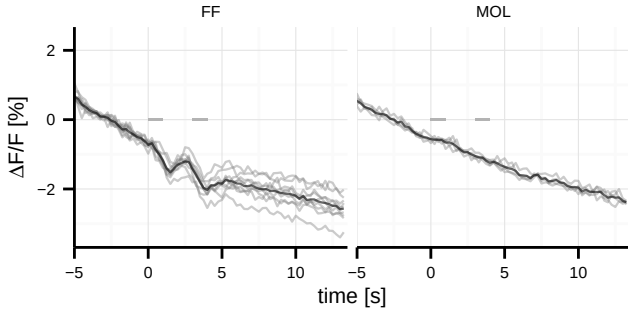

FIGURE S14: Response traces recorded from unstained antenna of wildtype CantonS flies (n=9 (FF) and 4 (MOL, solvent control mineral oil) recorded from two animals). Data was not bleach-corrected, individual response traces in *gray*, mean trace in *black*, *gray* dashes indicate stimulus pulses.

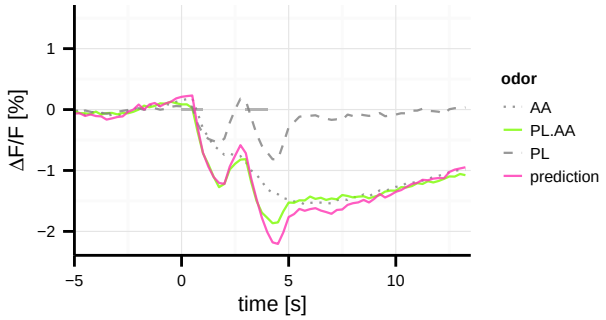

FIGURE S15: Mean traces for PL.AA mixture, prediction and components. PL.AA mixture is almost identical to the summation of both component traces. *Gray dashed* lines indicate component responses, *blue* line: mixture, *magenta* line: prediction, calculated as the sum of component responses. *Gray* dashes indicate stimulus pulses.

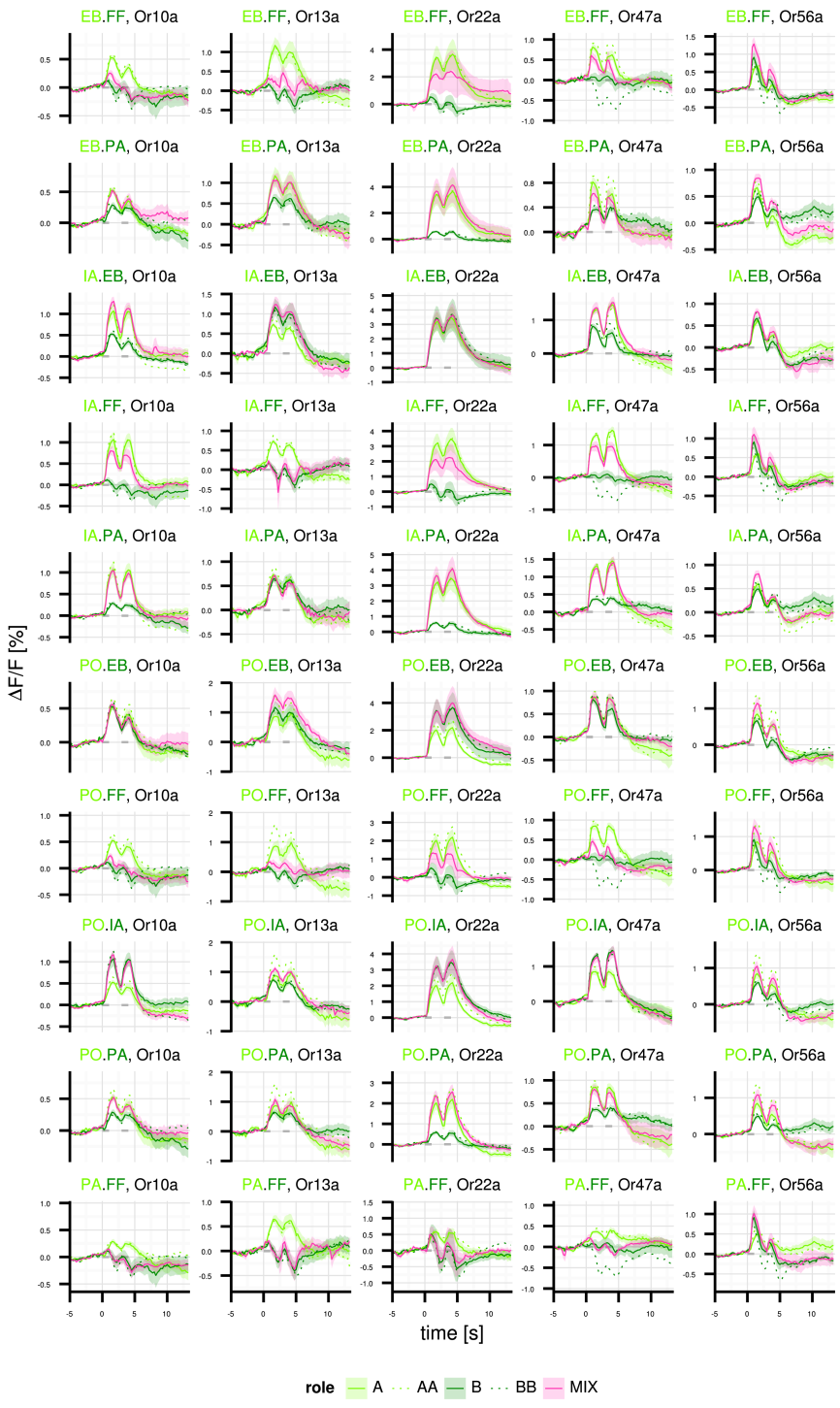

FIGURE S16: Mean response traces of all mixtures investigated. *Shaded* areas indicate SEM, *solid lines* indicate component responses at single concentration (10^{-3} dilution), *dotted lines* indicate component responses at double concentration. *Gray* dashes indicate stimulus pulses. (*Continued on next page*)

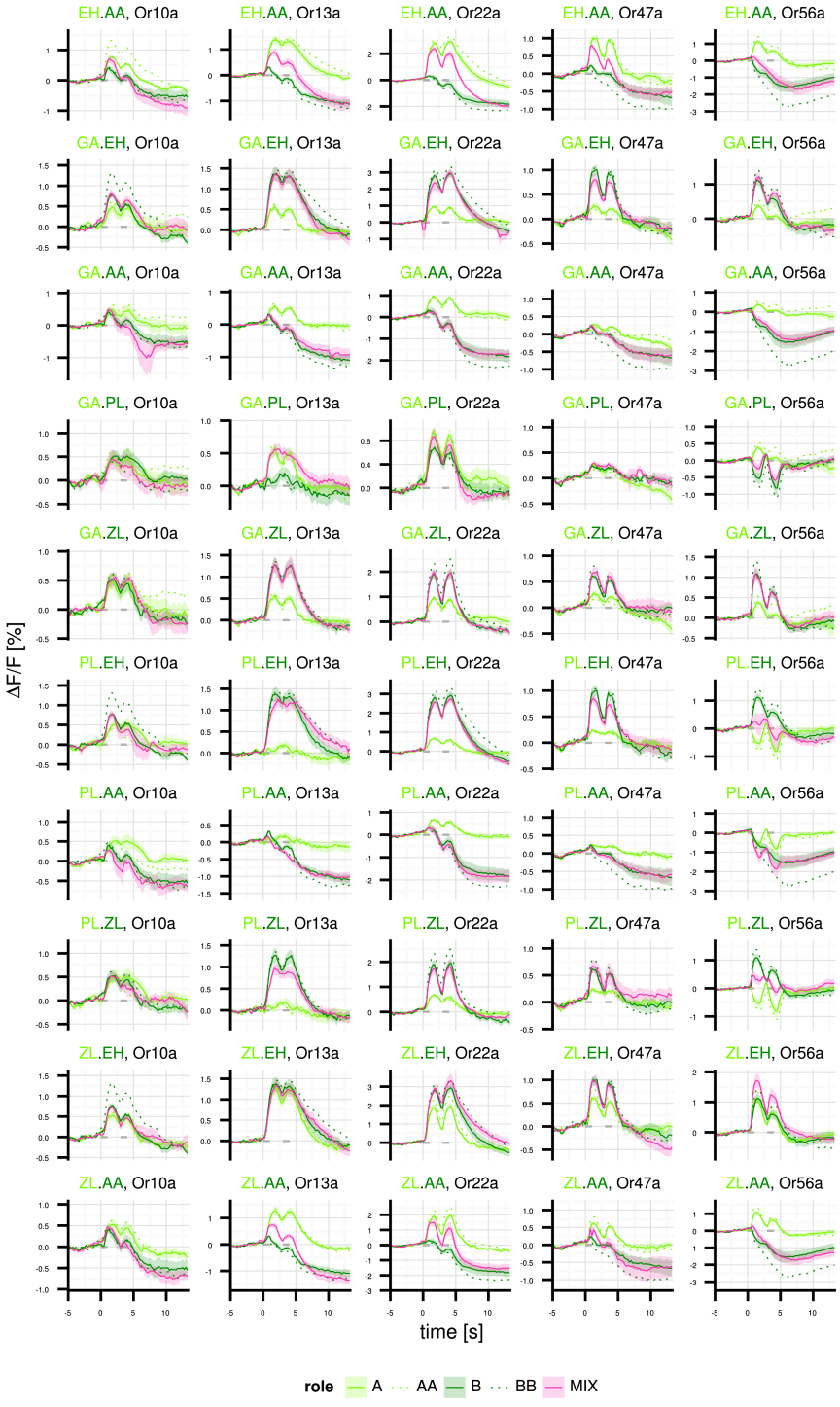

FIGURE S16: (*Continued*)

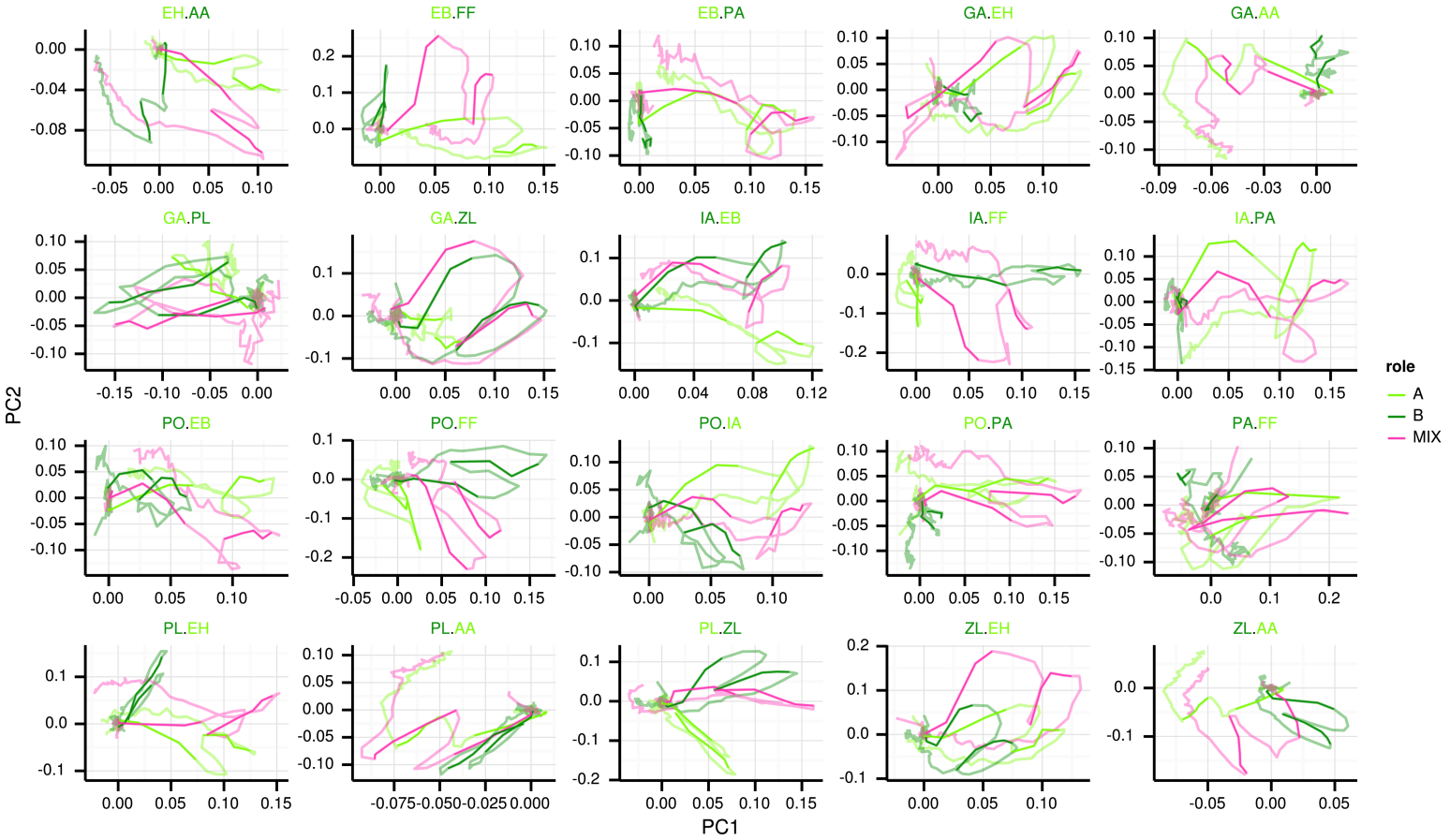

Figure S17: Principle component trajectories for all mixtures. Rotations were calculated in the five ORN dimensions for each individual mixture together with its components. Darker parts of the trajectories indicate stimulus-pulses.

Additional Publications

DoOR: The Database of Odorant Responses

Vol 13, No.4 September 2011

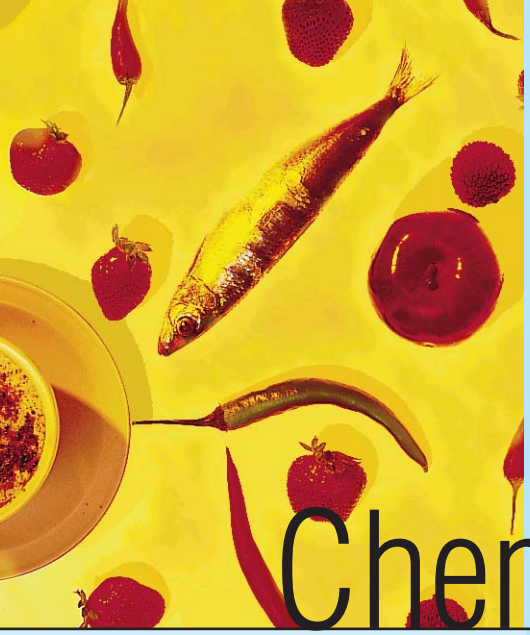

Chemo sense

EDITORIAL

ChemoSensory Science Noses Ahead

By Graham Bell
g.bell@e-nose.info

In the past decade since the tumult and tragedy of 9/11, science has not stood still.

Chemosensory receptor technology which began in the 1990s is pressing ahead and new forms of database are needed to keep track of information growth. One of these is presented by Daniel Münch and Giovanni Galizia in this issue. Their freely accessible web-based information system can provide new insights into receptor-odorant functionality, through inter-linkage of information, obtained separately from any number of independent researchers. The database is a new tool for discovery. We pay tribute to the inclusive generosity of its inventors.

cont. pg 2

DoOR: The Database of Odorant Responses

Daniel Münch and C. Giovanni Galizia,
giovanni.galizia@uni-konstanz.de

University of Konstanz, 78457 Konstanz, Germany

Both olfactory systems of animals, or artificial noses, can increase the capacity of the system exponentially by combining many sensors with overlapping response profiles, thanks to the power of combinatorial coding. Studying animal systems helps to understand the underlying mechanism, and knowledge of odor-response profiles, in this pursuit, is of paramount importance. We present here a new approach towards this goal: DoOR, the database of odorant responses, including a freely available access to it on the Internet.

THE COMBINATORIAL NATURE OF OLFACTORY CODING

The chemical environment provides the most complex sensory cues all living organisms on earth have to deal with, being composed of an uncountable number of different molecules. Many kinds of chemosensory systems have evolved and all organisms use some of them, but the most elaborate one is olfaction. This sense is amazingly efficient and enables organisms to orient and communicate within this incredibly complex chemical world.

Many technologies deal with detection or analysis of chemicals, but real olfactory systems

cont. pg 2

INSIDE:

TM
E-Nose Pty Ltd
Graham Bell and Associates Pty Ltd
Centre for ChemoSensory Research
www.chemosense.info www.e-nose.info
ISSN 1442-9098

EDITORIAL CONTINUED

ChemoSensory Science Noses Ahead

continued

Australians lay claim to the discovery of, and national addiction to a white, sugary, fruit and cream-lashed tart, called Pavlova. The release of digitised back numbers of Sydney newspapers, spanning centuries, provides new resources on the historical voracity of such claims. While helping correct errors in the digitisation process, Robert Marks made interesting insights on the origin, recipe and name of this popular dessert. Whether in New Zealand or Australia, Pavlova performs gustatory ballet on your sensory perception.

ChemoSense congratulates Alan Mackay-Sim on his award of a Eureka Prize.

Will you attend the 2011 AACSS scientific meeting in New Zealand? Make bookings now to avoid disappointment ■

DoOR: The Database of Odorant Responses

continued

still appear to be the most powerful.. We may think of a dog searching for drugs, dangerous substances or missing people, or of a winemaker or whisky distiller creating a special flavor. Indeed, even though it is much easier to describe a color or a tone as compared to a complex odor, and even though our vocabulary for odors quickly reaches its limits and we have to borrow words like "dense", "green" or "robust" from other contexts, we are still able to recognize and differentiate amazing numbers of complex odors..

Humans have around350 types of olfactory receptors (ORs), dogs over 1000. Even a rather simple olfactory system like that of the fruit fly *Drosophila melanogaster*, with about60 OR types, is able to detect and differentiate hundreds or thousands of different odors. Olfactory receptor neurons (ORNs) always express a single OR, so that 60 OR types in a species corresponds to 60 ORN types. The huge coding capability of countless different cues by only a few sensors arises from the combinatorial code created across ORN types. However, in order to decipher the code, it is necessary to know not only the best ligand of each ORN type (i.e. to "deorphan" it), but ideally its entire response spectrum across many substances: in other words, we need to know what is called the "olfactome".

THE WAY TOWARDS THE OLFACTOME

It follows that "deorphaning" ORs (or ORNs) is a major challenge in olfactory research: very few ORs have had that honor yet. The animal species for which the best data is available is the fruit fly. Many labs around the world decided to use the fruit fly for olfactory experiments because these animals are easily modified genetically. Since the *Drosophila* OR genes were published in 1999 (Clyne et al. 1999; Gao et al. 1999; Vosshall et al. 1999), responses of hundreds of ligand/OR combinations have been measured, with each data set contributing a small part to the *Drosophila* "olfactome" (e.g. de Bruyne et al. 2001; Hallem et al. 2006; Pelz et al. 2006). However, assembling these data remained a challenge.

OUR APPROACH TOWARDS ASSEMBLING THE OLFACTOME

With so many data sets of olfactory responses in *Drosophila*, a notable part of the olfactome is known, and one would think that we are already close to the full picture. But far from it: these data are very heterogeneous and cannot be compared easily. Different labs use different techniques, based on slightly different research questions: ORN responses can be recorded *in situ* using electrophysiology (de Bruyne et al. 2001), or in transgenic animals, where the OR of interest is expressed ectopically (Hallem et al. 2006). ORN responses can also be recorded *in situ* as changes in intracellular calcium (Pelz et al. 2006). ORs can be expressed in cell culture, and their responses to odors measured using either electrophysiology or calcium imaging (Kiely et al. 2007). Additional heterogeneity comes from different approaches: some labs record odor responses to single concentrations, other to full dose response curves, odor pulse length and/or temporal dynamics vary across labs, etc. Nevertheless, one rule should always be fulfilled (give or take experimental variability): a better ligand gives a stronger response, irrespective of the technique or the lab involved.

Using this notion, we decided to develop a technique that allows merging all available data into a consensus database,

cont. pg 3

DoOR: The Database of Odorant Responses

continued

the Database of Olfactory Responses – DoOR (Galizia et al. 2010).

MERGING HETEROGENEOUS DATA

Merging data is performed stepwise, whereby in each step we integrate two data sets from different studies of the same OR into a new merged data set, and iteratively repeat the procedure with the data from the next study until all existing responses for a given OR are used. We use the following strategy. First, the odorant responses (e.g. spike counts, fluorescence change, half-optimal concentrations) are scaled from zero to one within each study. Then, they are plotted against each other (Fig. 1). Five monotonic functions (linear, exponential, sigmoid, asymptotic, and asymptotic with an offset) are fitted to the overlapping data points (i.e. the odorants measured in both studies). Next, we select the function with the best fit. As the function describes the relationship of the two studies only within the range of overlapping measurements, extrapolation beyond that range follows a linear identity relationship. All measurements are then projected orthogonally onto the function, producing a new, merged data set containing more odors than each of the parent data sets. This data set is again scaled from zero to one according to the position of the responses along the curve, and the merging now continues iteratively until all data sets are used. This way, in the end all the data sets describing a given OR/ORN end up in one consensus data set, scaled from 1 (best ligand) to 0 (either no response, or corresponding to an antagonistic, inhibitory response).

Merging of two data sets is only performed when they overlap at least by four odors and the fit performance is good. The sequence of merging data set pairs affects the outcome: suitable methods were developed to select the best sequence (Galizia et al. 2010). As a result we obtain a database that combines all currently available information about odor responses in the fruit fly. This database is open access, and can be used interactively or as a downloaded package. In the following, we present how to use the database, and show a few study cases where such a tool can be put to good use. Most importantly, such a database can be evaluated from two points of view that are orthogonal to each other: for a given receptor, it is possible to obtain all available responses as an odor-response profile, or for a given odor it is possible to obtain the combinatorial odor-response pattern across all receptors.

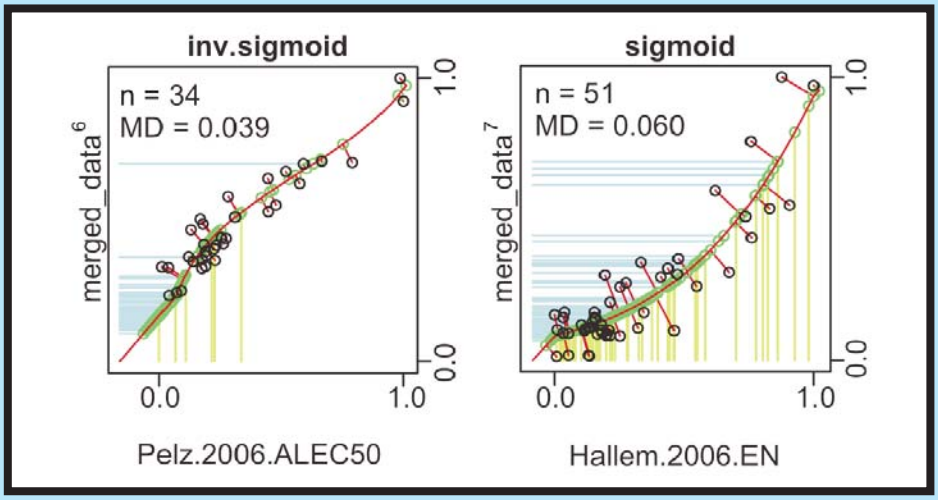

Figure 1: *Merging process for data sets of receptor Or22a. Best fitting function is given above each plot, black circles are odorants measured in both data sets, their number is indicated as n, MD = mean distance, blue and yellow lines are projections of odors present in only one study.*

USING DoOR: HOMEPAGE

The interactive mode is the fastest: any particular OR response profile or odor-response pattern is available as the newest DoOR data in form of tables and figures on the DoOR homepage (http://neuro.uni-konstanz.de/DoOR). In addition, we list chemical information on the odor molecules, data on each given receptor, and all the studies used that deal with a given receptor or odorant together with links to corresponding external resources from PubChem (http://pubchem.ncbi.nlm.nih.gov/) or FlyBase (http://www.flybase.org).

The example in Fig. 2a shows the response to the odor 2-heptanone (a substance that smells somewhat like glue; the structure is shown in figure 2c). The response is shown as a *virtual* activity pattern across olfactory glomeruli in the antennal lobe of the fruit fly (the antennal lobe forms a spatial mapping of all olfactory receptors in the fly brain, akin to what happens in the human olfactory bulb), with the four frames showing four sections going deeper into the brain. The odor elicits strong activity in some glomeruli (red), an inhibition in others (blue) and no activity in the rest (white). The responses for some glomeruli are as yet not known (gray),

cont. pg 4

DoOR: The Database of Odorant Responses

continued

and for some glomeruli not even the receptor innervation is known (black). Receptor responses can be shown as a histogram (Fig. 2b), with glomeruli/receptors sorted so that the strongest response is in the center, and weak or inhibitory responses to the sides. Such histograms are useful to describe overall response properties, e.g. odors that activate only a few receptors (with a pointed shape) or those that activate many receptors (with a flat shape). In this case, the histogram is moderately broad, with two inhibited glomeruli. Because the antennal lobe is a three-dimensional structure in the brain, we also mapped the responses onto a 3-D model (Fig. 3). On the homepage, this model is interactive, and can be rotated by the user in order to see the response from whatever angle is needed.

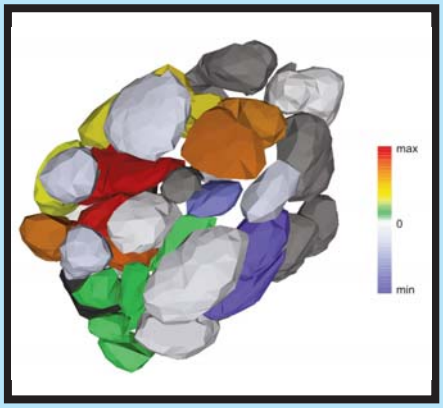

Figure 3: *Responses to 2-heptanone mapped onto 3-D model of the antennal lobe.*

DoOR-PACKAGE

If you are interested in more detailed data and tools for further calculations you can download the complete Database of Odorant Responses (http://neuro.uni-konstanz.de/DoOR). DoOR is written in Gnu-R (R Development Core Team 2011), a statistical programming language which is available for free from http://www.R-project.org. The DoOR download contains all available data, and all programs needed to compute the consensus database. Furthermore, several tools for plotting data, performing various calculations on it, and tools for adding data sets are included.

The DoOR package consists of two parts, one containing all the functions and one containing all the data. The advantage of this separation is that updating the data is independent from updating the functions. Importantly, with each update, all previous versions of the database (both functions and data tables) remain as downloadable links, and therefore stay available as fully referable snapshots.

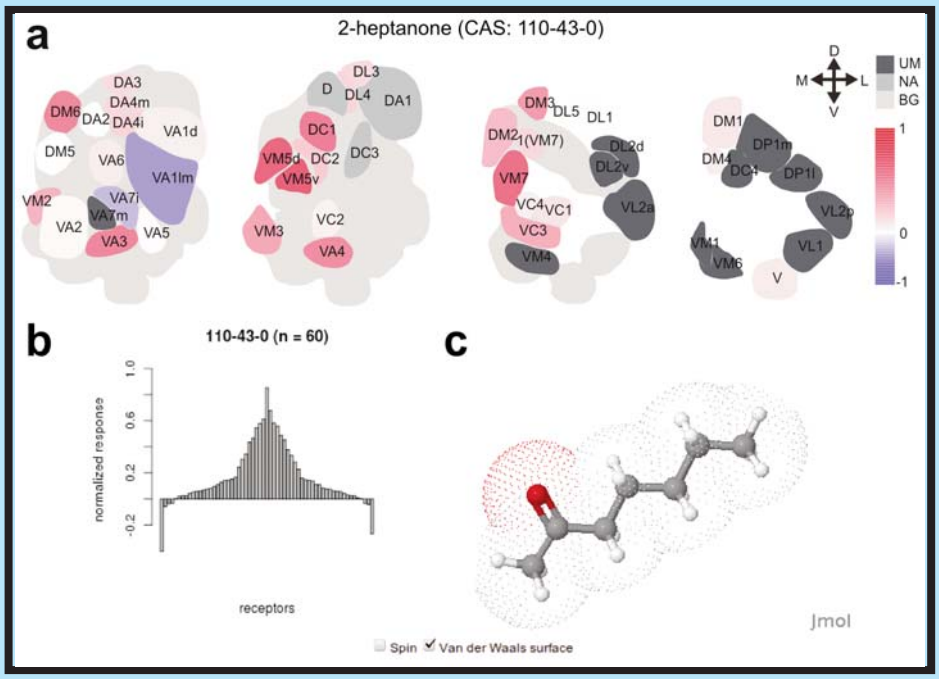

Figure 2: *Odorant profile of 2-heptanone as found on the DoOR homepage. a: The DoOR data for 2-heptanone visualized as a false color coded representation of the antennal lobe. UM: OR for these glomeruli is still unknown; NA: no data available for 2-heptanone in this glomerulus; BG: background, glomeruli from deeper layers. b: Odorant response histogram for 2-heptanone. c: 3-D model of 2-heptanone.*

USING THE DoOR

Accounting for negative responses

A feature of ORNs is that they do not only respond with excitation but that some ligand/receptor combinations lead to an inhibition of that cell. The DoOR data consists of values scaled from 0 to 1 after merging, not yet accounting for negative responses. Therefore, during the merging process, we treat the spontaneous firing rate of a receptor (SFR, the firing rate in absence of any stimulus) as a normal odorant. We then set the SFR to zero, so that all the values lower than SFR become negative. The range SFR – maximum is rescaled from zero to one and the inhibitory responses are as large as dictated by the linear remapping.

Global scaling

The most important feature of an olfactory response to an odorant is the

cont. pg 5

DoOR: The Database of Odorant Responses

continued

combinatorial code represented by the responses across all receptors. In order to reveal the combinatorial features of the DoOR, the data sets that have been computed for each receptor have to be rescaled relative to each other. Thus, we recalculate the responses using inter-receptor information gained from studies that measured more than one receptor. This information is important for a correct interpretation of the data. For example, in Fig. 4 (top), the odor-responses of the two receptors Or65a (left) and Or67a (right) are shown as histograms (again in center-lateral order, with best responses at the center, and increasingly weak responses to the sides). Or65a has a pointed shape (few good ligands) with many inhibitory responses (the two downwards pointing tails), while Or67a has a broad response profile (many intermediate ligands with varying affinity) and no negative responses. However, when scaling is corrected for differences across receptors (Fig. 4, bottom), it is apparent that the picture for Or65a changes: even the best known ligand is a very weak ligand, eliciting a weak response. Similarly, the inhibitory responses are weak. This result has two possible interpretations: either

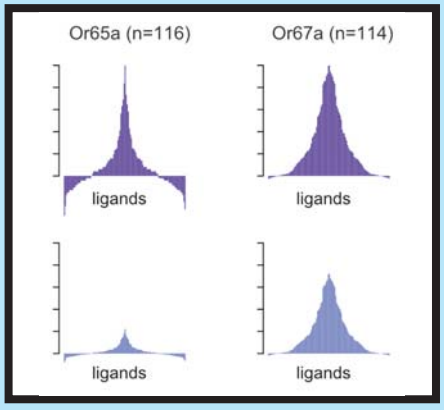

Figure 4: *Receptor tuning plots before (top) and after (bottom) global normalization for the two ORs Or65a (left) and Or67a (right).*

the best ligand for this receptor is not known (meaning that more odor-response screening is needed), or this is indeed a very weak receptor (which would have far-reaching implication for how the brain extracts information from combinatorial response patterns).

Back projection

When working with a particular technique, 0-1 information in the DoOR database is useful, but abstract and different from the values in the physiological data (e.g. spikes, Ca^{2+} increase). For this reason, we included a tool for back projection of the consensus data onto the value-space of any of the input data types. This tool uses the same algorithms that are used for merging the single data sets, but calculates in reverse, transforming the 0-1 data to the unit of interest.

Identifying ORs from an orphan response profile

Another tool is useful when the mapping of OR and ORN is not yet known. In these cases you may have an orphan response profile and want to know to which OR/ORN it belongs. One example is receptor Or13a which we were measuring using Ca^{2+} imaging. The Ca^{2+} reporter was expressed under control of the Or13a promoter, but the corresponding ORN was not known by then.

In *Drosophila*, each OR gene (e.g. Or22a, a name related to its position in the genome) is expressed in a particular population of receptor neurons (e.g. ab3A, for "cell **A** in the **a**ntennal **b**asiconic sensillum number **3**"), and these receptor neurons send their axons to a particular glomerulus (e.g. DM2 for dorso-medial glomerulus number 2). This isomorphism is also the reason why activity patterns across receptor types can be shown as patterns across glomeruli (see above). The specific mapping of gene-receptor-glomerulus (e.g. Or22a -> ab3A -> DM2) is not yet known in all cases. Therefore where data sets are available for a particular neuron type (e.g. ab6A), they have been included as such when the corresponding OR is not known.

The program performs fits between the orphan data set and all the data in DoOR and thereby finds the best matching partner. In our case Or13a had the best match to ab6A, a receptor neuron that had been characterized before but for which the expressed receptor was not yet known (de Bruyne et al. 2001; Galizia et al. 2010). We confirmed this result by mapping another data set from a recent study measuring Or13a (Kreher et al. 2008) (Figure 5).

OUTLOOK

The DoOR project is a first step towards the complete olfactome, and is intended as a service to the broader scientific community, not only Drosophila researchers.. Clearly, the database does yet completely solve the "olfactome" problem: information about odor-concentration is not yet included, because too few reported data sets contain sufficiently detailed information. Similarly, odor mixtures are not covered, and natural odors (e.g. plant extracts) are also missing. DoOR is, however, the most complete and most comprehensive step towards the olfactome currently available.

We will keep DoOR up to date and upload new versions as soon as new olfactory data is published. Any additional data set is welcome and will be added: the more data is fed into the database, the more reliable and complete

cont. pg 6

DoOR: The Database of Odorant Responses

continued

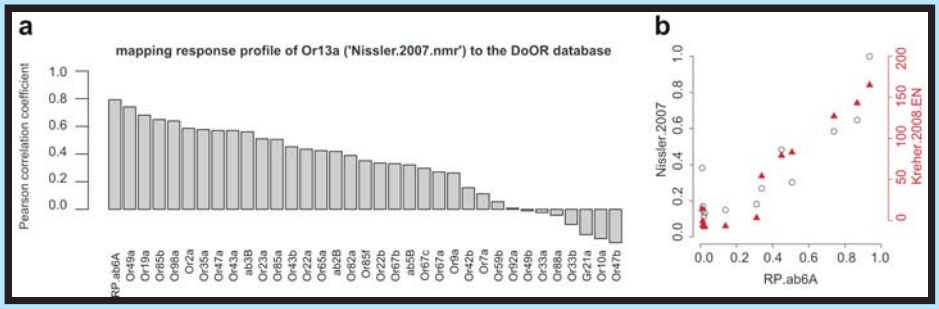

Figure 5: *Mapping response profiles to ORs. a: Pearson's correlation coefficient of the Or13a response profile to the consensus responses of all ORs existing in DoOR, the best match was found for RP.ab6A. b: Plotting the data from the known receptor gene (left ordinate: Ca^{2+} imaging; right ordinate: electrophysiological recording) against the measured response profile of receptor neuron ab6A (abscissa).*

the overall result. While the current data only covers the fruit fly, algorithms and the program package can be immediately ported to any other species (or even to a set of artificial odor sensors). Whenever enough information is available, a new DoOR to other olfactomes can be opened ■

REFERENCES

Bruyne, M. de, Foster, K., and Carlson, John R. (2001). Odor Coding in the *Drosophila* Antenna. *Neuron* **30**, 537-552.

Clyne, P. J., Warr, C G, Freeman, M. R., Lessing, D., Kim, J, and Carlson, J R (1999). A Novel Family of Divergent Seven-Transmembrane Proteins: Candidate Odorant Receptors in *Drosophila*. *Neuron* **22**, 327-38.

Galizia, C. G., Münch, D., Strauch, M., Nissler, A., and Ma, S. (2010). Integrating Heterogeneous odor Response Data into a Common Response Model: A DoOR to the Complete Olfactome. *Chemical Senses* **35**, 551-63.

Gao, Q., and Chess, A. (1999). Identification of Candidate Drosophila Olfactory Receptors from Genomic DNA Sequence. *Genomics* **60**, 31-9.

Hallem, E. A., and Carlson, John R (2006). Coding of Odors by a Receptor Repertoire. *Cell* **125**, 143-60.

Kiely, A., Authier, A., Kralicek, A. V., Warr, Coral G, and Newcomb, R. D. (2007). Functional Analysis of a Drosophila melanogaster Olfactory Receptor Expressed in Sf9 Cells. *Journal of Neuroscience Methods* **159**, 189-94.

Kreher, S. A., Mathew, D., Kim, Junhyong, and Carlson, John R (2008). Translation of Sensory Input into Behavioral Output via an Olfactory System. *Neuron* **59**, 110-24.

Pelz, D., Roeske, T., Syed, Z., Bruyne, M. de, and Galizia, C. G. (2006). The Molecular Receptive Range of an Olfactory Receptor In Vivo (Drosophila melanogaster Or22a). *Journal of Neurobiology* **66**, 1544-63.

R Development Core Team (2011). R: A Language and Environment for Statistical Computing.

Vosshall, L. B., Amrein, H., Morozov, P. S., Rzhetsky, A., and Axel, R. (1999). A Spatial Map of Olfactory Receptor Expression in the *Drosophila* Antenna. *Cell* **96**, 725-36.